Utilising Unmanned Aerial System (UAS) for precision agriculture and yield estimation of Tasmanian Poppy

by

Faheem Iqbal

MS (Remote Sensing and GIS)

National University of Science and Technology

Submitted in fulfilment of the requirements for a Degree of Doctorate of Philosophy

University of Tasmania (November, 2018)

Declaration of Originality

This thesis contains no material which has been accepted for a degree or diploma by the University or any other institution, except by way of background information and duly acknowledged in the thesis, and to the best of my knowledge and belief no material previously published or written by another person except where due acknowledgement is made in the text of the thesis, nor does the thesis contain any material that infringes copyright.

Faheem Iqbal

9 November 2018

Authority of Access

This thesis may be made available for loan and limited copying and communication in accordance with the Copyright Act of 1968.

Publications included in this thesis

This thesis contains three manuscripts that have been published in peer reviewed literature and have been incorporate as Chapter 3, 4 and 5.

Chapter 3: Iqbal, F., Lucieer, A., Barry, K., and Wells, R., 2017. Poppy Crop Height and Capsule Volume Estimation from a Single UAS Flight. *Remote Sensing*, 9 (7), 647.

Chapter 4: Iqbal, F., Lucieer, A., and Barry, K., 2018. Simplified Radiometric Calibration for UAS mounted multispectral sensor. *European Journal of Remote Sensing*, 51 (1), 301–313.

Chapter 5: Iqbal, F., Lucieer, A., and Barry, K., 2018. Poppy crop capsule volume estimation using UAS remote sensing and random forest regression. *International Journal of Applied Earth Observation and Geoinformation*, 73, 362–373.

Statement of Co-Authorship

The following people contributed to the publication of work undertaken as part of this thesis:

Faheem Iqbal, School of Technology, Environment and Design, University of Tasmania
Arko Lucieer, School of Technology, Environment and Design, University of Tasmania
Karen Barry, Tasmanian Institute of Agriculture, University of Tasmania
Reuben Wells, Ag Logic; University of Tasmania (adjunct appointment)

Author details and their roles:

Paper 1: Iqbal, F., Lucieer, A., Barry, K., and Wells, R., 2017. **Poppy Crop Height and Capsule Volume Estimation from a Single UAS Flight**. *Remote Sensing*, 9 (7), 647.

Located in chapter 3

Contribution of Authors: Faheem (85%), Arko (10%), Karen (3%) Reuben (2%)

All authors contributed to design and development. Faheem and Arko performed all field work. Faheem performed all analysis and writing. Arko, Karen and Reuben provided editorial advice.

Paper 2: Iqbal, F., Lucieer, A., and Barry, K., 2018. **Simplified Radiometric Calibration for UAS mounted multispectral sensor**. *European Journal of Remote Sensing*, 51 (1), 301–313.

Located in chapter 4

Contribution of Authors: Faheem (90%), Arko (5%), Karen (5%)

All authors contributed to design and development. Faheem and Arko performed all field work Faheem performed all analysis and writing of chapter. Arko and Karen provided editorial advice.

Paper 3: Iqbal, F., Lucieer, A., and Barry, K., 2018. **Poppy crop capsule volume estimation using UAS remote sensing and random forest regression**. *International Journal of Applied Earth Observation and Geoinformation*, 73, 362–373.

Located in chapter 5

Contribution of Authors: Faheem (90%), Arko (5%), Karen (5%)

Faheem and Arko contributed to design and development. Faheem and Arko performed all field work. Faheem performed all analysis and writing of chapter. Arko and Karen provided editorial advice.

Paper 5: Iqbal, F., Lucieer, A., and Barry, K., 2018. **Prediction of poppy alkaloid concentration using UAS remote sensing**. *Precision Agriculture*, PRAG-D-18-00157.

Located in chapter 7

Contribution of Authors: Faheem (90%), Arko (5%), Karen (5%)

Faheem and Arko contributed to design and development. Faheem and Arko performed all field work. Faheem performed all analysis and compiled the written chapter. Arko and Karen provided editorial input and advice.

We the undersigned agree with the above stated "proportion of work undertaken" for each of the above published (or submitted) peer-reviewed manuscripts contributing to this thesis:

Signed:

Associate Prof. Arko Lucieer
Supervisor
School of Technology, Environment and Design
University of Tasmania
Date: 13 November 2018

Signed:

Prof. Kirsten Orr
Head of School
School of Technology, Environment and Design
University of Tasmania
Date: 14 November 2018

List of Abbreviations

Acronym	Index
VARI	Visual Atmospherically Resistant Index
MCARI	Modified Chlorophyll Absorption Ratio Index
mTVI	Modified Triangular Vegetation Index
NDVI	Normalized Difference Vegetation Index
GI	Greenness Index
RGI	Red/Green Index
RDVI	Renormalized Difference Vegetation Index
SPVI	Spectral polygon vegetation index
OSAVI	Optimized Soil Adjusted Vegetation Index
GNDVI	Green NDVI
MSAVI	Improved Soil Adjusted Vegetation Index
mSR	Modified Simple Ratio
NDRE	Normalized Difference Red Edge Index
EVI	Enhanced Vegetation Index
TVI	Triangular Vegetation Index
GCI	Green Chlorophyll Index
CVI	Chlorophyll Vegetation Index
DVI	Difference Vegetation Index
ExR	Excess Green Minus Excess Red
UAS	Unmanned Aerial System
RS	Remote Sensing
RF	Random Forest
RFR	Random Forest Regression
RFRM	Random Forest Regression Model
CMS	Crop Surface Model
DSM	Digital Surface Model
CHM	Crop Height Model
DTM	Digital Terrain Model
PH	Plant Height
SVIs	Spectral Vegetation Indices
PA	Precision Agriculture
H	Hook
CF	Capsule Formation
F	Flowering

Abstract

The state of Tasmania, Australia is the largest licit producer of poppy opium. The poppy industry in Tasmania cultivates poppies for morphine or thebaine as the main alkaloid product, and supplies up to 40% of the world's opiates used for medication. The global pharmaceutical industry depends on reliable supply of opium poppy from Tasmania, thus, accurate prediction of opium production is important to fulfill national and international demands. Yield prediction well before crop maturity enables precision management of agronomic practices applied to the crop for enhancing the yield. Commonly, traditional direct methods are used to estimate poppy crop yield, whereby samples are collected from the field and appropriate laboratory analyses are performed. These methods are regarded as time-consuming, labour-intensive, costly, and can be biased as often samples do not represent the spatial variability in the field. Alternatively, remote sensing can provide a spatial continuous and efficient assessment of a poppy field. Using satellite imagery for obtaining spatiotemporal information about the crop's phenological status during critical growth periods, however, is very challenging due to frequent cloud cover in Tasmania and due to limitations in spatial resolution of current satellite sensors. Data acquired with an unmanned aerial system (UAS) fills this gap by delivering timely high spatial resolution data. This study aims to investigate the potential of ultra-high spatial and temporal resolution UAS data in predicting poppy capsule volume and alkaloid yield in order to provide timely and reliable spatial information to the farmers and pharmaceutical industry for managing and monitoring crop growth and development prior to harvesting, ultimately improving yield potential.

The research presented in this thesis was conducted between 2014 and 2017. Studies in 2014 and 2015 were used to estimate the poppy capsule volume, while the 2016 and 2017 studies were used to predict the capsule volume prior to harvesting. In the capsule volume estimation study, UAS images acquired using a visible (RGB) camera were investigated to generate crop height estimates. This study provided a novel approach to estimate crop height based on a single UAS flight. UAS-derived plant height and field measured plant height were strongly correlated with R^2 values ranging from 0.93 to 0.97. The robustness of the proposed methodology was successfully tested on a second study site. Field-based experiments showed that plant height and poppy capsule volume were strongly related (R^2 0.74), with relative error of 19.62%. The plant height generated from UAS data was used to estimate capsule volume, and it was concluded that plant height can be reliably estimated for poppy crops based on a single UAS flight and can be used to predict opium capsule volume at capsule formation stage.

The second study aimed to determine whether the combination of structural and spectral derivatives of UAS data could provide improvement in capsule volume prediction results using a random forest (RF) machine learning approach. Investigation was undertaken using multiple

sensor dataset integration, field based spectroscopy data, UAS based multispectral data and crop height. Convolved field spectra were used to compute spectral vegetation indices (SVIs), and a combination of SVIs and plant height was used to train and test the random forest model. It was found that poppy capsule volume can be estimated using a combination of SVIs (NDVI, mSR, mTVI and RDVI) with RF regression and significantly higher prediction accuracy with an RMSE value of 15.60 cm^3 (10.27 %) based on training dataset and an RMSE value of 25.63 cm^3 (14.45 %) with validation dataset was observed. The proposed RF model provides improvement in capsule volume estimation as compared to that estimated using plant height only. The proposed RF model was successfully tested on UAS data acquired from two different experiment locations.

To predict the poppy capsule volume prior to harvesting, multi-temporal UAS data was collected using a 4-band Parrot Sequoia multispectral sensor. Data was collected from hook, flowering and capsule formation stages. This experiment investigated the potential to predict capsule volume of poppy crop based on multi-temporal SVIs and green vegetation fractional cover, using random forest regression and multi linear regression techniques. The combination of green vegetation fractional cover from flowering stage with spectral indices from hook stage (RDVI, SPVI and mTVI) provided optimal results with an R^2 of 0.88 and RMSE of 13.45 % using RF regression. Multi-temporal data of hook, flowering and capsule formation stage was also used to estimate the alkaloid yield in poppy capsule. It was found that the RF model with MSAVI, mSR, OSAVI, NDVI and EVI from capsule formation stage can provide optimal results to estimate thebaine with a relative error of 13.56 % to 22.36 % with training and validation dataset, respectively.

The findings in this thesis demonstrate that UAS based visible and multispectral imaging delivers valuable data for poppy crop yield estimation and prediction. The demonstrated results for plant height and yield open new possibilities in precision agriculture by capturing in-field variability and methods developed in this thesis provide tools to support operational decisions for site specific precision agriculture. The results achieved from methods developed in this thesis are robust and can be applied to other crops as well.

Acknowledgements

In the name of Allah ﷲ (God), the most Gracious, and the most Merciful, who aided me with eloquence and provided me with guidance to complete this research. Prophet Muhammad ﷺ (Peace Be Upon Him) and his contributing prayers and exemplary lifestyle cannot be forgotten, that has guided me throughout my life and particularly in my research journey.

After Allah SWT and his beloved prophet Muhammad ﷺ (Peace Be Upon Him) I would like to convey very special thanks to my parents. I will always be very grateful for all of the support and love they have given me. Thank you for giving me a positive upbringing, and pushing me for education. I could never have done this without them, so I would like to thank them from the bottom of my heart. May Allah give them the best of this world and hereafter Ameen.

Also, I would like to acknowledge University of Tasmania, Australia for providing me the scholarship to carry out this research work. I would like to acknowledge my diligent supervisors who helped and encouraged me to move forward leading me to this day of completing my research. I wholeheartedly express my gratitude to my inspiring supervisors Associate Professor Arko Lucieer, Dr Karen Barry and Dr Reuben Wells for their support and help throughout my research. I am grateful for the opportunity of being supervised by knowledgeable and passionate supervisors. I give my special thanks to my primary supervisor Associate Professor Arko Lucieer for accepting me as his PhD student and for offering his kind advice and guidance throughout my PhD. In addition to that, I would like to acknowledge Dr Darren Turner for organising and conducting the UAS field campaigns for Cambridge and Cressy. I thank Iain Clarke for his help in conducting the GPS survey and Dr Zbynek Malenovsk for his help during the UAS and spectral measurement campaign at Cambridge, Tasmania.

I would like to acknowledge Tasmanian Alkaloids Pty. Ltd. for their valuable support, especially for conducting alkaloid analysis and for providing access to the Sorell and Cressy site. I would like to acknowledge GlaxoSmithKline for providing access to the Cambridge site.

I don't think I can even begin to describe how much of this project is owed to my wife and my daughter. The amount of support and love they have given me over the last four years is something that I could never even begin to repay you. Finally yet importantly, I am grateful to my brothers and sisters especially my elder brother Furqan Iqbal who encouraged and supported me throughout my life. May Allah give them best of this world and hereafter Ameen.

Table of Contents

List of Figures

List of Tables

Chapter 1

1. Introduction

1.1. Background and context

1.1.1. Precision agriculture

Crop management is a critical part of agricultural productivity, and efficiently maximising crop yields to meet demand is a pressing global challenge. However, many current agricultural practices seek to meet this yield demand by applying an overabundance of inputs (e.g. agrochemicals), which is inefficient and leads to soil and ground water contamination (Nelson 1972, Novotny 1999, Doran 2002, Horrigan *et al.* 2002, Schloter *et al.* 2003, Tirado 2007, Roger-Estrade *et al.* 2010, Leh *et al.* 2013, Chartzoulakis and Bertaki 2015, Lu *et al.* 2015). To enhance crop yield while overcoming environmental challenges, the concept of precision agriculture (PA) was introduced. This relates to sustainable site-specific management by applying the right management practices at the right place and right time using variable rate technologies by taking into account the spatial variability of agronomic conditions of crops. The PA approach is in contrast to traditional farming, where farms under conventional management receive uniform application of agronomic inputs. Uniform crop management based on the field average would apply too much fertilizer on areas in a field where crop yield potential was low and would apply too little fertilizer where crop yield potential was high. In practice, farmers apply fertilizer at rates in excess of requirements for areas in the field with the highest yield potential. Today, precision agriculture embraces all agricultural inputs and management options based on site-specific information. With precision agriculture, fields can be divided into management zones that each receive customised management inputs based on varying soil properties, plant condition and management history. This concept deals with efficiently maximising crop yields without unnecessarily depriving resources or without degrading soil with intensive agricultural practices. Sustainable agriculture through precision farming has been recognised as a need of the day, effectively responding to the challenges in hand (Stafford 2000, Oudemans et al. 2002, Zhang et al. 2002, Iqbal 2010, Primicerio et al. 2012, Zhang and Kovacs 2012, Guo et al. 2018). Far and Rezaei-Moghaddam (2018) found that in Iran, PA technologies lead to a mean increase in crop productivity of around 4%; however most experts considered the increase to be up to 3-4 fold higher. Investigation of van Evert et al. (2017) reported an increase in profitability up to 21 % for potato crop.

1.1.2. Role of remote sensing in precision agriculture

Methods exist today in which farmers and field officers can estimate various crop parameters such as biomass, yield and nitrogen concentration (Ncube *et al.* 2018). However, the benefit of these methods is reduced by the fact that often a small sample size is used to infer the status of an entire field or farm. To more effectively maximise yield while minimising chemical applications, data can be collected using field-based instruments. Field based data can help micro-level management with the potential for optimising the return of each individual plant. What is truly desired then, is a capability to monitor the status of an entire crop, down to individual plants, and report the relevant information in near-real-time to enable farmers to make timely changes to management as needed. One way to efficiently schedule irrigation, fertiliser and pesticide applications, is to collect high spatial resolution data related to crop needs and application of agronomic inputs with spatial and temporal variation.

Achieving spatial-temporal information requires technological tools that can assist in crop monitoring. Such tools are offered by spatial sciences and remote sensing technologies that have an ability to provide valuable spatial-temporal information for PA. Remote sensing applications in agriculture are based on the interaction of electromagnetic radiation with soil and plant material (Brisco *et al.* 1998, Kempeneers *et al.* 2006). Remote sensing refers to non-contact measurements of spectral radiance reflected from agriculture fields. The radiant energy reflected from plants is related to radiance absorbed and radiance transmitted by plant pigments, and varies with the wavelength of incident radiation. Plant pigments such as chlorophyll absorb radiation strongly in the visible spectrum from 400 nm to 700 nm, particularly in blue and red region of visible spectrum. In contrast, plant reflectance is high in the near infrared region as a result of leaf density and canopy structure effects. This contrast in reflectance behaviours between red and NIR portions of the spectrum is used for the development of spectral vegetation indices that are based on ratios of reflectance values in these spectral regions. Spectral indices are often used to assess biophysical and biochemical variability of crops.

Common platforms used to collect remote sensing data are satellites and manned aircraft with the ability to acquire images covering large areas within a short time (Oudemans *et al.* 2002, Bastiaanssen and Ali 2003, Zhang and Kovacs 2012). Such images are used to monitor the crop growth, crop stress, and yield variability. For precision agriculture, site-specific information is required at specific times with higher spatial resolution within a cropping season. However, satellite remote sensing for real-time

crop management is typically limited to cloud free days. Only radar imagery is unaffected by cloud cover. Other challenges include lack of imagery with optimum spatial resolutions, and unfavourable revisit time (temporal resolution) for crop stress and disease detection applications (Han-Ya *et al*. 2010, Gevaert *et al*. 2015). Such limitations restrict the use of satellite based remote sensing for precision agriculture. Given these limitations, there has been significant interest in low-altitude and flexible UASs remote sensing as an affordable tool for precision agriculture (Berni, Zarco-Tejada, Suarez, *et al.* 2009, Zhang and Kovacs 2012, Gómez-Candón *et al.* 2014, Candiago *et al.* 2015, Yang *et al.* 2017, Salvatore *et al.* 2018). Moreover, comparative investigation of three remote sensing approaches including UAS, proximal sensing, and satellite-based imagery demonstrated that UAS-based remote sensing performed best for acquiring canopy temperature and NDVI (Tattaris *et al.* 2016). Therefore, UAS remote sensing is becoming an important tool for precision agriculture and near real-time crop monitoring.

1.1.3. UAS remote sensing – advantages and challenges

In the early 1980s, a number of research groups published their research on imagery acquired from UASs (Wester-Ebbinghaus 1980, Tomlins and Lee 1983). The limitations of satellite remote sensing had already been determined for crop management. To overcome these limitations, Jackson and Youngblood (1983) suggested establishing a UAS for precision agriculture. Herwitz *et al.* (2004) used UAS for agricultural surveillance two decades earlier. Other studies examined a wide variety of UASs: a fixed-wing aircraft was used for range and resource management (Quilter and Anderson 2000) and small radio-controlled helicopters was used for grass and forest monitoring (Hongoh *et al.* 2001).

During the last twenty years, UASs have shown a great potential as an imagery system platform that can be used for diverse problems including precision agriculture (Murray-Krezan *et al.* 2008). UAS imagery systems are considered a low-cost alternative for regular remote sensing systems for precision agriculture (Zhang and Kovacs 2012). The spatial resolution obtained from a UAS is much higher as compared to conventional remote sensing platforms, such as satellite. Typically, sub-metre spatial resolution is available from commercial satellite sensors and sub-centimetre (15 - 25 cm) spatial resolution is achieved from commercial aerial photography platforms. UASs provide ultrahigh spatial resolution as they fly at lower altitudes, where it is capable of providing sub-decimetre spatial resolution even as detailed as 1 cm / pixel. This enables UAS with the acquisition of spectral information with similar detail to ground based

measurements but with higher spatial coverage. UAS imagery minimises the problem of mixed pixels and allows differentiating the spectral information of soil from vegetation pixels, and thus has the potential to provide better accuracy. Moreover, UASs have the ability to fly at different altitude to obtain dataset at various spatial resolutions. Also, UASs can provide high temporal resolution imaging that are capable of real-time/flexible image acquisition (Saari *et al.* 2009, Zhang and Kovacs 2012, Dandois and Ellis 2013, Grenzdorffer 2014). In addition, technological advancement in the field of UAS-based remote sensing provides customised sensors that are available for precision agricultural applications (Zhang and Kovacs 2012). Continuous development in the field of electronics has allowed the production of lightweight navigation systems and controllers making UASs more cost-effective (Joseph *et al.* 2016). On the other hand, the latest developments in plastic technology in replacing metal components (Zhu *et al.* 2004, Ajayan and Tour 2007) and production of high performance polymer materials, providing the same mechanical strength with dramatic reduction in weight, has allowed carrying of heavier and larger payloads and has resulted in increased flight time.

In addition, there are numerous types of sensors that can be used for data collection. Sensors for image capture include digital cameras (Saari *et al.* 2011) and even modified digital cameras with a near infrared band (Stagakis, Gonzalez-Dugo, *et al.* 2012, Wang and Myint 2015). Specific UAS cameras have also been used for precision agriculture, including the ADC multispectral camera (Swain *et al.* 2010, Primicerio *et al.* 2012) and the MCA mapping camera (Berni, Zarco-Tejada, Suarez, *et al.* 2009). Spectral vegetation indices used for satellite remote sensing (Tucker *et al.* 1980) have been among the top indices used for agriculture using UAS based multispectral imagery. Instead of relying on broad-band vegetation indices, hyperspectral sensors are used more frequently to measure physiological processes such as photosynthesis with their ability to measure narrow-band spectral features. The photochemical reflectance index (PRI), for example, uses narrow spectral bands at two green wavelengths (531 and 570 nm) to track changes in leaf xanthophyll pigments in direct response to changes in photosynthetic rate (Hernández-Clemente *et al.* 2012, Zarco-Tejada, Guillen-Climent, *et al.* 2013). Other leaf parameters may be retrieved by inverting the PROSAIL model, which estimates unknown model inputs from measured model outputs (Zarco-Tejada, Morales, *et al.* 2013). In addition, lightweight thermal sensors are also available to map the spatial variability of temperature used it to determining the amount of water stress (Rud *et al.* 2014). Other studies examined a wide variety of UAS mounted thermal sensors for water stress, combining canopy temperature, fluorescence, and PRI (Primicerio *et al.* 2012, Stagakis, Gonzalez-Dugo, *et al.* 2012).

Apart from apparent advantages of UAS remote sensing, there are many challenges associated with routine operations, such as restricted spatial coverage, small payload capacity, poor geometric and radiometric performance, low software automation, sensitivity to atmospheric conditions, short flight endurance, and possibility of equipment damage. Moreover, UAS users need to consider the cost and expertise involved in repairs and maintenance, transportation, weather conditions and regulations for flying small UAS.

1.1.4. Examples of UAS in precision agriculture

UAS-based remote sensing technology has demonstrated the potential for precision agriculture by providing data at high temporal and spatial resolution (Zhang and Kovacs 2012). Some applications of UAS remote sensing are listed in table 1.1. UAS remote sensing has been used to monitor crop growth and health by computing a range of spectral vegetation indices (Rufino and Moccia 2005, Jaakkola *et al.* 2010, Mäkynen *et al.* 2011, 2012, Rasmussen *et al.* 2016). Calderón *et al*. (2014) identified downy mildew of opium poppy using high-resolution multispectral and thermal imagery acquired with an unmanned aerial vehicle. Thermal and multispectral images acquired using UAS can also be used to estimate water status variability in vineyards (Berni, Zarco-Tejada, Suarez, *et al.* 2009, Baluja *et al.* 2012, Stagakis, González-Dugo, *et al.* 2012, Zarco-Tejada, González-Dugo, *et al.* 2012). Multiple studies have shown the potential of early weeds detection using UAS acquired images, when the small plants of crop and weeds have high spectral similarity (Lopez-Granados 2011, Pérez-Ortiz *et al.* 2015). Bah *et al.* (2018) and De Castro *et al.* (2018) applied object-based classification and deep learning techniques on UAS acquired images to automate the weed detection process. Several studies have shown an estimation of biophysical characteristics, such as plant and tree height and biomass (Ehlert *et al.* 2008, Bendig *et al.* 2014, Tilly *et al.* 2014, Zarco-Tejada *et al.* 2014, Li *et al.* 2016). In this context, several studies have shown crop productivity estimation in certain crop types e.g. maize, barley, wheat, corn, rice and sunflower. Moreover, RGB, multispectral and hyperspectral cameras have been used to estimate crop yield (Zhu *et al.* 2010, Yin *et al.* 2011, Geipel *et al.* 2014, Vega *et al.* 2015, Du and Noguchi 2017, Zhou *et al.* 2017). Zhu *et al.* (2010) and Hernández-Clemente *et al.* (2012) estimated the bio-chemical properties of crop leaf using UAS remote sensing. Leaf area and flower fraction are also assed using UAS remote sensing (Córcoles *et al.* 2013, Fang *et al.* 2016). Crop height is an important factor for poppy yield estimation and crop management (Bernath 1986, Mahdavi-Damghani *et al.* 2010, Jia *et al.* 2011).

Table 1.1. Some UAS application in agriculture

Application	Reference
Vegetation monitoring and UAS system development	
Forest and agriculture monitoring	(Makynen *et al.* 2012)
Natural disaster monitoring	(Rufino and Moccia 2005)
Low coast mapping	(Jaakkola *et al.* 2010)
Light weight system development	(Makynen *et al.* 2011)
SVIs estimation using consumer grade camera	(Rasmussen *et al.* 2016)
Water stress and fruit quality monitoring	
Thermal remote sensing for vegetation monitoring	(Berni, Zarco-Tejada, Suarez, *et al.* 2009)
Thermal remote sensing of vineyard	(Baluja *et al.* 2012)
Orange water street and fruit quality monitoring	(Stagakis, González-Dugo, *et al.* 2012)
Water stress estimation	(Zarco-Tejada, Gonzalez-Dugo, *et al.* 2012)
Biomass, crop and tree height estimation	
Canopy height and biomass of maize	(Li *et al.* 2016)
Biomass estimation of barley	(Bendig *et al.* 2014)
Crop biomass	(Ehlert *et al.* 2008)
Biomass estimation of rice crop	(Tilly *et al.* 2014)
Tree height estimation	(Zarco-Tejada *et al.* 2014)
Crop yield estimation	
Rice nitrogen status and yield estimation	(Zhu *et al.* 2010)
Rice yield estimation	(Zhou *et al.* 2017)
Sunflower yield estimation	(Vega *et al.* 2015)
Corn yield and plant height estimation	(Yin *et al.* 2011)
Corn yield estimation	(Geipel *et al.* 2014)
Wheat yield estimation	(Du and Noguchi 2017)
Disease estimation	
Detection of *Downy Mildew* of poppy opium	(Calderón *et al.* 2014)
Weed detection	
Early weed detection	(Lopez-Granados 2011, Pérez-Ortiz *et al.* 2015)
Automated weed detection	(Bah *et al.* 2018, De Castro *et al.* 2018)
Bio-Chemical estimation	
Leaf carotenoid content estimation	(Zarco-Tejada, Guillen-Climent, *et al.* 2013)
Rice nitrogen status and yield estimation	(Zhu *et al.* 2010)
Leaf Area and fractional cover estimation	
Flower and vegetation fraction estimation of sunflower	(Fang *et al.* 2016)
Leaf Area Index estimation in onion crop	(Corcoles *et al.* 2013)

1.1.5. Introduction to alkaloid poppy

Poppy (*Papaver Somniferum L*) is one of the few medicinal plants that has been cultivated and used in prehistoric times (Schiff 2002, Shukla *et al.* 2006). Poppy is a dicotyledonous

annual herb belonging to the family *Papaveraceae* and generally grow to a height of 1.4 m. Poppies have four petals (typically pale pink) with a dark basal blotch. The capsules are spherical with a flat cap, 20-40 mm in diameter and contain a large number of very small seeds (Mahdavi-Damghani *et al.* 2010). Poppies differ from most crops as the capsule, being the major site of alkaloid deposition, is the most economically important component of the plant at maturity (Chung 1987). The importance of poppy opium is its alkaloid concentration which is found in all parts of the plant except the seed (Yadav *et al.* 2006). Poppy opium is grown in several parts of the world (Turkey, India, France, Spain, Hungary, Czech Republic and China). The state of Tasmania in Australia is the largest licit producer of poppy opium, supplying up to 40% of the world's opiates used for medicines with morphine and thebaine as the main alkaloid product. Tasmania is a major producer of thebaine and fulfils 90% of the demand of world's pharmaceutical industry (Lisson 2007). The island state also accounts for a quarter of the world's morphine and codeine, two older painkillers (Harvest *et al.* 2009). Tasmania produces $60 to $80 million of product a year for opiate painkillers (Frappell 2010). In Tasmania, poppy farmers focus not only on the capsule yield but also on alkaloid concentration, as processors determine the price based on the poppy alkaloid concentration of the crop. Therefore, accurate yield estimation prior to harvesting in high value alkaloid poppy crop can offer improved decision making for farmers, managers and the pharmaceutical industry.

The amount of alkaloid concentration varies from plant to plant within a field and is influenced by a number of physical, biological, environmental factors, and incidence of pests and diseases. Many studies have highlighted the effect of irrigation, temperature, light and nutrients on alkaloid yield (Harrison and Schmitt 1972, Yadav *et al.* 1984, Bernath 1986, 1988, Bernath and Tetrnyi 1986, Chung 1987, Dieu and Dunwell 1988, Jain 1990a, Acock and Pausch 1997, Solanki *et al.* 1999, Ey *et al.* 1999, Shukla *et al.* 2006, Landa *et al.* 2007, Harvest *et al.* 2009, Mahdavi-Damghani *et al.* 2010, Jia *et al.* 2011, Lecina *et al.* 2011, Singh *et al.* 2011, Waine *et al.* 2014, Calderón *et al.* 2014). Each factor has complex influences in relation to other factors at each developmental phase within the same field.

In earlier studies, different physiological indicators have been assessed to predict opium capsule volume and alkaloid yield (Harold *et al.* 1920, Laughlin and Chung 1990, Acock, Wang, Acock, *et al.* 1996, Yadav *et al.* 2007, Mahdavi-Damghani *et al.* 2010, Jia *et al.* 2011, Waine *et al.* 2014). Such studies found a positive correlation of various physiological indicators with poppy gum extracted from poppy capsules. The gum extracted is further processed to obtain opium alkaloid and thus, we can assume that it would also

result in positive correlation with opium alkaloid yields. The physiological indicators used were Leaf Area Index (LAI), plant height, number of capsule per plant, weight of volume of capsules and dry mass of crop (Chung 1987, Laughlin and Chung 1990, Laughlin *et al.* 1998, Scott *et al.* 2004, Cheng *et al.* 2006, Mahdavi-Damghani *et al.* 2010, Jia *et al.* 2011, Calderón *et al.* 2014, Morel *et al.* 2014, Waine *et al.* 2014).

The question is how poppy farmers can use this literature to enhance the yield potential using optimal management. Therefore, there is a need for the investigation of methods to estimate the potential of poppy capsule yield at field scale to manage the crop effectively.

1.2. Problem statement

Understanding the influence of each factor (temperature, light, irrigation and nutrients) on crop physiology particularly on capsule volume and alkaloid yield can assist in proactive crop management, which can enhance the value of the crop. It is thus critical that growers know the importance of these factors at each developmental phase along with the condition of their farms so that they can analyse and control the controllable factors in a timely fashion to produce a high-quality crop with optimal alkaloid content. The controllable factors are the application of irrigation and nutrients, whereas, temperature and light cannot be practically controlled at a commercial field level. However, these decisions should ideally be based on accurate and timely spatial information of integrated physio-ecological factors at the appropriate spatial scale. Therefore, to optimise yield and minimise inputs, this dissertation explores the use of UAS-based visible and multispectral sensors for Tasmanian poppy crop yield estimation and prediction.

Spectral indices have been reported to estimate capsule volume and showed a significant correlation between NDVI and capsule volume from flowering till harvesting stage (Waine *et al.* 2014). Crop height was reported as a significant indicator of yield estimation in maize (Yin *et al.* 2011), whereas, in barley, UAS driven crop height has been utilised to estimate biomass (Bendig *et al.* 2014). In the case of poppy crops, only one study has looked at the use of remote sensing methods, in which crop height and Leaf Area Index (LAI) were found to be two suitable indicators for estimating opium yield (Jia *et al.* 2011). Several studies show that the growth and development of poppy are influenced by agronomic and environmental factors along crop development (Mika 1955, Acock, Wang, and Acock 1996, Acock and Pausch 1997, Lisson 2007, Jackson 2009, Dean 2011). Poppy crop growth is spatially highly heterogeneous and requires a substantial amount of data collection to develop models for yield estimation

(Kang and Primack 1991). Thus, monitoring within farm spatial variability of crop condition during multiple phases needs to be investigated to understand the spatiotemporal growth variation within farm. Vega *et al.* (2015) and Zhou *et al.* (2017) investigated multiple-temporal SVIs using simple linear or multiple linear regression models to predict sunflower and rice yield. Selected studies have used a combination of remote sensing and random forest regression techniques to estimate yield (Abdel-Rahman *et al.* 2013, Jeong *et al.* 2016, Wang *et al.* 2016, Saeed *et al.* 2017), although, none of them have been focused on poppy crops.

UAS remote sensing techniques can help to capture detailed information about crop height and spectral variation. Modern machine learning techniques can help to identify the most important variables (height, SVIs) to estimate and predict capsule volume and help decision-making for precision agriculture. Thus, there is a need to investigate the spectral and structural variables derived from UAS acquired imagery to estimate poppy capsule yield.

1.3. Research aims and objectives

The aim of this dissertation is to estimate and predict poppy crop capsule yield from ultrahigh-resolution UAS imagery acquired at critical stages of the crop growth cycle.

In order to address the aim and answer the research question several objectives have been defined:

Objective 1: To investigate the use of visible (RGB) imagery acquired using a single UAS flight for estimation of poppy crop height and capsule volume.

Objective 2: To develop a machine learning workflow for estimating poppy capsule volume from UAS-based multispectral remote sensing data.

Objective 3: To assess the potential of multi-temporal UAS remote sensing with machine learning and linear regression techniques to predict poppy capsule volume.

Objective 4: To develop a methodology for poppy opium alkaloid estimation before harvesting using multispectral imagery acquired from a UAS.

1.4. Thesis structure

The structure of this thesis is by publication, and therefore, Chapters 3-7 comprise material that has been published in peer-refereed journals (Chapter 3, 4, 5) or submitted

to scientific journals for publication (Chapter 6 and 7). The thesis structure diagram (Figure 1.1) is divided into three major portions; Introduction, Biophysical estimation and Biochemical estimation. The research objectives are addressed by each of the publications as illustrated in Figure 1.1. Each chapter separately addresses the relevant literature and includes detailed methods, results, discussions, and conclusions. A conclusion chapter (chapter 8) summarises the overall outcomes and contributions of the thesis in the context of the objectives and provides an overview of limitations and discusses future work.

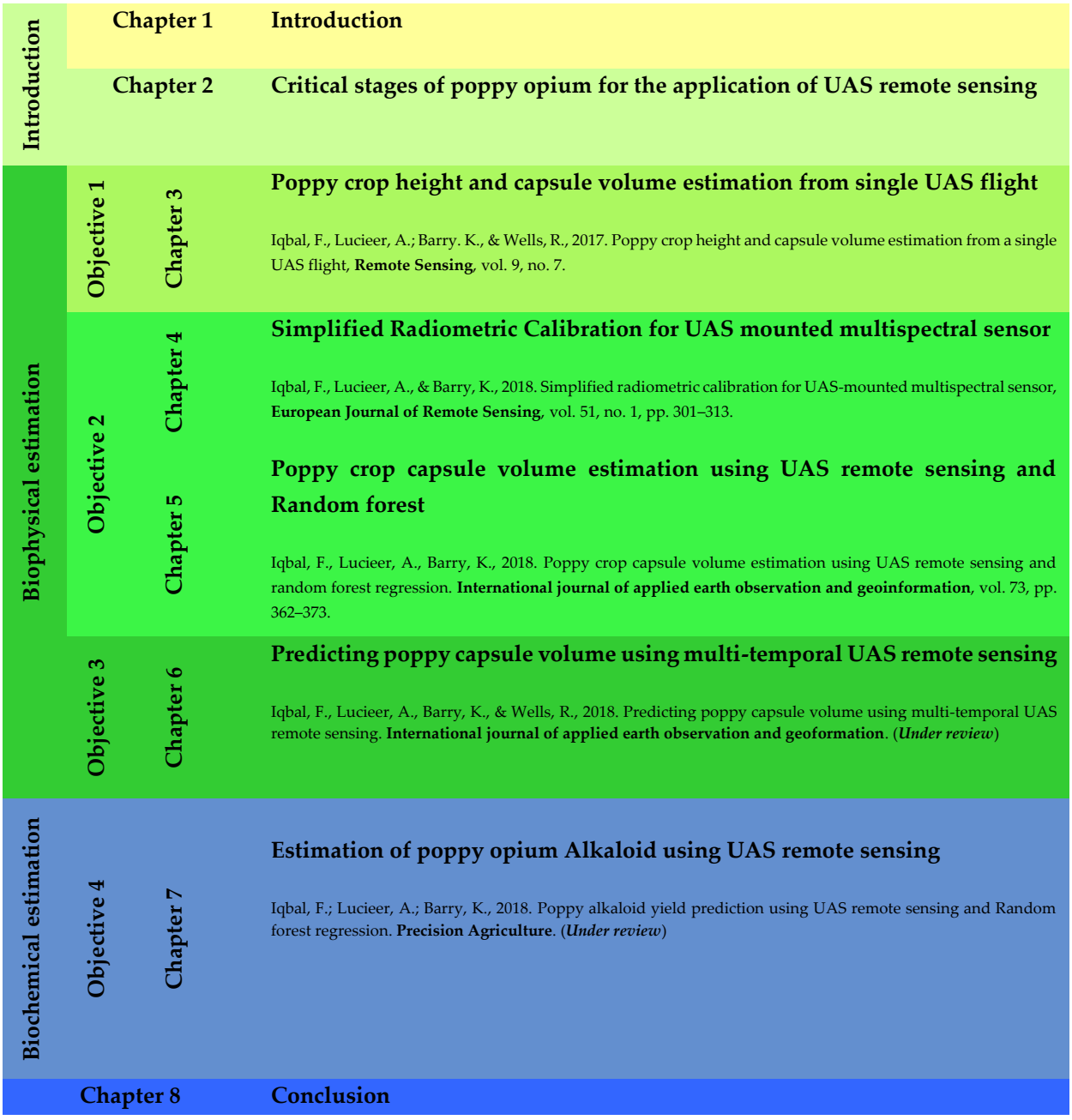

Figure 1.1. Structure of thesis and achievement of objectives

Chapter 2

2. Critical stages of poppy opium for the application of UAS remote sensing

Abstract

Opium poppy (*Papaver Somniferum L*) is one of the highest value annual broad acre crops. Precision crop management is a worthy investment. Precision farming strategies promote variable agricultural management practices according to site-specific conditions, which enable efficient resource use. However, site-specific crop management requires a clear understanding of optimal plant growth requirements and real-time assessment of limiting conditions (e.g. water, nutrients, light). These requirements also vary with the developmental phases of the crop. The increase or decrease of these limiting factors at certain developmental stages may result in high differences in yield. Thus, the information on crop growth stages needs to be transformed into tangible information that can be utilised for sustainable precision agriculture. In addition, monitoring plant health and detecting plant stress at critical growth stages is central to precision management. This review focuses on key aspects of poppy crop management, and outlines the use of high-resolution spatio-temporal remote sensing imagery to support decision making for precise and timely management. This review highlights the significant environmental factors needed at critical growth stages that would facilitate advancement in poppy crop management. It describes the factors affecting alkaloid yield in the poppy opium capsule and delineates critical growth stages of the poppy crop that determine optimum yield. It has also been proposed that UAS based imagery at critical stages can inform management decisions and increase the efficiency of alkaloid production. Therefore, developing systems and methodologies to easily retrieve crop information from UAS should be a priority for the near future.

2.1. Introduction

Poppy (*Papaver Somniferum L*) is one of the few medicinal plants that has been cultivated and used since prehistoric times (Schiff 2002, Shukla *et al.* 2006). It is a plant of the dicot family *Papveraceae*, cultivated for seed, oil and opium. Poppy is a herbaceous plant with an erect stem, having an attractive flower varying in colour according to varieties. The end product of poppy crop is the capsule that contains latex and seeds (Mahdavi-Damghani *et al.* 2010). Latex is a rich source of around twenty different pharmaceutical

alkaloids including morphine, codeine, thebaine, narcotine, papaverine, although, its analgesic activities are attributed to morphine, the primary alkaloid (Apuya *et al.* 2008). Alkaloids are found in all parts of the plant except the seed (Yadav *et al.* 2006). However, the amount of alkaloid varies from plant to plant and within fields and is influenced by a number of physical, biological (e.g. pests and diseases) and environmental factors (Wang *et al.* 1997, Lisson 2007). Extensive investigations have been done to develop growth models to determine the influence of factors affecting yield; the key environmental factors affecting yield are light, temperature, nutrients and irrigation application (Harold *et al.* 1920, Mika 1955, Bernath 1986, Shukla *et al.* 2006, Harvest *et al.* 2009, Dean 2011). Each factor has complex interactions with other factors at each developmental phase. In earlier studies, different physiological indicators have been assessed to predict final opium alkaloid yield. Such studies have found a positive correlation between various physiological indicators with poppy gum extracted from poppy capsules (Harold *et al.* 1920, Bernath and Tetrnyi 1981, Acock, Wang, Acock, *et al.* 1996, Wang *et al.* 1999, Jia *et al.* 2011). The gum extracted is further processed to obtain opium alkaloid and thus, we can assume that it would also result in positive correlation with opium alkaloid yields (Acock, Wang, Acock, *et al.* 1996). The physiological indicators used were Leaf Area Index (LAI), plant height, number of capsules per plant, capsule weight and crop dry mass (Laughlin *et al.* 1998, Scott *et al.* 2003, Haboudane *et al.* 2004, Jia *et al.* 2011, Waine *et al.* 2014). Understanding the influence of each environmental factor on crop physiology, particularly on alkaloid yield, can assist in strategic and proactive crop management. It is thus critical that growers know the optimal status of these environmental factors at each developmental phase so that they can develop and implement timely remedial practices if conditions become sub-optimal. Key factors that can be controlled include the application and timing of irrigation and nutrients along with pest and disease management. Decision-making for remedial actions can be supported by accurate and timely spatial information. Therefore, to optimise yield and minimise inputs, this review proposes the use of spatially explicit information on crop physiology and site-specific environmental factors.

Integration of spatial and temporal crop measurements with associated physiological measures (i.e. LAI, plant height, crop density etc.) can provide better understanding of within-crop variability and therefore can be used for precise management. The concept of adjusting agronomic practices based on spatial and temporal variation in agricultural fields is known as Sustainable Precision Agriculture (SPA) (Bakhsh and Kanwar 2006, Abdullah *et al.* 2011, Primicerio *et al.* 2012, Bellvert *et al.* 2013). SPA involves applying agricultural inputs precisely according to the needs of the soil and crop to improve the

crop yield and environmental quality. Spatial technologies offer a variety of tools and techniques that can be utilised to maximise the crop production (Iqbal 2010, Awan, Tischbein, *et al.* 2011, Bellvert *et al.* 2013). Among spatial technologies, remote sensing is a key component of SPA that provides a synoptic view of the earth and facilitates to collect data of crop for better agricultural management.

Spectral remote sensing for precision agriculture relies on the fact that every part of the crop (leaf, head, stem and flower) has a unique spectral signature and can therefore be differentiated from each other. Similarly, any changes in the normal spectral signatures of these parts would indicate that the crop may be subject to a biotic (i.e. pathogen) or abiotic (e.g. water deficiency) stressor, which has impacted plant health or development. Thus, in this way, stressed crops can be detected through spectral signatures (Chuinsiri *et al.* 2010, Wang 2013, Calderón *et al.* 2014) and the variability of stress in crops within a field can also be mapped using remote sensing. Satellite remote sensing has been widely used as a tool in spatial sciences. Using satellite remote sensing for real-time crop management is limited by two critical factors; 1) lack of imagery with optimal spatial and spectral resolution; 2) an unfavourable revisit time (temporal resolution) for rapid crop stress detection. There are alternatives such as piloted airborne sensor platforms that are difficult to use operationally due to their high cost. Due to this reason, the use of the UAS for capturing ultra-high resolution imagery has become increasingly important in remote sensing applications including crop management (Bos *et al.* 1994, Kempeneers *et al.* 2008, Zhu *et al.* 2010, Mäkynen *et al.* 2011, 2012, Uto *et al.* 2013, Bendig *et al.* 2014). Location-based agriculture requires crop information at specific times and locations for accurate management. UAS meets these needs as a remote sensing platform for SPA and provide significant advantages over space-borne remote sensing.

UAS represent a low-cost platform with flexible temporal resolution. Moreover, high-quality hyperspectral and multispectral sensors mounted on UAS can capture data having higher spatial, spectral and temporal resolution. The use of UAS-based sensing ensures availability of data when it is required (i.e. at critical growth stages) and could rapidly inform precise and site-specific proactive management decisions. Therefore, the main objective of this review is to investigate the fundamental concepts of poppy opium physiology along its development stages and to delineate the critical growth stages, while also highlighting the environmental factors affecting these stages. The rationale of this study is that each environmental factor plays a significant role in the development of the crop, and altering any of these factors at critical stages may influence poppy opium yields. Thus, monitoring crop variability to investigate the influence of

environmental factors at critical stages is imperative and UAS acquired imagery can be a helpful tool for poppy crop precision management.

2.1.2. Poppy opium and its characteristics

Total yield potential of a crop is a theoretical estimation of yield under optimum environmental conditions. Yield can be classified as biological yield (i.e. total growth of plant containing stem, leaves, and capsule) or economic yield (the plant material that generates revenue, such as seed and opium). This review considers poppy opium capsule gum and alkaloid concentration in opium as economic yield. Alkaloids are secondary plant metabolites that evolve as protection against predation by insects and pathogens (Zenk and Juenger 2007). Alkaloids contains a nitrogenous base and are often categorised on their amino acid predecessor (Dewick 2002). Tyrosine is the base of a morphine and codeine formed in poppies (Hagel *et al.* 2007). Alkaloid concentrations are affected directly or indirectly by environmental factors. Alkaloids are the main pharmaceutical content of poppy opium and Tasmanian alkaloid products are mainly used as anaesthetics. The economic yield of the poppy crop is determined by the quantity and type of alkaloid that is found in all parts of the plant, except the seeds (Harvest *et al.* 2009, Lisson and Cotching 2011).

2.1.3. Development stages of poppy

The growth and development life cycle of poppy is divided into the following stages: growth of seedlings, the formation of rosette-type leaves, budding, flowering, capsule formation and maturity (Shuljgin 1969, Bernath 1986, Wang *et al.* 1999, Miura and Huete 2009, Mahdavi-Damghani *et al.* 2010). In Tasmania, poppy is mainly sown in spring and on average, the vegetation growth period of spring sown poppy varies between 120-160 days (Bernath 1988). The average duration of each phase in optimum conditions is shown in Figure 2.1, which illustrate that rosette stage is the longest stage in the poppy life cycle. In this figure, the duration of vegetation period has been divided into various growth stages (Shuljgin 1969, Mahdavi-Damghani *et al.* 2010) and each growth stage has a different duration which varies with changes in conditions of light and temperature (Bernath and Tetrnyi 1981, 1986, Kamkar *et al.* 2012, Baser and Arslan 2014). Each phase of poppy development requires different optimal temperature conditions, with a progressive rise in temperature required towards maturity, as shown in Figure 2.2. The duration of a winter sown poppy crop is more prolonged than spring sown crop. Opium poppy in Tasmania is grown beyond the green capsule stage and harvested when the capsules are dry (Chung 1987, Laughlin and Chung 1990), while in most of

parts of the world it is harvested green. Figure 2.3 illustrate the typical timing of growth stages of poppy in Tasmania conditions.

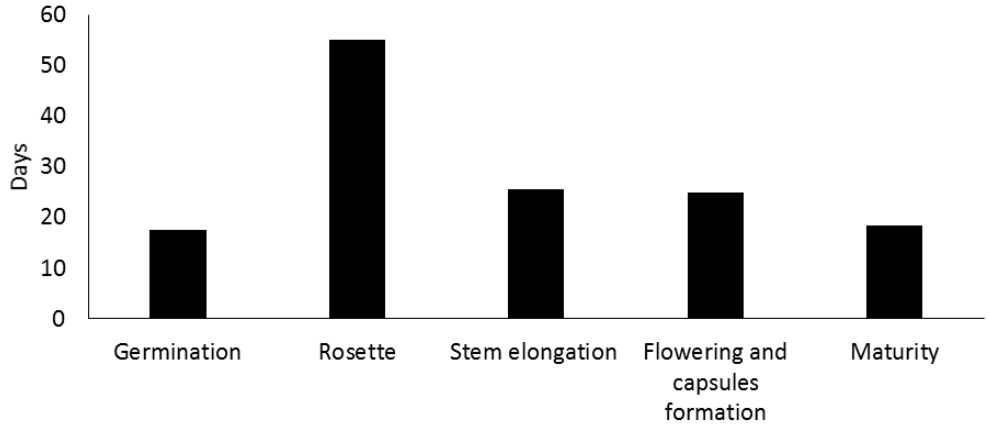

Figure 2.1. Duration of each development phase (Bernath 1988, Kamkar *et al.* 2012, Baser and Arslan 2014)

The first stage is categorised by germination of the seed, which starts from the separation of the tesla until the appearance of the first leaf (Mika 1955, Bernath and Tetrnyi 1986, Mahdavi-Damghani *et al.* 2010, Baser and Arslan 2014). Poppy is moderately tolerant to cold temperature during initial stages of plant development. The average temperature required at the germination phase is 4.5°C (Kamkar *et al.* 2012, Baser and Arslan 2014). Under optimum circumstances, the average duration of this stage is around 17 days (Shuljgin 1969, Bernath and Tetrnyi 1981, 1986, Acock, Wang, and Acock 1996, Wang, Zhongchun and Acock, Mary C and Acock 1997, Lisson 2007) (Figure 2.1). Leaf rosette is known as the next stage after germination. This stage advances from the appearance of the first leaves until the start of flower shoot formation (Mahdavi-Damghani *et al.* 2010). This is the longest stage in the growth cycle and is significantly influenced by climatic conditions and management practices. The average duration of this stage is around 55 days and optimum average temperature for this stage is around 13 °C (Bernath 1988). In hot and dry weather conditions, the duration of this stage becomes short and adversely affects the flower and capsule formation, thus, resulting in yield reduction (Bernath and Tetrnyi 1981). A plant with a healthy root system and development of six to eight rosette leaves is required for the development of a good stem that leads to better capsule development. Investigations by Baser & Arslan (2014) and Mahdavi-Damghani *et al.* (2010) show that the rosette stage is critical in terms of plant health and end yield.

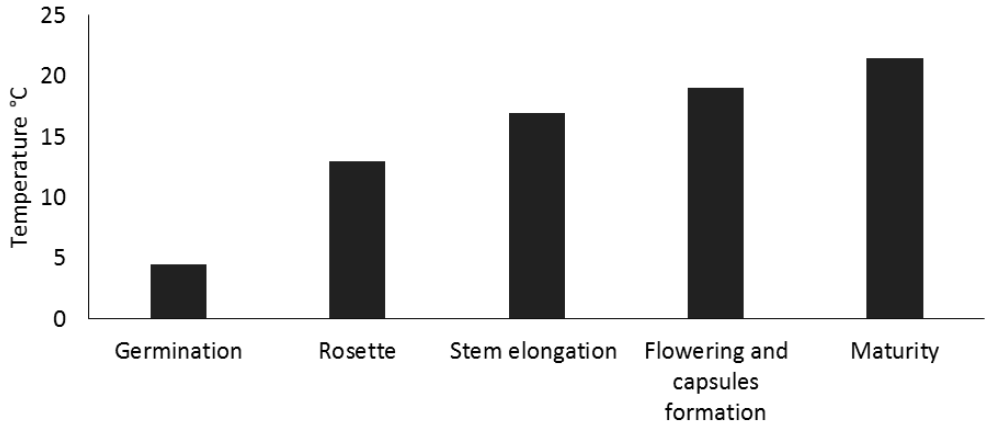

Figure 2.2. Optimum average temperature at each development phase (Bernath 1988, Shibata *et al.* 1991, Kamkar *et al.* 2012, Baser and Arslan 2014)

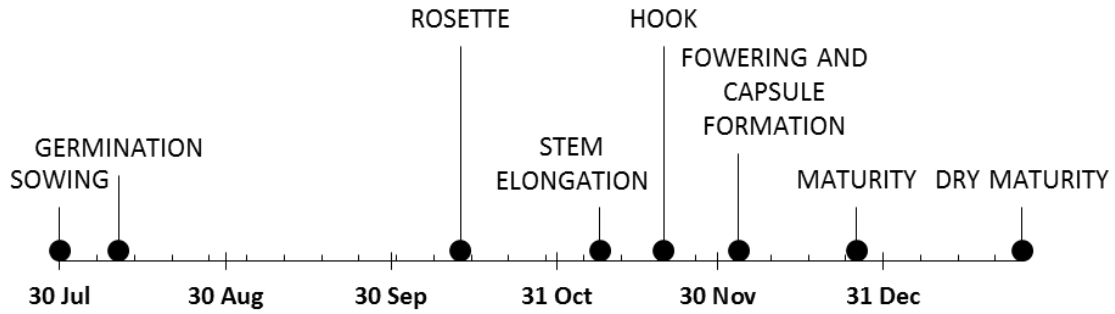

Figure 2.3. Poppy opium growth time frame for Tasmania

After leaf development, the poppy plant stem starts to elongate and branches are initiated, which is considered as the third phase in the poppy life cycle starting from the beginning of shooting until blossoming of the main axis. The optimum temperature for stem elongation stage has been reported as 17 °C and the average duration of this phase is around 25 days (Bernath and Tetrnyi 1986, Bernath 1988, Acock and Pausch 1997, Lisson 2007). After stem elongation phase a transition phase incites know as hook stage. Hook stage very quickly converts to flowering starts over two to five days. Poppy flourishes in the sun and hot weather, especially during the flowering stage the optimal temperature is around 19°C (Bernath and Tetrnyi 1981, Bernath 1988, Shibata *et al.* 1991). Insect pollination is required to initiate capsule formation and therefore flower health is a major predictor of final yield (Shibata *et al.* 1991). Extremely hot weather with lower humidity during the flowering phase hinders pollination and affects the end yield. On the other hand, rain during the flowering stage also reduces pollination (Baser and Arslan 2014). Furthermore, higher moisture at this stage can cause fungal infections as well (Laughlin and Munro 1982, Landa *et al.* 2007, Calderón *et al.* 2014). The

time span between flowering and capsule formation is around 25 days (Bernath and Tetrnyi 1981, Bernath 1988). The temperature during capsule development is critical for yield and the average optimal temperature is around 21.5 °C. At the end of this stage, water requirement increases dramatically as the capsule starts to accumulate opium gum, and the optimum temperature requirement relatively increases (Mahdavi-Damghani *et al*. 2010). The last and final stage is the dry maturity of the capsule, which takes 20 to 25 days and temperatures above 20 °C are required for this stage.

2.1.4. Physiological indicators predicting yield

Physiological characteristics of plants play a vital role in the development of capsule and alkaloids. Positive correlations have been found between the yield of morphine and the total volume of capsules per plant (Harold *et al.* 1920, Mika 1955, Acock, Wang, and Acock 1996, Cotching *et al.* 2004, Chuinsiri *et al.* 2010, Jia *et al.* 2011, Wang 2013). There have also been extensive investigations into the relationships between alkaloid yield and morphine percentage (Shukla *et al.* 2006, Yadav *et al*. 2006, Waine *et al.* 2014). Poppy crop development and yield found to be heterogeneous nature, and studies indicate significant relationships of yield with various physiological characteristics of a plant e.g. plant height, the number of capsule per plant, and size of each capsule (Annett 1920). In earlier studies, different physiological characteristics, serving as indicators of yield have been assessed to predict final opium alkaloid yield. Such studies found a positive correlation between various physiological indicators with poppy gum extracted from poppy capsules. The gum extracted is further processed to obtain opium alkaloid, thus it can be assumed that the gum would also result in positive correlation with opium alkaloid yields. The physiological indicators used to investigate the association with yield were Leaf Area Index (LAI), plant height, number of capsules per plant, weight of capsules, volume of capsules and dry mass of the crop (Chung 1987, Laughlin *et al.* 1998, Zarco-Tejada *et al.* 2003, Cheng *et al.* 2006, Kempeneers *et al.* 2008, Zheng and Moskal 2009, Mahdavi-Damghani *et al.* 2010, Jia *et al.* 2011, Morel *et al.* 2014, Pradhan *et al.* 2014, Waine *et al.* 2014). One of the major indicators dominantly influencing alkaloid production is the quantity of crop dry matter (Bernath and Tetrnyi 1986). Parameters of plant height, stem volume, as well as number of leaves and seeds contribute to the quantity of crop dry matter (Bendig *et al.* 2014, Geipel *et al.* 2014). With the above-cited literature, it can be assumed that the parameters contributing to crop dry matter will also be of high significance to alkaloid production (Chung 1987, Acock, Wang, Acock, *et al.* 1996, Acock and Pausch 1997, Wang *et al.* 1997, 1999).

Chapter 2

2.2. Environmental factors affecting poppy opium yield

2.2.1. Environmental factors

It is evident from the previous studies (Bernath and Tetrnyi 1981, 1986, Acock, Wang, and Acock 1996, Acock and Pausch 1997, Wang *et al.* 1997, Wang, Zhongchun and Acock, Mary C and Acock 1997, Lisson 2007, Jackson 2009, Mahdavi-Damghani *et al.* 2010) that the main environmental factors affecting yield are light, temperature, nutrients and irrigation application. These factors determine 80% of dry mass production and similarly have a greater impact on alkaloid quantity (Bernath and Tetrnyi 1981, 1986, Bernath 1986, Fist 2000, Schiff 2002, Veres 2011). Whereas, the remaining 20% depend upon biotic stressors (e.g. pathogens, insect damage, herbivores, weeds etc). These environmental factors (light, temperature, nutrients and irrigation) determine photosynthetic potential, which enables the plant to develop and produce dry matter. Overall, optimal water availability is the largest factor, which contributes to the production of dry matter as shown in Table 2.1. In the absence of biotic constraints such as pest and disease damage, these four factors drive net primary productivity. Based on the above literature, a diagram (Figure 2.4) has been developed, which also highlights plant genotype as an additional key factor in determining alkaloid production, as specific genotypes have variable alkaloid production (Yadav *et al.* 2006, Mishra *et al.* 2010, 2013, Kumar *et al.* 2011, Verma *et al.* 2011).

However, each genotype or variety generates an optimum yield in certain specific environmental conditions. Thus, the interaction of plants with their environment (irrigation, nutrients, temperature, and light) plays an important role in potential yield production. There is substantial interaction between these factors, for example water availability in the presence of optimal temperature with extended light conditions enhances the nutrients uptake of plant and is essential for stem development (Bernath and Tetrnyi 1981, 1986, Bernath 1986, Laughlin and Chung 1990, Mahdavi-Damghani *et al.* 2010). All of these factors also interact with biotic stress, including pests, weeds and diseases, the latter of which is of particular importance to Tasmanian poppy management and will be expanded upon in a later section. Furthermore, healthy stem development is a function of increase in leaf area in the presence of water and nutrients under appropriate climatic conditions. Stronger stem and greater plant height has been reported to determine healthier capsule formation (Apuya *et al.* 2008, Harvest *et al.* 2009, Mishra *et al.* 2010, Jia *et al.* 2011). The majority of investigations seeking to estimate alkaloid yield reported capsule size as the most highly correlated (Laughlin 1977, Chung 1987, Laughlin and Chung 1990, Waine *et al.* 2014). However, within each

paddock, biophysical parameters of plants vary and need investigations to understand the response of crop at different development stages in field conditions (Laughlin *et al.* 1998, Wang *et al.* 1999, Alam *et al.* 2011).

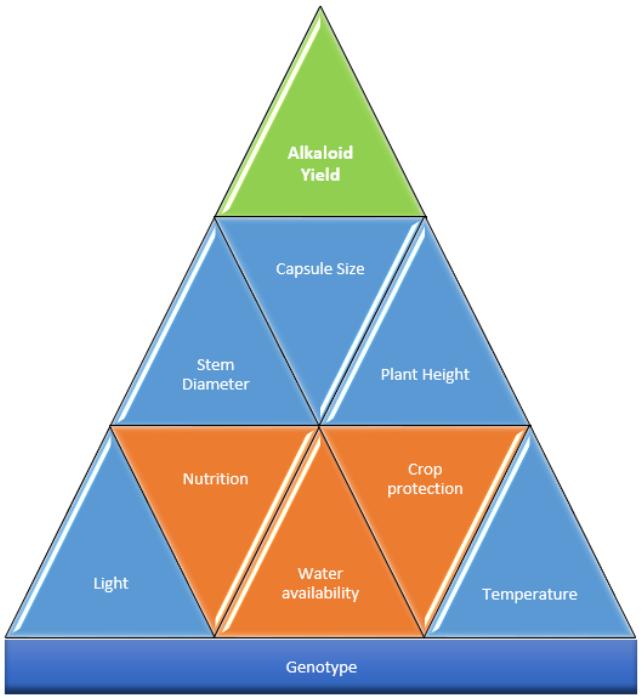

Figure 2.4. Factors Affecting Alkaloid Yield

Table 2.1. Percentage of environmental factors that determine the production of dry matter (Bernath 1986)

	Light	Temperature	Nutrients	Irrigation
Dry Mass	12 %	20 %	17 %	51 %

2.2.2. Effect of temperature on plant yield

As outlined in section 2.2.1, temperature has a significant impact on the development of poppy opium and each developmental stage has an optimum temperature range (Figure 2.2). After seeds germination, increase in temperature reduces the duration of each growth stage. Poppy is tolerant to cooler temperatures, which elongates the duration of the rosette phase and modifies the initiation of stem development (Bernath 1988), which ultimately increases the time for stem elongation and delays the initiations of flowering (Mahdavi-Damghani *et al.* 2010). In this case, plant height increases more compared to when grown at higher temperatures, and flowering time is postponed (Bernath and Tetrnyi 1981). The delay in flowering gives more time for plant development and produces more dry mass and significantly larger capsules (Brunet *et al.* 1991, Acock, Wang, and Acock 1996, Acock and Pausch 1997, Lisson 2007). Increase

in temperature beyond optimal limits reduce the rosette and stem elongation phase and causes the hastening of flowering which results in up to 12% reduction of plant height compared to growth at optimum temperature (Bernath and Tetrnyi 1981, Acock, Wang, and Acock 1996, Huang *et al.* 2001, Lisson 2007). Thus, increase in temperature during the early growth stages can reduce capsule mass up to 30% (Bernath and Tetrnyi 1981, Mahdavi-Damghani *et al.* 2010) and reduce yield. Capsule alkaloid is a function of capsule volume and dry mass, in cooler temperature relative to warmer conditions higher alkaloid quantity was found (Mika 1955, Losak and Richter 2004). High temperatures also increase evapotranspiration and the need for adequate water to be maintained.

2.2.3. Effect of light on plant yield

Poppy opium is a long day plant with flowering promoted when day length increases (Acock, Wang, and Acock 1996, Wang *et al.* 1999, Lisson and Cotching 2011). Studies have shown that poppy opium plants grown in a photoperiod with less than 12 hours day length did not initiate flowering (Acock, Wang, and Acock 1996). The role of light also varies in different poppy varieties, although, the literature shows that highest illumination provides more yield at high-temperature experiments (Bernath and Tetrnyi 1981, 1986, Acock, Wang, and Acock 1996). Moreover, light plays a vital role in the utilization of nutrients (Bernath and Tetrnyi 1986), and high dose of nutrients under insufficient light conditions can lead to toxicity of some elements. The minimum reported light illumination found is 16 kilo lux (klx) (Bernath and Tetrnyi 1986, Acock, Wang, and Acock 1996). Overall, increase in the amount of light can promote the development of the plant as a whole along with flowering specifically.

2.2.4. Effect of nutrients on plant yield

The amount of plant dry matter is a major contributor towards yield (Chung 1987) and dry matter has a direct relationship with nutrient availability and uptake (Losak and Richter 2004, Losak and Palenicek 2005). Nutrient requirements can vary spatially within a crop, and more nutrient uptake leads to more dry matter production. Edelbauer & Stangl (1993) highlighted the amount of nutrient uptake by poppy opium during its life cycle and reported that poppy opium plants producing 14.30 g dry matter use 0.26 g nitrogen (N), 0.10 g phosphorus (P), 0.34 g potassium (K), 0.30 g calcium (Ca) and 0.05 g magnesium (Mg). Out of total dry matter, 41.5 percent dry matter has been reported as capsule and the remainder was stem and leaves. Crop dry matter has been reported vital for capsule volume (Losak and Richter 2004, Jia *et al.* 2011, Waine *et al.* 2014) and opium yield is a product of capsule mass and volume (Jia *et al.* 2011, Waine *et*

al. 2014). Thirty-three percent of the total uptake of nutrients is used for capsule formation (Edelbauer and Stangl 1993).

Nitrogen is vital for alkaloid production and formation of morphine is higher when N is applied at hook, flowering and capsule development stage, whereas, N deficiency after flower initiation causes reduction in morphine yield (Laughlin 1982). Phosphorous has been reported vital for straw yield (Laughlin 1977, Losak and Palenicek 2005). and the application of N, P and K is recommended at seed sowing stages (Laughlin 1977, Baser and Arslan 2014). By application of N, P and K at sowing stage, a significant increase in yield has been reported (Laughlin and Chung 1990). Losak & Richter (2004) emphasised the increase in yield by applying the first dose of N at early growth stage and a second dose at flowering stage. Studies showed that a split dose of N (sowing, rosette and pre-flowering) provides a highly significant positive effect on the end yield as compared to the single application of N and reported 25% increase in yield (Losak and Richter 2004) and significant increase in latex quantity and morphine concentration (Jain 1990a). In addition to this, P and K nutrients are also considered very important for opium development. P nutrients are vital for the synthesis of proteins and phospholipids that serve as a major component of all cell membranes (Laughlin 1977, Solanki *et al.* 1999, Baser and Arslan 2014). Moreover, P application at the time of sowing increases the tolerance at lower temperatures and helps plant germination and enhances the amount of latex, seed and capsule husk yields (Jain 1990a, Losak and Palenicek 2005). Moreover, pre-sowing application of sodium borate with N, P and K fertiliser and later application at hook stage gave a significant increase in capsule yield (Laughlin 1979, Temple-Smith *et al.* 1983). However, the excessive application of nutrients can affect the crop adversely.

2.2.5. Effect of irrigation on plant yield

Precision irrigation management and scheduling have long been recognised as important factors to increasing crop production in a sustainable way (Rowshon *et al.* 2003, Awan, Ibrakhimov, *et al.* 2011). Moreover, applying water according to crop water requirement minimises the chance of over-irrigation and nutrient leaching. Consequently, there is less crop failure and more economic benefit in terms of end yield. However, there are few studies available to highlight the effect of irrigation on poppy opium yield. This section covers the review of studies published to highlight the effect of irrigation on poppy opium yield.

Seed germination is a complex process, with temperature and water being the key factors affecting germination (Singh *et al.* 2011). Poppy opium seed germination starts

when the soil is at 60 percent of available soil moisture with optimal average temperature (Bernath 1986, Mahdavi-Damghani *et al.* 2010, Singh *et al.* 2011, Baser and Arslan 2014). Crop water requirement along crop development varies due to the biological need of the plant. Penka (1968) highlighted crop water requirements of poppy and illustrated that the variation of water requirement changes according to transpiration rate during the crop growth cycle. After germination, vegetative growth of poppy opium starts (rosette phase) and water requirement changes accordingly. This stage is important for plant health and development, and normally good rosette formation provides more production (Laughlin and Chung 1990). Similarly, Bernath (1986) highlighted the consequence of water deficiency at rosette stage and reported that water stress at this stage affects the end yield dramatically. Mahdavi-Damghani *et al*. (2010) reported water stress at rosette stage as a serious cause of restricted health and consequently a factor of yield reduction. Numerous studies emphasise the effect of variation in moisture content of soil on crop growth. Studies indicate that decrease in soil moisture content from 60 percent field capacity in the rosette stage causes a severe reduction in yield (Mika 1955, Chung 1987, Laughlin and Chung 1990, Mahdavi-Damghani *et al.* 2010). Likewise, Yadav *et al.* (2006) showed that highest opium yield can be obtained by maintaining soil moisture at field capacity of 60 percent and above. Moreover, Penka (1968) reported the effects of water on crop yield and suggested two critical stages for irrigation application; initiation of stems and flower formation. Water stress at these critical stages has been found to reduce the yield. Good rosette formation leads to better root growth, which in turn assists plants in extracting water and nutrients from root-zone, thus, assisting in stem elongation. The hook stage is the next critical stage in poppy development and is crucial as it comes prior to flowering. The research of Chung (1987) illustrates that water stress at hook stage till flowering stage causes intensive reduction in end yield. On the other hand, split irrigation i.e. one application before flowering stage and one at the end of flowering stage, increases the yield by 4-13 kg/ha. Mahdavi-Damghani *et al* (2010) illustrated that hastening of flowering as effect of high temperature thus water deficiency before flowering reduces capsule mass and ultimately leads to alkaloid yield reduction. Moreover, water deficit directly reduces the biomass accumulation and causes reduction in the concentration of alkaloids indirectly. Previous studies have demonstrated that irrigation has a direct relationship with dry matter production and leaf area index (Bernath 1986, Chung 1987).

Irrigation application of Tasmanian poppy is different from the rest of the world, as poppies elsewhere are harvested at green capsule (opium) stage, whereas, in Tasmania

poppy is grown beyond the opium stage and harvested at the dry maturity stage. Hence, for Tasmanian poppy, irrigation application at opium stage is vital for higher yield. Leaf size and structure plays a vital role in production of food for plants in the presence of light. Thus, an extended photoperiod will enhance the yield as well as water requirement (Mahdavi-Damghani *et al.* 2010). Moreover, irrigation until leaf senescence increases end yield by 5-20kg/ ha. Delaying leaf senescence requires irrigation before flowering stage till maturity. However, early morning rain or overhead irrigation at flowering retards opening of petals and negatively affects the pollination and reduces the yield (Baser and Arslan 2014). Irrigation from flowering till capsule formation is critical due to the requirement of the biological processes in capsule (Chung 1987, Mahdavi-Damghani *et al.* 2010). Irrigation after the flowering stage shows promising results and increase in yield (Laughlin and Chung 1990). A key findings of the above studies (Mika 1955, Penka 1968, Bernath 1986, Chung 1987, Laughlin and Chung 1990, Mahdavi-Damghani *et al.* 2010, Kumar *et al.* 2011, Baser and Arslan 2014) highlighted that water stress at critical stages i.e. at rosette, hook and flowering stages result in yield reduction. In Tasmania, irrigation at the end of the flowering stage and two weeks after the flowering stage is also suggested (Chung 1987). In addition, full irrigation throughout the growing cycle increases the yield by 95 percent (Chung 1987, Laughlin and Chung 1990). Conversely, Hofman & Menary (1984) suggested that heavy irrigation at capsule stage may result in leaching of morphine from capsules. Thus, maintenance of an optimal irrigation management is critical.

2.2.6. Effect of pests, weeds and disease on plant yield

Crop protection is an important part of poppy crop management and includes diseases, insect pests and weed control. Poppy is prone to at least two bacterial, two viral and more than fifty fungal diseases (Harrison and Schmitt 1972), and as such fungal diseases are the main concern of the Tasmanian poppy industry. Insect pest damage is a more minor issue in Tasmania, but risk remains and damage can occur (Laughlin and Munro 1982). Thus, application of insecticides and fungicides at the time of sowing is recommended (Ireson 1993, Alam *et al.* 2011, Baser and Arslan 2014). To minimise the effect of weeds pre-emergent herbicides are recommended within one to two days after germination. Moreover, the post-emergent application of herbicide at rosette growth stage is also recommended (Fejer and Salamon 2011, Murray 2014). In Addition, weeds are also controlled through the use of crop rotations. Cereal crops are commonly used as an opportunity to control broad leafed weeds. For instance, there are a range of weed species that threaten poppies, but decades of cultivation of the plant have led to a number of control methods.

Ireson (1993) showed the infestation of springtails (*Collembola sp*) on poppies in Tasmania and reported that it attacks newly germinated poppy plants or plants at early rosette stages. Moreover, Laughlin *et al.* 1998 found evidence of springtails and native bud worm (*Heliothis punctigera*) in Tasmania. Native bud worm is an infrequent pest and attacks the capsule resulting in yield reduction. In addition, springtail growth has been recorded on moist leaves and dead plants, whereas, no evidence of springtails has been found on mature leaves. Moreover, red legged earth mites, lucerne flea, snails and cutworms are main insects in Tasmania (Murray 2014) affecting poppy growth.

Growth of fungal diseases are associated with moisture and humid conditions, the exception being of seed borne diseases (Hofman and Menary 1984). After the hook stage, higher moisture around leaves with poor air movement expedites the fungal development consequently reducing the alkaloid concentration (Laughlin and Munro 1982, Hofman and Menary 1984, Landa *et al.* 2007, Calderón *et al.* 2014). Most common recorded disease incidence around the globe on poppies are downy mildew (*Peronospora meconopsidis*) (Thangavel *et al.* 2017), collar rot (*Rhizoctonia solani*), damping off (*Pythium aphanidermatum*), root rot (*Fusarium semitectum*), stem and capsule rot (*Erwinia carotovora subsp. carotovora*), powdery mildew, sclerotinia, entyloma fuscum and poppy mottle (*potyvitus*) (Kothari and Verma 1972, Ireson 1993, Cotterill and Pascoe 1998, Laughlin *et al.* 1998, Scott *et al.* 2003, Turechek and Mahaffee 2004, Pethybridge *et al.* 2005, Alam *et al.* 2011, Fejer and Salamon 2011, Calderón *et al.* 2014). It has also been reported that Downy mildew and Damping off are common occurring diseases in Tasmanian poppies (Alam *et al.* 2011, Thangavel *et al.* 2017). It is evident from investigation conducted on downy mildew that canopy density can be used for incident severity, higher canopy density is more vulnerable towards down mildew (Scott *et al.* 2003). Scott et al. (2003) demonstrated rapid development of downy mildew from 60 to 85 days after sowing. The application of fungicide around this time can delay the severity of its occurrence (Danielsen and Munk 2004, Turechek and Mahaffee 2004, Montes-Borrego *et al.* 2008). Thus, the application of fungicides at the right time and appropriate location is critical.

2.2.7. Effect of growth regulators on plant yield

Plant metabolisms are divided into two types, primary and secondary metabolism. Primary metabolites, are molecules that are found in all plant cells, such as sugars, amino acids, proteins and nucleic acids (Raven *et al.* 1999). In addition, secondary metabolites serve as chemical indicators that enable the plant to respond to environmental effects and diseases (Zenk and Juenger 2007, Ziegler and Facchini 2008). There are different types of secondary metabolites and alkaloids are among them

(Raven *et al.* 1999). The first alkaloid (morphine) was identified in 1806, from poppy opium (Annett 1920, Kassem and Jacquin 2001, Schiff 2002, Yadav *et al.* 2006, Bendig *et al.* 2014). Efforts have been made to increase the concentration of alkaloid in poppy opium (Bernath and Tetrnyi 1981, Bernath 1986, Kassem and Jacquin 2001, Schiff 2002, Schulz *et al.* 2004, Yadav *et al*. 2006, Khan *et al.* 2011, Xing *et al.* 2011). Research studies illustrate the benefits of plant growth regulators (PGRs) on increasing alkaloid concentrations (Srivastava and Sharma 1990, Gross and Parthier 1994, Apuya *et al.* 2008, Dean 2011, Xing *et al.* 2011). PGRs are synthetic substances that are similar to natural plant hormones.

Plants have different types of hormones; five recognised groups of hormones are classified as auxins, gibberellins, cytokinins, abscisic acid and ethylene (Chiwocha *et al.* 2003, Davies 2010). They play a pivotal role for the growth and development of cells and work as messengers for intercellular communication. Auxins stimulate cell elongation and influence a host of other developmental responses, such as root initiation, development of auxiliary buds, flowers and fruits (Galewsky and Nessler 1986, Kassem and Jacquin 2001, Apuya *et al.* 2008). Cytokinins can help to stimulate cell division and induce shoot bud formation Moreover, they are involved in chlorophyll biosynthesis and transpiration control (Sagare *et al.* 2000). In addition to this, gibberellins are used for stem elongation and incitation of flowering (Tripathi and Tripathi 2005, Khan *et al.* 2007). Abscisic acids (ABA) are primarily involved in seed germination, inducing storage protein synthesis. It is commonly known as stress hormone and is widely used for modulating plant stress (Kuo *et al.* 2002). ABA plays an important role in somatic embryogenesis, particularly during maturity and early stages of germination. Ethylene is a simple gaseous hydrocarbon, and is mainly involved in flower senescence in plants. However, it can have a significant impact on development of plant root and sprouts (Facchini *et al.* 1996, Park and Facchini 2000, Ziegler and Facchini 2008).

Research conducted on the application of PGRs showed that it alters the alkaloid profile and enhances vegetative growth while restricting plant height (Dean 2011). It has been suggested that the plant height can be restricted with application of Sunny (uniconazole), that leads to the reallocation of plants nutrients and increase in alkaloid yield. Moreover, it is reported that the application of moddus (trinexapac) strongly influences the dioxygenases activities and alters the proportion of thebaine to oropavine which results in more morphine content. Moddus application at mid-late stem elongation showed reduction in seed yield and increased straw and capsule yield (Dean 2011). On the other hand, Investigation of Khan *et al*. (2007) showed that the application of gibberellic acid (GA) and n-triacontanol (TRIA) ninety days after sowing enhances

the opium yield. Split application of GA and TRIA at hook stage and flowering stage enhances the morphine yield. The application of GA + TRIA showed promising results to increase the chlorophyll content (Srivastava and Sharma 1990, Khan *et al.* 2007). In addition, application of GA + TRIA enhances the water uptake in plants and resulting in higher the number of capsules per plant (Sagare *et al.* 2000). Moreover, Srivastava & Sharma (1990) reported significant increase in plant dry weight, plant height, number of capsules, leaf chlorophyll and morphine concentration with the induction of TRIA (Srivastava and Sharma 1990). Leaf chlorophyll concentration at critical growth stages has been reported as a good indicator for alkaloid yield estimation (Jain 1990b, Kassem and Jacquin 2001, Omidi *et al.* 2012).

2.3. Critical stages of poppy opium for UAS remote sensing

From the above-cited literature, it is clear that multiple environmental factors affect the growth and development of plant. Proactive measures required to be taken even before sowing to get optimum yield and thus, are essential for the germination stage. Critical stages along poppy opium development are illustrated in Figure 2.5, highlighting the critical growth stages and biophysical and bio-chemical variable that can be estimated using UAS-based remote sensing technologies. Figure 2.5 illustrates the importance of environmental factors (temperature, light irrigation and nutrient) at germination, rosette, stem elongation, hook, flowering and at capsule formation stages. Horizontal red bars represent temperature, yellow bars illustrate light, blue represents irrigation requirements, and green represents nutrient importance. Vertical boxes along y-axis represent the growth stages and colour coded line length along x-axis within each box represent the importance of particular factor duration during within each phase.

UAS-based remote sensing at germination stage can be used to estimate the germination density (Hernández-Clemente *et al.* 2012). Initial stages of development are vulnerable to a number of factors and need proper attention, pesticide and herbicide need to be applied (Harrison and Schmitt 1972, Brunt *et al.* 1996, Alam *et al.* 2011, Fejer and Salamon 2011, Baser and Arslan 2014). Nutrients and irrigation stress at this stage can cause major reduction in end yield (Bernath and Tetrnyi 1986, Chung 1987, Laughlin and Chung 1990, Laughlin *et al.* 1998, Losak and Richter 2004, Losak and Palenicek 2005, Mahdavi-Damghani *et al.* 2010). UAS campaign with a multispectral sensor at this stage can provide the information of crop nutrient status (Zhu *et al.* 2010), chlorophyll concentration (Zarco-Tejada, Morales, *et al.* 2013) and can provides information on irrigation requirements (Stagakis, Gonzalez-Dugo, *et al.* 2012). Moreover, UAS remote sensing with the combination of thermal and multispectral sensors has been used to

monitor crop stress (Baluja *et al.* 2012, Stagakis, Gonzalez-Dugo, *et al.* 2012). On the other hand, excess application of nutrients in limited sunlight can cause a toxic effect on the plant (Bernath and Tetrnyi 1981, Bernath 1988, Ey *et al.* 1999, Wang *et al.* 1999) and irrigation also plays a vital role in the movement of nutrients and helps the plant to uptake nutrients. Thus, application of proper nutrients and irrigation according to the climatic conditions are essential requirements in the rosette stage. UAS-based remote sensing provides the opportunity to investigate the occurrence of disease and plant nutrient requirements (Calderón *et al.* 2014) using thermal and multispectral sensors (Berni, Zarco-Tejada, Suarez, *et al.* 2009, Zhu *et al.* 2010). Researchers have already tested UAS acquired data to estimate crop health using spectral indices (e.g. Berni, Zarco-Tejada, Suarez, *et al.* 2009, Waine *et al.* 2014) and LAI (Mäkynen *et al.* 2012), which has been found to have good relationship with opium yield, plant height (Iqbal *et al.* 2017) and in turn with capsule volume.

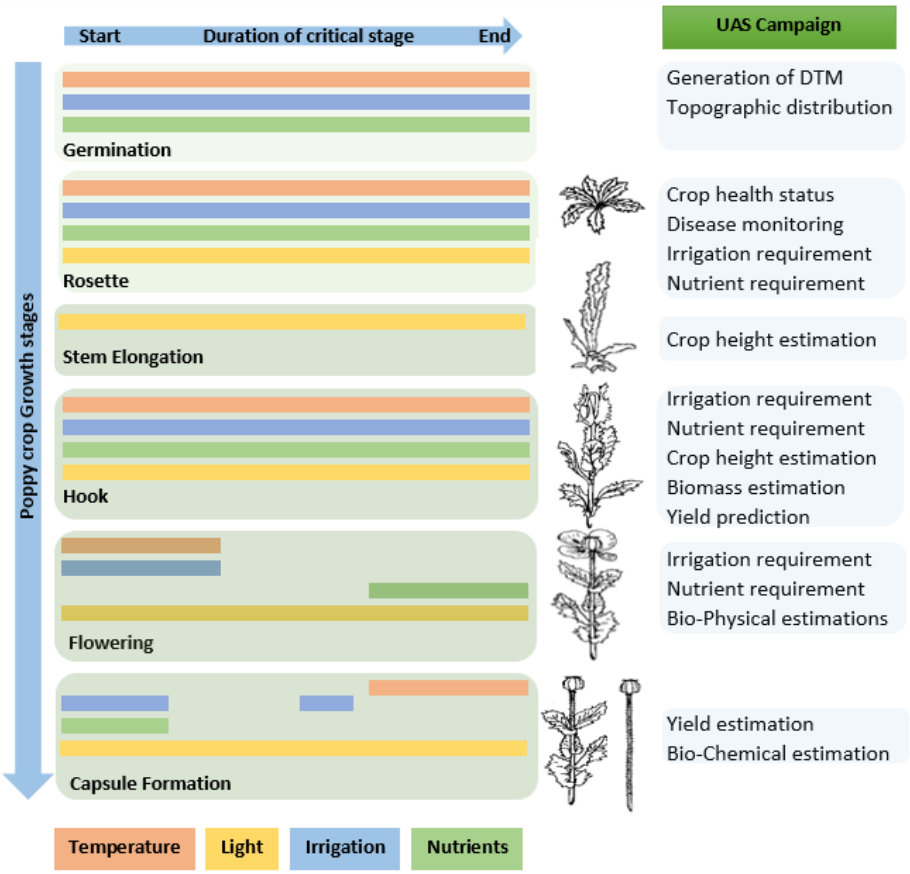

Figure 2.5. Critical factors at each phase of poppy development and important stages to estimate capsule yield. Light green boxes along y-axis illustrating growth stages of poppy crop from germination to capsule formation stage. Coloured lines within green boxes (Green, blue, yellow and red) along x-axis representing important stages for nutrient, irrigation, light and temperature application.

As shown in figure 2.5, UAS can provide an indication of crop irrigation (Berni, Zarco-Tejada, Sepulcre-Canto, *et al.* 2009, Baluja *et al.* 2012, Stagakis, Gonzalez-Dugo, *et al.* 2012) and nutrient requirements (Zhu *et al.* 2010) and provide a useful tool to estimate the biophysical parameters of crop health i.e. plant height (Iqbal *et al.* 2017), LAI (Jia *et al.* 2011). Spectral vegetation indices were also used to estimate crop biomass and yield (Bendig *et al.* 2014, Du and Noguchi 2017, Zhou *et al.* 2017). Start of the hook stage needs optimal nutrients and irrigation in the presence of long daylight periods and slightly warmer temperatures. Development of plants with higher leaf density normally creates humid conditions in plants. Thus, this stage can be regarded as critical for the occurrence of downy mildew and may need application of fungicides.

2.4. Conclusion

The aim of this chapter was to examine the cause and effect of environmental factors along the poppy growth cycle. The crucial stages for irrigation and nutrient application are the early stages of vegetative growth and in later stages, from initiation of hook stage till capsule formation. Crop management from germination till rosette stage is important for crop development, whereas, hook, flowering and capsule formation stages are important for capsule formation and alkaloid yield. Thus, monitoring of these stages is important for better crop growth and can result in yield enhancement. Precise monitoring requires data that can be achieved using a low-cost UAS remote sensing platform. UASs provide higher spatial and temporal resolution and enable the user to get the required data at required stages. Spectral indices and crop surface models derived from UAS imagery can provide detailed data for poppy crop management to get better yield. Stress related to sub-optimal nutrient and water availability, or plant yield potential, can be monitored using variability of spectral and structural variables driven using UAS remote sensing. This research has endeavoured to highlight the important growth stages for the application of UAS-based remote sensing for the estimation of poppy opium yield that can be most useful for poppy crop management.

2.5. Thesis context

Chapter 2 describes the critical stages of poppy crop that play a crucial role in biophysical and biochemical development of capsule yield. The findings of Chapter 2 indicate that hook, flowering and capsule formation stages are critical for capsule and alkaloid development. Thus, this chapter provides a strong foundation to conduct and organise UAS and field campaigns.

Chapter 3

3. Poppy crop height and capsule volume estimation from a single UAS flight

Chapter 3 described a novel method to estimate poppy crop height and capsule volume using a single UAS flight and has been published in **Remote Sensing** 22nd June 2017.

Iqbal, F., Lucieer, A., Barry, K., & Wells, R., 2017, 'Poppy crop height and capsule volume estimation from a single UAS flight', **Remote Sensing**, vol. 9, no. 647.

Abstract

The objective of this study was to estimate poppy plant height and capsule volume with remote sensing using an Unmanned Aircraft System (UAS). Data was obtained from field measurements and UAS flights over two poppy crops at Cambridge and Cressy in Tasmania. Imagery acquired from the UAS was used to produce dense point clouds using structure from motion (SfM) and multi-view stereopsis (MVS) techniques. Dense point clouds were used to generate a digital surface model (DSM) and orthophoto mosaic. An RGB index was derived from the orthophoto to extract the bare ground spaces. This bare ground space mask was used to filter the points on the ground, and a digital terrain model (DTM) was interpolated from these points. Plant height values were estimated by subtracting the DSM and DTM to generate a Crop Height Model (CHM). UAS-derived plant height (PH) and field measured PH in Cambridge were strongly correlated with R^2 values ranging from 0.93 to 0.97 for transect one and transect two, respectively, while at Cressy results from a single flight provided R^2 of 0.97. Therefore, the proposed method can be considered an important step towards crop surface model (CSM) generation from a single UAS flight in situations where a bare ground DTM is unavailable. High correlations were found between UAS-derived PH and poppy capsule volume (CV) at capsule formation stage (R^2 0.74), with relative error of 19.62%. Results illustrate that plant height can be reliably estimated for poppy crops based on a single UAS flight and can be used to predict opium capsule volume at capsule formation stage.

3.1. Introduction

UAS-based remote sensing technology has demonstrated the potential for precision agriculture by providing data at high temporal and spatial resolution (Zhang and Kovacs 2012). In precision agriculture, remote sensing has been used to monitor crop

growth and health by computing a range of spectral vegetation indices (Berni, Zarco-Tejada, Suarez, *et al.* 2009, Saari *et al.* 2011, Baluja *et al.* 2012, Stagakis, Gonzalez-Dugo, *et al.* 2012, Zarco-Tejada, Guillen-Climent, *et al.* 2013, Waine *et al.* 2014, Brandao *et al.* 2015, Kaur *et al.* 2015). However, recently more attention has been given to the use of crop height modelling for yield estimation (Yin *et al.* 2011, Bendig *et al.* 2014, Tilly *et al.* 2014). In this context, several studies have shown that crop productivity, in certain crop types (e.g. maize, potato, barley, wheat, corn, rice, sunflower and poppy (Wang *et al.* 1999, Hasnain *et al.* 2006, Mahdavi-Damghani *et al.* 2010, Jia *et al.* 2011, Papadavid *et al.* 2011, Bendig *et al.* 2014, Gao *et al.* 2015, Vega *et al.* 2015, Erten *et al.* 2016, Li *et al.* 2016, Sharma *et al.* 2016), can be assessed from biophysical characteristics, such as crop height and biomass. Crop height is an important factor for yield estimation and crop management (Bernath 1986, Wang *et al.* 1999, Mahdavi-Damghani *et al.* 2010, Jia *et al.* 2011, Bendig *et al.* 2014, Vega *et al.* 2015). Crop height is a significant indicator of yield estimation in maize (Yin *et al.* 2011), whereas, in barley, crop height has been utilised to estimate biomass (Bendig *et al.* 2014). In the case of poppy crops, only a single study has looked at the use of remote sensing methods, in which crop height and Leaf Area Index (LAI) were found to be two suitable indicators for estimating opium yield (Jia *et al.* 2011).

UAS have become a viable and cost-effective alternative to manned airborne or satellite remote sensing for precision agriculture, given their ability to collect high spatial resolution data at critical times during the growing season (Zarco-Tejada, González-Dugo, *et al.* 2012, Zhang and Kovacs 2012, Gago *et al.* 2015, Verhoeven and Vermeulen 2016, Wu *et al.* 2017). Moreover, UAS aerial photography allows overlapping imagery to be collected, which is widely used for three-dimensional (3D) image reconstruction and facilitates change analysis (Jaakkola *et al.* 2010, Harwin and Lucieer 2012, Bendig *et al.* 2014, Lucieer, de Jong, *et al.* 2014, Zarco-Tejada *et al.* 2014). Three-dimensional measurements of crop structure are possible by generating Crop Surface Models (CSMs), which enable crop height measurement (Bendig *et al.* 2014, Geipel *et al.* 2014, Verhoeven and Vermeulen 2016, Wu *et al.* 2017). Availability of CSM at high spatial resolution and high vertical accuracy is of increasing importance for site-specific precision agriculture. The change in height values between the DTM at the time of sowing and DSM at crop maturity can be used to derive plant height, which can improve understanding of the relation between plant height, biomass, and yield (Bendig *et al.* 2014, Geipel *et al.* 2014). For the reliability and accuracy of estimated crop biomass or crop yield, the availability of timely information on crop height is important. In recent years, automated image orientation technique Structure from Motion (SfM) complemented by dense image-matching through Multi-View Stereo (MVS) has become

a popular technique to derive 3D information about terrain and vegetation from UAS images (Harwin and Lucieer 2012, Remondino *et al.* 2012, Bendig *et al.* 2013, Geipel *et al.* 2014, Harwin *et al.* 2015, Verhoeven and Vermeulen 2016, Wu *et al.* 2017). The SfM-MVS workflow starts with automated image feature detection and identification followed by feature matching between overlapping images. Next, SfM-MVS uses bundle adjustment algorithms to simultaneously estimate the 3D geometry, the different camera poses (extrinsic calibration) and the camera intrinsic parameters (intrinsic calibration) (Remondino *et al.* 2012, Nex and Remondino 2014, Harwin *et al.* 2015, Smith *et al.* 2016). The output of the SfM stage is a sparse, unscaled 3D point cloud in arbitrary units along with camera models and orientation (Harwin and Lucieer 2012, Remondino *et al.* 2012, Lucieer, de Jong, *et al.* 2014, Smith *et al.* 2016). The 3D point cloud can be registered to a projected coordinate system by identifying and incorporating ground control points in the bundle adjustment (Harwin and Lucieer 2012, Turner *et al.* 2014, Verhoeven and Vermeulen 2016, Wu *et al.* 2017). A dense image matching algorithm is then employed to extract a dense 3D point cloud from the images (Doneus *et al.* 2011, Harwin and Lucieer 2012, Remondino *et al.* 2012, Verhoeven *et al.* 2012, Mancini *et al.* 2013, Green *et al.* 2014, Nex and Remondino 2014, Harwin *et al.* 2015).

The SfM-MVS workflow has been successfully applied for estimation of crop height (Bendig *et al.* 2014, Geipel *et al.* 2014, Li *et al.* 2016, Wu *et al.* 2017). DTMs have been produced with imagery acquired at the sowing stage, and subsequent DSMs have been derived from UAS imagery at several critical crop stages (Bendig *et al.* 2014). The vertical difference of both surface models (DSMs) and the DTM was used to estimate the crop height. A challenge with this method is that it requires either a precise DTM or at least two flights to collect the DTM before crop sowing and crop DSM during the growing season. It is not always feasible to collect a DTM at the start of the growing season, and therefore, our study aims to estimate crop height from a single UAS flight.

In this study, we focus on a high-value alkaloid poppy crop (*Papaver Somniferum L*), grown for pharmaceutical applications, to demonstrate the application of UAS-based crop height assessment. In earlier studies, different physiological indicators, such as plant height, have been assessed to predict opium yield (Annett 1920, Jain 1990b, Kang and Primack 1991, Acock, Wang, Acock, *et al.* 1996, Khan *et al.* 2007, Harvest *et al.* 2009, Mahdavi-Damghani *et al.* 2010, Jia *et al.* 2011). Spectral indices have been reported to estimate capsule volume and showed a significant correlation between NDVI and capsule volume from flowering till harvesting stage (Waine *et al.* 2014). In most fields, poppy crop growth is spatially highly heterogeneous and requires a substantial amount of data collection to develop models for yield estimation (Kang and Primack 1991).

Several studies have highlighted this phenomenon based on field observation of poppy crops grown under controlled conditions (Annett 1920, Bernath and Tetrnyi 1981, Kang and Primack 1991, Lisson 2007, Harvest *et al.* 2009). Few studies have used remote sensing technologies for poppy yield estimation (Jia *et al.* 2011, Waine *et al.* 2014). Data collected from field measurements, particularly physical measurements of the crop, provides reference information on crop growth. The spatial coverage of detailed field measurements is often limited; however remote sensing techniques can help to identify the spatial variability of key yield indicators at a much broader scale. This paper aims to investigate the potential use of low-cost image acquisition using a UAS-based platform for the estimation of poppy crop height and capsule volume. More specifically, the first objective of our study is to develop a new approach that facilitates crop height estimation from a single UAS flight. The second objective is to assess the potential of UAS-based CSM to predict poppy capsule volume (CV) using plant height as the predictor variable.

3.2. Materials and methods

3.2.1. Study area

This research was conducted in Tasmania, Australia on opium poppy, which was grown for the pharmaceutical industry subject to government licensing. Two different field sites were selected for this study (Figure 3.1). The first study area was a commercial poppy crop located at Cambridge, Tasmania (42°47'50" S, 147°25'33" E, altitude 32 m) and the total sown area was ~16 hectares. The field was irrigated with a centre pivot irrigation system. Poppy seed was sown in late July 2014 in a well-cultivated field using seed drills, with seedling emergence in the following 1-2 weeks. Flowering occurred in November, with capsule formation starting in late December and poppy capsules were harvested in late January 2015. The crop was sown with a seed drill to maintain a row distance of 6 cm with a seeding density of 80 seeds per square metre.

The second study area was located in Cressy, Tasmania (41°41'S, 147°05'E) and the assessment was conducted in the subsequent field season. Many aspects of the crop were similar to the Cambridge site. The Cressy field was also irrigated with a centre pivot system, seed was sown in mid-August 2015 in a well-cultivated field using a seed drill, and the months of flowering, capsule formation and harvest (late January 2016) were the same. However, the crop was sown with a higher density (90 seeds per square metre) in 210 separate sample plots. This site was used to conduct an independent UAS campaign to verify the robustness of the single flight method.

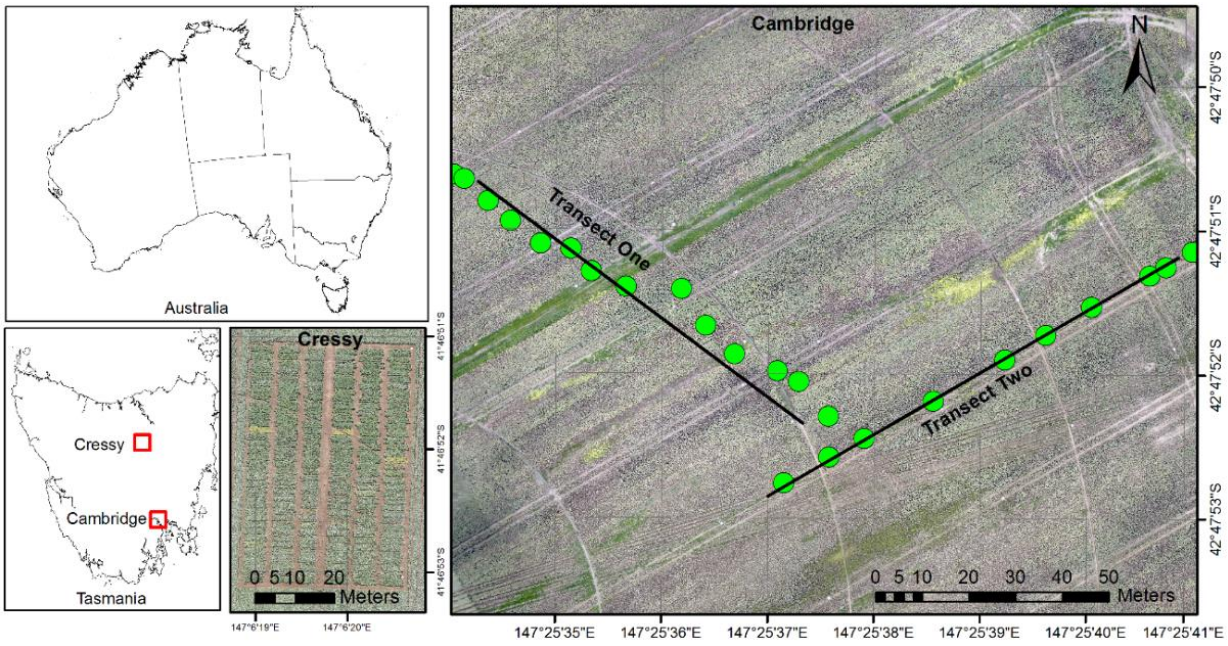

Figure 3.1. The general location of the study sites (Cambridge and Cressy) and the overview of the image obtained from unmanned aircraft system (UAS).

3.2.2. Data collection

3.2.2.1. Field measurement

For the Cambridge site, physical data was collected at four time points (Table 3.1). Field measurements were conducted along two transects, each a total length of ~90 metres. Transect one (T1) was selected based on topographical variation, as it crossed a drainage channel in the field (Figure 3.2a). In contrast, transect two (T2) was located in a part of the field with less topographical variability (Figure 3.2b). The location of both transects is shown in Figure 3.1. Field data collection was organised in 25 (0.25 x 0.25 m) sample plots (sampled at every 5 to 8 m in each transect), which included the physical measurements of 125 plants along the two transects (five plants in each sample plot). Sampling plots were selected randomly along the transect lines and were marked to allow for repeat data collection at different growth stages, i.e. flowering, capsule development and capsule formation (Table 3.1). At each sample plot, physical parameters including the number of plants and capsules, horizontal and vertical dimensions of each capsule, and plant height (PH) were measured using Vernier calipers and steel measuring tape respectively (Figure 3.3). Average plant height and average capsule dimensions per plot were determined. Capsule volume was calculated by assuming the capsule to be an ellipsoid (Wang *et al.* 1999). Linear regression was computed for plant height (PH) at three stages against capsule volume (CV) at the capsule formation stage (Table 3.1). For capsule volume estimation, an empirical

relationship between crop height and capsule volume was developed from the field observations at capsule formation stage. This relationship was used to estimate capsule volume using UAS acquired plant height information.

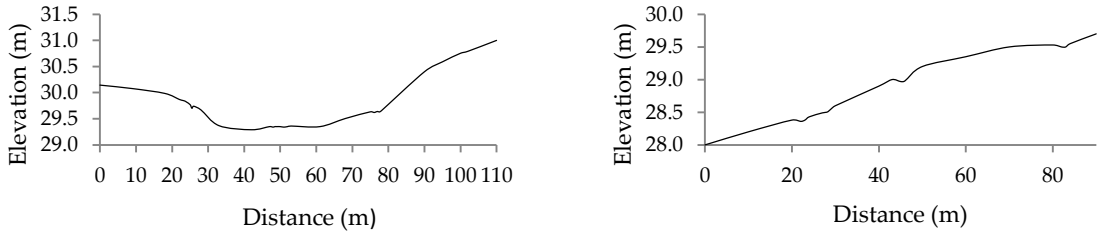

(a) (b)

Figure 3.2. Topographical profile of transects at Cambridge farm (ASL), (a) transect one, and (b) transect two. (derived from DSM generation, ref: section 3.3)

(a) (b) (c)

Figure 3.3. Overview of the field physical measurement of plant height and capsule height and diameter; (a) diameter of capsule measured with a Vernier caliper, (b) height of capsule measured with Vernier caliper, (c) height of each plant was measured with measuring tape.

Table 3.1. Field assessments and UAS campaigns at the study locations

Survey date	Growth stage	Observation
Cambridge		
28/11/2014	Flowering	Physical
16/12/2014	Capsule development	Physical
21/12/2014	Capsule formation	Physical
22/12/2014	Capsule formation	Physical, UAS, GPS
Cressy		
17/9/2015	Sowing and germination	UAS, GPS
3/12/2015	Capsule formation	Physical, UAS

For the Cressy site, two assessment periods were included (Table 3.1). Field measurement was conducted from 210 (5 m x 1.8 m) sample plots, with data obtained

from 20 plants per plot. Plant height was measured at capsule formation stage (3/12/2015).

3.2.2.2. GPS survey

Accurate GPS coordinates of each sample plot and Ground Control Points (GCPs) were measured with survey-grade dual frequency RTK GPS (2 – 4 cm absolute coordinate accuracy). Photo targets generated with Agisoft Photoscan were printed on 0.5 m X 0.5 m plastic boards and were distributed in the field to be used as GCPs for UAS-based image processing (Harwin and Lucieer 2012). 20 GCPs were distributed evenly in the both experiment area. For the Cambridge site, fourteen GCPs were used as constraints in the bundle block and were used to automatically georeference the whole camera network, while six GCPs were used for the validation of processed imagery results. For the Cressy site, 5 GCPs were used for 3D model construction, whereas, 15 GCPs were used for model validation.

3.2.2.3. UAS campaign

In this study, three UAS campaigns were conducted (Table 3.1). We used an OktoKopter UAS platform to acquire the imagery (Harwin and Lucieer 2012). An OktoKopter is a multi-rotor platform and has a total take-off weight of 3 kg. This platform has a camera stabiliser gimbal with capacity to carry a payload of up to 2 kg for flight duration of around 5 to 10 minutes, which is sufficient to capture UAS-MVS imagery for a 1-2 ha area. Two separate flights were conducted to cover the whole area. This platform was controlled with an autopilot and navigation-grade GPS receiver (with the expected accuracy of 5 – 10 m) to collect (x, y) positions and altitude for the camera stations. The RGB images, with a 5184 x 3456 pixel array, were acquired with a Canon 550D DSLR digital camera (18 Megapixels). The camera was operated with a 20 mm fixed focal length lens on manual focus mode fixed to infinity. The exposure time of the camera was set to a fast shutter speed of 1/1600th of a second to reduce motion blur and the ISO was set to 125 to reduce noise in the image with an aperture of f/2.8. The camera was triggered by the flight controller to capture the image after every ~1.5 seconds. The images were acquired at an altitude of approximately 50 m with a mean spatial resolution of 1 cm. Finally, the images were acquired along evenly spaced flights with ~90% forward overlap and ~70% side overlap between images in cloudless illumination condition at 12:30 PM to 1:30 PM.

3.3. UAS data analysis and DSM generation

The main methodology of this research is summarised in Figure 3.4. The study was based on crop height estimation using SfM-MVS image reconstruction approach with Agisoft PhotoScan software (Jaakkola *et al.* 2010, Harwin and Lucieer 2012, Bendig *et al.* 2014, Lucieer, de Jong, *et al.* 2014, Zarco-Tejada *et al.* 2014, Harwin *et al.* 2015). As detailed further below in section 2.3.1, UAS images were processed to generate DSMs and orthomosaics of the study areas. As poppy crop growth is relatively dense compared to other crops, it is not always possible to detect bare ground patches within the crop. Therefore, mosaicked orthophotos with R, G, and B bands were used to classify crop and bare soil pixels (Geipel *et al.* 2014). The bare soil pixel masks were used to extract the corresponding height values from the 3D model generated using Agisoft PhotoScan. Extracted soil height values were spatially interpolated using a Spline algorithm to generate the DTM surface. DSM (height values of crop) and DTM (height values of ground) data were subtracted to estimate the crop height. The results were compared against field measurements of crop height (at sample plot level) in order to assess the accuracy of the method. Finally, the relationship of plant height and capsule volume developed from the Cambridge field data was used to estimate capsule volumes using UAS determined crop height.

The single flight method for estimation of crop height used at Cambridge (Figure 3.4), was tested at the Cressy site. In this verification process, comparison was made between a single UAS flight and the traditional methodology for crop height estimation using two separate flight campaigns (Bendig *et al.* 2015, Wu *et al.* 2017). A bare ground DTM was created by conducting a UAS campaign over the bare field at the time of sowing (17/9/2015). The second flight campaign was conducted at capsule formation stage (3/12/2015) and the UAS images were used to develop a DSM and orthophoto mosaic. Data of proposed (single flight) and traditional CSMs were statistically compared to quantify the accuracy of the new method.

3.3.1. DEM generation

The workflow involved in processing UAS-mounted RGB camera imagery is represented in Figure 3.4. UAS-MVS acquired imagery and corresponding GPS data were used to geotag all images. The process of geotagging images speeds the process of extracting orientation information and reducing the computation required for feature identification and feature-matching to estimate camera parameters (Lucieer, de Jong, *et al.* 2014). Computation of 3D object geometry information from overlapping images is

possible using feature matching in multiple views through SfM-MVS algorithms (Lucieer, Malenovský, *et al.* 2014).

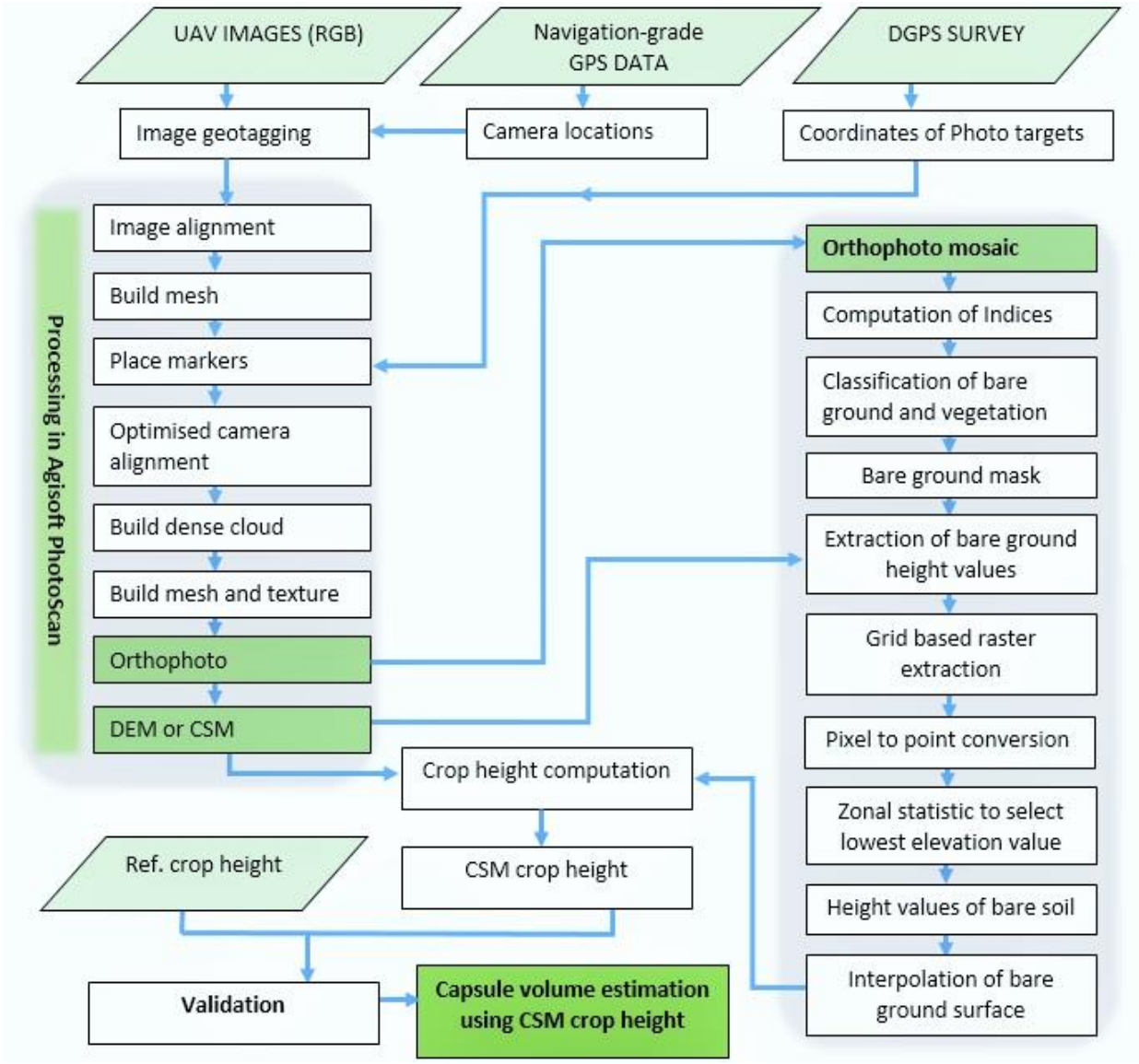

Figure 3.4. Flowchart illustrating the main steps for the estimation of plant height and capsule volume using imagery acquired from UAS flight campaign.

In this study, we utilized Agisoft PhotoScan Professional version 1.1.4 to generate 3D models and orthophotographs. The first step is the image feature detection, feature matching, and bundle adjustment. This process results in a sparse point cloud (based on the image features used in the bundle adjustment) and the initial camera locations. The "High Accuracy" and "Reference" pair selection settings were used to achieve accuracy high quality bundle adjustment. The resulting 3D model was used to build a 3D texture model to manually identify the GCP targets. This model was used to position the GCP markers approximately, after which the exact position of the markers was refined in

every image (Harwin and Lucieer 2012, Lucieer, de Jong, *et al.* 2014, Harwin *et al.* 2015). Based on GCP coordinates measured in the field using RTK GNSS (2—4 cm absolute accuracy), the camera alignment was optimised to generate the dense point cloud. For the production of the dense point cloud, the point quality was set to "High" and depth filtering setting was set as default "Aggressive". Finally, the orthophoto and DSM were exported with the standard procedure of Agisoft PhotoScan.

3.3.2. Vegetation indices and bare ground pixel extraction

In Tasmania, poppy crops are sown using seed drills that create areas of bare ground, which in this case was approximately from 0.5 to 1.0 m wide (Figure 3.7) and provides the visibility of ground areas from UAS imagery. Moreover, areas of bare ground were also visible in the orthophoto, either due to wheel tracks of spray equipment, or between plants in areas of weaker growth. The seeding density of 80-90 seeds per square metre with dense growth makes it difficult to classify ground points within the crop. Therefore, an orthophoto mosaic with R, G, and B bands was used to compute RGB indices for the delineation of crop and soil pixels (Geipel *et al.* 2014). The Red-Green index (Gitelson *et al.* 2002, Motohka *et al.* 2010) was computed using DN values (unsigned integer) to classify the crop and bare ground pixels. The output index values ranged between -1.0 to +1.0. Index layer pixels were classified as bare ground when pixel values were below zero and as vegetation when above zero.

$$\frac{\text{Rgreen}-\text{Rred}}{\text{Rgreen}+\text{Rred}}$$ (Gitelson *et al.* 2002, Motohka *et al.* 2010)

The classified bare ground areas were used to mask all bare ground areas throughout the image. Masked areas were used to extract the pixel-based height values from the DSM. To ensure the classification of real ground values, polygon grids of 0.5 x 0.5 m were created and used to extract the height values from masked bare ground areas. Each pixel bare ground height value was converted into a point. To ensure the selection of real ground surface height value, zonal statistics for each zone were calculated in ArcGIS 10.3 to determine the lowest elevation points in each zone. These were used to generate the DTM with spatial Spline interpolation, which minimises the overall surface curvature. This results in a smooth surface that passes exactly through the input points. A CSM is calculated by subtracting the DTM from the DSM (Bendig *et al.* 2014, Geipel *et al.* 2014). For plot-based analysis, a square buffer of 0.25 m was placed around each surveyed point for each sample plot. Finally, from the CSM layer, pixels falling in each sample plot were extracted. Based on the CSM, individual plant heights were extracted

solely from crop classified pixels and used for statistical analysis and accuracy assessment.

3.3.3. Plant height and capsule validation

PH estimates derived from the UAS-CSM at Cambridge were compared to the reference measurements on the ground to assess the accuracy of this method. The height error was calculated as the difference between actual PH measured in the field and estimated PH from the UAS CSM. The root mean square error (RMSE) of the errors was calculated along with the regression fit and the R^2 between measured and estimated PH. PH derived from the UAS CSM was used to estimate CV and the simulated results were also verified with field observations. Moreover, Cressy site PH obtained from a single flight and from traditional methodology were compared with field measured data.

3.4. Results

3.4.1. Field measurements

Field-based plant measurements showed that PH at the capsule development stage is the strongest predictor for CV estimation, based on the stages assessed in this study (Figure 3.5). The highest correlation of PH with CV was observed at capsule formation stage (R^2 of 0.71) in T1, whereas, at capsule development and flowering stage the correlations were lower (R^2 0.69 and 0.67 respectively). The significant and moderately strong correlation between PH (measured) and CV (measured) observed at capsule formation stage were found for both transect 1 and 2 data (Figure 3.6). During the flowering stage, the poppy opium capsule still needs time to develop, however, the increase in plant height stops at this stage and the plant moves towards the next phenological stage.

Figure 3.6 shows a significant relationship between PH and capsule volume at capsule formation stage. We selected this stage for analysis because the yield prediction at this stage can be used to appropriately manage the required resources to optimize yield. The relationship is more apparent during the capsule formation stage (as evident from Figure 3.5), showing an increase in CV with an increase in PH (Figure 3.6 and Table 3.2). High PH is an indicator of vigorous plant growth and typically is associated with multiple and larger capsules per plant. During the capsule formation stage, the correlation between PH and CV at plant level shows $R^2 = 0.711$ at T1 and $R^2 = 0.723$ at T2. Thus, it can be concluded that the PH during flowering and capsule formation stage is the best indicator for capsule volume estimation. The model developed based on T1

field data was validated on T2 and vice versa yielding RMSE of 20.80 % and 15.0 % respectively (Table 3.3). Data obtained from T1 showed greater variation in CV compared to T2, ranging from 13.71 cm^3 to 60 cm^3 in T1 and 16.08 cm^3 to 49.35 cm^3 in T2 (Table 3.2). Similarly, a wider range of PH was observed in T1, i.e. 49 cm to 110 cm as compared to T2 ranging from 59 to 89 cm.

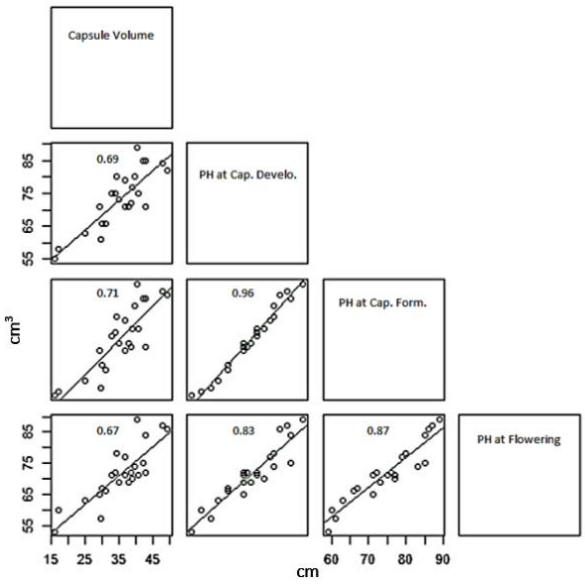

Figure 3.5. The coefficient of determination (R^2) for capsule volume (Y axes - cm^3) at capsule formation stage and plant height (X axes – cm) at different growth stages, for transect 1.

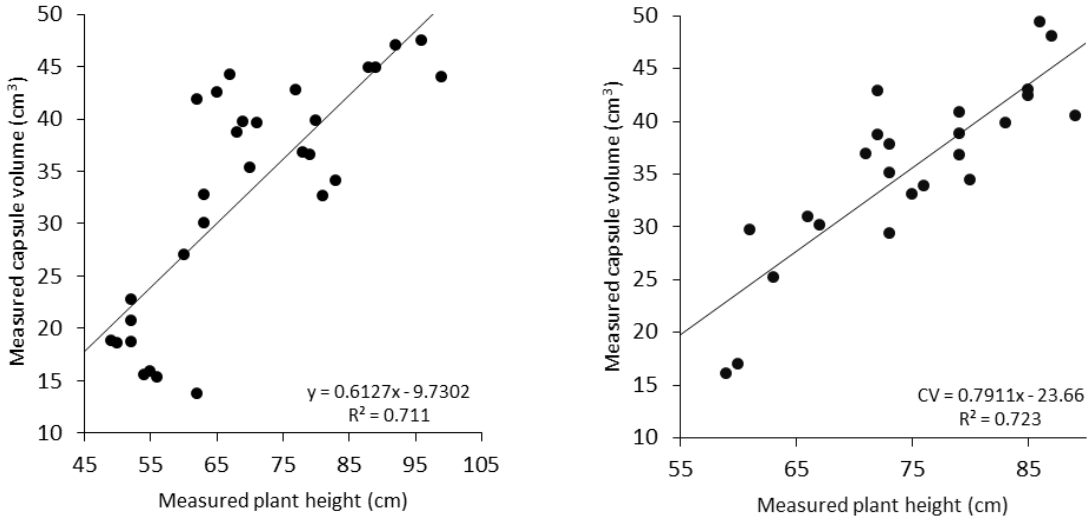

Figure 3.6. The empirical relationship between poppy plant height and capsule volume at capsule formation stage: (a) transect one (T1), (b) transect two (T2).

Table 3.2. Field measured data of plant height and capsule volume for two transects at individual plant level (n = 65 for T1 and n = 60 for T2). PH, plant height; CV, capsule volume

	Transect 1		Transect 2	
	PH (cm)	CV (cm^3)	PH (cm)	CV (cm^3)
Min PH	49.00	13.71	59.00	16.08
Median PH	69.00	36.79	74.00	36.86
Mean PH	72.55	34.71	74.46	35.44
Max PH	110.0	60.00	89.00	49.35

Table 3.3. Regression of plant height versus capsule volume from field measurement of two transects. T1: transect one, T2: transect two. N = number of sample; SE = standard error; R^2 = coefficient of determination; with $p < 0.0001$; RMSE = root mean squared error; RMSE = relative root mean square error

	Regression Model	N	SE (cm^3)	R^2	RMSE (cm^3)	RMSE%
T1	CV = 0.6127 x PH -9.730	65	6.33	0.71	7.23	20.80
T2	CV = 0.7911 x PH -23.66	60	4.30	0.72	5.32	15.00

3.4.2. Crop surface model generation

The Cambridge site analysis of the 3D model generated in Agisoft PhotoScan with reference to GCPs resulted in an overall RMSE of 7.60 cm. Theaccuracy of using the Red Green Index to classify vegetation from bare ground was checked by conducting a survey of bare ground patches in the field. In the survey, 152 points were collected from both classes (bare ground and cropping area) and the overall accuracy of classification was 93.72%. Extraction of the actual bare ground surface was achieved by eliminating false classification points. The resultant areas were then used to extract the height values of bare ground from the DSM. The extracted height values were interpolated using a Spline interpolation algorithm to generate the DTM. The height values of DTM pixels were compared with the corresponding surveyed points. For each point, the error was calculated as the difference between actual ground elevations measured in the field using DGPS with the ground elevation obtained from the interpolated DTM layer. The accuracy assessment indicated an overall RMSE of 9 cm. In the case of the Cressy site, the overall RMSE of the surface model derived from the campaign at the sowing stage was 2.5 cm. For the model generated at capsule formation stage, results yielded an overall horizontal RMSE of 6 cm and the vertical RMSE of 4 cm.

3.4.3. Relationship between CSM-derived PH and measured PH

The accuracy of the CSM generated from UAS imagery was calculated using average height values of the pixel on each plant with measured values. The difference between

height values obtained from field and CSM were derived to quantify the error in the CSM. The results showed (Table 3.5 and Figure 3.7) a clear underestimation of height in both transects, which is a common observation found in previous studies (Bendig *et al.* 2014). In both transects, the difference of observed vs estimated mean height was found to be variable, ranging from 12.55 to 9.96 cm. In T1, the difference between measured and estimated CSM height of smaller plants revealed underestimaton of approx. 10 cm and approx. 18 cm for larger plants. In contrast, the values of T2 showed an underestimation of 7 cm for larger plants and 12 cm for smaller plants. RMSE also varied depending on the transects, with the relative error ranging from 13.60 to 18.72 percent (Table 3.4).

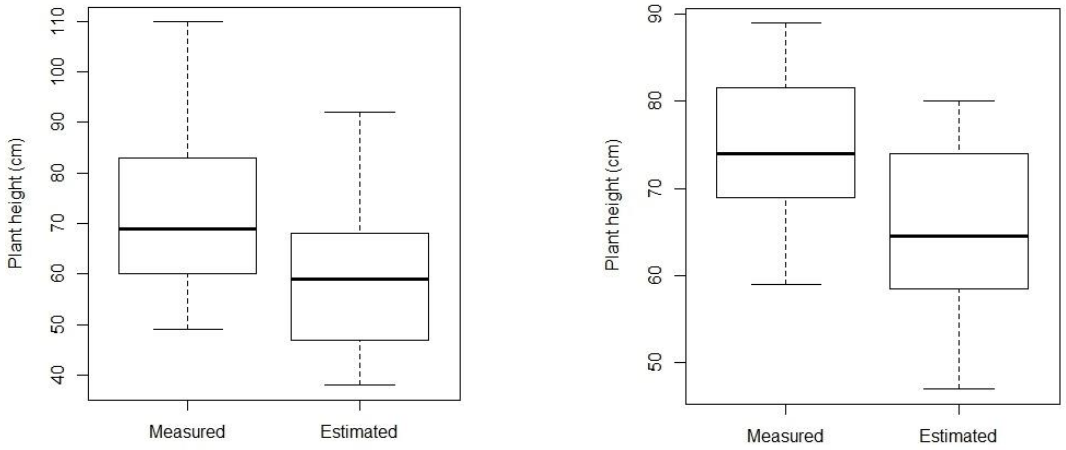

(a) (b)

Figure 3.7. Box plot of the measured and estimated plant height for the two transects at the individual plant level (n = 65 for transect one (a) and n = 60 in transect two (b)).

Figure 3.8 shows the linear fit and coefficient of determination between measured and estimated plant height at the individual plant level; the results are highly significant with R^2 of 0.93 for T1 and 0.97 for T2. The underestimation of plant height in the CSM is likely a result of local averaging in the creation of the grid-based CSM.

Table 3.4. Root mean square error (RMSE) and relative root mean square error (RMSE %) compared with average of measured plant height (PH) for transect one (T1) and transect two (T2) at the Cambridge site.

	RMSE (cm)	**Average PH (cm)**	**RMSE%**
PH (T1)	13.58	72.54	18.72
PH (T2)	10.12	74.45	13.60

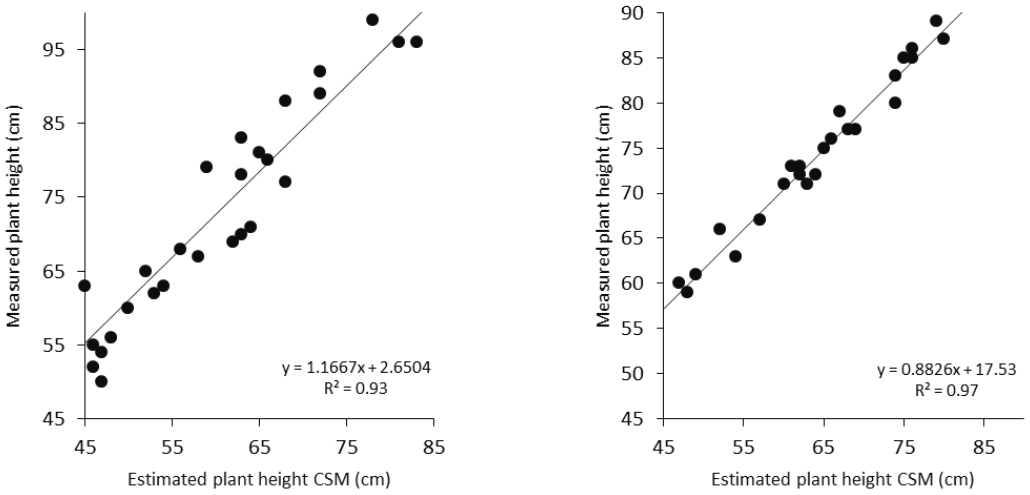

(a) (b)

Figure 3.8. Linear fit between measured and estimated plant height of two transects at the individual plant level. (a) PH of transect one, (b) PH of transect two.

3.4.4. Relationship between single flight PH and traditionally measured PH

Figure 3.9 (c) illustrates that the DTM extracted (b) at capsule formation stage varied between -4.3 cm to 4.1 cm compared to the DTM estimated (a) when the field was bare. Moreover, the estimated DTM (single flight) showed smoother boundaries as compared to the true DTM (two flights), which is caused by interpolation. Overall, both DTMs show almost the same elevation values and illustrate the same general spatial variability. It was found that the crop height estimated from a single flight was strongly correlated with the crop height estimated from two flights, with an R^2 value of 0.97 (Figure 3.10). Whereas, R^2 of 0.99 was achieved in case of two flights in relation to measured values. However in both methodologies, the difference of mean height was found to be slightly variable, ranging from 58 cm to 59 cm.

The difference of CSM derived height of smaller plants was approximately 3 cm, whereas in larger plants the CSM showed a maximum height of 85 cm and 84 cm based on a single and two-flight method respectively. The accuracy of the proposed one-flight methodology is similar to results of crop height estimation in other studies for other crops [11,28–31]. Overall, the RMSE varied from the single flight to two flight method, with the relative error ranging from 11.01 to 10.36 percent. However, the extracted height values from both methods were lower than the field measured values.

Table 3.5. Measured and estimated plant height (cm) for two transects at the individual plant level PH for transect one and two at the Cambridge site.

	Transect 1		Transect 2	
	Measured (cm)	Estimated (cm)	Measured (cm)	Estimated (cm)
Min PH	49.00	38.00	59.00	47.00
Median PH	69.00	59.00	74.00	64.50
Mean PH	72.55	60.00	74.46	64.50
Max PH	110.0	92.00	89.00	82.00

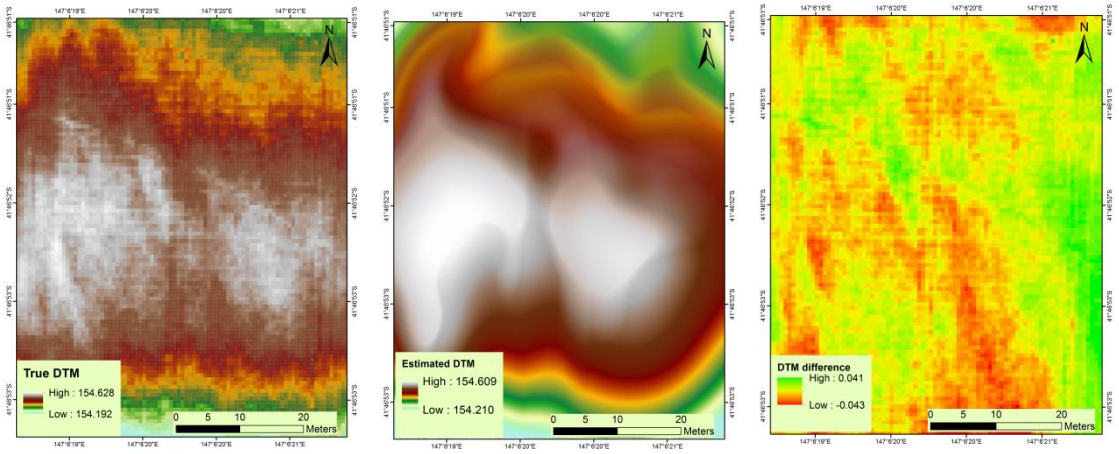

(a) (b) (c)

Figure 3.9. Map of DTM generated from UAS flight when the soil was bare (a), DTM extracted from the flight at capsule formation stage (b) and difference between a and b (c).

3.5. Discussion

In this research, the analysis was carried out to estimate capsule volume from plant height determined at different developmental stages, and it was concluded that the capsule formation stage gives the best results in predicting capsule volume ($R^2 = 0.71$), which is in accordance with a previous study (Jia *et al.* 2011). Capsule volume can also be predicted at the flowering stage, but with lower accuracy ($R^2 = 0.67$). The coefficient of determination at the flowering stage was found to be low, as plant development was not uniform (i.e. some plants had progressed to the flowering stage while others remained at the stem elongation stage). This shows that at intermediate developmental stages of the crop the accuracy of the relationship between PH and CV is limited, as reported previously (Waine *et al.* 2014). PH plays an important role in providing information on crop development. Healthier plant development in early stages supports formation of larger capsules (Kang and Primack 1991, Mahdavi-Damghani *et al.* 2010). The current research shows that plant height information can be estimated using UAS-MVS remote sensing. Apart from apparent advantages of UAS remote sensing, there are

many challenges associated with routine operations, such as small payload capacity, low spectral resolution, poor geometric and radiometric performance, low software automation, sensitivity to atmospheric conditions, short flight endurance, and possibility of equipment damage. Moreover, UAS users need to consider cost involved in repairs and maintenance, transportation, weather conditions and regulations for flying small UAS. Thus, multiple flight campaigns are not always possible. The weather, especially in Tasmania, is also a restricting factor. Spring and early summer can have high rainfall, so, it can be difficult to conduct UAS campaigns during this period at the relevant crop stages. Therefore, in this study, a simple and reliable method has been developed and tested for robust estimation of PH, based on a single UAS flight campaign, thereby overcoming the restriction of multiple flight campaigns and providing promising results for precision agriculture.

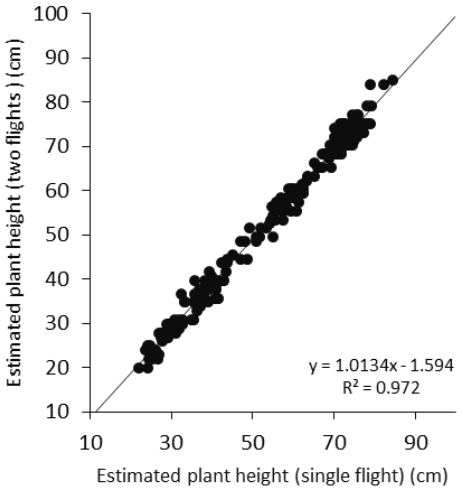

Figure 3.10. Linear fit between plant height estimated from single and two flights.

In this study, the visible ground areas within the field were utilised to detect the elevation of bare ground and were used to interpolate the DTM. The height values of soil points could also be extracted from vegetated imagery (Bendig *et al.* 2014, Verhoeven and Vermeulen 2016). The accuracy of the DTM obtained from the single flight method depends on the distribution and size of bare ground patches visible in the mosaicked image. The error analysis of the Cambridge site DTM showed an underestimation, expressed by an RMSE of 9 cm. This indicates that a smaller number of bare ground patches cannot represent an accurate distribution of height values. Moreover, the accuracy of the DTM depends upon the terrain variation in the field. If the topography throughout the field is highly variable, then a large number of bare ground patches are needed to obtain an accurate DTM. In the case of the Cressy site

with flatter topography but fewer bare ground patches, similar results were obtained (Figure 3.10). The Cressy site results illustrate that the difference in DTM extracted at capsule formation stages and DTM generated at sowing stage varied approx. ± 4 cm which is much lower than the result of Cambridge site, and therefore more accurate. An accuracy assessment of the CSM resulted in an RMSE of 12.24 cm for the Cambridge site, whereas, Cressy resulted in RMSE of 5.60 cm, in accordance with the result of previous studies (Harwin and Lucieer 2012, Lucieer, de Jong, *et al.* 2014, Turner *et al.* 2014, Harwin *et al.* 2015).

Crop height is generally underestimated, which is a common issue with vegetation height assessment with SfM-MVS (Bendig *et al.* 2014). Crop height estimated from UAS compared with measured crop height resulted in a coefficient of determination of 0.93 in the case of T1, while in T2 it was slightly higher and reached up to 0.97. Cressy site results with a single campaign provide R^2 of 0.972, in accordance with a previous study (Bendig *et al.* 2014). Results with two flights showed higher R^2 of 0.988, in accordance with other findings (Ehlert *et al.* 2008). Overall, the RMSE also varied depending on topography. In Cambridge farm, the relative error being 13.60 and 18.72 percent for transect T1 and T2 respectively. Whereas in Cressy experiment, results illustrates that the crop height extracted with the single flight can provide similar results as compared to two flight campaigns, with the relative error ranging from 11.01 to 10.36 percent respectively. This is because topography of Cressy farm was well levelled as compared to Cambridge site. Moreover, well distributed bare soil patches were available to detect, therefore, resulted in better estimation.

UAS remote sensing derived PH estimates used to simulate capsule volume showed the coefficient of determination of $R^2 = 0.738$ with RMSE of 6.95 cm^3 with a relative error of 19.62% at T2. The error is slightly higher for UAS derived CV as compared to the field-based model because of underestimation of UAS-derived plant height. The results showed a higher agreement between the estimated capsule volume and estimated plant height. To improve the model prediction for future research, the error inherited from DTM and DSM can be minimised by using an on-board RTK GNSS receiver as it will enable collection of accurate location and position information associated with each image and improve the georeferencing of acquired imagery. Moreover, an important factor is the size and distribution of bare ground patches. A larger number of bare ground patches with larger GCPs can be used to cover the whole variation of terrain, which would improve the accuracy of the DTM and DSM, resulting in a higher accuracy of the CSM.

The poppy capsule volume estimation model used in this study is an empirical model, and if implemented elsewhere, would require a new regression analysis based on field survey data, as the slope and offset of the regression equation would alter based on environmental circumstances and impacts of treatments, such as growth regulators. In Tasmania, poppy is grown as a legal crop and farmers are paid based on the alkaloid output of crops. Therefore, the poppy industry selects specific varieties for cropping, thus, the applicability of this model would need to be investigated on other varieties as well. Other factors that may change the relationship of PH with CV include different soil types, irrigation applications, and nutrients. Crop height estimation using the proposed methodology provides a cost-effective and time-saving way to acquire crop information. The proposed method reduces the time for field campaigns and reduces the cost of each flight campaign (GPS, UAS pilot, transportation, image processing etc.), which can help farm managers and researchers to manage crop zones according to crop requirement and therefore optimise yield.

3.6. Conclusions

In this study, we used a UAS platform with a standard digital camera and GPS to acquire very high resolution RGB images of poppy crops. Structure from Motion (SfM) and multi-view stereopsis (MVS) methods were used by deploying Agisoft Photoscan software to generate a DSM and orthophoto. This study demonstrates a novel method to estimate plant height using a single-flight UAS survey. The bare ground patches were classified using red green index and were used to extract the height value of the ground and were used to generate a DTM. In Cambridge farm experiment, UAS-derived plant height and field-measured PH was strongly correlated with R^2 values ranging from 0.93 to 0.97 for T1 and T2 respectively. In Cressy farm experiment, the extracted crop height from single flight method showed very high correlation with two flights estimated and field measured height, with a R^2 value of 0.97 and 0.98 respectively. It can be concluded that to estimate PH and therefore CV, a single flight method can provide almost similar results to that of two flights, saving cost and time. This provides an important approach for CSM generation from a single UAS flight where a prior DTM is unavailable. Moreover, this study estimated poppy capsule volume based on UAS derived crop height. Poppy capsule volume estimation using UAS derived plant height is a novel approach which has not been formally tested before and has predicted 81% of the capsule volume variation. The coefficient of determination ($R^2 = 0.73$) demonstrates that plant height derived from UAS imagery is a suitable indicator for capsule volume. Capsule volume can be used as a proxy for alkaloid yield (Wang *et al.* 1999), which is vital to estimate for the pharmaceutical industry.

3.7. Thesis context

Chapter 3 addressed the first objective of the thesis and described a novel method to estimate poppy crop height and capsule volume using a single UAS flight. Chapter 4 will focus on the use of multispectral UAS data to further improve capsule volume estimates.

Chapter 4

4. Simplified radiometric calibration for UAS mounted multispectral sensor

Chapter 4 described a successful methodology for radiometric calibration using low-cost single pseudo target approach for image acquired using Mini-MCA sensor and has been published in **European Journal of Remote Sensing** 6th February 2018.

Iqbal, F., Lucieer, A., & Barry, K., 2018, 'Simplified radiometric calibration for UAS-mounted multispectral sensor', **European Journal of Remote Sensing**, vol. 51, no. 1, pp. 301–313.

Abstract

Unmanned Aircraft System (UAS) in combination with multispectral sensors stimulate the utilisation of site-specific technologies to monitor and manage crop production according to intra-field variability. Crop monitoring requires accurate conversion of raw digital numbers (DNs) to surface reflectance. However, radiometric calibration methods in practice are difficult to implement for UAS remote sensing as every single image requires correction due to smaller field of view and changes in light. Therefore, this paper proposes an easy and cost effective radiometric calibration process for UAS-based Mini-MCA multispectral sensor. Prediction equations for six multispectral bands were developed between image DN and surface reflectance values obtained from five radiometric calibration and one white pseudo target. Results showed linear relationship between spectral reflectance and raw DN values with y-intercept value close to zero. It is the minimal possible surface reflectance recorded by sensor and can be used as a first point for equation development. The spectral quantification of white pseudo target was used as a second point of equation. Quantitative spectral information was generated by developing equation for every single image. An accuracy assessment was undertaken by comparing image driven reflectance values against reflectance values measured in the field from soil and crop. The overall accuracy based on the root mean square error (RMSE) for the six bands ranged from 0.025 % to 0.064 %. The results of this study showed that the proposed method can be used for the calibration of UAS based multispectral image for the conversion of raw UAS based DN to surface reflectance data.

Chapter 4

4.1. Introduction

Precision agriculture generally involves better management of farm inputs at the right place and the right time to optimise crop yield (Mulla 2013). While the general practice in field management is to apply even applications of irrigation, pesticides and fertilisers etc. throughout the paddock. Remote sensing technology has paved a great importance in the field of sustainable agriculture (Zhang and Kovacs 2012). The use of remote sensing technologies provides data to retrieve crop variability information (Carbone *et al.* 1996, Oudemans *et al.* 2002, Zarco-Tejada, Ustin, *et al.* 2005, Zhang and Kovacs 2012, Morel *et al.* 2014, French *et al.* 2015, Stadler *et al.* 2015). RS helps in the division of a field into different variability zones that facilitates crop management by customising variable inputs (Zhang *et al.* 2002). On the global scale, studies have used satellite remote sensing to monitor plant growth by computing different spectral indices (Saari *et al.* 2011, Baluja *et al.* 2012, Stagakis, Gonzalez-Dugo, *et al.* 2012, Zarco-Tejada, Guillen-Climent, *et al.* 2013, Waine *et al.* 2014, Brandao *et al.* 2015, Kaur *et al.* 2015). Crop health information derived from satellite data have a potential to forecasts economic return and help policy makers to take precautionary measures for food security at national level (Bastiaanssen *et al.* 2000, Bastiaanssen and Ali 2003, Fedotov and Osmani 2010, Dempewolf *et al.* 2014, Morel *et al.* 2014). However, in majority part of the world agriculture is mainly driven by small farms (Thornton 2002). Land owners of small farms need to grow multiple crops in order to fulfill their food requirements, resulting in enormous variability of crop type and management practices within the farm. Usually, this variability cannot be captured over the canvas of satellite imagery due to the small size of the farm and low spatial resolution of imageries (Boschetti *et al.* 2004, Leroux *et al.* 2014). This variability restricts the use of satellite imagery at local scale due to spatial resolution (Lausch *et al.* 2013). Moreover, crop management on farm scale requires availability of crop information at specific time during the crop cycle and requires repeated measurements (Zarco-Tejada, Miller, *et al.* 2004, Cohen *et al.* 2005, Cheng *et al.* 2006, Iqbal 2011). Thus, satellite remote sensing is not a suitable option for small land farmers (Stafford 2000). There exist alternatives such as piloted airborne platforms that allows to acquire very high spatial resolution data at a required time, but are difficult to use due to their high costs (Rango *et al.* 2009). Recently, growing attention has been given to the use of Unmanned Aircraft Systems (UAS) to overcome the limitations of satellite remote sensing, especially where small farm areas have to be monitored (Swain *et al.* 2010, Zhu *et al.* 2010, Harwin and Lucieer 2012, Lucieer, de Jong, *et al.* 2014, Lucieer, Malenovský, *et al.* 2014, Torres-Sánchez *et al.* 2015). The use of UAS as a remote sensing platform has demonstrated the potential for small farm management by providing multi-temporal

data (Bendig *et al.* 2013, Zhou *et al.* 2017). It provides flexibility in acquisition at much lower costs as compared to aerial and satellite data. Images captured using UAS generally have spatial resolution within a few centimetres. Therefore, UAS acquired images could be a practical alternative to aerial and satellite remote sensing. For small farm management, UAS remote sensing driven spectral signatures have been used to estimate biophysical characteristics of plants (Berni, Zarco-Tejada, Suarez, *et al.* 2009, Jaakkola *et al.* 2010, Baluja *et al.* 2012, Mäkynen *et al.* 2012, Zhang and Kovacs 2012) to monitor plant growth and health (Berni, Zarco-Tejada, Suarez, *et al.* 2009, Zhu *et al.* 2010, Saari *et al.* 2011, Kelcey and Lucieer 2012, Bendig *et al.* 2014).

UAS-based remote sensing technology has developed remarkably and customised sensors are available for agricultural applications (Zhang and Kovacs 2012). Continuous development in the field of electronics allows the production of lightweight navigation systems and controllers which makes UASs cost effective (Joseph *et al.* 2016). On the other hand, the latest developments in plastic technology are replacing metals (Zhu *et al.* 2004, Ajayan and Tour 2007) and high performance polymer materials providing same mechanical strength with dramatic reduction in weight, which allows carrying of more payload and results in increase in UAS flight time (Ajayan and Tour 2007). For these reasons, the use of UAS remote sensing for small agriculture farms is increasing and its use is anticipated to increase in future (Stellman *et al.* 2001, Baluja *et al.* 2012, Zhang and Kovacs 2012, Uto *et al.* 2013).

UAS systems are often operated under suboptimal conditions, such as below a full or partial cloudy cover. Despite the challenging conditions, the images must be processed accurately so that object characteristics can be interpreted on a quantitative geometric and radiometric basis using the data. Radiometric calibration of images is a prerequisite, especially for precision agriculture (Moran *et al.* 2001), where change in spectral signatures across the paddock is used to develop management zones (Pinter Jr *et al.* 2003, Bakhsh and Kanwar 2006, Whiting *et al.* 2006). The data retrieved from an image is in the form of digital numbers, which is not a true representative of the surface reflectance (Del Pozo *et al.* 2014). The sensor records the radiance and converts it to digital numbers, which is not a quantitative value (Smith and Milton 1999) and changes with illumination conditions and consistency of sensor.

UAS campaigns with smaller field of view (FOV) results in large number of very high resolution images over a small paddock (Oovergaard *et al.* 2010, Del Pozo *et al.* 2014, Wang and Myint 2015). Smaller FOV results in variation in range of DN values and generates an un-reliable data (Warren *et al.* 2011, Herrero-Huerta *et al.* 2014), which can

be associated to change in illumination (Wang and Myint 2015). Therefore, for reliable crop zonation each UAS based image needs to be radiometrically corrected to maintain the spectral consistency throughout the campaign (Smith and Milton 1999).

Several levels of radiometric correction for remote sensing data are available (Chavez Jr 1989, Smith and Milton 1999, Vicente-Serrano *et al.* 2008). The first level is to convert the sensor digital numbers (DNs) to sensor radiance, which requires camera calibration information. The second step is transformation of the sensor radiance to radiance at the earth surface (Mattar *et al.* 2014), which requires removal of atmospheric distortions. Multiple methods have been developed to remove the effect of atmospheric distortion including radiative transfer model and empirical line method (Smith and Milton 1999, Moran *et al.* 2001, Miura and Huete 2009, Saari *et al.* 2011, Wang and Myint 2015).

The altitude of UAS a campaign is restricted by Civil Aviation Safety Authority (CASA) Australia for remote pilot aircraft (RPA) and allows flight below 120 metres. In case of small farms, UAS is flown around 50 to 100 metres that passes through a very small atmospheric column. Therefore, the difference of radiance at sensor and surface is minimal, and is thus, ignored. The use of empirical line correction method is based on relationship between DN value and surface reflectance in which the DN values are converted to the units of reflectance (Smith and Milton 1999, Moran *et al.* 2001, Wang and Myint 2015). The role of ground targets in radiometric correction of imagery is vital and thus, are used for the calibration and validation of data (Baugh and Groeneveld 2008, Staben *et al.* 2012).On field, the reflectance of ground targets are recorded with spectrometre and the DN values of the same targets are extracted from the image. The radiance values from the image are plotted on the independent axis and the reflectance values from the ground targets are plotted on dependent axis. This gives a linear or near-linear relationship, depending on the number of targets used (Stow *et al.* 1996, Smith and Milton 1999, Karpouzli and Malthus 2003).

Most researchers have used two calibration targets (black and white) to cover the range of dark and bright pixels in the image (Chavez Jr 1989, Baugh and Groeneveld 2008, Del Pozo *et al.* 2014, Herrero-Huerta *et al.* 2014). This process assumes that the distribution of DN to reflectance within image is linear (Smith and Milton 1999, Baugh and Groeneveld 2008). However, this is not always true, especially when working with crops (Stow *et al.* 1996). Some researchers use multiple calibration targets to improve the calibration accuracy and assume that illumination is uniform throughout the campaign with lambertian properties and the relationship remains the same for all images (Staben *et al.* 2012). However, in case of multiple images with smaller FOV, this case is not

always true due to illumination conditions and therefore, every image needs to be calibrated to achieve consistency in results (Stow *et al.* 1996, Wang and Myint 2015). Dozens of calibrations targets are required over a field such that each UAS based acquired image should capture one target for the purpose of calibration. As the calibration targets with lambertian properties are very expensive making the overall field campaign cost intensive, thus, a feasible, accurate and cost effective method needs to be developed for the radiometric correction of UAS images. Therefore, for this study, photo targets were tested as pseudo calibration targets in order to make the campaign more cost effective. The objective of this study was to test the performance of pseudo photo targets in place of calibration targets by developing a relationship between multiple image derived DN values acquired through Mini-MCA sensor and field measured reflectance. The relationship developed by using pseudo photo targets was then utilised to convert image DN values to surface reflectance for achieving radiometric calibration of UAS based imageries.

4.2. Materials and methods

4.2.1. Materials

This research was conducted at a research farm of University of Tasmania (42°47′50.84″ S, 147°25′33.06″E, attitude 32m), at Cambridge located around 20 km east of Hobart, Tasmania, Australia (Figure 4.1). In summer 2014, a commercial crop was sown at a selected paddock. UAS campaigns were conducted along two transects almost perpendicular to each other. The images acquired over transect one was used for the development of calibration equation and imagery acquired over transect two was used to check the consistency.

In this study, Miniature Multiple Camera Array (Mini-MCA) was used (Figure 4.2), which is a low-cost influential instrument used for crop mapping. It can provide the data to investigate the development stages of the crop. This sensor was mounted on multirotor aircraft to acquire the spectral images from multiple discrete bands. For the field spectral data, ASD spectroradiometer was used to collect the spectral reflectance of photo targets and calibration targets. Details of all the steps undertaken are elaborated in subsequent sections.

4.2.2. Multispectral sensor

A multispectral sensor is a powerful and dominating instrument for environmental remote sensing (Stow *et al.* 1996). It can provide the data to investigate the development

of the crop (Del Pozo *et al.* 2014). UAS-mounted multispectral sensors can acquire the spectral data from multiple discrete bands, which can be used for the computation of indices (Herrero-Huerta *et al.* 2014). Studies have been published in past to highlight the potential use of indices in crop yield modelling (Zarco-Tejada, Ustin, *et al.* 2005, Papadavid *et al.* 2011, Dempewolf *et al.* 2014, Geipel *et al.* 2014, Kross *et al.* 2015). The miniature camera array (Mini-MCA) of Tetracam Inc. was used for this research. It consists of an array of six individual channels, each channel consisting of a lens, a filter, a memory card and a complementary metal-oxide-semiconductor (CMOS) sensor that records the light passing through the filter within a channel as an image on the memory card. The spectral response of image sensors is uniform through the range with optimum sensitivity (100%) between 750 nm to 800 nm and gradual decrease to 20% at 450 nm in visible region and 1050 nm in near-infrared region (Kelcey and Lucieer 2012). Every channel of Mini-MCA has a place of band-pass spectroscopic filters and is placed between lens and image sensor. Spectroscopic filters restrict radiation allowing a narrow band of wavelength to reach the image sensor. The amount of light received by each image sensor is directly dependent on the bandpass filter. Camera sensors produces finest image at full width half maximum (FWHM) of 10 nm as it provides optimum light, although, exceptions prevail at the far ends of the sensors sensitivity range. In this case, more light passes through the far end filter and is balanced by the sensor's diminished affectability. In our study, we used the filters with a central wavelength of 530, 550, 570, 670, 700 and 800nm. Corresponding FWHM and peak transmission wavelength of each filter are listed in Table 1. Filters are interchangeable depending upon the purpose of UAS campaign.

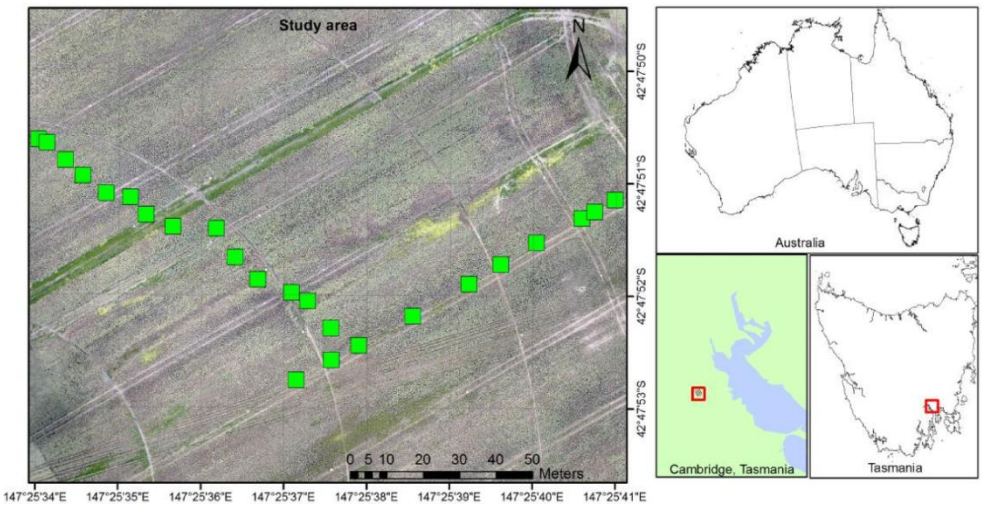

Figure 4.1. The general location of study site and the overview of the image obtained from UAS showing sampling locations in green for surface reflectance comparison.

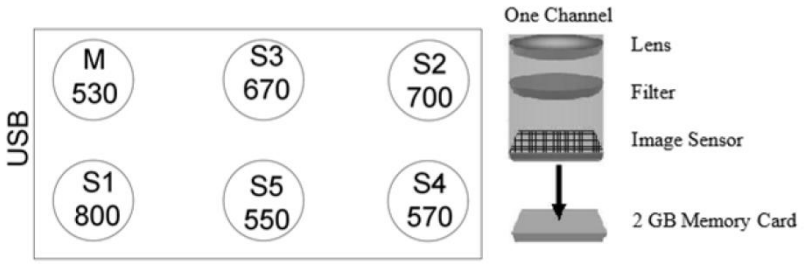

Figure 4.2. Modified tetracam miniature multiple camera array (Mini-MCA).

Table 4.1. Mini-MCA channel specifications.

Channel	Filter	FWHM	Peak wavelength (nm)	Band width range (nm)	Peak transmission (%)
Main	530	10	530.50	510 – 550	59.71
S1	800	10	799.60	780 – 820	59.61
S2	700	10	702.20	680 – 720	69.44
S3	670	10	670.50	650 – 690	70.17
S4	570	10	571.80	550 – 590	62.99
S5	550	10	549.60	530 - 550	55.01

4.2.3. Spectral campaign of calibration targets

To measure field reflectance five radiometric calibration targets and twenty photo targets (pseudo targets) were used in this study. All five calibration targets were placed along the transect and spectral measurements of each calibration target was taken using ASD FieldSpec3 spectroradiometer (Analytical Spectral Device, Inc., Boulder, co, USA). ASD FieldSpec3 is a passive device which depends on solar illumination and acquires the data from 325nm to 1075nm. Reflectance measurements were taken during the flight campaign (1:00 pm to 2:00 pm) under solar light. During spectral data collection, spectroradiometer calibration measurements were taken with a reference panel (white colour Spectralon) and dark current before and after taking readings from radiometric calibration targets. Twenty spectral readings were taken from each target from a distance of 1 metre without blocking sunlight with sample counts of 15. Every spectral reading per calibration panel was averaged for further analysis and average of all twenty spectral readings was used for image calibration analysis.

UAS campaign acquired hundreds of very high resolution images over a small farm and every image required one calibration target for calibration. It is not feasible to place a large number of radiometric calibration targets during each flight campaign as it increases the cost of each campaign. Moreover, this UAS sensor does not cater for the illumination specific data and thus requires more detailed calibration data. As the intensity of ambient light varies, the amount of reflected light energy from the surface

will alter resulting in inaccurate information. To cope with illumination variability, accurate calibration is imperative. Therefore, this study tested one pseudo calibration target per image, thus, distributing 20 pseudo targets throughout the study area of around 60 × 180 m to make sure one target is captured by each image. For this purpose, matte finish plastic boards of 0.5 × 0.5 m photo targets were used for geometric correction as pseudo radiometric calibration targets for each image. Spectral readings from white portion of pseudo targets were measured using spectroradiometer. To make sure the readings were taken from the white portion of the targets, pointing light of the spectroradiometer was used as a marker and measurements were taken from a distance of 0.5 m. The calibration target was then tested for lambertian material properties for which, twenty spectral measurements were taken from four different viewing angles.. To compare the collected field spectra with Mini-MCA imagery, spectral signals were resampled to Mini-MCA band positions. In this research, FWHM values and central wavelength of each Mini-MCA band values were used to resample the reference field measured spectral signatures. This was carried out using R package Prospect-R, which uses Gaussian model with FWHM spacing (Stevens and Ramirez-Lopez 2014).

4.2.4. UAS platform

In this study, UAS platform was used for the collection of multispectral sensor data with a Multirotor Oktokopter. The payload capacity of UAS platform used in this study was 2 kg. The flight duration was 5 to 10 minutes, depending on batteries and payload. To maintain near nadir position of sensor, gimbal was used. An on-board Autopilot system with GPS, 3D advanced compass and barometric altimeter permits the system to follow the predefined flight path. According to CASA laws, flying height within three nautical miles of aerodrome is restricted and UAS cannot be operated above 120 metres. For this research, as the study site was within three nautical miles from controlled aerodrome, thus, it was necessary to maintain an allowed range of flying height during the campaign. Flying height being a crucial factor was calculated beforehand based on the size of calibration target. For the purpose of calibration, multiple numbers of pixels from each calibration target need to be present, for which, flight height was calculated using the relation between flight height and pixel size. Moreover the length and pitch of propeller time and distance travelled by each flight was calculated to manage the number of batteries required to complete the mission. A planned campaign was conducted at the altitude of ~45 metres to acquire a pixel resolution of 3 cm using four flights. UAS system was equipped with gimbal to mount the Mini-MCA camera. Finally, five-hundred images were captured from the study site.

4.2.5. Image processing

UAS campaign captured five hundred images that required enormous rectification followed by radiometric calibration to obtain seamless, homogenous spectral reflectance data from a non-homogenous raw image. To reduce the processing load, two hundred and forty images were selected by eliminating every second image and systematic noise and vignetting affect were corrected (Kelcey and Lucieer 2012). To completely remove the influence of vignetting, outer edges of each image were removed. As Mini-MCA consists of six separate channels and the channel images produced are not co-registered with each other, therefore, all channel images were geometrically registered before conversion of DN to surface reflectance (Turner *et al.* 2012).

4.2.6. Radiometric calibration

All corrected images were converted to 10 bit Tagged Image File Format (TIFF). Multiple overlapping images capturing the calibration targets were selected for analysis. Points were generated on a centre point of each radiometric and pseudo calibration target and a boxed buffer was generated over each target. Vectors of overlapped boxes were converted to raster format with pixel size equal to image. Each pixel of overlapped layer was converted to points and each point was used to extract the DN values from multiple images. To compare in situ measurements with imagery, it was found that DN value of every pixel recorded by sensor had a direct relationship with surface reflectance of target. The relationship can be represented by the following simple linear equation.

$$\text{Surface reflectance} = \text{Slop} \times \text{DN} \pm \text{Inetcpet}$$

For ease of analysis, polygon grid was used for extracting image DN values from each calibration and pseudo target for all bands. This polygon grid was used to calculate the statistics of DN values from each target. Therefore, the resulting 40 pixel values of each target (calibration and pseudo) were used to compute the mean DNs of corresponding targets for each image separately. The DN values of multiple images were then plotted against the in situ mean convolved reflectance values at central wavelength of each sensor image. Relationships were computed between the sensor corrected spectral bands generated by the mini-MCA and the corresponding at-surface reflectance measurements. The linear relationship between the DN and reflectance showed y-intercept close to zero. Theoretically, it is the minimum reflectance value which can be recorded by an image sensor. Multiple equations were developed from overlapping images to check the consistency of minimum possible reflectance recoded by sensor.

Moreover, the relationship between calibration targets and pseudo targets were tested by computing multiple equations. Finally, zero reflectance being minimum possible reflectance recorded by the sensor was used as one data point and maximum reflectance point was used as pseudo target point. Prediction equation for each image was developed using resampled spectral and DN values of pseudo target. Sensor measurements were converted into reflectance measurements by applying each linear equation to its corresponding image.

4.2.7. Ground comparison and verification

The overall accuracy of the proposed method was assessed by comparing image driven reflectance values with the field measured reflectance values. Summary statistics were computed to assess the performance of each band with field-measured values. Spectral data of 25 sample plots were collected from ASD spectrometer by using 0.25 m x 0.25 m square frame to compare the performance.

4.3. Results

4.3.1. Calibration target

In this study, five calibration panels and one pseudo target was used to collect the field spectra for the quantification of image DN to surface reflectance. Figure 4.3 shows the spectral reflectance of each calibration panel. The mean reflectance value of each target for each spectral region of sensor waveband was plotted. The results show an increase in reflectance associated with the decrease in grey level. Results of this study showed that white pseudo target represents maximum reflectance whereas; minimum reflectance is covered by dark antracit calibration panel. These two panels covered both the extremes of reflectance and can be used to prepare the prediction equation for each image. Remaining four panels covered the middle portion of spectral reflectance ranging from ~10% to ~60%. The reflectance value of white target was gradual decreasing from 570nm to 800nm wavelength. However, the reflectance of calibration panel remained the same from 570 to 800 nm wavelengths. In contrast, there was a sharp increase in reflectance of cream panel from 530 nm to 570 nm and a slight increase in pearl target from 530 nm to 570 nm.

4.3.2. Prediction equation

The combination of calibration panels and field targets enabled the development of linear relationship between image DN and surface reflectance. Six targets (5 calibration and one pseudo calibration) were used to derive the calibration equation from all

images. Figure 4.4 shows the linear fit and coefficient of determination between image DN and spectral reflectance measured in the field from each calibration target. Results showed statistically significant relationship in all spectral bands. Coefficient of determination R^2 = 0.97 to 0.99 was achieved in all bands, indicating that relationship between the image DN and reflectance is linear. At the wavelengths of 530 nm, 550, 570, 700 and 800 nm, equation showed R^2 = 0.99 and at 670 nm, the equation showed R^2 = 0.97 (Figure 4.4 a, d). The use of pseudo target showed maximum reflectance in all equations ranging from ~0.75% to ~0.85%. This white colour plastic target ensures that predicated reflectance values were interpreted within the limits of the prediction equation. While, dark antracit calibration panel reflectance values covered the lower end of prediction equation ranging from 0.059% to 0.062%. Prediction equation of all images showed that the value of y-intercept was close to zero and thus, can be excluded from calculation (Table 4.2).

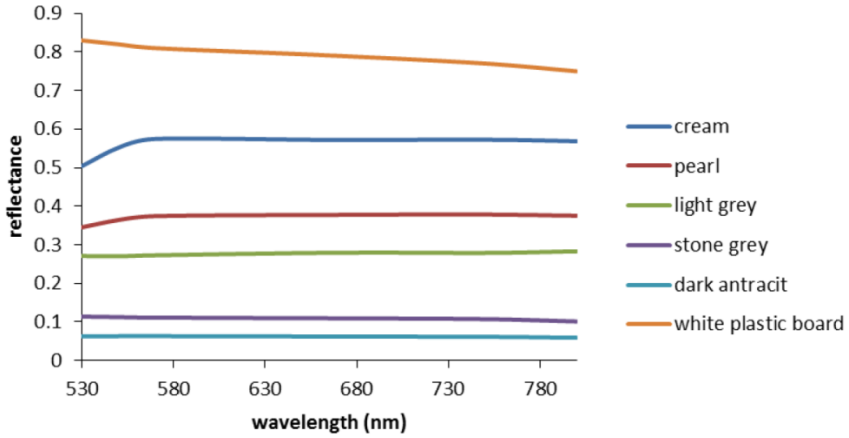

Figure 4.3. Mean spectral signature from 530 to 800 nm of the calibration panels obtained in the field using ASD spectroradiometer.

Table 4.2. Mini-MCA calibration constant (*y*-intercept).

Wavelength	530	550	570	670	750	800
Y-intercept	-0.0307	-0.0203	-0.0048	-0.0306	-0.0098	-0.0561

4.3.3. Simplified prediction equation

Based on six calibration targets, it was found that the relationship between image raw DN and the spectral reflectance values is linear and y-intercept of the prediction equation can be used as a constant parameter for each waveband, which is in accordance with the results of (Del Pozo *et al.* 2014). By considering reflectance of dark target as zero (starting point of equation as zero), only one target was required to cover

the brightest portion of image. This process made the conversion of DN to reflectance easy to adopt. Table 4.3 showed the calibration equation for each single waveband with summary statistics derived from validation targets. The overall RMSE value of each band showed that there was high degree of agreement between the UAS driven reflectance and field measured reflectance for calibration targets.

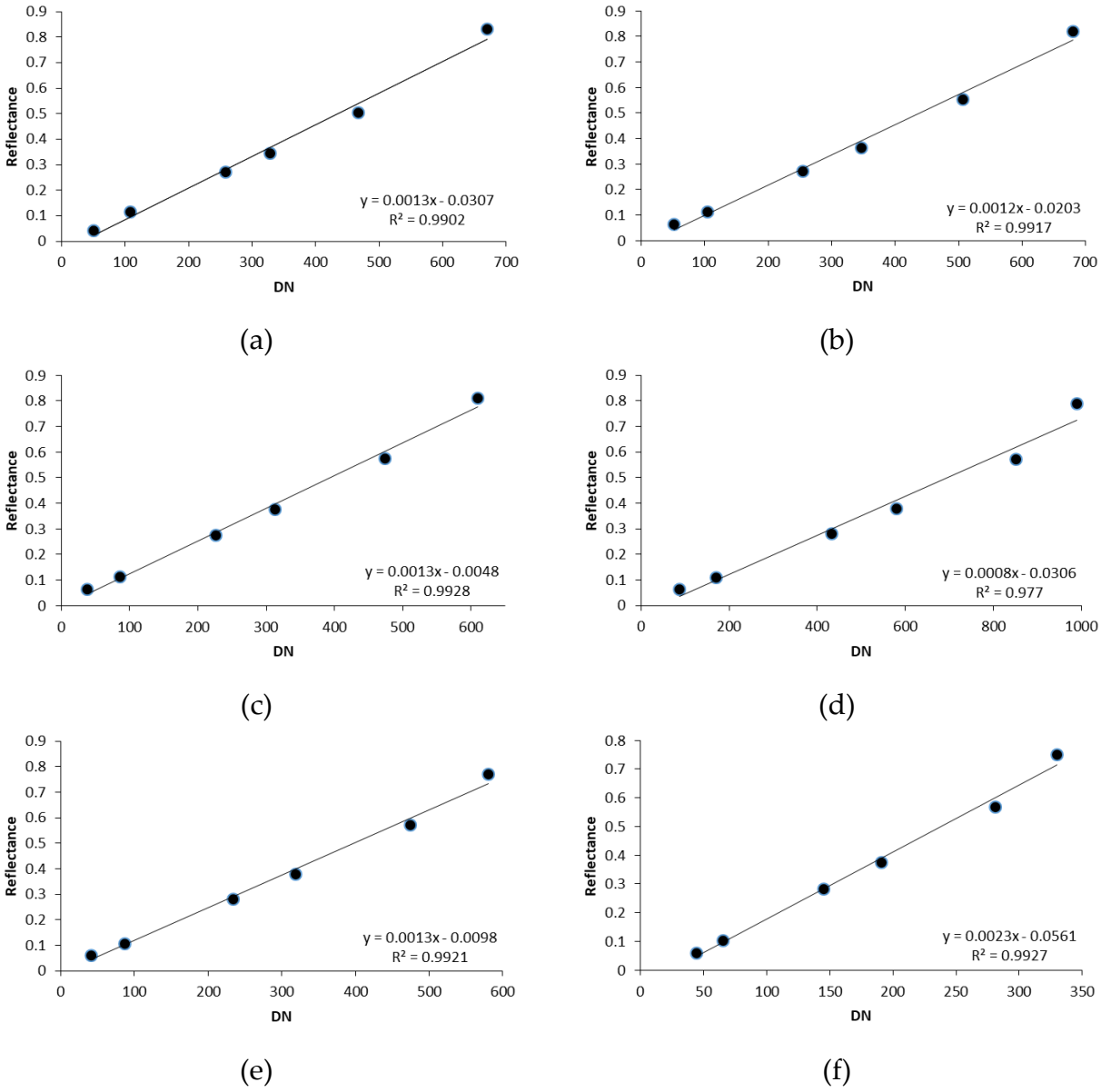

Figure 4.4. Relationship between mean image DN and mean reflectance of the calibration panels for each waveband of Mini-MCA sensor. Each data point represents one calibration target. (a) 530 nm, (b) 550 nm, (c) 570, (d) 670 nm, (e) 700 nm and (f) 800 nm.

Table 4.3. Summary statistics derived from the simplified prediction calibration equation for each waveband of Mini-MCA.

Channel	Simplified prediction equation	RMSE (%)	MAPE (%)
530	$\rho_\gamma = 0.0013 \times DN$	0.063	16.56
550	$\rho_\gamma = 0.0012 \times DN$	0.060	15.56
570	$\rho_\gamma = 0.0013 \times DN$	0.025	7.82
670	$\rho_\gamma = 0.0008 \times DN$	0.064	17.16
750	$\rho_\gamma = 0.0013 \times DN$	0.027	7.72
800	$\rho_\gamma = 0.0023 \times DN$	0.054	29.11

Two out of five bands recorded RMSE values below 0.025%, while 570 nm band recoded the lowest RMSE value 0.025%. The MAPE values of 570 nm and 750 nm bands were also in agreement with the RMSE values of 570 nm and 750 nm bands and showed lowest values of 7.72 and 7.82. The 530 nm, 670 nm and 550 nm bands recorded the highest RMSE values of 0.063, 0.064 and 0.060 % respectively. The RMSE value of 800 nm band was 0.054 %. However, the MAPE value showed that the 800 nm bands recorded highest error in the spectrum.

4.3.4. Surface reflectance comparison

Radiometrically calibrated image driven surface reflectance was compared to field measured reflectance using ASD. The green crop cover showed sharp rise in the surface reflectance values from 700 nm to 800 nm. The comparison of image driven surface reflectance and field measured surface reflectance of green crop is illustrated in Figure 4.5a. The prediction outcomes showed that the image driven results were predicting less reflectance as compared to the ASD reflectance results in all bands. For the 530 nm and 550 nm bands, the surface reflectance values reduced to 0.0114 % in relation to the ASD measurements. In case of 670 nm and 700 nm bands, reflectance reduction was 0.0157% and 0.0063% respectively. Highest underestimation of 0.057% was observed in case of 800 nm band and the least underestimation was observed in 570 nm band with an average reduction of 0.0043%.

The results obtained for diseased and dry vegetation are illustrated in Figure 4.5b. For the 530 nm and 550 nm bands, the surface reflectance values reduced to 0.0025 % and 0.0023 % respectively in relation to the ASD measurement. In case of 670 nm and 700 nm bands, reflectance reduction was 0.0022% and 0.0030%, respectively. Highest underestimation of 0.0110% was observed in case of 800 nm band and the least underestimation was observed in 570 nm band with an average reduction of 0.0019%.

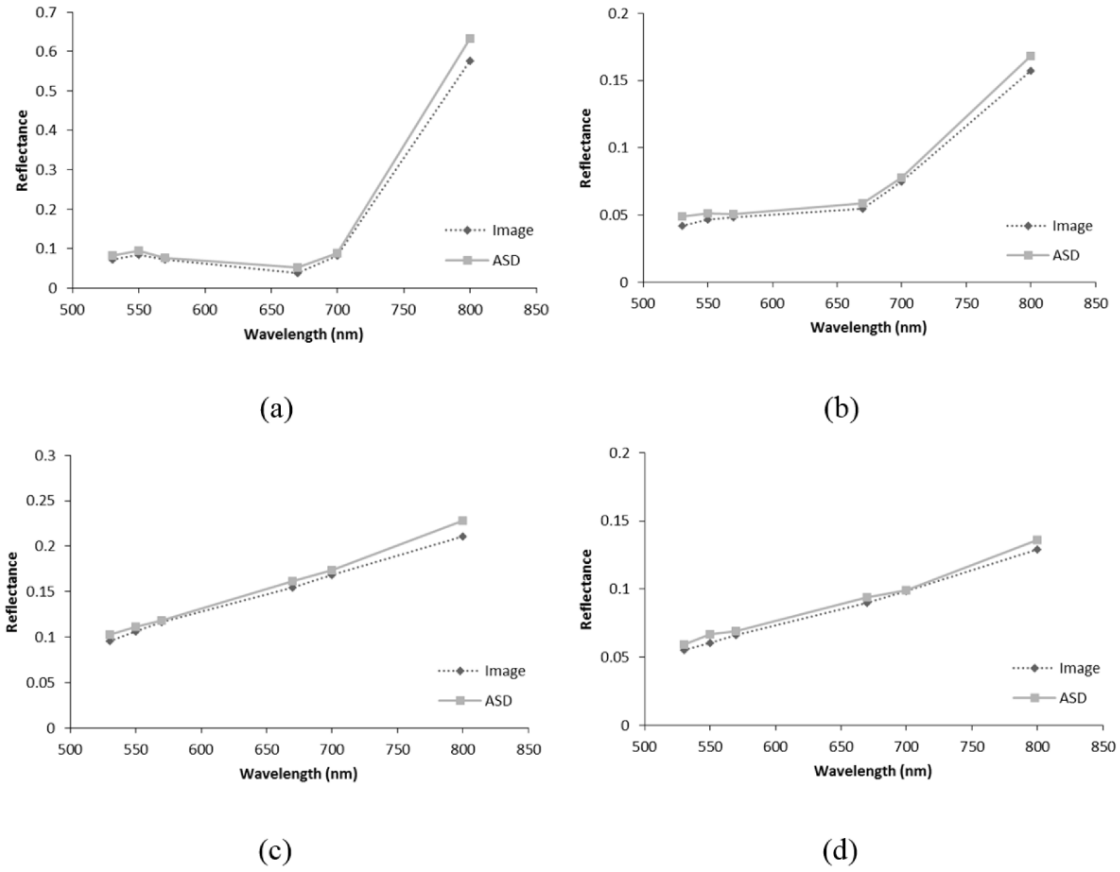

Figure 4.5. Reflectance estimated from ground measurement and UAS data (530, 550, 570, 670, 750 and 800 nm). Each data point represents reflectance values of poppy crop (a), diseased plants (b), dry soil (c) and wet soil (d).

The compression of dry soil reflectance from image and ASD is presented in Figure 4.5c. For the 530 nm and 550 nm bands, the surface reflectance values diminished to 0.0048 % and 0.0032 % respectively. Highest underestimation of 0.0169% was observed in case of 800 nm band and the least underestimation was observed in 570 nm band with an average reduction of 0.0023%. In case of 670 nm and 700 nm bands, reflectance reduction was 0.0062% and 0.0051%, respectively. In case of moist soil, the highest underestimation of 0.0071% was observed in case of 800 nm band and the least underestimation was observed in 700 nm band with an average reduction of 0.0006% (Figure 4.5d). For the 530 nm and 570 nm bands, the surface reflectance values were underestimated to 0.0019 % and 0.0021%, respectively. The reflectance values of 550 nm and 670 nm bands were reduced to 0.0025%.

4.4. Discussion

Real time, fast and accurate processing of UAS imagery is an area of active research and is the future of remote sensing technologies. In this research, the analysis was carried

out to perform radiometric calibration of UAS images. Generally, empirical line method with multiple calibration targets are used to convert raw image DN to surface reflectance, which requires cost intensive calibration panels with lambertian properties (Teillet *et al.* 2007, Miura and Huete 2009, Del Pozo *et al.* 2014, Herrero-Huerta *et al.* 2014). In this study, the empirical line method for radiometric calibration used was unlike the methods used in previous literature (Teillet *et al.* 2007, Miura and Huete 2009, Del Pozo *et al.* 2014, Herrero-Huerta *et al.* 2014).

In case of satellite imagery, satellites are equipped with advanced systems that collect the information on weather and sun illumination conditions and records the metadata corresponding to each image as a header file. Metadata provides the calibration coefficients which help researchers to rectify the data before further processing. Moreover, a large amount of investigation has already been done on satellite data that makes calibration process more standardised, whereas, no standardised process is available for UAS remote sensing. UAS mounted sensor provides cost effective solution to collect the remote sensing data at required time. Although, widely used UAS sensors do not collect illumination specific data, yet advanced UAS sensors are coming with Sunshine Sensors that are capable of collecting illumination condition data and thus, allows to calibrate the data. In this research, the sensor used did not contain data on illumination conditions, thus, the intensity of the ambient light would have varied due to the sky being overcast for some time. Therefore, the amount of reflected light energy from the surface must have altered resulting in error in data accuracy. To cope with illumination variability, accurate calibration is imperative. Studies that have carried out calibration for elimination of errors due to changes in weather and illumination for UAS mounted sensors may not be replicated to other regions due to differences in site conditions. As a standardised method for radiometric calibration of UAS based imagery does not exist, therefore, this study tested an empirical line method using only one pseudo calibration target per image to make the process simpler and replicable without compromising on accuracy. This method uses only one pseudo calibration target per image to build empirical line calibration equations, instead of two or more lambertian calibration targets, which has dramatically simplified the procedure to conduct field campaign. In this study, the results demonstrated the feasibility and usefulness of using pseudo calibration targets (white plastic board) as compared to calibration targets with lambertian properties that are expensive, thus reducing the cost of UAS campaign. This method requires one pseudo target in each image, thus, allowing each image to be rectified with the help of that target resulting in a homogeneous image mosaic.

For the development of an empirical line equation, at least two data points are required. The results achieved showed that the first point for the equation can be considered as zero representing the minimum reflectance detected by the sensor, whereas, the second point can be taken as the reading of one pseudo target. In such case, the slope and DN value of the image can be used to convert DN values to surface reflectance making the process more robust and replicable.

The pseudo target used in this study was found to be highly lambertian, although, it did not provide equal reflectance at different wavelengths (Figure 4.3). Relatively more reflectance was observed in the visible region than the NIR region of the spectrum and gradual decrease in reflectance was observed from 530 nm to 800 nm. Therefore, one calibration equation was required for each band image (n=6). It was assumed that the reflectance of pseudo calibration target does not change abruptly. Moreover, the protocol used to collect the ASD field measurement also allowed to mitigate the changes in reflectance over the time and to minimise the effect of changing illumination condition, whereas, UAS image recorded DNs of a target do change with changing illumination condition. As a result, UAS image acquired in clear and sunny condition could show high DN values and lower DNs in cloudy condition. Similarly, the change in sun angle due to changing seasons also influence the DN values of the image (Wang and Myint 2015). Thus, change in illumination condition alters the slope and offset of empirical line equation, and if implemented elsewhere, would require a new empirical line equation based on field measured reflectance data.

The result of our study demonstrated that the y-intercept value is close to zero and can be taken as the minimum amount of reflected light that can be recorded by each CMOS image sensor (n = 6). Although, y-intercept value can be changed over longer time as it associates to sensor stability (Del Pozo *et al.* 2014, Herrero-Huerta *et al.* 2014). But for this study we considered zero as a first data point and value of pseudo calibration target as a second point to develop empirical line equation (Table 4.3). This allows the derivation of surface reflectance with the RMSE ranging from 0.025 to 0.064 % (Table 4.3). Highest MPAE of 29.11 % was observed in 800 nm band and least MPAE of 7.82 % was observed in 570 nm band. Results obtained from single pseudo target calibration method proves that it can be used as radiometric calibration target, which is in accordance with the results obtained with digital camera (Wang and Myint 2015).

The comparison of calibrated image driven surface reflectance to field measured reflectance showed that each band is underestimating the reflectance in all bands ranging from 0.0169 to 0.0006%. Highest difference was observed in 800 nm band and

least was observed in case of 700 nm band. Relatively less accuracy can be associated to the material used for calibration panel; as white plastic board reflects more light, although, spectral reflectance alters by changing surface roughness and thinness of board (Hoppert and LaPlante 1992, Ham *et al.* 1993, Moroni *et al.* 2015). Plastic materials (Polyethylene Terephthalate, Polycarbonate and Polymethyl Methacrylate) provide almost consistant spectral signatures in visible portion, whereas. Signatures slightly decline at near infrared region (Moroni *et al.* 2015). Moreover, it is associated to sensors sensitivity at far end range at 800 nm where more light passes through filter. The highest error is observed in case of vegetation 0.057% and it is reduced in case of moist soil to 0.0071%. Relatively highest error in case of vegetation reflectance is associated to angular reflectance, crop heterogeneity and difference of scale (Baugh and Groeneveld 2008, Herrero-Huerta *et al.* 2014). Overall the difference of reflectance is very small and can be ignored, thus, it can considered as a step forward for UAS image calibration in accordance with the findings of previous studies (Staben *et al.* 2012, Del Pozo *et al.* 2014, Herrero-Huerta *et al.* 2014, Wang and Myint 2015). Although, proposed method can provide easy and cost effective calibration method and has dramatically simplified the procedure and reduced the field workload, there exist some limitations when implementing for other sensors. Calibration parameters vary for every sensor, and the sensitivity of sensors differ from each other. Thus, the lowest possible reflectance of zero observed with this sensor, may not be measured with other sensors. Therefore, to check the applicability of this method on other sensors, calibration equations for each sensor bands need to be developed using multiple targets and tested with the proposed method before implementation. It is recommended to use white pseudo target as it will cover the maximum possible reflectance. Moreover, the size of a calibration target should be large enough to cover large number of pixel in each target.(Smith and Milton 1999). Overall, proposed methodology is very useful for precision agriculture applications and can assist to calibrate UAS images using single calibration target.

4.5. Conclusion

This paper describes a successful methodology for radiometric calibration using low cost single pseudo target method for each image of a Mini-MCA sensor. The quantitative analysis of field measured and image estimated reflectance confirms the validity of the proposed method. For this purpose, UAS two flight campaigns were conducted over a study area with distributed pseudo and calibration targets for converting DN values to spectral reflectance. Calibration equation derived from radiometric calibration targets was simplified by using two points, first point (y-intercept) zero and second point was used as the DN and reflectance of white pseudo

target. The result achieved from this method provided accurate and cost effective solution for radiometric calibration of UAS based images. Based on the results from this study, it can be concluded that a single pseudo target based calibration method can be used for easy and accurate UAS based image calibration.

4.6. Thesis context

Chapter 4 addressed part of the second objective and described a successful methodology for radiometric calibration using a low-cost single pseudo target approach for images acquired using the 6-band Mini-MCA multispectral UAS sensor. In Chapter 5, the use of multispectral data for estimation of capsule volume will be further investigated.

Chapter 5

5. Poppy crop capsule volume estimation using UAS remote sensing and random forest regression

Chapter 5 described a successful methodology to improve capsule volume estimation results as compared to result presented in chapter 3 by combining structure and spectral derivative analysed using random forest (RF) machine learning approach and has been publication to **International Journal of Applied Earth Observation and Geoinformation** 15th July 2018.

Iqbal, F., Lucieer, A., and Barry, K., 2018, 'Poppy crop capsule volume estimation using UAS remote sensing and random forest regression', **International Journal of Applied Earth Observation and Geoinformation**, 73, 362–373.

Abstract

Improved prediction of poppy capsule volume is essential for optimal management of poppy crop. In order to estimate poppy capsule volume accurately using remotely sensed imagery, the selection of most appropriate models and predictor variables is essential. Multiple spectral indices with random forest (RF) regression were tested to estimate poppy capsule volume using an Unmanned Aircraft System (UAS). Data were collected from field-based physical measurements, in-field spectral measurements and from UAS flights with multispectral sensors over two poppy crops at Cambridge and Sorell in Tasmania, Australia. Field measured spectral signatures were convolved to the multispectral bands of a UAS mounted sensor. These convolved UAS spectral signatures were used to compute multiple spectral indices to develop the RF model, and select optimal model parameters based on root mean squared error (RMSE). In addition, the RF variable importance scores were used to rank the model variables, and to identify the best performing vegetation indices. In Cambridge, an RF model based on convolved UAS spectral signatures predicted capsule volume with an R^2 values ranging from 0.70 to 0.86 from validation and training dataset, respectively, indicating a strong relationship between SVIs and field measured capsule volume. An RF model trained on UAS multispectral data (measure not simulated) resulted an R^2 value of 0.82 based on training data set and an R^2 value of 0.77 with validation dataset. The Cambridge site model parameters and optimal variables were applied to the Sorell data, which showed a significant relationship between measured and predicted capsule volume, with an R^2 value of 0.72. The results showed that the RF model developed using selected variables can help to predict capsule volume 2-3 weeks prior to harvest.

Chapter 5

5.1. Introduction

Poppy (*Papaver Somniferum L*) is one of the few medicinal plants that has been cultivated and used since prehistoric times (Schiff 2002, Shukla *et al.* 2006). It is a plant of the dicot family *Papveraceae*, cultivated for seed, oil and opium. Poppy is a herbaceous plant with an erect stem, with an attractive flower varying in colour according to the variety. At later development stages, flowers develop capsules that contain latex and seeds (Mahdavi-Damghani *et al.* 2010). The latex is located mainly in the capsule walls and is a rich source of around twenty different pharmaceutical alkaloids. These include morphine, codeine, thebaine, narcotine, papaverine, although, its analgesic activities are attributed to morphine and thebaine, the primary alkaloid (Apuya *et al.* 2008). Capsule volume is one of several variables that can predict the alkaloid content (Chung 1987, Yadav *et al.* 2006, Waine *et al.* 2014).

Poppy opium is grown in several parts of the world but the state of Tasmania in Australia is the largest licit producer of poppy opium, supplying up to 40% of the world's opiates used for medicines with morphine and thebaine as the main alkaloid product. Tasmania is a major producer of thebaine and fulfils 90% of the world's demand (Lisson 2007). The island state also accounts for a quarter of the world's morphine and codeine, two older painkillers (Harvest *et al.* 2009). Tasmania produces $60 to $80 million of product a year for opiate painkillers (Frappell 2010). Therefore, the global medicine industry depends on reliable supply of opium poppy from Tasmania and accurate prediction of opium production is important for pharmaceutical industries to fulfil the requirement of the national and international markets. Moreover, yield prediction well before crop maturity enables precision management of input factors (e.g. nutrients, pesticides, irrigation) to enhance the yield outcome. Commonly, farmers and field officers use their experience for yield prediction. Estimations are made based on the practical field knowledge and improved estimations can be made from destructive sampling. However, destructive sampling is time and cost intensive. Thus, reliable information about actual yield potential would be improved with methods that are more accurate.

Several studies have demonstrated the importance of crop growth models to predict yield (Tan and Shibasaki 2003, Steduto *et al.* 2009, Frappell 2010) although, their practical applicability may be limited due to the need of extensive input data. For studies at both global and local scales, satellite remote sensing has been used to monitor crop condition by computing different spectral indices (Saari *et al.* 2011, Baluja *et al.* 2012, Stagakis, Gonzalez-Dugo, *et al.* 2012, Zarco-Tejada, Guillen-Climent, *et al.* 2013,

Waine *et al.* 2014, Brandao *et al.* 2015, Kaur *et al.* 2015). Several studies have demonstrated that crop health can be assessed from biophysical characteristics, such as biomass and crop height (Thenkabail *et al.* 2000, Rufino and Moccia 2005, Ehlert *et al.* 2008, Jaakkola *et al.* 2010, Mäkynen *et al.* 2011, Bendig *et al.* 2014, Iqbal *et al.* 2017). Crop height and biomass are important factors for crop yield estimation and can be predicted using vegetation indices (VIs) (Bernath 1986, Wang *et al.* 1999, Mahdavi-Damghani *et al.* 2010, Jia *et al.* 2011, Bendig *et al.* 2014, Vega *et al.* 2015, Iqbal *et al.* 2017). Many researchers recommended utilisation of precision agriculture technologies to aid in crop management decision-making (Bakhsh *et al.* 2005, Whiting *et al.* 2006, Iqbal and Mehdi 2008). Remote sensing platforms with sensors for measuring crop spectral reflectance offer the opportunity to identify spatial and temporal patterns of crop condition and inform yield estimation (Carbone *et al.* 1996, Dempewolf *et al.* 2014, Waine *et al.* 2014). For example, spectral indices such as NDVI (Normalised Difference Vegetation Index), RVI (Ratio Vegetation Index) and MTVI (modified Triangular Vegetation Index) have been reported to be a significant predictor of corn biomass (Trishchenko *et al.* 2002, Haboudane *et al.* 2004, Van Leeuwen *et al.* 2006, Teillet *et al.* 2007, Zarco-Tejada, Gonzalez-Dugo, *et al.* 2012, Zarco-Tejada, González-Dugo, *et al.* 2012, Cilia *et al.* 2014) and a significant relationship has been found between SAVI (Soil-Adjusted Vegetation Index), MTVI and biomass in rice (Tan and Shibasaki 2003). There have been applications of VIs to estimate crop yield in sugar beet, wheat, barley, poppy and maize (Gitelson *et al.* 2002, Vincini *et al.* 2006, Liu *et al.* 2008, Barati *et al.* 2011, Pradhan *et al.* 2014, Waine *et al.* 2014, Wang *et al.* 2014, Bendig *et al.* 2015, Fang *et al.* 2016, Li *et al.* 2016, Zhou *et al.* 2017). Leaf Area Index (LAI) has been found to be a suitable indicator for estimating opium yield in poppy (Jia *et al.* 2011). Gao et al. 2013 reported that biomass and yield of maize can be estimated by a combination of VIs derived from satellite data and radar polarimetric parameters.

Remote sensing can be categorised into satellite, aerial, low altitude Unmanned Aircraft System (UAS) and field based remote sensing (Zhang and Kovacs 2012). Methods that take advantage of remote sensing, particularly the use of UAS-based campaigns, have demonstrated the potential for precision agriculture by providing higher temporal and spatial resolution, non-destructive, cost effective, and near real-time monitoring for the estimation of crop condition. UAS-mounted multispectral sensors enable acquisition of spectral bands across visible and infrared regions of the electromagnetic spectrum. Spectral bands can be used for the computation of indices to highlight or enhance information contained in spectral signatures, such as plant health and density (Primicerio *et al.* 2012, Zhang and Kovacs 2012, Mulla 2013). Studies have been

published in the past to highlight the potential use of indices derived from UAS platform for crop yield modelling (Liu *et al.* 2006, Berni, Zarco-Tejada, Suarez, *et al.* 2009, Saari *et al.* 2011, Bendig *et al.* 2013, Zhou *et al.* 2017). The use of ultra-high resolution imagery (<10 cm pixel size) from UAS has laid the foundations for site-specific cropping, which supports on-farm decision making according to crop requirements.

UAS remote sensing has the potential to provide cost effective and repetitive techniques for monitoring crop yield. Multispectral data are characterised by multiple wavelengths which allowed computing multiple VIs. In order to predict any feature of interest from these spectral indices a large number of field samples are required to reduce the problem of overfitting, but this is not often possible. Therefore, researchers have explored techniques and methods that could be used to reduce the redundancy and co-linearity in the data without losing the important information to the feature of interest. Some studies used stepwise linear regression techniques for data reduction and variable selection for the application of remote sensing (Kempeneers *et al.* 2006, Abdel-Rahman *et al.* 2013, Vega *et al.* 2015). To improve the feature of interest, prediction accuracy artificial neural network (ANNs) and support vector regression (SVRs) have been used in combination with multiple VIs (Pal and Mather 2005, Wang *et al.* 2016). Multiple linear regression (MLR) methods based on more than two spectral indices have been used in estimating biomass (Bendig *et al.* 2015). However, selection of suitable variables for developing a multiple regression model is often critical. Therefore, a suitable method for identifying the most useful vegetation indices to improve crop yield prediction is required. As an alternative to the empirical approach, machine learning models have been used to estimate crop yield. Researchers have used "ensemble learning" methods that generate many regression trees and aggregate their results. Boosting (Schapire and Singer 1999) of regression trees and bootstrap (Breiman 1996) are well known methods used for feature of interest prediction. Ensemble method random forests (Breiman 2001, Saeed *et al.* 2017) have successfully been used to enhance the crop yield prediction accuracy in the field of agriculture. Random forest is an advanced form of bootstrap method with an additional feature of randomness (Cutler *et al.* 2007, Adam *et al.* 2012, 2014, Qi 2012, Jones and Linder 2015, Jeong *et al.* 2016). Random forest is widely used for feature selection method to reduce the redundancy in the data (Williams 2008, Siroky and others 2009, Jones and Linder 2015). The usefulness of RF techniques has been investigated to predict the crop yield (Abdel-Rahman *et al.* 2013, Jeong *et al.* 2016, Saeed *et al.* 2017). Compared with other variable selection and regression methods such as stepwise regression, the random forest approach performs well when a large number of input variables are analysed to build a model using a small

number of samples for prediction (Prasad *et al.* 2006, Sandri and Zuccolotto 2006). Random forest is a robust method and can handle a large number of input variables as well as an unbalanced data set. The variable importance is a very helpful measure in gaining insight on most useful spectral index for prediction when implemented on high dimensional data (Siroky and others 2009, Jones and Linder 2015).

In this study, we developed RF models using spectral indices derived from convolved to multispectral bands and resulted RF parameters and optimal variables were guided to build a RF model using UAS acquired data. In earlier studies, spectral indices have been used to estimate crop yield (Laughlin *et al.* 1998, Scott *et al.* 2003, Haboudane *et al.* 2004, Jia *et al.* 2011, Waine *et al.* 2014, Saeed *et al.* 2017). NDVI has been reported to be a significant indicator for poppy capsule volume (Waine *et al.* 2014) and significant relationship has been found between LAI and opium yield (Jia *et al.* 2011). Crop height has been found to be a suitable indicator for capsule volume estimation (Iqbal *et al.* 2017). Selected studies have used remote sensing and random forest techniques for crop yield estimation (Abdel-Rahman *et al.* 2013, Jeong *et al.* 2016, Wang *et al.* 2016, Saeed *et al.* 2017), although, none of them have been focused on poppy crops. The spatial coverage of detailed field measurements is often limited; however, UAS remote sensing techniques can help to identify the most important index to predict capsule volume at a much broader scale. Thus, based on our previous study (Iqbal *et al.* 2017) and findings of other researchers (Jia *et al.* 2011, Waine *et al.* 2014) there is need to investigate the combination of SVIs and plant height to estimate poppy capsule volume using RF regression technique. Therefore, the aim of the study is to model the combination of plant height and spectral information based on multi-sensor UAS data to predict poppy capsule volume using RF regression techniques.

5. 2. Material and methods

5.2.1. Study area

This research was conducted in Tasmania, Australia on opium poppy, which was grown for the pharmaceutical industry subject to government licensing. Two different field sites were selected for this study (Figure 5.1). The first study area was a commercial poppy crop located at Cambridge, Tasmania (42°47′50″ S, 147°25′33″ E, altitude 32 m) and the total sown area was ~16 hectares. Poppy seed was sown using seed drills in late July 2014 in a well-cultivated field, with seedling emergence in the following 1-2 weeks. Flowering occurred in November, with capsule formation starting in late December and poppy capsules were harvested in late January 2015.

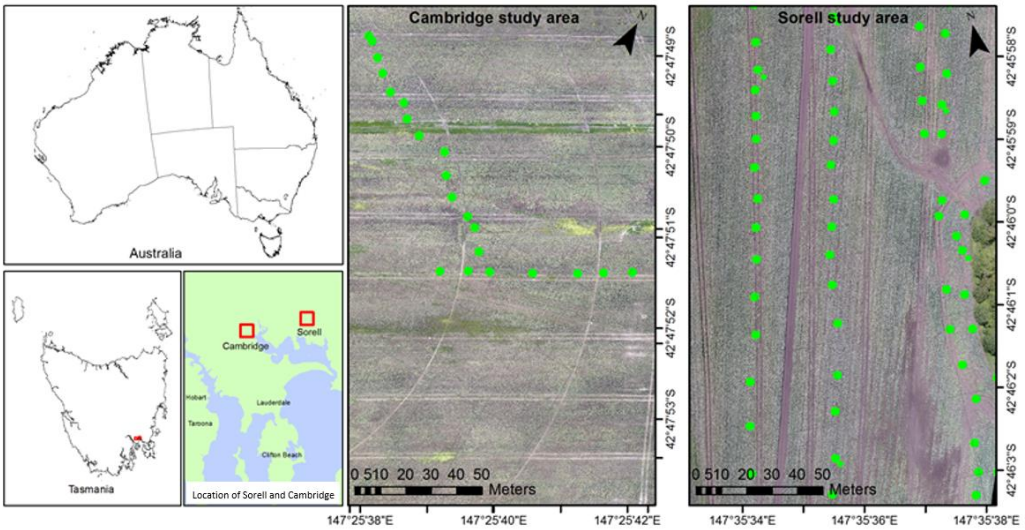

Figure 5.1. The location of the study sites (Cambridge and Sorell) and the field site overview images obtained from unmanned aircraft system (UAS).

The second study area was located in Sorell, Tasmania, Australia (42°45′ 58″S, 147° 35′ 38″E) on commercial opium poppy (Figure 5.1). The poppy crop was sown in mid-July 2016 in a well-cultivated field using a seed drill, with seedling emergence in the following 1-2 weeks. Flowering occurred in early December, with capsule formation starting in late December and poppy capsules were harvested in mid-January 2017.

5.2.2. Field data collection

For the Cambridge site, the field campaign was carried out between 16th December and 22nd December 2014 at the capsule formation stage. This period is characterised as a suitable time for capsule volume estimation (Waine *et al.* 2014, Iqbal *et al.* 2017). Field measurements were conducted from 25 (0.25 x 0.25 m) sample plots, which included the physical measurements of 125 plants (5 plants per plot), which is the same as already outlined (Iqbal *et al.* 2017). The green points in Figure 5.1 represent the location of sample plots. At each sample plot, parameters including the number of capsules, horizontal and vertical dimensions of each capsule were measured using vernier calipers (Iqbal *et al.* 2017). Average capsule volume per plot was then calculated from the physical measurements. For the Sorell site, data collected at capsule formation stage (22nd December 2016) was investigated. Field measurement was conducted from 70 (0.5 m x 0.5 m) sample plots, with capsule volume measured from all capsules. In order to ensure that the size and location of each plot was consistent, wooden pegs were used to mark the southwest corner of each plot location. A PVC quadrant (0.5 m x 0.5 m) was used to confine the plots during field sampling. Moreover, GPS coordinates of each sample plot and Ground Control Points (GCPs) (0.5 m 0.5 m) were measured with

survey-grade dual frequency real-time kinematic (RTK) GPS (2 – 4 cm absolute coordinate accuracy).

5.2.3. Analytical workflow

Figure 5.2 illustrates the methodology used to estimate capsule volume using data computed from convolved and UAS acquired imagery. To develop a RF regression model for capsule volume estimation using spectral indices that are applicable to field conditions, field-based spectral signatures were collected using an ASD HandHeld2 spectroradiometer (explained in section 5.3.1). These spectra were convolved to the spectral resolution of the multispectral UAS sensors to simulate the spectral response for typical UAS surveys. The convolved signatures were used to compute spectral vegetation indices (SVIs). A combination of spectral indices and plant height (measured in chapter 3) (Iqbal *et al.* 2017) was tested using RF to predict the poppy capsule volume. The most optimal RF model developed using field-based spectra were implemented on UAS mini-MCA sensor data (section 5.3.1). The robustness of the model trained on Cambridge data was then tested on the Sorell datasets (section 5.3.2).

5.2.3. Spectral data collection

Spectral measurements of the upper leaves of each plant within each sample plot were obtained using an ASD HandHeld2 spectroradiometer (Analytical Spectral Device, inc., Boulder, co, USA). This is a passive device that depends on solar illumination and acquires the data from 325 nm to 1075 nm at one nm intervals. Reflectance measurements were taken between 12 pm and 2 pm local time under incident light. Calibration measurements were taken with a Spectralon reference panel and dark current after every five minutes, depending on illumination, or after every five spectra. Spectra were taken at a distance of 5 to 8 cm from the target to collect the precise readings of the required plant with sample counts of 15 per observation. For the Cambridge site, one upper leaf per plant within the plot was recorded, whereas for the Sorell site, fifteen of the most dominant leaves per plot were scanned. In either case, reflectance values of each sample plot were averaged to one value for analysis.

5.2.4. Spectral resampling of field based data

For the multiple sensor integration, spectral signals were convolved to the multispectral bands. We used FWHM (Full Width Half Maximum) values and central wavelengths of the TetraCam Mini-MCA bands to resample the reference field measured spectra of crop and radiometric calibration panels using R statistical analysis package prospect-R (R Core Team 2015).

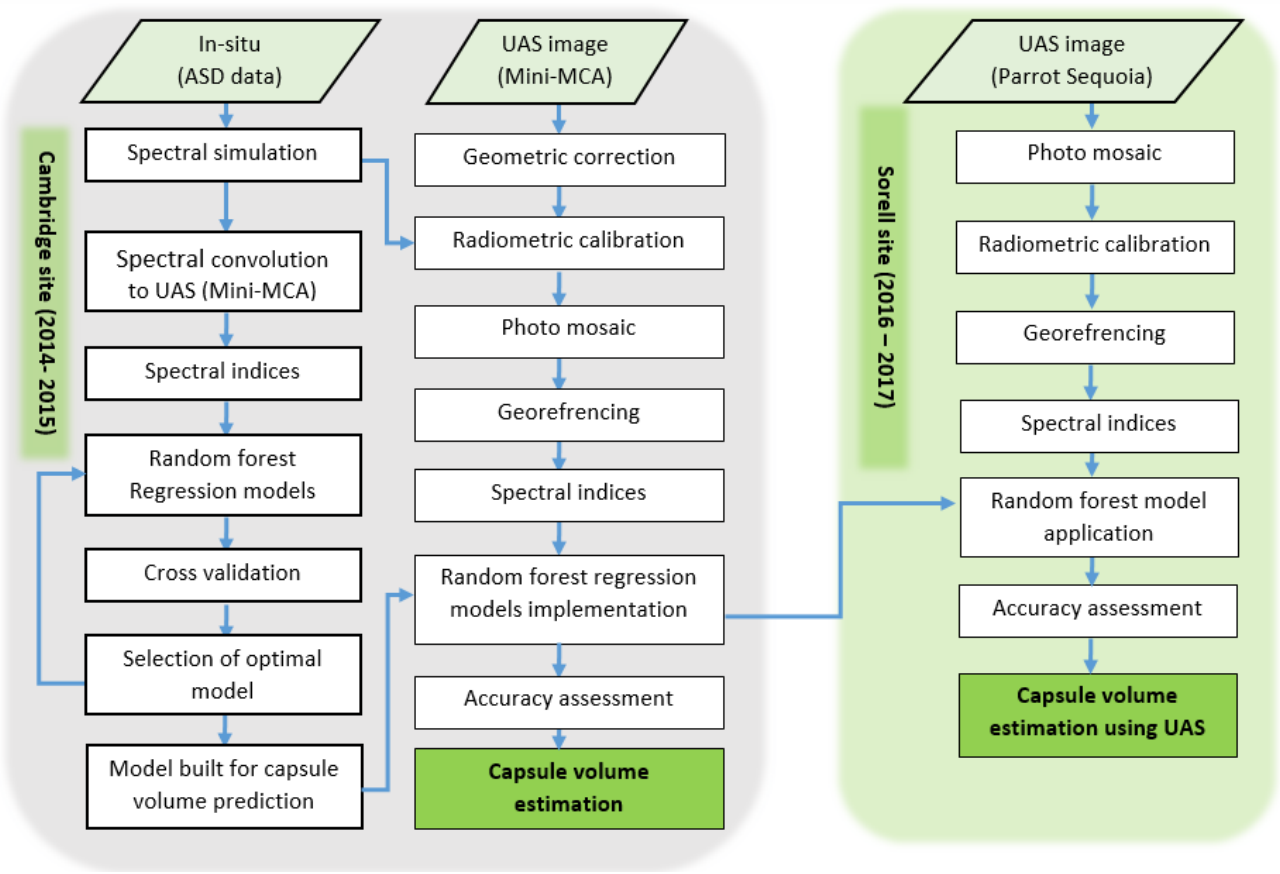

Figure 5.2. Flow diagram of capsule volume estimation model using spectral vegetation indices.

5.2.4. Computation of vegetation indices

A large number of studies have proposed double or multi band spectral indices to estimate crop yield (Table 5.1) and Waine et al. 2014 proved that NDVI is highly correlated with poppy capsule volume. Thus, vegetation indices (VIs) were computed using resampled field data. Average spectral values of each sample plot were used to compute VIs. Computed VIs were used for a random forest regression model to measure the importance of each index to predict capsule volume.

5.2.5. Random forest regression

The Random Forest (RF) regression is a popular machine-learning algorithm that is largely insensitive to noisy data sets and has good predictive capability for high dimensional datasets (Breiman 2001). To model the relationship between VIs, crop height and poppy crop capsule volume, random forest (Breiman 2001) was implemented within the R environment software (R Core Team 2015). RF is commonly used to aid in selection of optimal variables for developing models where there is

a large number of variables and a need to reduce this to a smaller set of most influential variables (Adam *et al.* 2012, 2014). The RF algorithm is bootstrapping method based on the classification and regression tree (CART) that can be used for regression for predicting a continuous response variable. The RF performs recursive partitioning of dataset, and makes no assumptions about the distribution of input data. Random forest regression fits an ensemble of decision tree models to a set of data. The trees are created by extracting a subset of training samples through replacement. This means that the same sample can be selected several times, while the remaining data is not seen at all. For each tree, the data are recursively split into subsamples, which are commonly refers to nodes, in order to improve the predictability of the response variable. Split points are based on values of predictor variables.

Table 5.1. Vegetation indices investigated in this study.

Acronym	Formula	Reference
VARI	(ϱ 550 - ϱ 660) / (ϱ 550 + ϱ 660)	(Gitelson *et al.* 2002)
MCARI	1.2 [2.5(ϱ 790−p660)−1.3(ϱ 790−p550)]	(Haboudane *et al.* 2004)
mTVI	1.2 [1.2(ϱ 790 - ϱ 550)-2.5(ϱ 660 - ϱ 550)]	(Haboudane *et al.* 2004)
NDVI	(ϱ 790 - ϱ 660) / (ϱ 790 + ϱ 660)	(Rouse Jr 1972)
GI	ϱ 550 / ϱ 660	(Zarco-Tejada, Berjón, *et al.* 2005)
RGI	ϱ 660 / ϱ 550	(Zarco-Tejada, Berjón, *et al.* 2005)
RDVI	(ϱ 790 - ϱ 660) / (ϱ 790 + ϱ 660)$^{0.5}$	(Roujean and Breon 1995)
SPVI	0.4[3.7(ϱ 790 - ϱ 660)-1.2|ϱ 550 + ϱ 660|]	(Vincini *et al.* 2006)
OSAVI	1.16(ϱ 790 - ϱ 660)/(ϱ 790 + ϱ 660+0.16)	(Rondeaux *et al.* 1996)
GNDVI	(ϱ 790 - ϱ 550) / (ϱ 790 + ϱ 550)	(Gitelson *et al.* 1996)
MSAVI	[2(ϱ 790 +1-[2* ϱ 790+1)^2-8(ϱ 790 - ϱ 660)$^{0.5}$]/2	(Qi *et al.* 1994)
mSR	(ϱ 790 / ϱ 660 − 1)/ (ϱ 790 / ϱ 660 + 1)$^{0.5}$	(Chen and Cihlar 1996)
NDRE	(ϱ 790 - ϱ 735) / (ϱ 790 + ϱ 735)	(Clevers *et al.* 2002)
EVI	2.5 (ϱ 790 - ϱ 660) / (1+ ϱ 790 + 2.4 x ϱ 670)	(Jiang *et al.* 2008)
TVI	0.5 [120(ϱ 735 - ϱ 550)-200(ϱ 660 + ϱ 550)]	(Broge and Leblanc 2001)
GCI	(ϱ NIR / ϱ green) -1	(Hunt *et al.* 2013)
CVI	(ϱ NIR - ϱ green) / (ϱ red + ϱ green)	(Vincini *et al.* 2008)
DVI	ϱ NIR - ϱ red	(Jordan 1969)
ExR	1.4 ϱ red - ϱ green	(Woebbecke *et al.* 1995)

For this study, 150 random forest models and their variable importance features were utilised to compare relative importance among predictor variables. To find number of trees: (N_{tree}) and number of variables (M_{try}) values that can best predict the poppy capsule volume, the two parameters (M_{try} and N_{tree}) were optimised based on the RMSE The N_{tree} values were tested from 500 to 9500 with 1000 interval. Optimised 'N_{tree}' and 'M_{try}' were tested based on OOB estimate of error (Liaw *et al.* 2002, Adam *et al.* 2012). Optimal parameters were used to generate variable importance.

Variable importance was evaluated based on how much poorer the prediction would be if the data for that predictor were permuted randomly (Prasad *et al.* 2006). The importance of variables were assessed by their impact on the accuracy of predictions, which allows for a quick assessment of the relevance of a predictor for the outcome of interest (Jones and Linder 2015). In this study, percentage increase in mean square error (% IncMSE) was used as a measure for variable importance (Williams 2008). The importance measure shows how much MSE or impurity increases when that variable is randomly permuted or, in other words, how much the model accuracy decreases if we drop that variable. If a variable is randomly permuted and no gain is achieved in the prediction, then there is evidence that removing that measure will substantially degrade predictions; with the converse also true: a high change in % IncMSE indicates an important variable (Prasad *et al.* 2006, Williams 2008, Siroky and others 2009). The difference between the accuracy of the prediction before and after permutation provides the importance of the i^{th} variable for one tree, and the importance for the forest is calculated by averaging trees (Breiman 2001, Sandri and Zuccolotto 2006). While generating the variable importance through random forest, a training sample of 70% (n = 17) was assigned that is called 'in bag' data, whereas a calibration sample of 30% (n = 8) was allocated, and referred to as 'out of bag' (OOB) data for the Cambridge dataset. The OOB sample, which is the set of observations that are not used for building the current tree, is used to estimate the prediction error (OOB error) and then to evaluate variable importance (Williams 2008). As the OOB sample is not used to build trees in the ensemble, therefore, the OOB estimate of error is considered as a reliable form of cross-validation and a good source of prediction accuracy (Breiman 2001, Prasad *et al.* 2006, Siroky and others 2009).

After ranking the predictor variables with RF, the challenge was to select the fewest number of VIs that offer the best prediction and help in the interpretation of the final model. In this regard, variable importance (M_{try}) ranking received from each iteration (K1, K2 …. K10) was added up to obtain the cumulative importance value of each input variable. Finally, the optimal number of M_{try} (top four most important variables) with lowest RMSE was then selected to generate the RF model to predict the capsule volume. To check the consistency and robustness of the model, the dataset was randomly split into 10 equal size subsamples. During each iteration 70% of data was used for training and the remaining 30 % dataset was used for validation. During the 10 iterations (K1 to K10), dataset for validation and training was rotated in such a way that all the data points could be used for training and validation. However, a data point used in training was not used for validation simultaneously in a single iteration (Kohavi and John 1997,

Breiman 2001, Cutler *et al.* 2007, Apuya *et al.* 2008). The performance of training and validation dataset during each iteration was calculated using well-known error statistics to analyse the difference between measured and predicted capsule volume, including RMSE and relative root mean square error. The model generated using convolved to UAS spectral data (convolved from the field measurements) were applied to data derived from UAS multispectral imagery.

5.3. UAS image acquisition and pre-processing

5.3.1. Cambridge site

For the Cambridge site, we used an OktoKopter UAS platform to acquire the imagery (Harwin and Lucieer 2012). An OktoKopter is a multi-rotor platform and has a total take-off weight of 3 kg. This platform has a camera stabilising gimbal that has the capacity to carry a payload of up to 2 kg with flight duration of around 5 to 10 minutes. This platform was controlled with an autopilot and navigation-grade GPS receiver to collect positions and altitude for the camera stations. To capture the multispectral data, a miniature camera array (mini-MCA) developed by Tetracam, Inc., USA was utilised. It consists of an array of six individual channels, each consisting of a CMOS sensor with mountings for interchangeable band-pass filters that provides the data in a dynamic range of 10 bits. The spectral response of image sensors is not uniform through the range with optimum sensitivity (100%) between 750 nm to 800 nm and gradual decrease to 20% at 450 nm in the visible region and 1050 nm in the near-infrared region. Every channel of the mini-MCA sensor has spectral band-pass filter in front of the lense (mini-MCA model 1). Filters with a central wavelength of 530, 550, 570, 670, 700 and 800 nm (with a 10 nm full-width at half maximum, FWHM) were used for this research. Finally, data was captured with ~80% forward overlap and 60% side overlap between images.

The UAS campaign at this site captured 500 images, which required georectification. To reduce the processing load 240 images were selected. Systematic noise and vignetting effect were corrected following (Kelcey and Lucieer 2012). To completely remove the influence of vignetting, the outer edges of every image were removed. After removing the radiometric distortion, images were geometrically corrected to remove the lens distortion effect (Turner *et al.* 2012, 2014). In this study, the empirical line approach was used to convert image Digital Numbers (DN) to surface reflectance (Iqbal *et al.* 2018). To ensure the geo-referencing accuracy of images, survey-grade dual frequency GPS receivers were used for a survey of the GCPs. Photo targets of 0.5 m x 0.5 m were distributed in the field to be used as GCPs for geo-referencing (Harwin and Lucieer

2012). The orthophoto of the field was generated by mosaicking all images in ENVI software.

5.3.2. Sorell site

Data was acquired using a 4-band multispectral MicaSense/Parrot Sequoia" sensor, mounted on a 3DR Solo quadcopter (3D Robotics, Inc, city of supplier). The sensor had a spectral range of 530 to 810 nm with a spectral resolution of 40 nm. The Sequoia sensor contains an RGB 16 megapixel sensor (4608 × 3456 pixel) with four single band sensors; the green band is sensitive to the reflected energy in the 530–570 nm region, red band records the reflectance in the 640–680 nm spectral band, while the red edge is a very narrow band covers the portion of 730–740 nm and captures the rapid change from low red reflectance to near infrared reflectance. The fourth band corresponds to the near infrared portion of spectral wavelength 770 nm to 810 nm. The spectral sensitivity of image sensors provides optimum sensitivity of 70% in the green band and gradual decrease to 55% at 650 nm, 35% at 730 nm and 30% around 800 nm in near-infrared. The sensor has a built-in GNSS and IMU for positioning and orientation. Moreover, it operates with an irradiance sensor, which allows self-calibration of spectral bands and provides good quality spectral reflectance values. The sensitivity of the irradiance sensor is 98% in the red region and 82% to 84% in the near-infrared, red edge and green regions.

The UAS campaign was conducted under clear sky and low wind conditions between 12:00 pm and 2:00 pm local time. The Tower app was used for flight planning and automated flight with 75% side overlap, flight speed of 2.5 m/s and altitude of 50 m AGL. The Sequoia was set to capture one image every second (1 Hz). For spectral calibration, pre- and post-flight images of a spectral calibration target were collected. Tower mobile application was connected with 3DR solo controller and mission was planned. After finalising mission, it was uploaded to 3DR solo to fly over the field while the under-mounted multispectral sensor captured the images of the ground. Acquired imagery containing orientation and locational information of each camera with photos taken from calibration targets were uploaded to micasense atlas to generate the orthophotos. Finally, radiometric calibration was performed using empirical line approach to convert image Digital Numbers (DN) to surface reflectance (Smith and Milton 1999, Moran *et al.* 2001, Karpouzli and Malthus 2003, Baugh and Groeneveld 2008, Staben *et al.* 2012, Iqbal *et al.* 2018).

5.3.3 Extracting image spectra and computation of vegetation indices

A point map of the sample plots was developed using DGPS surveyed data. The square buffer was generated around each sample plot point to create a region for each sample plot. These buffers were overlayed on the UAS mosaicked image to extract pixel values of the image from each sample plot with an area of (0.25 × 0.25 m). To make sure the spectra were collected only from sample plot area, the pixels that entirely fell within the blocks were included in the spectral dataset, while the pixels that partially fell inside each plot were discarded. Zonal statistics were computed using ArcGIS 10.3 from a raster file for a given set of plots. Thus, extracted spectral values were averaged for each sample plot by considering all pixel values within a plot. Finally, vegetation indices (VIs) values computed from each sample plots were used as an input for RF model. Similarly, the data of the Sorell site were extracted using sample plots of 0.5 × 0.5 m to compute comparable spectral indices and used to test the robustness of the random forest model developed from Cambridge site.

5.3.4. Accuracy assessment

Capsule volume, estimated from the optimal random forest model with data from the Cambridge site, was compared to the reference measurements on the ground to assess the accuracy. The error was calculated as the difference between actual and measured capsule volume. The RMSE of the errors was calculated along with the regression fit, expressed as the R^2 between measured and estimated capsule volume. Moreover, UAS-based models developed from the Cambridge site were evaluated at the Sorell site and the predicted capsule volumes were compared with field measured data.

5.5. Results

5.5.1. Model results and accuracy assessment

The results of random forest parameters (M_{try} and N_{tree}) are shown in Figure 5.3. The optimisation was done based on the RMSE of the calibration datasets (n = 17). Results indicate that RF parameters affect the prediction accuracy. As shown in Table 5.2, the tuning parameters were set and determined. Overall, the high number of N_{tree} and the combination of more variables increase the prediction accuracy. After reaching maximum accuracy point, results become stabilised and nominal improvement is illustrated in prediction accuracy. Figure 5.3 indicates that 500 N_{tree} with 4 M_{try} provides optimal results and yield predictions with the lowest RMSE (24.2 cm^3). Moreover, the second most optimal results were observed at 500 N_{tree} with 4 variables.

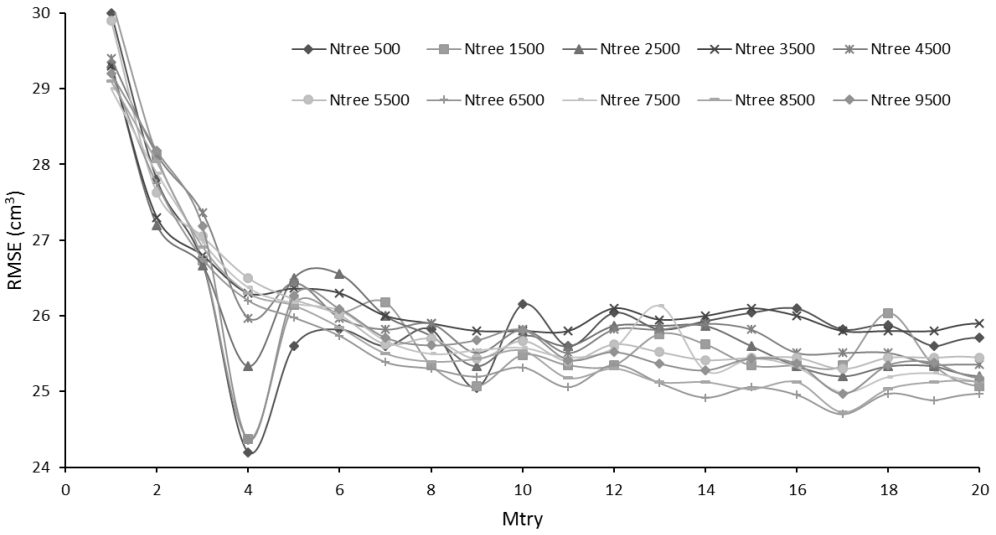

Figure 5.3. Optimization of random forest parameters (N_{tree} and M_{try}) using RMSE.

Table 5.2. Tuning parameters and settings of Random Forest regression model

Parameters	Parameter range	Interval	Optimal setting
N_{tree}	500-9500	1000	500
M_{try}	1-20	1	4

5.5.2. Variables importance at optimal N_{tree} and M_{try}

Using RF model with 500 trees, the importance of the contribution of each variable to predict the capsule volume was computed using a 10-fold cross-validation method. The mean decrease in accuracy displayed in Figure 5.4 is the contribution of each variable to the regression model generated by SVIs and plant height. Variables that have high mean decrease accuracy value are considered to be more important for model prediction accuracy. According to the mean decrease in accuracy, the most relevant variables in the RF model were NDVI, SR, mTVI, RDVI, VARI, EVI and GI. In contrast, plant height was found to provide a minor contribution to the model as compared to SVIs. The combination of SVIs overrides the importance of plant height. In general, NDVI and SR contributed significantly to increase the prediction accuracy during each iteration and has been ranked among top four variables in this research. Finally, the OOB estimates of error were used to measure the importance of each variable. Ten important variables were shown in Figure 5.4 by their importance in estimating capsule volume. The four most important SVIs (NDVI, SR, mTVI and RDVI) in predicting opium capsule volume were used for further analysis.

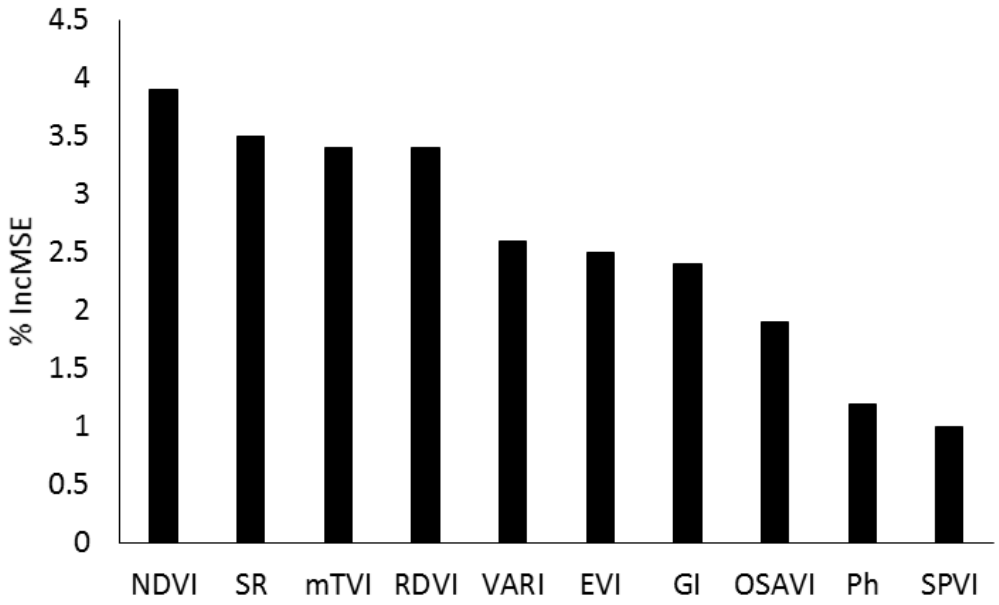

Figure 5.4. Importance of 10 variables representing mean decrease accuracy values of optimal Random Forest regression model.

5.5.3. Predictive performance of the model using selected variables using convolved data

The best performing RF model developed using NDVI, mTVI, SR and RDVI was used to estimate capsule volume. Performance based on training (n =17) and validation (n = 7) data were determined by average 10-fold cross validation RMSE. As shown in Table 5.4, the RMSE was achieved from training data ranging from 15.60 cm^3 (10.27 %) to 18.80 cm^3 (12.38 %) with an average RMSE of 17.49 cm^3 (11.56 %), whereas, RMSE based on validation dataset was found to be ranging from 17.90 cm^3 (12.19 %) to 35.82 cm^3 (24.39 %) with an average RMSE of 25.63 cm^3 (17. 45 %).

The results showed (Table 5.3 and Figure 5.5) a slight underestimation of capsule volume in validation datasets, whereas, minor overestimation was observed based on training dataset. In both datasets, the difference of measured vs predicted mean capsule volume is less than one percent. The difference between measured and predicted capsule volume of smaller capsules based on the training dataset showed an overestimation of 20 % (14.57 cm^3), and 1.14 % (2.72 cm^3) in case of multiple capsules. In contrast, the OOB dataset showed an underestimation of 10.25 % (7.43 cm^3) for smaller capsule volume and 9.31 % (22.11 cm^3) for larger and multiple capsules per plot. Figure 5.5 shows the scatter plot and coefficient of determination between measured and predicted capsule volume achieved from 10-fold of training and validation datasets. The results are highly significant with R^2 of 0.86 for training and 0.70 for validation data.

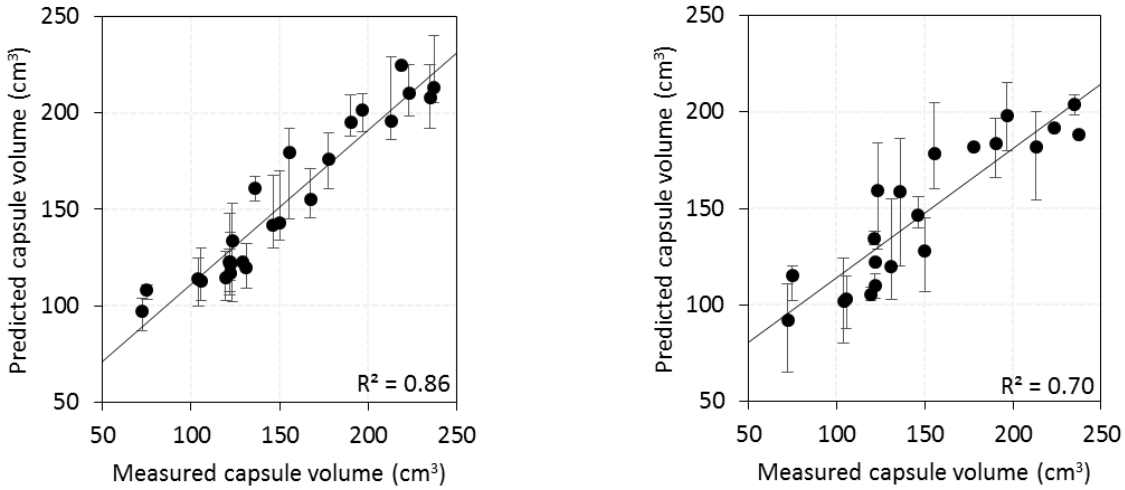

(a) **(b)**

Figure 5.5. Scatter plot between measured and predicted capsule volume: (a) training data; and (b) validation data.

Table 5.3. Measured and predicted capsule volume (cm^3) using simulated Mini-MCA data.

	Training		**Validation**	
	Measured (cm^3)	Predicted (cm^3)	Measured (cm^3)	Predicted (cm^3)
Min	72.43	87.00	72.43	65.00
Median	136.10	141.47	146.43	145.00
Mean	151.76	151.71	146.82	146.75
Max	237.28	240.00	237.28	215.17

Table 5.4. Regression model fitting statistics calculated with 10 random subsets for estimating poppy capsule volume. R^2 = coefficient of determination; with $p < 0.0001$; RMSE = root mean squared error.

Model	**RMSE** (cm^3)										**Avg. RMSE**
	1	2	3	4	5	6	7	8	9	10	
Training	16.75	18.31	18.74	17.61	17.20	**18.47**	16.86	**15.60**	18.80	16.56	17.49
validation	24.92	30.35	19.26	**35.82**	**17.90**	29.40	19.93	28.51	23.22	27.00	25.63

5.5.4. Capsule volume estimation using UAS data of Cambridge site

The random forest model using selected variables was implemented on UAS acquired image derived SVIs. Similar to the RF results from the convolved field spectra, the highest R^2 (0.82) was achieved using a combination of four SVIs with RMSE was found ranging from 15.06 cm^3 (9.94 %) to 23.10 cm^3 (15.25 %) and an average RMSE of 19.39 cm^3 (12.80 %) (Table 5.5 and Figure 5.6). Implementation of RF model on the validation datasets showed coefficient of determination of 0.77 with RMSE ranging from 10.12 cm^3

(6.69 %) to 35.80 cm³ (21.71 %). Overall, an RMSE of 26.85 cm³ (17.77 %) was achieved using validation dataset.

Table 5.5. Regression model fitting statistics calculated with 10 random subsets for estimating poppy capsule volume. R^2 = coefficient of determination; with $p < 0.0001$; RMSE = root mean squared error.

Model	**RMSE** (cm³)										**Avg. RMSE**
	1	2	3	4	5	6	7	8	9	10	
Training	15.41	**15.06**	18.16	22.40	20.18	**23.10**	19.95	20.90	19.65	19.18	19.39
validation	**35.80**	34.20	31.40	22.27	31.36	**10.12**	20.21	26.26	29.86	27.05	26.85

Table 5.6 illustrates that the difference of measured vs predicted mean capsule volume is quite small. In the analysis based on training datasets, the difference between measured and predicted capsule volume of plots with smaller and fewer capsules revealed an overestimation of 27.87 % (20.19 cm³), and an underestimation of 8.20 % (19.47 cm³) in case of plots with multiple and bigger capsules. In contrast, the OOB dataset showed an overestimation of 43.00 % (31.52 cm³) for smaller capsule volume and an underestimation of 10.09 % (23.95 cm³) for larger and multiple capsules per plot.

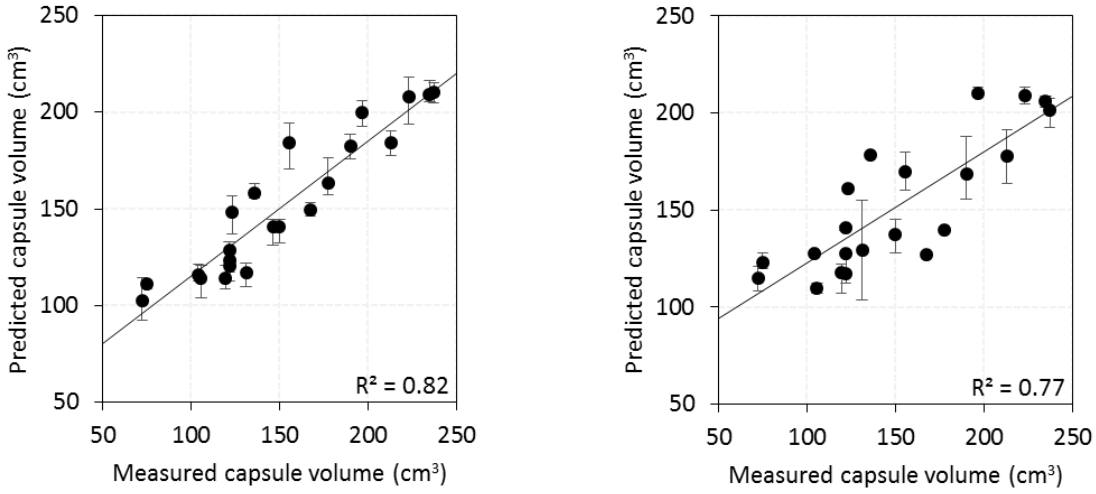

(a) (b)

Figure 5.6. Scatter plot between measured and predicted capsule volume: (a) training data; and (b) validation data.

5.5.5. Model validation on Sorell site

In addition to model performance with convolved and UAS driven dataset from the Cambridge site, examination of model performance was tested across the farms as well. However, RF can only predict the range of values used in the training dataset to grow

regression tree and thus it was not possible to implement the Cambridge site model on Sorell site data due to the difference in sample plot size. Thus, the RF model parameters (N_{tree} and M_{try}) achieved from Cambridge site were used to train and test the model based on Sorell dataset. Tables 5.7 shows that the RMSE value of training and validation dataset ranges from 62.72 cm^3 (15.97 %) to 96.16 cm^3 (24.49 %) and 77.00 cm^3 (20.72 %) to 111.70 cm^3 (30.00 %), respectively.

Table 5.6. Measured and estimated capsule volume (cm^3) using Mini-MCA data acquired from Cambridge site.

	Training		Validation	
	Measured (cm^3)	Predicted (cm^3)	Measured (cm^3)	Predicted (cm^3)
Min	72.43	92.62	72.43	103.95
Median	146.43	145.34	133.66	141.29
Mean	151.44	151.59	151.08	152.39
Max	237.28	217.81	237.28	213.33

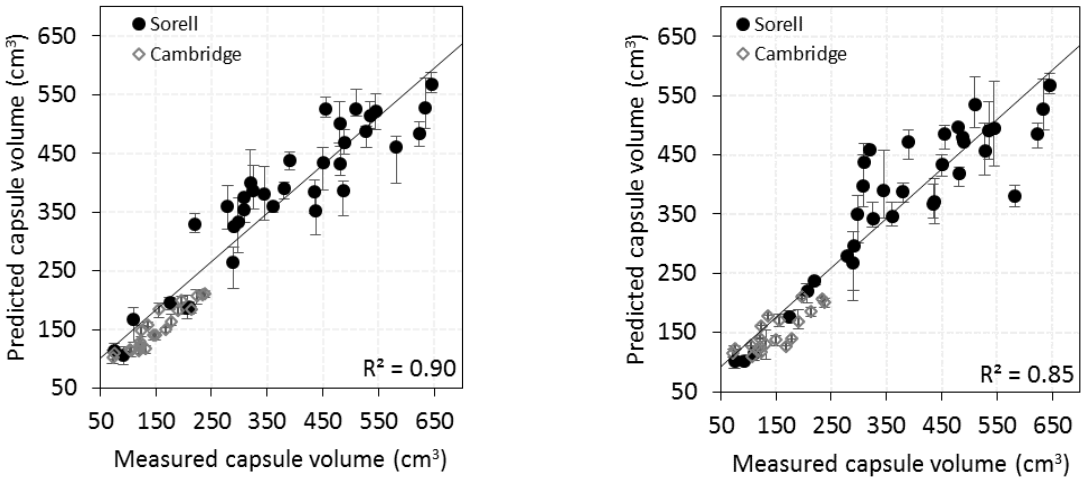

(a) (b)

Figure 5.7. Scatter plot between measured and predicted capsule volume: (a) training data; and (b) validation data.

Overall, an average RMSE of 72.85 cm^3 (18.85 %) and 96.50 cm^3 (25.70 %) was found for training and validation datasets respectively. The difference between measured and predicted capsule volume showed an overestimation of 20.00 % (15.00 cm^3) in lower volume plots, and an underestimation of 8.88 % (57.32 cm^3) in higher capsule volume plots. In contrast, the validation dataset showed an overestimation of 20.00 % (15.00 cm^3) for smaller capsule volume and an underestimation of 10.07 % (65.00 cm^3) for larger and multiple capsules per plot. Significant relationships between measured and estimated capsule volume was observed based on Sorell data with an R^2 of 0.84 for

training and 0.80 for validation dataset. To check the applicability of inter site models, results of both sites were combined (Figure 5.7). Combined training data of both sites showed similar trend and improved the coefficient of determination from 0.82 to 0.90. Similarly, the combined plots of both sites improved the coefficient of determination of validation dataset from 0.77 to 0.85. Figure 5.8 illustrates the robustness of the optimal models. Coefficient of determination of 0.72 with relative error of 26.25 % is achieved by implementing the Cambridge site model on Sorell data, for this analysis the capsule volume of each sample plot for Sorell site was divided by four to make it comparable to Cambridge sample plot range.

Table 5.7. Regression model fitting statistics calculated with 10 random subsets for estimating poppy capsule volume. R^2 = coefficient of determination; with $p < 0.0001$; RMSE = root mean squared error.

Model	**RMSE** (cm^3)										**Avg. RMSE**
	1	2	3	4	5	6	7	8	9	10	
Training	96.16	65.51	65.77	62.72	73.85	71.33	72.76	74.57	71.93	73.92	72.85
validation	111.7	101.6	103	92.9	77.00	78.70	101.3	99.95	98.95	99.95	96.50

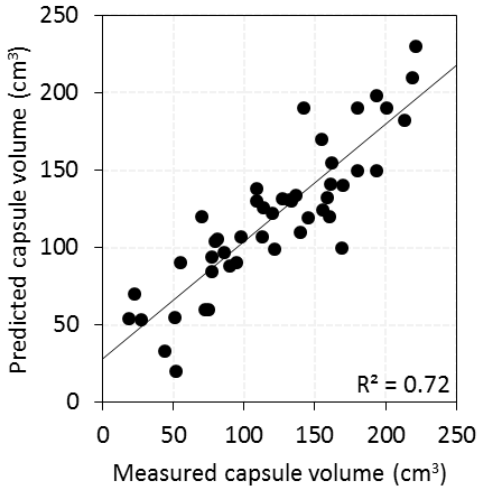

Figure 5.8. Scatter plot between capsule volume measured and predicted from Sorell site.

5.6. Discussion

In this research, the analysis was carried out to estimate capsule volume from SVIs computed at capsule formation stage. Nowadays, the real-time prediction of crop yield is an area of active research. Different SVIs have been investigated to estimate crop yield

in sugar beet, wheat, barley, poppy and maize (Gitelson *et al.* 2002, Vincini *et al.* 2006, Liu *et al.* 2008, Barati *et al.* 2011, Pradhan *et al.* 2014, Waine *et al.* 2014, Wang *et al.* 2014, Bendig *et al.* 2015, Fang *et al.* 2016, Li *et al.* 2016, Zhou *et al.* 2017). Multiple SVIs have been proposed for crop yield estimation. Compared to studies investigating field based proximal sensing to estimate biophysical crop parameters, the studies using UAS image provides detailed spatial data. Several studies tested ground based and fixed sensors as a real time proximal sensing system for resource management. They related either the vegetation index with LAI, biomass and yield (Jia *et al.* 2011, Waine *et al.* 2014, Wang *et al.* 2014, Zhou *et al.* 2017) and reported R^2 value of 0.75 to 0.87 for yield (Zhou *et al.* 2017). In this study, the results demonstrated the feasibility and usefulness of convolved leaf spectral reflectance in the visible and near-infrared region for poppy capsule volume estimation. Field based leaf spectral data collected three weeks prior to harvesting was spectrally convolved to simulate UAS mounted Mini-MCA sensor data using FWHM and central wavelength of each band. The vegetation index values of convolved to Mini-MCA sensor data were used to build RF regression models to estimate capsule volume. Variable importance achieved from RF showed that the SVIs with the combination of visible and NIR bands are ranked on top and showed maximum influence to predict capsule volume, as reported previously (Waine *et al.* 2014). SVIs in combination with NIR and visible bands have been reported as the most significant for estimating crop yield (Waine *et al.* 2014, Saeed *et al.* 2017). However, the significance of SVIs to demonstrate the yield prediction varies during growth stages (Aparicio *et al.* 2000). At early growth stage (before flowering), there is more absorption of light in the visible region because of the higher amount of photosynthetically active plant tissues, but plants reflect more light in NIR region. Although, at capsule formation stage when plant tissues mature, there is increase in reflectance of visible light and decrease in reflectance of NIR. Therefore, SVIs with the combination of NIR and visible bands showed the decrease in index value near maturity because of senescence of leaves. Importance of SVIs to predict capsule volume can also be related to spatial variability of irrigation application. Normally, irrigation is stopped around the end of December which causes reduction of green leaf area and start of leaf senescence, resulting in lower index value. On the other hand, irrigation until leaf senescence increases end yield by 5-20 kg/ha (Mahdavi-Damghani *et al.* 2010). Thus, the importance of RF variable can be associated to field management and leaf senescence (Chung 1987, Mahdavi-Damghani *et al.* 2010). Sample plot distribution indicates that the area under water stress showed that lower index value represent lower capsule volumes, whereas, higher index values represent bigger and multiple capsules. Moreover, variable importance showed that the use of a combination of four SVIs with RF model enhanced

the prediction accuracy as compared to the use of plant height only (Iqbal *et al.* 2017). The importance of plant height is reduced by the combination of SVIs. It can be associated to the crop biomass (Leaf fractional cover, LAI and plant height) which is also related to NDVI (Haboudane *et al.* 2004) and mTVI suitable to predict chlorophyll contents of crop (Zarco-Tejada, Gonzalez-Dugo, *et al.* 2012). This means, horizontal spread of green leaves is a more important variable to predict capsule volume as compared to vertical growth.

The main objective of this study was to employ accurate and robust RF machine-learning algorithm to accurately estimate opium capsule volume. Some of the spectral vegetation indices in this study are correlated but the RF model is insensitive to collinearity (Wang *et al.* 2016), which is very valuable in predictive modelling. In case of higher number of correlated variables, where it becomes difficult to decide which variable to remove, the RF algorithm has the ability to rank them based on their importance, thus making it easy to remove less important variables (Adam *et al.* 2012). The RF model developed using selected variables (NDVI, SR, mTVI and RDVI) provide an average relative error of 11.56 % based on training dataset, whereas, average relative error of 17. 45 % was observed using validation dataset. Overall, the model developed using the spectrally convolved dataset explained 83.65 % to 88.44% variation of capsule volume and showed significant relation between measured and estimated capsule volume (Figure 5.5). Higher prediction accuracy of training data is associated to higher number of sample points included for training, whereas relatively lower accuracy is observed using validation dataset with fewer sample points, which is in accordance with the results of previous studies (Adam *et al.* 2012, Jeong *et al.* 2016, Wang *et al.* 2016, Saeed *et al.* 2017). Moreover, by eliminating the data point from water stressed plot (results not shown, as the focus of this study was not irrigation, therefore, detailed plant water stress data was not collected), higher accuracy is observed.

The RF model generated using calibration data were trained and tested using UAS driven SVIs. Results from UAS data were similar to spectrally convolved field data with highest R^2 = 0.82 and an average relative error of 12.80 %, whereas, R^2 = 0.77 with relative error of 17.77 % was observed using validation dataset. The performance of training dataset is reduced as compared to simulated data as UAS based training dataset is associated to radiometric and geometric calibration factors, such as atmospheric variables, solar and observational geometries and spatial resolution (Trishchenko *et al.* 2002, Van Leeuwen *et al.* 2006, Teillet *et al.* 2007), thus contributing to the lower accuracy of training dataset. Similarly, as the field data represents the spectral values of poppy leaves, whereas UAS driven data represents canopy scale spectral data,

which is a combination of leaves, capsules and background, thus reducing the prediction accuracy of a UAS driven dataset. To check the consistency and robustness of RF models based on data from the Cambridge site, selected variables were used to train and test the model on Sorell site. As the size of Sorell site sample plots was four times larger than Cambridge site sample plots, a separate model was trained and tested based on Sorell data. Overall, the average relative error of 18.85 % and 25.70 % were observed for training and validation dataset respectively, which is relatively less accurate as compared to Cambridge data. Relatively lower accuracy may be associated with different genotype, variability in soil moisture content and variation in crop stage that alters the model performance. There exists a varying photosynthetic activity at different crop stages, thus depicting change in spectral reflectance values as well as index values, in turn resulting in varied model performance. Overall, the accuracy of 74.30 % to 81.15 % can be achieved with the RF developed based on selected variables to predict poppy capsule volume.

In general, RF only uses the values included in training dataset to grow regression tree and thus it is not possible to predict beyond the training data range as RF has an inherited inability to extrapolate to the data range where no training data has been used. Therefore, predicting capsule volume from other sites where capsule volume range is beyond the range of training dataset is not possible, in accordance with previous study (Jeong *et al.* 2016). Hence, to check the performance of the model, results of Cambridge and Sorell were combined (Figure 5.7) to see the influence of data range limits. Points from Cambridge data only covered the lower limits of data, whereas, combined data from Cambridge and Sorell sites covered a larger range of data limits that enhanced the coefficient of determination, which was observed to be 0.90 and 0.85 for predicted and estimated values of training and validation data, respectively. Therefore, model accuracy can be improved by using training data covering a wider range of more critical variables (lower limit and upper limit). To compare the UAS data driven RF model, data of Sorell sample plots were divided into four subplots to make it comparable to Cambridge data and RF model developed from Cambridge were implemented to Sorell site. Results showed a coefficient of determination of 0.72 with an RMSE of 36 cm^3, relative error of 26.25%, which is in accordance with the model tested and implemented on Sorell data. Overall, the results showed a higher agreement between measured and predicted capsule volume using RF regression model. To improve the model prediction for future research, the balance of the variable distribution needs to be considered. The number of positive and negative responses in the model training data is unbalanced and causes false estimation (Breiman 2001).

Higher number of data points for training sample can minimise the issue of over and under estimation. Moreover, the simulated data from leaves spectra provides higher accuracy based on training data as compared to the performance of UAS driven model. Therefore, size and structural information of canopy needs to be investigated (Jia *et al.* 2011). The analysis of Jia *et al.* (2011) found a good correlation between opium yield and LAI using field measurements at hook, flowering and harvesting stage. Therefore, spatial extent of vegetation cover over different growth stages can improve the model accuracy.

The model for estimation of poppy capsule volume used in this study is developed using capsule formation stage data. Ideally, predicting capsule volume could be based on data of earlier stages, which would require training the model based on early stage data. In addition to this, several factors can influence the variable importance for estimating capsule volume. These factors include mainly the genotype of crop and environmental factors. This implies that model calibration will be required based on field survey data for a new study site. In addition, this study predicted the capsule volume of summer crop only, however, in other parts of the world, poppy is sown in winter, thus, the difference of prediction conditions need to be reconciled by quantifying the effect of weather and genotype. In Tasmania, the world's largest licit producer of opioids, continuous research and development aims to use genetically improved crops obtain higher yields, thus, the applicability of developed models would need to be investigated on new varieties as they are used. Overall, the combination of NDVI, SR, mTVI and RDVI can provide significant information about potential and predicted crop yield, which can be used to inform precision decision-making on-farm.

5.7. Conclusion

This study investigated the opportunity to enhance the utility and accuracy of UAS driven data to estimate poppy capsule volume using random forest (RF) machine learning approach. We used field based spectroscopy data to convolve to UAS based Mini-MCA sensor data. Convolved data was used to compute spectral vegetation indices (SVIs) and combination of SVIs and plant height measured from UAS remote sensing (chapter 3) were used to develop a random forest (RF) model. The optimal number of trees lowest RMSE value was used to rank the variable importance to predict poppy capsule volume. Finally, optimal numbers of variables (NDVI, SR, mTVI and RDVI) were used to train and test the RF model. Variables relevance and predictability indicates that indices formed using NIR and visible portion dominates for predating capsule volume. In Cambridge, Tasmania, Australia, RF model based on convolved to

UAS multispectral data were used to predict capsule volume, which was strongly related to field measured capsule volume with an R^2 value of 0.70 for validation and an R^2 value of 0.86 for training dataset, whereas, UAS based RF model provided an R^2 value ranging from 0.77 to 0.82 from validation to training dataset respectively. Selected variables based on the first study site (Cambridge) were used to generate an RF model using UAS acquired data at the second site (Sorell) and significant relationship between measured and predicted capsule volume was observed, with an R^2 value of 0.72 and relative error of 26.25 %. It can be concluded that poppy capsule volume can be estimated using combination of SVIs investigated with RF regression and has significantly higher prediction accuracy as compared to our previous study in which capsule volume was estimated from UAS driven plant height (Iqbal *et al.* 2017). Such information could be useful for crop management practices and yield enhancement.

5.8. Thesis context

Chapter 5 addressed the second objective of the thesis and described a successful methodology to improve capsule volume estimation compared to the results presented in chapter 3. Chapter 5 combined plant height and spectral derivatives using random forest (RF) machine learning approach. Chapter 6 builds onto this work by leveraging multi-temporal UAS data.

Chapter 6

6. Predicting poppy capsule volume using multi-temporal UAS remote sensing

Chapter 6 described a practical and effective method for capsule volume prediction in a quantitative manner using multi-temporal UAS remote sensing data analysed using random forest (RF) machine learning approach and will be submitted for publication to **IEEE Transactions on Geosciences and Remote Sensing**.

Abstract

Monitoring the dynamics in poppy crop development requires real-time observation with high spatial and temporal resolution due to complex factors influencing growth variability. The development of Unmanned Aerial System (UAS) has made it possible to acquire high spatio-temporal resolution imagery. In this study, Spectral and structural derivatives are used to estimate poppy capsule volume. Poppy capsule volume is predicted with the combination of single stage Spectral Vegetation Indices (SVIs), and multi-temporal SVIs derived from the UAS acquired multispectral images. The results showed that the hook stage provides optimal results for capsule volume prediction with SVIs at a single stage and the highest coefficient of determination achieved was 0.72 with RDVI. The sum of multi-temporal SVIs showed significant improvement in colour index using Linear Model (LM) and Random Forest Regression Model (RFRM) with an optimal R^2 of 0.72 achieved with RDVI and MSAVI with linear model and SPVI with RFRM. Analysis of multi-temporal SVIs showed significant improvement with RFRM yield having an R^2 of 0.81 with RDVI. The multiple multi-temporal SVIs investigated with RFRM showed significant improvement in results and an optimal result was achieved using $SPVI_{Hook}$, $RDVI_{Hook}$, $mTVI_{Hook}$ and $RDVI_{Flowering}$ yielding an R^2 of 0.84 as compared to single stage SVIs. In addition, the combination of multi-temporal SVIs ($SPVI_{Hook}$, $RDVI_{Hook}$, $mTVI_{Hook}$) and $GVF_{Flowering}$ with RFR showed superior results with an R^2 of 0.88 and RMSE of 13.45% as compared to multilinear regression model results. In conclusion, this study demonstrates that a combination of SVIs and GVF computed from hook and flowering stage provides reliable prediction of poppy capsule volume.

6.1. Introduction

Precision agriculture (PA) involves the integration of geospatial technologies that take into account the spatial variability of agronomic conditions affecting the crop to determine the most effective management strategy (Brisco *et al.* 1998). This allows the

producer to use variable rate technologies for sustainable site-specific management, leading to reduced inputs, while optimising yield (Bakhsh and Kanwar 2006). The main components of the precision agriculture system are field variability mapping and decision support systems that lead to the precise application of management practices (Zhang and Kovacs 2012). Remote sensing offers many tools that can be used to map field variability and inform yield forecasting (Warren and Metternicht 2005, Whiting *et al.* 2006, Gago *et al.* 2015). Field variability maps can help crop managers to use suitable strategies to manage crops according to the conditions and can be used as inputs in a variable rate application machinery to enhance yield (Zhang *et al.* 2002). Traditionally, crop yield prediction has relied on field-based destructive sampling, which is expensive and vulnerable to poor assessment (Bakhsh *et al.* 2005, Rodriguez *et al.* 2009). Therefore, developing low-cost and precise methods is essential for optimal crop management.

Remote sensing has been proven an efficient tool to monitor crop LAI (Haboudane *et al.* 2004, Zheng and Moskal 2009, Delegido *et al.* 2015), biomass (Morel *et al.* 2014, Pradhan *et al.* 2014, Kross *et al.* 2015, Wang *et al.* 2016), chlorophyll content (Gitelson and Merzlyak 1997, Gitelson *et al.* 2003, Moorthy *et al.* 2003, Zarco-Tejada, Morales, *et al.* 2013), water stress (Cohen *et al.* 2005, Baluja *et al.* 2012, Bellvert *et al.* 2013, De la Rosa *et al.* 2015) and yield (Abdullah *et al.* 2011, Jia *et al.* 2011, Dempewolf *et al.* 2014, Morel *et al.* 2014, Brandao *et al.* 2015), which can be estimated and assessed using spectral vegetation indices (SVIs) at one or several times during the crop growth cycle. Kaur *et al.* (2015) used a field-based spectroradiometer to identify the relationship between NDVI and wheat crop yield at tillering and botting stage. Tucker et al. (Tucker *et al.* 1980) showed a linear relationship between NDVI and wheat grain yield. Several studies used ratio NIR and Red band to predict wheat yield (Serrano *et al.* 2000). Waine et al. (2014) used satellite driven NDVI to predict opium capsule yield, while, some studies used remote sensing to estimate the total area under poppy crop (Chuinsiri *et al.* 2010, Wang 2013). Jia et al. (2011) showed a stronger relationship between LAI and opium capsule gum yield. Numerous studies have investigated the relationship between crop yield and NDVI (Zarco-Tejada, Ustin, *et al.* 2005, Morel *et al.* 2014, Brandao *et al.* 2015). Kogan et al. (2013) predicted yield using combination of NDVI, meteorological data, and biophysical models, whereas, multiple SVIs were used to improve prediction accuracy in another study (XUE *et al.* 2005). Some researchers achieved higher yield prediction accuracy with accumulated SVIs over entire growth cycle than with SVIs at a single stage (Wang *et al.* 2014). However, relatively coarse spatial resolution results in mixing of spectral signature, thus causing error. Whereas, higher spatial and temporal resolution enhances the prediction accuracy (Wang *et al.*

2014, Zhou *et al.* 2017). However, it is often difficult to acquire high temporal resolution data using satellite remote sensing (capturing key dates/events in the crop growth cycle). Moreover, due to the presence of clouds, it is not always possible to acquire satellite data. Therefore, acquiring crop data at optimal spatial and temporal resolutions is one of the key issues that can improve prediction accuracy for appropriate decision-making.

UAS-based remote sensing technology has developed remarkably in recent years and customised sensors are available for many agricultural applications (Swain *et al.* 2010, Laliberte and Rango 2011, Wang *et al.* 2014). The use of UAS as a remote sensing platform has demonstrated the potential for precision agriculture by providing multi-temporal data (Zhang and Kovacs 2012). UASs provide flexibility in acquisition at much lower cost as compared to aircraft and satellite data. Images captured using UAS generally have spatial resolution within a few centimetres. Therefore, UAS acquired images could be a practical alternative to aerial and satellite remote sensing. For PA, UAS remote sensing is used to monitor plant growth and health (Saari *et al.* 2011, Bendig *et al.* 2014, Geipel *et al.* 2014, Iqbal *et al.* 2017). Several studies have shown an estimation of biophysical characteristics, such as plant height, yield, LAI and biomass (Thenkabail *et al.* 2000, Rufino and Moccia 2005, Ehlert *et al.* 2008, Jaakkola *et al.* 2010, Mäkynen *et al.* 2011, Córcoles *et al.* 2013, Bendig *et al.* 2014, Li *et al.* 2016, Iqbal *et al.* 2017). UAS based imagery was used to estimate plant height for crop yield estimation (Bernath 1986, Wang *et al.* 1999, Mahdavi-Damghani *et al.* 2010, Jia *et al.* 2011, Bendig *et al.* 2014, Vega *et al.* 2015). Geipel, Link & Claupein (2014) estimated corn yield by operating MicroKopter mounted RGB camera. Baluja et al. (2012) acquired thermal and multispectral images using UAS system to estimate water status variability of the vineyard. Zhu et al. (2010) used UAS imagery to estimate crop nitrogen status. Thermal and multispectral imagery acquired from UAS platform for crop health assessment (Berni, Zarco-Tejada, Suarez, *et al.* 2009). Calderón et al. (2014) identified downy mildew of opium poppy using high-resolution multispectral and thermal imagery acquired with an unmanned aerial vehicle. Similarly, Córcoles et al. (2013) investigated the use of UAS acquired imagery for the estimation of leaf area index in onion. Du & Noguchi (2017) investigated colour vegetation indices (CVI) and accumulative CVI used to predict wheat yield. Rasmussen *et al.* (2016) examined the reliability of consumer grade camera by computing four vegetation indices, and concluded that vegetation indices of UAS mounted camera can be used to monitor vegetation status. Zhou *et al*. (2017) used UAS mounted multispectral sensor driven vegetation indices to predict rice yield and LAI, which showed multi-temporal NDVI and Visible Atmospherically Resistant Index

(VARI) provided higher predict accuracy as compared to single stage index. Vega *et al*. (2015) showed the linear relationship between NDVI and grain yield, aerial biomass and nitrogen content in the biomass. Fang *et al*. (2016) used UAS mounted multispectral sensor driven vegetation indices to estimate green vegetation fraction (GVF) and establish linear regression between vegetation fraction and the Spectral Vegetation Indices (SVIs). Moreover, multispectral and hyperspectral cameras have been used to monitor vegetation using different SVIs (Berni, Zarco-Tejada, Suarez, *et al.* 2009, Mäkynen *et al.* 2012, Zarco-Tejada, Gonzalez-Dugo, *et al.* 2012, Geipel *et al.* 2014, Zarco-Tejada *et al.* 2014). Zarco-Tejada *et al*. (2013b) inspected UAS driven SVIs and determined that structural indices related to LAI, i.e. Renormalised Difference Vegetation Index (RDVI), modified Triangular Vegetation Index (mTVI), and optimised Soil-Adjusted Vegetation Index (OSAVI), showed significant relationships with the cotton yield at early growth stage. Whereas, hyperspectral indices related to crop physiological status i.e. Modified Chlorophyll Absorption Index (MCARI) and Transformed Chlorophyll Absorption Index (TCARI), showed significant relationship near maturity.

UAS remote sensing has filled an important gap by providing high spatio-temporal data, and researchers that have used multi-temporal UAS data for timely yield estimation. Vega *et al*. (2015) showed that NDVI derived from crops before the flowering stage was significantly correlated with sunflower yield. In another study, Zhou *et al*. (2017) proved that NDVI at initial botting stage provided higher correlation with wheat yield. Whereas, a combination of multi-temporal SVIs using multilinear regression function enhances the prediction accuracy in wheat and rice (Wang *et al.* 2014, Zhou *et al.* 2017). To the best of our knowledge, however, only two studies (Wang *et al.* 2014, Zhou *et al.* 2017) have investigated the utility of multi-temporal UAS data for yield estimation, and none of them have been applied to high-value alkaloid poppy crops. The study of (Wang *et al.* 2014, Zhou *et al.* 2017) demonstrated that multi-temporal data has the capacity to improve the accuracy of prediction for real-time crop management. Similarly, these studies have explored SVIs and yield using simple linear or multiple linear regression models, although, machine-learning algorithms are yet to be tested for yield estimation using multi-temporal spectral data. Statistical modelling based on machine learning algorithms can provide a superior an alternative to traditional regression techniques. The Random Forest (RF) regression model is a data mining method (Breiman 2001) used for feature selection to reduce the redundancy of variables (Smith *et al.* 2013, Adam *et al.* 2014, Wang *et al.* 2016). RF is a robust method and can handle a large number of input variables as well as an unbalanced dataset. The

variable importance is a helpful measure in gaining insight about which SVIs contribute most to the prediction of an independent variable when implemented on high dimensional data (Siroky and others 2009, Jones and Linder 2015). Several studies have demonstrated the benefits of RF for crop yield prediction using multiple variables (Abdel-Rahman *et al.* 2013, Jeong *et al.* 2016, Wang *et al.* 2016, Saeed *et al.* 2017). Thus, there is an opportunity to explore the potential of RF regression in combination with multi-temporal SVIs data acquired using UAS to improve crop yield predictions.

In this study, we focus on a high value poppy crop (*Papaver Somniferum L*), which is one of the few medicinal plants that has been cultivated and used since prehistoric times (Bernath and Tetrnyi 1981, Schiff 2002, Shukla *et al.* 2006). It is a plant of the dicot family *Papveraceae*, cultivated for seed, oil, and opium. Poppy is a herbaceous plant with an erect stem and flower varying in colour according to varieties. At later development stages, flowers become capsules that contain latex and seeds (Mahdavi-Damghani *et al.* 2010). Latex is located mainly in the capsule walls and is a rich source of around twenty different pharmaceutical alkaloids including morphine, codeine, thebaine, narcotine, papaverine (Apuya *et al.* 2008). Poppy opium is grown in several parts of the world, but the state of Tasmania, Australia is the largest global licit producer of poppy opium used for medicine (Lisson 2007). However, the demand for opium-based medicines is increasing and poppy cropping is intensive as it utilises numerous resources and is therefore normally cultivated in a three to five-year rotation. Therefore, horizontal expansion of crop production is not a sustainable option. Predicting yield potential well before maturity is critical and managing the crop precisely is vital for fulfilling the requirements of national and international markets.

Several studies show that the growth and development of poppy are influenced by agronomic and environmental factors (Mika 1955, Acock, Wang, and Acock 1996, Acock and Pausch 1997, Lisson 2007, Jackson 2009, Dean 2011). Thus, assessment of crop during multiple phases needs to be investigated. Therefore, multi-temporal analysis of crop is vital to see the influence of each stage towards capsule volume. Remote sensing has been used in previous studies to estimate poppy crop yield (Jia *et al.* 2011, Calderón *et al.* 2014, Waine *et al.* 2014, Iqbal *et al.* 2017). Analysis of Jia *et al*. 2011 found a good correlation between opium yield and product of LAI and plant height. Whereas, research of (Waine *et al.* 2014) found good empirical relationships between NDVI and poppy capsule volume. Thus the aim of this study investigates the combination of multi-temporal SVIs, GVF to predict opium capsule volume. Therefore, multi-temporal SVIs and GVF were used to investigate the applicability of the RF regression algorithm to predict capsule volume. The performance of RF regression is compared with linear

and multilinear regression models. This paper analyses the quantitative relationship between estimated vegetation fraction, SVIs and opium capsule yield, and determines the best growth stage for prediction of capsule volume and the best combination of SVIs for predicting opium yield using random forest, linear and multi-linear regression models.

6.2. Material and methods

6.2.1. Study area

This research was carried out in Sorell, Tasmania, Australia (42°45′ 58″S, 147° 35′ 38″E) on commercial opium poppy (Figure 6.1). The terrain of the site has a gentle fall to the east. The average rainfall is 509 mm with 142 rainy days with relatively even yearly distribution. Average pan evapotranspiration is 1308 mm with evaporation exceeding rainfall for ten months of the year. The experiment was designed based on the single season from June 2016 to January 2017. Poppy crop was sown in mid-July 2016 in a well-cultivated field, with the seedling emergence in the following 1-2 weeks. Flowering occurred in early December, with capsule formation starting in mid-December and poppy capsules were harvested in mid of January 2017. The crop was sown with a commercial seed drill to maintain the seeding density of 80 seeds per square metre. To control the weeds, herbicides were applied prior to sowing and at early rosette stage.

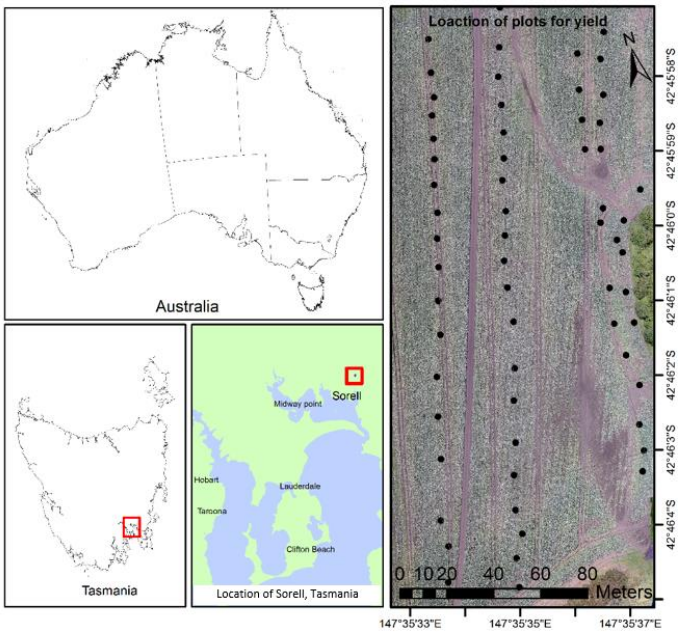

Figure 6.1. The general location of the study site and the overview of the image obtained from unmanned aircraft system (UAS) showing the location of field sampling plots.

6.2.2. Field data collection

The growth and development lifecycle of poppy is divided into the following stages; growth of seedlings, the formation of rosette-type leaves, stem elongation, hook, flowering and capsule formation (Shuljgin 1969, Bernath 1986, Wang *et al.* 1999, Miura and Huete 2009, Mahdavi-Damghani *et al.* 2010). The critical period in opium development is from the hook stage until the capsule formation stage (Waine *et al.* 2014). Thus, UAS and field campaigns were conducted at hook stage (17th November), flowering (4th December), and at capsule formation stage (22nd December 2016). In this study, the sown area of ~ 5 hectares was divided into three transects, each with a total length of ~260 metres. Transects were selected based on crop growth variability; transect one was located on healthier growth area (west side of the farm), whereas, transect two was selected in the middle to high crop growth category. The third transect was marked on the west side of the farm with very poor to heathier plant growth. All transects were selected to avoid any area of weed growth. Capsule volume was measured from capsule formation stage (22nd December 2016).

On marked transects, we set up 70 (0.5 x 0.5 m) plots for field data collection, which included the physical measurement of plants (number of plants and capsules, horizontal and vertical dimensions of each capsule and spectral measurement of leaf and flowers) (Iqbal *et al.* 2017). In order to ensure that the size and location of each plot was consistent, we used marker stakes to mark each plot location and used a PVC quadrant (0.5 m x 0.5 m) to confine the plots and assist with sampling. Moreover, global navigation satellite system (GNSS) coordinates of each sample plot and Ground Control Points (GCP) (0.5 m 0.5 m) were measured with a survey-grade dual frequency real-time kinematic (RTK) GNSS receiver (2 – 4 cm absolute coordinate accuracy).

6.2.3. UAS campaign

For this study, three images were acquired over the study area using a multispectral sensor, MicaSense/Parrot Sequoia, mounted on a UAS quadcopter (3D Robotics, Inc) (Table 6.1). The 3DR Solo has a payload capacity of ~ 0.5 kg, a flight duration of 20 min. The Sequoia sensor consists of an RGB 16 Mpixel sensor (4608 × 3456 pix) with four single band sensors: the green band is sensitive to the 530–570 nm spectral region, the red band is sensitive to 640–680 nm, red edge band is a narrow band that covers 730–740 nm and captures the rapid change from low red reflectance to near-infrared reflectance, and the near-infrared (NIR) band captures the 770–810 nm region. The spectral sensitivity of image sensors is changing in each region with optimum sensitivity of 70% in green band and gradual decreases to 55% at 650 nm, 35 % at 730 nm and 30% around

800 nm in NIR. The Sequoia sensor has an inbuilt GNSS and IMU for positioning and orientation. Moreover, it operates with a sunshine sensor that allows self-calibration of spectral bands and allows for conversion from imager digital number (DN) values to reflectance (with the aid of a spectral calibration panel).

Table 6.1. Field assessments and UAS campaigns at the study location

Survey date	Growth stage	Observation
17/11/2016	Hook	Field sampling, UAS, GPS
04/12/2016	Flowering	UAS
22/12/2016	Capsule formation	Field sampling, UAS

The UAS campaigns were conducted under a clear sky and low wind conditions between 12:00 and 2:00 local time. The Sequoia sensor was mounted under the UAS in a fixed position (angled forward slightly to allow for nadir image acquisition in forward flight) and the sunshine sensor was connected on top of 3DRsolo battery by attaching the sunshine sensor holder. The Sequoia data capture rate was set to 1 fps. For spectral calibration, pre and post flight images of the Sequoia spectral calibration target was collected.

The Tower app was used to define the flight UAS flight lines. The UAS mission was planned with 75% overlap between adjacent flight strips, flight speed of 2.5 m/s, and flying height of 50 m, 25 m and 15 m above ground level (AGL) for 17th November, 4th December, and 22nd December respectively. MicaSense ATLAS was used to generate seamless 4-band orthomosaics for each date. The orthomosaics where further georeferenced with the GNSS coordinates for the GCPs by performing a 1st order polynomial geometric transformation in ArcGIS.

6.3. UAS image pre-processing

In this study, the empirical line approach was used to convert image Digital Numbers (DN) to surface reflectance (Smith and Milton 1999, Moran *et al.* 2001, Karpouzli and Malthus 2003, Baugh and Groeneveld 2008, Staben *et al.* 2012). This approach is widely used for image radiometric calibration for UAS campaigns (Kelcey and Lucieer 2012, Del Pozo *et al.* 2014, Lucieer, Malenovský, *et al.* 2014, Wang and Myint 2015). To measure field reflectance, five radiometric calibration targets (0.5 X 0.5) were used. All five calibration targets were placed along the transect and spectral measurements of each calibration target were taken using ASD HandHeld2 spectroradiometer (Analytical Spectral Device, Inc., Boulder, co, USA). The ASD HandHeld2 acquires spectral signatures from 325 nm to 1075 nm. Reflectance measurements were taken during flight

(1:00 pm and 2:00 pm) under incident solar light. During spectral data collection, spectroradiometer calibration measurements were taken with a reference panel (white Spectralon) and dark current before and after taking every reading from radiometric calibration targets. Twenty spectral readings were taken from each target from four different viewing angles from a distance of 1 m without blocking sunlight with sample counts of 15. Every spectral reading per calibration panel from each direction was averaged for further analysis and all twenty spectra average was used for image calibration.

Table 6.2. Polynomial regression model used for image radiometric calibration.

	R-Squared		
Spectral Bands	**17 Nov.**	**4th Dec.**	**22nd Dec.**
Red	0.998	0.997	0.996
Green	0.997	0.998	0.997
Red Edge	0.997	0.998	0.995
NIR	0.998	0.996	0.995

The target actual digital number (DN) values were extracted from UAS acquired imagery and the reflectances measured with the spectroradiometer were used for empirical radiometric correction. The absolute reflectance of the calibration targets measured with the spectroradiometer was spectrally convolved to resample the four bands of Sequoia using R package prospect-R (Stevens and Ramirez-Lopez 2014). The DNs of targets extracted from the raw image was then modelled to transform into the convolved reflectance data (Table 6.2). Finally, the developed 2nd order polynomial models were used to transform each image into surface reflectance. Since orthophotos were processed with GPS location recorded by the inbuilt GPS receiver of the Sequoia sensor, the absolute positional of the orthophoto mosaic is relatively low (50 – 10 m). Accuratly coordinated GCPs were used to further georeferenced the orthomosaic using georeferencing tool of Arc GIS 10.3 Fifteen evenly distributed photo target (0.5 m x 0.5 m) coordinates were used to georeference using 1st order polynomial transformation. Eight photo target coordinates were used to evaluate the georeferencing.

6.3.1 UAS image analysis

The four band false-colour composite images were used for delineation of soil, vegetation, and flower. Poppy crop growth was highly heterogeneous in the field, thus, the 70 plots (0.5m x 0.5 m) were used for field data collection and image analysis. Based on visual interpretation and field-based data, pixels of flowers, leaves, and soil were carefully selected as training samples for supervised classification using maximum likelihood classifier. Classified soil and crop pixels were coloured independently in the

map layer, which was then set as 60% transparent and overlayed on the original image to visually evaluate the classification accuracy. To calculate the percentage of green vegetation cover, soil pixels were reclassified with zero value, whereas, green vegetation pixels were given a value of one. Area of each sample plots was extracted from the classified layer and percentage of green vegetation cover was computed. Finally, the classification accuracy was evaluated using field data collected from each plot (Figure 6.1).

6.3.2 Computation of vegetation indices

Spectral indices were computed for all multispectral orthomosaics, based on previous research on crop yield estimation(Carlson and Ripley 1997, Zarco-Tejada, Ustin, *et al.* 2004, Zarco-Tejada, Gonzalez-Dugo, *et al.* 2012, Pradhan *et al.* 2014, Bendig *et al.* 2015, Zhou *et al.* 2017). The study area orthophoto was clipped into 70 plots to collect the image spectra from each band (n = 4) to compute SVIs (Table 6.3) using Arc GIS 10.3.

Table 6.3. Vegetation indices investigated in this study.

Acronym	Formula	Reference
VARI	$(\rho\ 550 - \rho\ 660) / (\rho\ 550 + \rho\ 660)$	(Gitelson *et al.* 2002)
MCARI	$1.2\ [2.5(\rho\ 790 - \rho\ 660) - 1.3(\rho\ 790 - \rho\ 550)]$	(Haboudane *et al.* 2004)
mTVI	$1.2\ [1.2(\rho\ 790 - \rho\ 550) - 2.5(\rho\ 660 - \rho\ 550)]$	(Haboudane *et al.* 2004)
NDVI	$(\rho\ 790 - \rho\ 660) / (\rho\ 790 + \rho\ 660)$	(Rouse Jr 1972)
GI	$\rho\ 550 / \rho\ 660$	(Zarco-Tejada, Berjón, *et al.* 2005)
RGI	$\rho\ 660 / \rho\ 550$	(Zarco-Tejada, Berjón, *et al.* 2005)
RDVI	$(\rho\ 790 - \rho\ 660) / (\rho\ 790 + \rho\ 660)^{0.5}$	(Roujean and Breon 1995)
SPVI	$0.4[3.7(\rho\ 790 - \rho\ 660) - 1.2\lvert \rho\ 550 + \rho\ 660\rvert]$	(Vincini *et al.* 2006)
OSAVI	$1.16(\rho\ 790 - \rho\ 660) / (\rho\ 790 + \rho\ 660 + 0.16)$	(Rondeaux *et al.* 1996)
GNDVI	$(\rho\ 790 - \rho\ 550) / (\rho\ 790 + \rho\ 550)$	(Gitelson *et al.* 1996)
MSAVI	$[2(\rho\ 790 + 1 - [2 * \rho\ 790 + 1)^2 - 8(\rho\ 790 - \rho\ 660)^{0.5}]/2$	(Qi *et al.* 1994)
mSR	$(\rho\ 790 / \rho\ 660 - 1) / (\rho\ 790 / \rho\ 660 + 1)^{0.5}$	(Chen and Cihlar 1996)
NDRE	$(\rho\ 790 - \rho\ 735) / (\rho\ 790 + \rho\ 735)$	(Clevers *et al.* 2002)
EVI	$2.5\ (\rho\ 790 - \rho\ 660) / (1 + \rho\ 790 + 2.4 \times \rho\ 670)$	(Jiang *et al.* 2008)

6.3.3. Data analysis for capsule volume estimation

Spectral data derived from sample plots was used to develop the relationship between SVIs and capsule volume. For the remote prediction of poppy capsule volume, SVIs and GVF were used to develop single variable linear, multiple linear (MLR) and RF regression models. Yield prediction models were developed using single and multi-temporal stage data (hook and flowering). In this study, two different forms of multi-temporal SVIs were calculated; SVIs of hook and flowering stage examined with linear regression and multilinear regression function and, the sum of SVIs at hook and flowering stage using a linear model. The combination of multi-temporal SVIs was

analysed using multilinear regression. Moreover, selected variables from the multi-temporal sum of SVIs and multiple SVIs for two different stages were analysed using a multi linear model. Further selected SVIs were used in combination with multi-temporal GVF using multi linear regression to check the accuracy using multilinear model. The RF model was trained and applied using a combination of multi-temporal SVIs. Firstly, the sum of multi-temporal SVIs (SVI_{Hook} + $SVI_{Flowering}$) was used to check the prediction accuracy. Secondly, multi-temporal SVIs were also investigated to predict the capsule volume. Further analysis was conducted by a combination of multiple multi-temporal SVIs (SVI_{Hook}, $SVI_{Flowering}$) to check the performance of all variables. Based on variable importance, higher ranked variables were used to predict capsule volume using multi-temporal variables. Selected variable with an optimal number of N_{tree} and M_{try} were used to predict capsule volume using the sum of multi-temporal SVIs. Similarly, selected multi-temporal SVIs were also used to predict capsule volume. Further analysis was conducted by a combination of multi-temporal SVIs and GVF to investigate the change ranking of variable importance. Finally, higher ranked SVIs and GVF from hook and flowering stage were used to predict capsule volume. To check the consistency and robustness of the model, the dataset was randomly split into 10 equal size subsamples. A single subsample was used as the validation data for testing the model performance, and the remaining k-1 subsamples were used as training data. The cross-validation process was repeated k times (n = 10), with each of the k subsamples used exactly once as the validation data. The 10 prediction results from the folds were combined to produce a scatter plot of measured and predicted capsule volume. K-fold method provides better prediction accuracy as compared to splitting data to two halves for training and validation. As in the k-fold process, all the data points are used for both training and validation, and each data point is used for validation exactly once. Finally, the combined coefficient determination (R^2) and root mean square error (RMSE) of were computed to assess the performance of estimation models.

MLR and RF were used to evaluate the prediction accuracy using all SVIs of two growth stages and variable importance was determined. Based on significant variables, RFR and MLR models were generated to predict the capsule volume. The prediction accuracy received from model generated using selected multi-temporal SVIs were compared by incorporating multi-temporal SVIS and GVF in same model. To evaluate the results, coefficient of determination (R^2) and root mean square error (RMSE) and relative RMSE were computed to assess the performance of estimation models. Best prediction model was used to generate spatial distribution map of capsule volume in the study area.

6.4. Results

6.4.1 GVF estimation

The accuracy achieved with supervised classification was also tested with the index based methodology used in our previous study to distinguish soil patches (Iqbal *et al.* 2017). Overall, the classification accuracy of 93.9 % at hook, 91.23 % at flowering and 93.7 % at capsule formation stage was achieved. Figure 6.2 illustrates that vegetation cover increases on the 22nd December map as compared to the maps generated based on data collected at the two earlier (flowering and hook) stages. The flowering stage image was classified into three classes (flower, soil, and vegetation), but for the purpose of analysis, flowering cover area was combined into vegetation cover by applying a 5 x 5 majority filter.

6.3.2. Capsule volume estimation using green vegetation fraction

Table 6.6 shows the correlation between GVF and capsule volume with $R^2 = 0.72$ at hook, $R^2 = 0.67$ at flowering and $R^2 = 0.76$ at capsule formation stage. We found that the relative root mean square error (RMSE) also varied depending on growth stage, 20.46 % at the hook, 22.21 % at flowering and 19.61 % at capsule formation stage. Thus, the capsule formation stage was found to be optimal for capsule volume estimation based on the aerial cover of green vegetation. Overall, capsule volume can be predicted with green vegetation fraction with a relative root mean square of 20.79 %. The capsule volume measured from field measurement and predicted using GVF showed overestimation in smaller capsules, ranging from 130 cm^3 at hook stage, 130 cm^3 at flowering stage and 101 cm^3 at capsule formation stage (Table 6.6). Whereas, underestimation was observed for the large capsules at all three stages, ranging from 587 cm^3 at the hook, 582 cm^3 at flowering and 598 cm^3 at capsule formation stage. Similarly, median values also varied from 375 to 406 cm^3 and very small variations were observed compared the mean values.

Table 6.4. Regression of green vegetation fraction and capsule volume at different growth stages.

Growth stages	R^2	RMSE (cm^3)	RMSE (%)
Hook	0.72	76.43	20.46
Flowering	0.67	82.99	22.21
Capsule formation	0.76	73.26	19.61
Combined	0.67	77.67	20.79

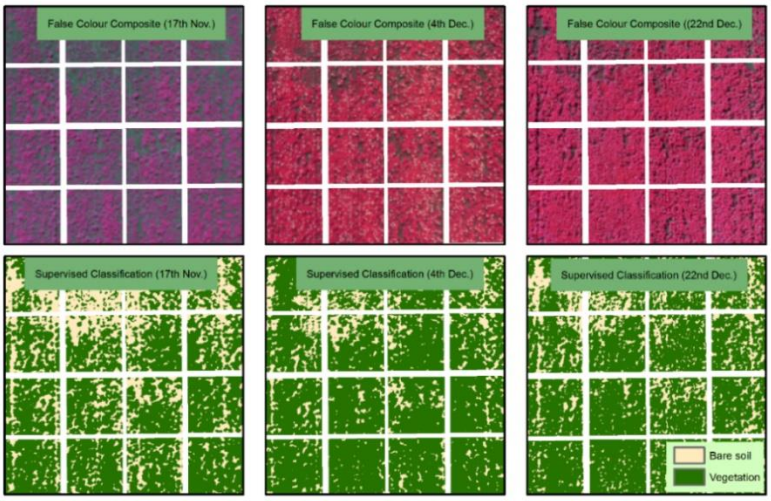

Figure 6.2. Classification results at different growth stages illustrating change in green vegetation cover.

Table 6.5. Measured capsule volume at capsule formation stage and predicted capsule volume using UAS data of hook and flowering stages.

		Hook	Flowering	Capsule formation
Statistics	**Measured (cm^3)**	**Predicted (cm^3)**	**Predicted (cm^3)**	**Predicted (cm^3)**
Min Volume	75	132	130	101
Median Volume	370	375	406	406
Mean Volume	373	372	371	375
Max Volume	645	587	582	598

6.4.3. Relationship between single growth stage SVIs and capsule volume

The relationship between opium capsule volume and spectral indices at different growth stages were investigated (Table 6.6). The results indicate that capsule volume was highly correlated with the spectral indices at hook stage, whereas, relatively lower correlation was observed at flowering and capsule formation stage. Overall, the coefficient of determination (R^2) at capsule formation stage ranged from 0.30 to 0.45 as presented in Table 6.6.

The maximum R^2 was 0.45 achieved with RDVI and GNDVI, whereas the relationship between capsule volume and SVI at hook stage showed significantly higher relationship as compared to capsule formation stage, ranging from 0.18 to 0.72. The highest achieved R^2 was 0.72 with RDVI and lowest R^2 of 0.18 was observed with NDRE. Relatively lower performance was observed at flowering stage, ranging from 0.41 to 0.66. Similar to the hook and capsule formation stage, the R^2 value of 0.66 was observed from RDVI at flowering stage. Overall, hook stages provided higher prediction accuracy with all SVIs excluding NDRE. Significant improvement from hook to flowering stage was observed

with NDRE with an R^2 0.18 to 0.42 provided a relative root mean square error improvement of 7 %.

Table 6.6. The coefficient of determination (R^2) between capsule volume and vegetation indices at different growth stages.

Spectral Index	Hook	Flowering	Capsule formation
NDVI	**0.66**	0.59	0.44
MCARI	0.59	0.58	0.36
mTVI	**0.69**	0.62	0.44
RDVI	**0.72**	**0.66**	0.45
SPVI	**0.66**	0.61	0.44
OSAVI	**0.66**	0.59	0.44
GNDVI	0.62	0.53	0.45
MSAVI	**0.67**	0.61	0.44
mSR	0.55	0.50	0.42
NDRE	0.18	0.42	0.30
EVI	0.64	0.58	0.36
VARI	0.49	0.46	0.36
GI	0.44	0.41	0.32
RGI	0.50	0.48	0.36

6.4.4. Determination of capsule volume using the multi-temporal spectral indices.

The investigation was conducted on the relationship of capsule volume to the combination of multi-temporal indices (through summation). In addition, slope and area under curve method were investigated as well but results were not found significant thus not reported. Table 6.7 illustrates the relationship between capsule volume and $\sum$ SVIs $_{(\text{Hook + Flowering})}$. For this analysis, we used the SVI values of hook and flowering stage to investigate the relationship with capsule volume. Results reveal that the sum of multi-temporal index values of flowering and hook stage improved the coefficient of determination, from 0.50 to 0.72 using linear regression model (LRM) and 0.32 to 0.72 using random forest regression model (RFRM). From LRM, the highest R^2 was achieved with MSAVI and RDVI resulting in an R^2 value of 0.72 with RMSE of 76.27 cm^3 and 75.23 cm^3, respectively. While, from RFRM, highest R^2 was achieved with SPVI resulting in an R^2 value of 0.72 with RMSE of 76.67 cm^3. Overall, an improvement in the performance of 11 out of 14 SVIs was achieved by using LRM excluding mTVI, RDVI and GNDVI, as compared to hook stage only. The highest improvement was observed with NDRE from an R^2 of 0.18 to 0.44. While, in relation to flowering stage, 13 out of 14 SVIs provided an improvement, with the only exception being GNDVI. Highest improvement was observed with colour index GI, providing an increase in R^2 value from 0.41 to 0.66. However, with RFRM 8 out of 14 SVIs provided improvement

in prediction accuracy as compared to hook stage SVIs only, where highest improvement was observed with NDRE from an R^2 value of 0.18 to 0.32. Moreover, 7 out of 14 SVIs provided improvement in prediction in comparison with flowering stage SVIs only, where highest improvement was observed with GI increasing from 0.41 to 0.53. Overall, the $\sum$ SVIs $_{(Hook + Flowering)}$ performed well as compared to single stage vegetation index of flowering and hook stage and showed the RMSE ranging from 19.55 cm^3 to 28.51 cm^3 using LRM and 19.92 cm^3 to 32.68 cm^3 using RFRM.

Table 6.7. The coefficient of determination (R^2) between capsule volume and sum of multi-temporal indices at two (Hook and Flowering) growth stages.

	LRM			RFRM		
$\sum$ SVI ($_{Hook\ and\ Flowering}$)	**R^2**	**RMSE (cm^3)**	**RMSE (%)**	**R^2**	**RMSE (cm^3)**	**RMSE (%)**
NDVI	**0.71**	77.24	20.07	0.53	101.05	26.25
MCARI	**0.71**	78.14	20.30	0.52	102.50	26.63
mTVI	**0.69**	80.48	20.91	**0.69**	80.27	20.85
RDVI	**0.72**	75.23	19.55	**0.67**	84.86	22.05
SPVI	**0.67**	83.34	21.65	**0.72**	76.67	19.92
OSAVI	**0.71**	77.24	20.07	0.53	101.51	26.37
GNDVI	0.50	88.28	22.94	0.50	104.88	27.25
MSAVI	**0.72**	76.27	19.82	0.53	99.35	25.81
mSR	0.64	86.88	22.57	0.56	97.27	25.27
NDRE	0.44	109.75	28.51	0.32	125.80	32.68
EVI	**0.71**	78.73	20.45	0.52	102.59	26.65
VARI	**0.67**	82.84	21.52	0.53	99.50	25.85
GI	**0.66**	84.62	21.98	0.53	100.55	26.12
RGI	**0.67**	82.13	21.34	0.53	100.3	26.06

Further investigation was conducted on the relationship of capsule volume to the multi-temporal SVIs. Table 6.8 illustrates the relationship between capsule volume and multi-temporal SVIs. For this analysis, the SVI values of hook and flowering stage were used in relation to capsule volume. Results reveal that the combination of multi-temporal SVIs improved the coefficient of determination as compared to sum of multi-temporal SVIs, ranging from 0.37 to 0.70 using the multi linear regression model (MLRM), and 0.36 to 0.81 using the RFRM.

From the MLR model, the highest coefficient of determination was achieved with NDVI, RDVI, OSAVI and MSAVI resulting in an R^2 value of 0.70 with RMSE of 78.07 cm^3, 77.76 cm^3, 78.00 cm^3 and 83.00 cm^3, respectively. Whereas, from the RFR model, the highest R^2 was achieved with RDVI resulting in an R^2 value of 0.81 with RMSE of 62.40 cm^3 and SPVI resulting in an R^2 of 0.79 with RMSE of 65.73 cm^3. Overall, no improvement was observed as compared to sum of SVIs. Also, the overall performance of 12 of 14 SVIs

was improved using the MLRM as compared to the sum of SVIs investigated using the RFR model. The highest improvement was observed with NDVI and MSAVI providing an R^2 value of 0.70. Whereas, only GNDVI showed improvement in comparison with the sum of SVIs inspected with LR model. Using RFR model, when SVI_{Hook} and $SVI_{Flowering}$ was analysed, 4 of 14 SVIs showed improvement in prediction accuracy as compared to sum of the SVIs analysis using LRM. Highest improvement was observed with OSAVI providing an R^2 value of 0.58, whereas, 11 of 14 SVIs showed implement in prediction accuracy observed with MLRM as compared to RFRM, in which the highest improvement was observed with RDVI providing an R^2 value of 0.81 with relative square error of 16.21%. The combination of multi-temporal SVIs investigated using RFR performed well as compared to sum of SVIs resulting in the RMSE of 16.21 cm^3 to 30.46 cm^3. Whereas, RMSEs ranging from 20.26 cm^3 to 30.60 cm^3 were observed using MLR.

Table 6.8. The coefficient of determination (R^2), RMSE = root mean square error, RMSE % = relative root mean square error between measured capsule volume and predicted capsule volume using multi-temporal SVIs.

		MLRM			RFRM	
SVI_{Hook}, $SVI_{Flowering}$	**R^2**	**RMSE (cm^3)**	**RMSE (%)**	**R^2**	**RMSE (cm^3)**	**RMSE (%)**
NDVI	**0.70**	78.07	20.28	0.58	94.55	24.56
MCARI	**0.68**	80.24	20.08	0.53	99.11	25.75
mTVI	**0.67**	82.53	21.14	**0.76**	71.54	18.59
RDVI	**0.70**	77.76	20.20	**0.81**	62.40	16.21
SPVI	**0.65**	84.83	22.03	**0.79**	65.73	17.08
OSAVI	**0.70**	78.00	20.26	0.58	94.57	24.57
GNDVI	0.59	108.0	28.05	0.52	102.39	26.60
MSAVI	**0.70**	83.00	21.30	0.58	94.58	24.57
mSR	**0.64**	92.04	23.90	0.58	94.57	24.57
NDRE	0.37	117.91	30.60	0.36	117.23	30.46
EVI	**0.68**	84.00	21.18	0.58	94.37	24.52
VARI	**0.65**	84.32	21.90	0.48	105.22	27.34
GI	0.64	85.74	22.27	0.48	105.03	27.29
RGI	**0.65**	83.84	21.78	0.48	105.16	27.32

6.4.5. Determination of the optimum model to predict capsule volume

Further analysis was conducted to find the optimal model for the prediction of capsule volume. Comparative analysis of results presented in section 6.4.3 illustrates that use of hook stage data was found to be optimal as compared to flowering stage data. The performance of $\sum SVI_{(Hook + Flowering)}$ investigated using LRM shows better prediction accuracy as compared to RFRM with all variables except mTVI and SPVI. Although multi-temporal $SVIs_{(Hook, Flowering)}$ investigated using RFR illustrate better performance

with RDVI, SPVI and mTVI, thus, providing an improvement of 3.34%, 4.57% and 2.32%, respectively. Figure 6.3, comparative analysis of results achieved from RFR and MLR using multi-temporal SVIs (Hook, Flowering) showed that RDVI, mTVI and SPVI performed better with RFR and resulted in an improvement of 3.99%, 2.55% and 4.95%, respectively. Moreover, the performance of RFR using multi-temporal SVIs (Hook, Flowering) was better with all spectral vegetation indices as compared to ∑ SVI (Hook + Flowering). Whereas, colour indices (VARI, GI, RGI) with ∑ SVI (Hook + Flowering) performed better as compared to SVIs (Hook, Flowering), providing an improvement of 1.49 %, 1.17 %, and 1.26 %, respectively. Overall, lowest RMSE value was observed with SVIs (Hook, Flowering) investigated with RFR, attaining lowest RMSE of 16.21 % with RDVI.

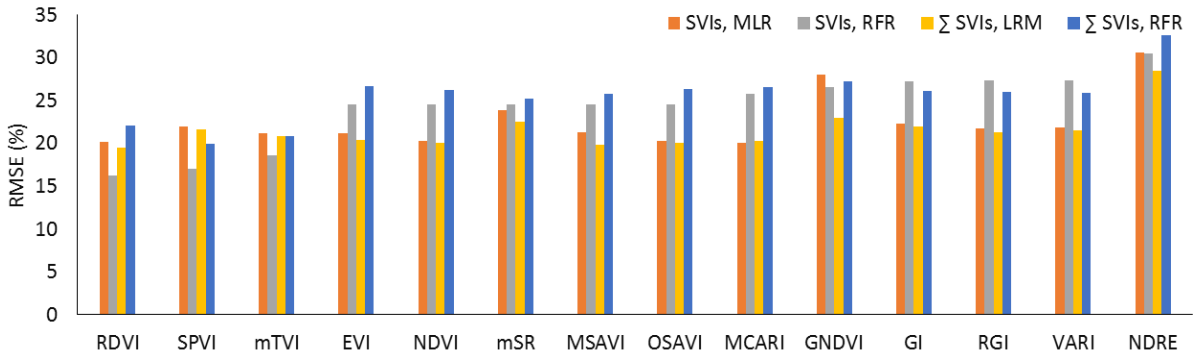

Figure 6.3. Relative RMSE variation in the prediction of capsule volume using linear regression model and random forest regression model. SVIs: SVIs of hook and flowering stage, ∑: the sum of SVIs Hook + Flowering. RFR: Random forest regression, MLR: multi linear regression, LRM: linear regression model.

6.4.6. Determination of capsule volume using a combination of important variables.

Further analysis was conducted to select the most important variable to achieve optimal results using MLR model. The first analysis was conducted using the sum of multi-temporal SVIs and optimal results were achieved using MCARI, mTVI providing an R^2 of 0.73 with RMSE 67.87 cm^3 (Table 6.10, Figure 6.5a). Whereas, in case of SVIs of two-stages as two variables for MLR, a combination of MCARI Flowering and SPVI Hook provided highest prediction accuracy with an R^2 value of 0.74 and RMSE 73.25 cm^3 (Table 6.10, Figure 6.5b). Based on results observed from the temporal SVIs using RFR, further analysis was conducted using all SVIs of two growth stages. The optimisation of parameters M_{try} and N_{tree} was done to obtain the lowest RMSE. Results indicate that RF parameters affect the prediction accuracy, as shown in Table 6.9, where the tuning parameters were set and determined. Optimal results were achieved at 500 N_{tree} with 4 M_{try} and yielded optimal prediction accuracy. Moreover, variable importance was

estimated in terms of the increase of error rate, which represents the determination of the predictive performance of the model when each predictor is permuted. The prediction accuracy decreased when the least important variables were incorporated. The use of four variables produced the highest accuracy using RDVI, mTVI, SPVI, and MCARI.

The most important variable $\sum SVI_{(Hook+Flowering)}$ in predicting poppy capsule volume as ranked by the RFR algorithm is shown in Figure 6.4. Based on the mean decrease in accuracy of prediction, RDVI, mTVI, SPVI, and MCARI were ranked most suitable variables. All the top-ranked SVIs use red – NIR region of the electromagnetic spectrum. In contrast, the RFRM uses SVIs of hook and flowering stage the importance of the contribution of each variable predicting the capsule volume is shown in Figure 6.4a. The mean decrease in accuracy displayed in Figure 6.4a is the contribution of all variable to the RFRM generated by SVIs and plant height. The variable that has high mean decrease accuracy value is considered more important for model prediction accuracy. According to the mean decrease in accuracy, the relevant variables in the RF model were $SPVI_{Hook}$, $RDVI_{Hook}$, $mTVI_{Hook}$ and $RDVI_{Flowering}$.

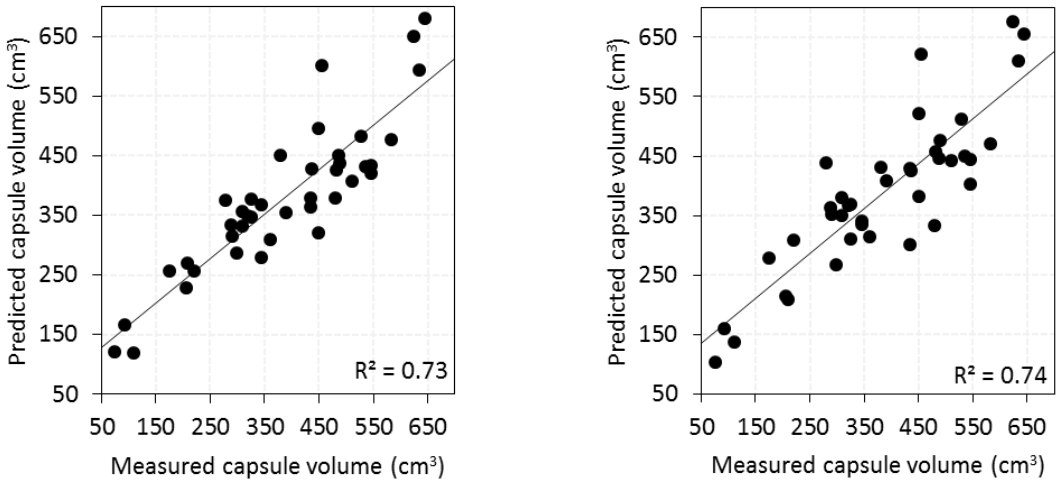

(a) (b)

Figure 6.5. The relationship between measured and predicted capsule volume using multi-linear regression model; (a) sum of multi-temporal SVIs, (b) multi-temporal SVIs.

The RFR model was developed and tested using selected variables. In case of multi-temporal SVIs using mathematical function ($\sum SVI_{(Hook+Flowering)}$), RDVI, mTVI, SPVI and MCARI were ranked as most important variables and provided an R^2 value of 0.72 with RMSE 78.02 cm^3 (Table 6.10 and Figure 6.6a). Whereas, in case of SVIs from two

different stages, SPVI $_{Hook}$, RDVI $_{Hook}$, mTVI $_{Hook}$ and RDVI $_{Flowering}$ were observed as most significant variables and provided an R^2 value of 0.84 with RMSE 58.03 cm^3 (Table 6.10 and Figure 6.6b). It was observed that SVIs of hook stage were more significant in predicting capsule volume as compared to flowering stage SVI. To check the influence of multi-temporal GVF, RF model with SPVI $_{Hook}$, RDVI $_{Hook}$, mTVI $_{Hook}$ and GVF were tested and significant improvement was observed in the model providing an R^2 0.88 with RMSE of 52.13 cm^3 (Table 6.10, Figure 6.6b).

Table 6.9. Tuning parameters and settings of Random Forest regression model

Parameters	Parameter range	Optimal setting
N_{tree}	500-9500	500
M_{try}	1-15	4

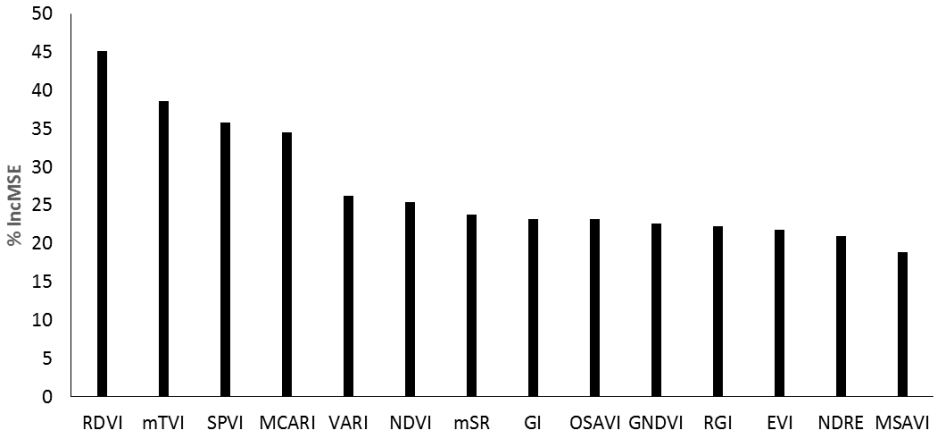

Figure 6.4. Importance of variables representing mean decrease accuracy values of optimal Random Forest regression model using the sum of SVIs of hook and flowering stage.

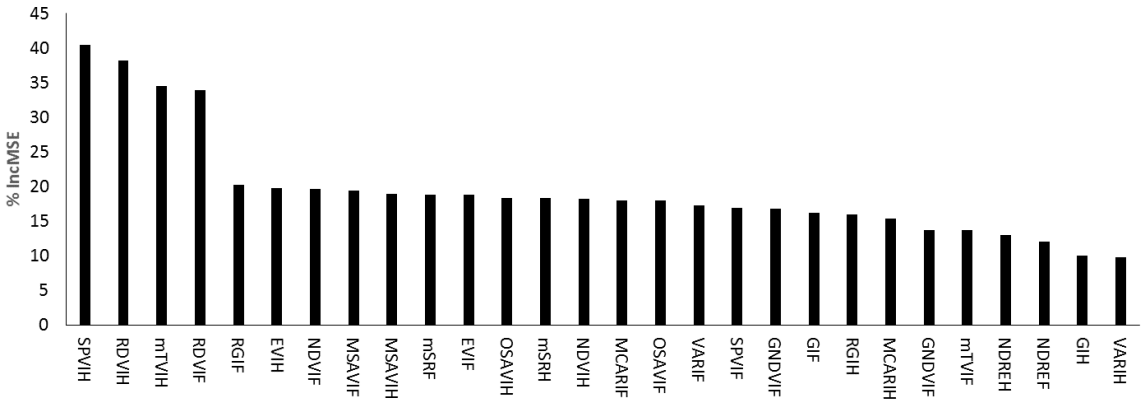

Figure 6.4a. Importance of variables representing mean decrease accuracy values of optimal Random Forest regression model using SVIs of two different growth stages.

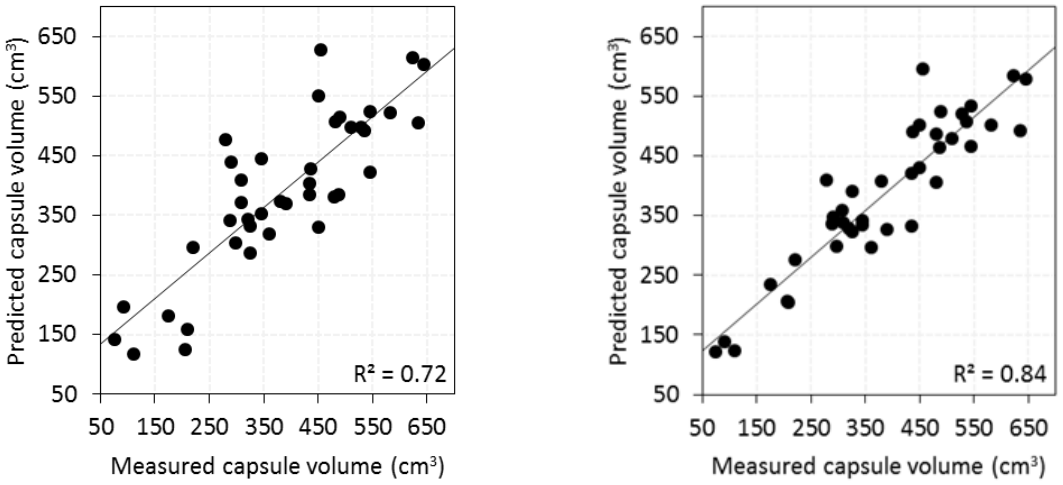

(a) (b)

Figure 6.6. The relationship between measured and predicted capsule volume using selected variable analysed with random forest regression model; (a) sum of multi-temporal SVIs ($\sum SVI_{(Hook + Flowering)}$), (b) multi-temporal SVIs (Hook, Flowering).

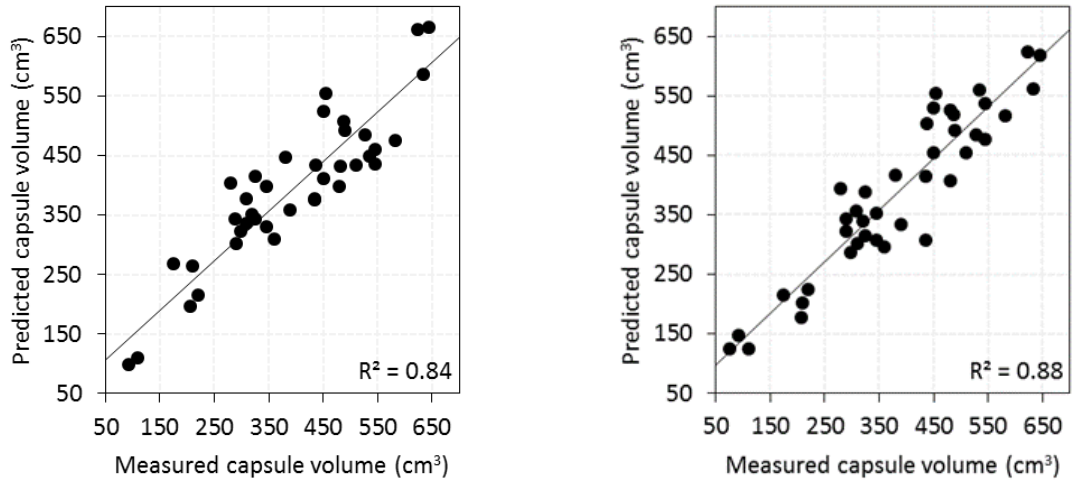

(a) (b)

Figure 6.7. The relationship between measured and predicted capsule volume using a combination of multi-temporal SVIs and GVF. (a) Multilinear model results (MCARI Flowering and SPVI Hook and GVF Flowering), (b) random forest model results (SPVI Hook, RDVI Hook, mTVI Hook and GVF Flowering).

It was observed that GVF of flowering stage resulted in significant improvement of results and predicted 86.46 % of the capsule volume as compared to RFRM based on SVIs only. In contrast, significant improvement was also observed with MLR using MCARI Flowering and SPVI Hook with GVF of flowering stage, providing an R^2 of 0.84 with an RMSE value of 59.57 cm^3 (Figure 6.5c). Overall, the highest accuracy was observed

with SVIs (Hook, Flowering) analysed using RFR, providing relative root mean square error value of 15.05 %. Similarly, a combination of multi-temporal SVIs and GVF investigated using RFR provided lowest relative root mean square error value of 13.54 %.

Table 6.10. Performance of the RFR and MLR for prediction of capsule volume using different variables.

Selected variables	MLR Model			RFR Model		
	R^2	RMSE (cm^3)	RMSE (%)	R^2	RMSE(cm^3)	RMSE (%)
Sum of Multi-temporal SVIs	0.73	67.87	17.62	0.72	78.02	20.27
Multi-temporal SVIs	0.74	73.25	19.03	0.84	58.03	15.05
Multi-temporal SVIs and GVF	0.84	59.57	15.47	0.88	52.13	13.54

6.4.7. Application of optimum index to see crop yield variability within a field.

The spatial distribution of the capsule volume was then predicted using developed models based on multi-temporal SVIs and GVF (Figure 6.8c). Results showed that the spatial variability ranged from 0 cm^3 to 645 cm^3, the low yielding areas are shown in light green through higher yielding areas in dark blue in Figure 6.8c, whereas, areas with negative yield are shown in red to yellow, illustrating no vegetation growth areas with bare ground patches. Yield maps illustrate higher yield areas in northern, southern areas of map, where irrigation water was not inundating. Although, the south-eastern side of area illustrates the areas under submerged condition with restricted and no growth (shown in red and yellow colour). Analysis based on seasonal spectral reflectance pattern reveals that NIR spectral reflectance is increased from hook to flowering stage whereas, NIR spectral reflectance is decreased from flowering to capsule formation stage. Spatial pattern of increase in NIR spectral reflectance from hook to flowering stage showed consistency with increase in capsule volume (Figure 6.8b). In contrast, increase in NIR spectral reflectance from flowering to capsule formation stage showed no relationship with yield pattern (Figure 6.8a).

6.5. Discussion

In this study, the relationship was investigated between poppy capsule volume and multi-temporal SVIs and GVF derived from multispectral images. Green vegetation fractional cover was estimated using supervised classification with an overall accuracy of 93.9 % at the hook, 91.23 % at flowering and 93.7 % at capsule formation stage, which was found to be in accordance with our previous study, in which accuracy of 93.72 % was achieved for the capsule formation stage (Iqbal *et al.* 2017). In this study, a slight reduction in accuracy at flowering stage image as compared to other growth stages is associated with the presence of flowers. The flowers present in the flowering stage

image were purposefully classified as vegetation cover due to flowers having understory vegetation. Results of green vegetation showed significant correlation with capsule volume and capsule formation stage provided optimum results with a relative RMSE of 19.61 %, however, a decrease of 0.85 % (20.46 %) at hook and 2.6 % (22.21) at flowering stage was observed, which is in agreement with the a previous investigation using LAI (Jia *et al.* 2011).

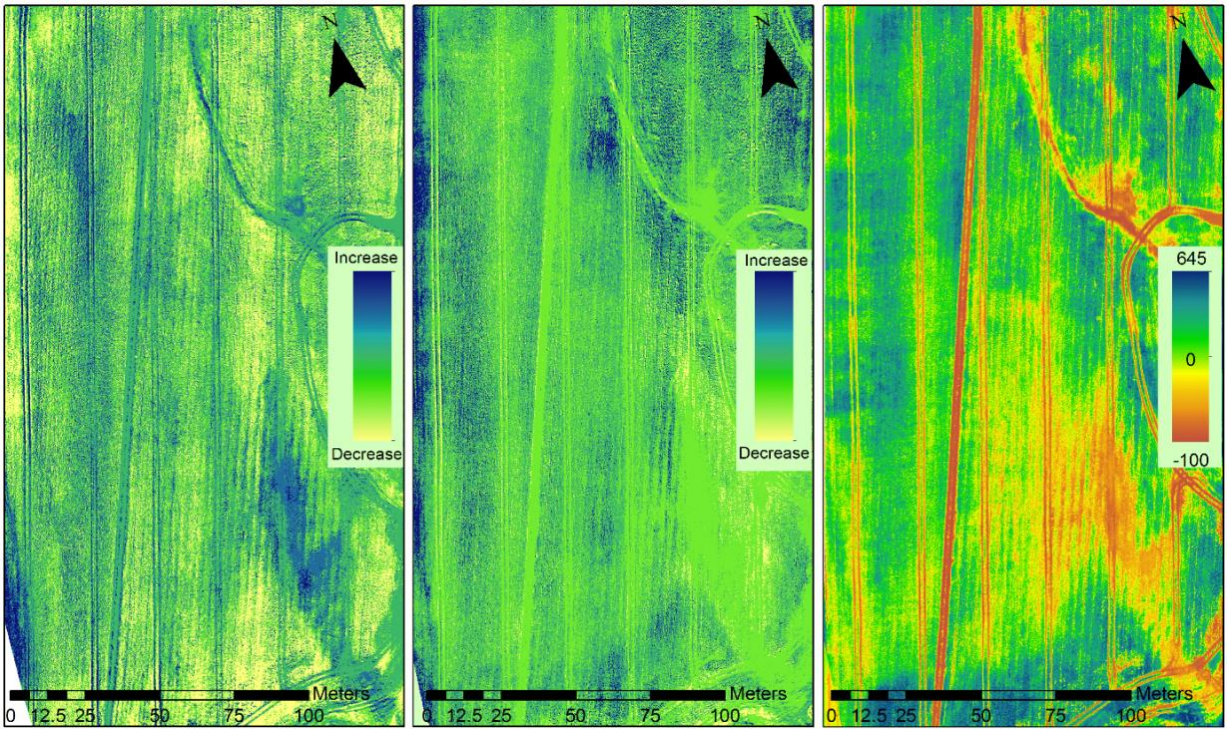

(a) (b) (c)

Figure 6.8. Spatial distribution of difference in spectral reflectance and capsule volume, (a) difference of NIR reflectance between capsule formation and flowering stage, (b) difference of NIR reflectance between flowering and hook stage, (c) spatial distribution of poppy capsule volume predicted (cm^3) based on RFRM in the study area.

Further investigation showed that the SVIs computed at hook, flowering and capsule formation stage had significant correlation with poppy capsule volume with R^2 = 0.72, 0.66 and 0.45, respectively. A significant relationship with NDVI has been reported in a previous poppy related study (Waine *et al.* 2014). The relatively weaker relationship at flowering stage can be associated with the presence of flowers, which has also been reported in a previous study (Fang *et al.* 2016). Investigation of spectral reflectance at flowering stage and growth stage without flowers showed a spectral signature similar to normal vegetation, i.e. low reflectance in red region and peak in green, red-edge and NIR portion. This indicates that understory leaves are absorbing visible light and are active in chlorophyll process. Overall, the magnitude of reflectance at flower stage was

slightly higher as compared to hook stage, which illustrates the presences of green leaves absorbing light (Figure 6.8b). Change in green vegetation fraction from flowering to capsule formation stage was not obvious, which is in accordance with previous studies (Acock, Wang, Acock, *et al.* 1996, Mahdavi-Damghani *et al.* 2010), however, capsule volume showed obvious reduction relationship with SVIs. The absorption in red bands at flowering stage was lower than the (flower free) hook and capsule formation stages, as the presence of flowers also lead towards scattering, thus, resulting in higher reflectance. This change in reflectance at the flowering stage likely resulted in the change in relationship between capsule volume and SVIs. The shift from flowers to capsules at the capsule formation stage resulted in less significant relationships between SVIs and capsule volume ranging from $R^2 = 0.32$ to 0.45. This can be associated with the presence of mature capsules and leaves. The relationship of SVIs with capsule volume is observed to change with the changing condition of crop and thus, altering the prediction accuracy. Overall, during the growth cycle, the condition of plant at hook and flowering are closely related to capsule volume, which is in accordance with previous studies (Jia *et al.* 2011, Waine *et al.* 2014). However, the capsule formation stage displayed a very weak relationship. Moreover, the capsule volume prediction at capsule formation stage is generally too late to inform crop management and agronomic practices to enhance the yield of the current crop (Acock, Wang, Acock, *et al.* 1996, Waine *et al.* 2014). Thus, investigation was further conducted on hook and flowering stage. Some studies have indicated that the sum of temporal SVIs can improve the accuracy of crop yield prediction (Pradhan *et al.* 2014). Our research confirmed this in poppy crop and strongly emphasises that summation of $SVI_{(Hook + Flowering)}$ improved the prediction accuracy.

The linear relationship between capsule volume and visible indices $\sum VARI_{(Hook + Flowering)}$, $\sum GI_{(Hook + Flowering)}$ and $\sum RGI_{(Hook + Flowering)}$ increase from 0.49 to 0.67, 0.44 to 0.66, and 0.50 to 0.67, respectively as compared to hook stage only. Similar improvement has been reported previously (Wang *et al.* 2014, Zhou *et al.* 2017). Optimal results were achieved with $\sum RDVI_{(Hook + Flowering)}$ and $\sum MSAVI_{(Hook + Flowering)}$, which yielded an $R^2 = 0.72$ with RMSE 19.55% and 19.82%, respectively. Moreover, $\sum SVIs_{(Hook + Flowering)}$ was investigated using RFR, which showed no improvement in prediction accuracy as compared to linear regression, and the result was in accordance with previous studies (Abdel-Rahman *et al.* 2013, Smith *et al.* 2013). The R^2 values for the linear model were higher than the proportion of variance explained for the RFRs, i.e. 6 of 15 of linear models as compared to 1 of 15 of RFRs had $R^2 \geq 0.70$. The RMSE values of all linear models were lower than those for the RFRs excluding the SPVI.

Moreover, previous studies reported that the MLR can provide better prediction accuracy (Vega *et al.* 2015). Our study confirmed this and indicated significant improvements in results. The combination of SVIs ($SVIs_{(Hook)}$ $SVI_{(Flowering)}$) was tested, where optimum prediction accuracy was achieved with $RDVI_{..}$ This increased the R^2 from 0.67 to 0.70 and RMSE decreased from 22.05 % to 20.20 % as compared to $\sum RDVI_{(Hook + Flowering)}$ investigated using RFR. Whereas, multi-temporal SVIs investigated using RFR showed significant improvement in prediction accuracy using RDVI, mTVI, SPVI and GNDVI with RMSE of 16.21 %, 18.59 % and 17.08 %, respectively. The prediction accuracy and importance of SVIs has been observed to change with growth stages in this study and thus, plays a vital role in prediction accuracy, and is found to be in accordance with previous studies (Jia *et al.* 2011, Waine *et al.* 2014, Iqbal *et al.* 2017). Multiple variables provide better prediction accuracy using RFR model, whereas, prediction results are significant with single variable using linear model.

Many scientists have developed methodologies to predict crop yield well before the time of harvest (Dempewolf *et al.* 2014, Pradhan *et al.* 2014, Waine *et al.* 2014, Wang *et al.* 2014, Saeed *et al.* 2017, Zhou *et al.* 2017). During this research, multi-temporal variables using MLRs and RFRs were tested. The most important variables selected to predict crop yield have also been reported in the literature (Haboudane *et al.* 2004, Zarco-Tejada, Ustin, *et al.* 2004, 2005). Results of this study showed that RFRs provided better prediction accuracy using multiple variables selected from hook and flowering stage. In the case of $\sum SVIs_{(Hook\ and\ Flowering)}$, MLR provided superior results as compared to RFR (Table 6.7, Figure 6.3). Whereas, multiple SVIs used without any mathematical function provided significant improvement using RFRs, which is associated to selected SVIs ($SPVI_{Hook}$, $RDVI_{Hook}$, $mTVI_{Hook}$ and $RDVI_{Flowering}$). RDVI and SPVI incorporates spectral signatures of visible and NIR portion and researchers have the leverage to estimate leaf fraction cover (Patel *et al.* 2007, Barati *et al.* 2011, Jiapaer *et al.* 2011). mTVI when incorporated into the model improves the accuracy as it has shown significant relationship with chlorophyll concentration in leaves (Haboudane *et al.* 2004, Zarco-Tejada, Ustin, *et al.* 2004, Stagakis, Gonzalez-Dugo, *et al.* 2012). RDVI at flowering stage was found as one of the important variables for yield prediction, as it incorporates the leave cover information at flowering stage. MLR and RF using multi-temporal SVIs showed that spectral indices with stronger relationship with chlorophyll and green vegetation fraction are highly suitable to estimate poppy capsule volume, which is in accordance with previous research in which the relationship of LAI with opium yield was investigated (Jia *et al.* 2011). Further investigation using $SPVI_{Hook}$, $RDVI_{Hook}$, $mTVI_{Hook}$ and $GVF_{Flowering}$ were tested and significant improvement was observed with RFRs

model providing an R^2 0.88 with RMSE of 52.13 cm^3 (Table 6.10, Figure 6.7 b), whereas, incorporation of $GVF_{Flowering}$ with MCAR and SPVI showed improvement in prediction accuracy using MLRs. The prediction accuracy has been found to change with changing growth stages of GVF and SVIs, supported by previous studies (Jia *et al.* 2011, Waine *et al.* 2014, Iqbal *et al.* 2017).

Results of spatial distribution of the capsule volume predicted using developed models showed that the spatial variability ranged from 0 cm^3 to 640 cm^3. The spatial pattern of capsule volume is strongly influenced by topographical variation, which in turn influences irrigation efficiency. The performance of SVIs is influenced by irrigation application as it changes the plant condition (Baluja *et al.* 2012). Thwe south-eastern side of farm with lowest elevation accumulated water causing saturation, which showed restricted or no crop growth (Mahdavi-Damghani *et al.* 2010). Whereas, areas with higher relative elevation provided well-drained soil showing higher yield. Therefore, crop health can be improved by improving irrigation efficiency and drainage condition. Moreover, spectral reflectance of crop showed increase in NIR region from hook till flowering stage, whereas, decrease in NIR reflectance was observed from flowering till capsule formation stage. Increase in NIR reflectance can be associated with the presence of photosynthetically active tissues at hook stage and decrease in NIR reflectance can be associated to capsule maturity at capsule formation stage. Spatial pattern of increase in NIR reflectance till flowering has been found to be in agreement with the spatial pattern of capsule volume. Therefore, SVIs with the combination of NIR and visible bands showed the decrease in index value near maturity due to senescence of leaves, thus, altering the performance of prediction model.

Overall, results illustrate that multi-temporal SVIs and GVF derived from UAS imagery were correlated significantly with capsule volume. Higher correlation was observed at hook stages, but correlation was found to be poor at flowering and capsule formation stage. Therefore, the hook stage SVIs in combination with GVF of flowering stage is suitable for capsule volume estimation. While, the combination of $\sum SVIs_{(Hook + Flowering)}$ provided significant improvement with visible band indices (VARI, GI and RGI). In addition, modified SVIs with red, NIR and green band (mTVI, RDVI and SPVI) provided better results with $SVIs_{(Hook)}$ and $SVIs_{(Flowering)}$ and $GVF_{(Hook)}$. Capsule volume can also be predicted at flowering stage, but with lower accuracy. To improve the prediction accuracy, images acquired one or two days after the end of flowering stage can make a significant difference. As time after flowering stage is critical for the development of capsules, and soil, plant-water relationship after flowering stage plays a vital role in capsule yield (Acock, Wang, Acock, *et al.* 1996, Mahdavi-Damghani *et al.*

2010, Dean 2011). Moreover, images acquired at the end of flowering stage and at the onset of capsule formation stage would provide spectral information of capsule, which would improve the prediction accuracy and help farmer to modulate agronomic practices for enhancing the yield. Results showed that GFV is an important factor for capsule volume prediction, thus, the early capsule formation stage will also be significant, as it would provide the information of peak GVF at capsule formation stage. Green vegetation fraction provides medium to absorb sunlight and to convert it into food required for capsule yield (Acock, Wang, Acock, *et al.* 1996, Lisson 2007, Apuya *et al.* 2008). Moreover, sunlight and chlorophyll alters water and nutrient requirement (Mahdavi-Damghani *et al.* 2010). Therefore, data collected between flowering and capsule formation will improve the prediction and would help to investigate the soil, plant-water relationship. In addition to this, random forest regression models can improve the prediction accuracy as they can handle nonlinear relationship between variables.

Several factors can influence the selection of suitable types of model for estimating capsule volume. Results showed that linear models performed better than RFRs model using single variables, whereas, inclusion of multiple variables provided superior results with RFRs, supported by previous research (Smith *et al.* 2013). RFR is less sensitive to overfitting, due to a large number of decision trees produced by randomly selecting a subset of training sample and subset of variables for splitting at each tree node. The RFR model has been shown to be suitable for variable selection for high dimensional dataset and can provide better prediction accuracy with multiple variables. In addition, model performance can be influenced by crop species, agronomic factors and extent of weed invasion. This implies that model calibration will be required based on field survey data for any new study site. From the test results, the developed model based on selected variables (GVF, SPVI, RDVI, mTVI) can be tested on other sites, although further tests are desirable with the data of multiple growing seasons and varied production scale. In addition, this study predicted the capsule volume of a summer crop only; however, in other parts of the world, poppy is sown in winter, thus, the difference of prediction conditions need to be reconciled by quantifying the effect of weather and genotype. In case of Tasmania, continuous research is taking place, which is foreseen to improve crop genetically for higher yield, thus, the applicability of developed models would need to be investigated on other varieties. Overall, the GVF and SVIs can provide significant information on crop yield potential, thus, assisting farmers in predicting the crop yield well before harvest, in turn contributing in enhancing yields by modulating the agronomic practices.

6.6. Conclusion

In this study, a UAS platform with a 4-band Parrot Sequoia multispectral sensor was used to acquire very high spatio-temporal images of a poppy crop. This study demonstrated the potential to estimate capsule volume of poppy crop using multi-temporal SVIs and GVF investigated using RFRs and MLR. The GVF of each critical stage was estimated using supervised classification. UAS-derived GVF was strongly correlated with R^2 value 0.67, 0.72 and 0.76 at flowering, hook and capsule formation stage, respectively. Moreover, the relationship between SVIs and capsule volume was investigated and the hook stage was identified as the best stage for yield estimation. The corresponding optimal single stage SVIs were RDVI, mTVI and MSAVI with R^2 of 0.72, 0.69 and 0.67, respectively. The capsule volume prediction accuracy was found to increase when RFR was conducted using multi-temporal SVIs and GVF. The combination of $GVF_{Flowering}$ with $RDVI_{Hook}$, $SPVI_{Hook}$ and $mTVI_{Hook}$ performed best with RMSE of 13.54% using RFRs, whereas, with MLR combination of $MCARI_{Hook}$, $SPVI_{Hook}$ and $GVF_{Flowering}$ provided optimal results with RMSE of 15.47 %. Poppy capsule volume estimation using combination of RFRs with UAS computed GVF and SVIs is a novel approach, which has not been tested before. The results showed that variables computed from hook and flowering stage were able to predict capsule volume accurately (R^2 = 0.88). This can provide valuable information for farmers and the pharmaceutical industry for enhancing crop productivity by modulating nutrient and irrigation application.

6.7. Thesis context

Chapter 6 addressed the third objective and described a successful methodology to predict capsule volume two months prior to harvest using multi-temporal UAS data. The analysis was based on spectral vegetation indices and applied a random forest (RF) machine learning approach. Chapter 7 builds onto this work, and focuses on retrieval of alkaloid concentration.

Chapter 7

7. Prediction of poppy alkaloid concentration using UAS remote sensing

Chapter 7 described a practical and effective method for thebaine prediction in a quantitative manner using multi-temporal UAS remote sensing data analysed using random forest (RF) machine learning approach and has been submitted for publication to **precision agriculture journal** June 2018.

Abstract

Alkaloid concentration, which represents the quality of industrial poppy, needs to be estimated in a spatially explicit manner to predict the value of crop prior to harvesting. Current practice is to estimate alkaloid concentration using destructive sampling and laboratory analysis, however, in order to estimate the value of the whole crop a method that could predict alkaloid concentration in field conditions prior to harvesting is needed. In this study, an Unmanned Aerial System (UAS) with multispectral imaging was tested for estimation of alkaloid concentration of a poppy crop before harvest, which was sown for pharmaceutical purposes in Tasmania, Australia. This study presents the result of a Random Forest (RF) regression analysis to evaluate the contribution and predictive ability of spectral and structural variables derived from the images. It was found that UAS imagery with an RF model has the potential to estimate thebaine concentration well before harvesting and without laboratory analysis. It was found that an RF model with the combination of MSAVI, mSR, OSAVI, NDVI and EVI spectral indices can provide optimal results to estimate thebaine with a relative error of 13.56% to 22.36% with training and validation dataset, respectively. The thebaine concentration predicted using the proposed RF model was strongly correlated to the laboratory measured thebaine concentration, with an R^2 value ranging from 0.63 to 0.82 for the training and validation datasets, respectively. These results indicate that poppy thebaine concentration can be estimated with reasonable accuracy three weeks prior to harvesting.

7.1. Introduction

Tasmania, Australia is considered the world's most efficient licit producer of industrial poppies with the highest yield of alkaloids, which are formed within the capsule (Lisson 2007). Tasmanian summers have long day lengths, providing a competitive advantage over other growing areas, and a dry climate at harvesting time in Tasmania ensures

high alkaloid concentrations. Moreover, the island state is isolated with a small population, and thus risk of illegal activities is perceived as easier to manage. Poppy is the highest value field crop of Tasmania (Murray 2014). In Tasmania, poppy farmers focus not only on the capsule yield but also on alkaloid concentration, as processors determine the price based on the poppy alkaloid concentration of the crop. There are three main alkaloids that contribute to the value of the poppy crop: morphine, codeine and thebaine (Bernath and Tetrnyi 1981). Accurate yield estimation in high value alkaloid poppy crop can offer improved decision making for farmers, managers and the pharmaceutical industry.

To enable higher alkaloid yield, optimal management of soil nutrients and irrigation is required during critical growth stages from hook till capsule formation (Chung 1987, Laughlin and Chung 1990, Laughlin *et al.* 1998, Mahdavi-Damghani *et al.* 2010). The increasing demand for cultivable land in Tasmania has resulted in moving cultivation to less well drained soils that are vulnerable to water-logging. This results in restricted root growth in poppy plants. To cope with the water logging problem, raised bed sowing was introduced allowing early sowing by farmers. Early sowing allows longer growth periods and results in more optimal use of water and nutrients and higher capsule yield. During the crop growth cycle, short segments of the cycle need to be monitored precisely for enhanced yield. Traditionally, crop monitoring is conducted using chemical testing with physical sampling methods, which is complex and time consuming. Generally, poppy growth is highly heterogeneous within the field and traditional sampling methods are impractical for monitoring the distribution of crop at a high degree of accuracy (Jia *et al.* 2011, Wang 2013, Waine *et al.* 2014, Iqbal *et al.* 2017). In addition, timely monitoring is difficult to achieve through traditional methods and destructive sampling cannot be avoided. If alkaloid concentration in capsules could be estimated well before harvesting, the input resources (irrigation and nutrients) could therefore be optimized to maximize yield.

Satellite remote sensing has been widely used in agriculture, as it has the ability to non-destructively predict biochemical properties of crops in a spatial context using spectral vegetation indices (SVIs) (XUE *et al.* 2005, Wang *et al.* 2014, Zhou *et al.* 2017). A number of studies have predicted crop yield and showed a linear relationship between the normalised difference vegetation index (NDVI) and yield in wheat and poppy (Oudemans *et al.* 2002, Zarco-Tejada, Ustin, *et al.* 2005, Morel *et al.* 2014, Vega *et al.* 2015, Onoyama *et al.* 2017). However, acquiring satellite data can be expensive (for high spatial resolution imagery), the spatial and temporal resolution is relatively low, and the required cloud-free conditions can seldom be obtained in Tasmania. In contrast, with

Unmanned Aerial Systems (UAS) and recent sensor technology, high spatial resolution image data can be collected anytime except in rainy and very windy conditions (Nex and Remondino 2014, Iqbal *et al.* 2017). Therefore, UAS acquired images could be a practical alternative to satellite remote sensing. Several sensors have been mounted on UAS to capture data for crop growth monitoring, disease detection, and estimation of vegetation cover, LAI, biomass, plant height and yield. Moreover, multispectral and hyperspectral cameras have been used to monitor vegetation using different SVIs (Berni, Zarco-Tejada, Suarez, *et al.* 2009, Mäkynen *et al.* 2012, Zarco-Tejada, Gonzalez-Dugo, *et al.* 2012, Geipel *et al.* 2014, Zarco-Tejada *et al.* 2014).

Some researchers inspected UAS derived SVIs and determined that structural indices are related to LAI, i.e. Renormalised Difference Vegetation Index (RDVI), modified Triangular Vegetation Index (mTVI), and optimised Soil-Adjusted Vegetation Index (OSAVI) showed significant relationships with cotton yield at an early growth stage (Roujean and Breon 1995, Rondeaux *et al.* 1996, Haboudane *et al.* 2004, Malenovský *et al.* 2006, Albrechtova *et al.* 2008, Stagakis, Gonzalez-Dugo, *et al.* 2012, Zarco-Tejada, Gonzalez-Dugo, *et al.* 2012, Zarco-Tejada, Morales, *et al.* 2013, Cilia *et al.* 2014). Narrow-band hyperspectral indices related to crop physiological status, i.e. Modified Chlorophyll Absorption Index (MCARI), Enhanced Vegetation Index (EVI) and Transformed Chlorophyll Absorption Index (TCARI), showed a significant relationship near maturity stage (Qi *et al.* 1994, Haboudane *et al.* 2004, Jiang *et al.* 2008). SVIs derived from NIR and visible bands have been reported as the most significant for estimating crop yield, nitrogen and chlorophyll estimation (Curran *et al.* 1991, Liu *et al.* 2012, Abdel-Rahman *et al.* 2013, Waine *et al.* 2014, Wang *et al.* 2014, Saeed *et al.* 2017). Nitrogen is vital for alkaloid production (Laughlin 1977) and nitrogen application from hook till capsule development stage showed significant increases in alkaloid yield (Losak and Palenicek 2005). Thus, spatial variability information of chlorophyll and nitrogen can help to predict yield potential before harvesting. This allows farmers to take proactive action regarding the variable rate application of irrigation, nutrients and pesticides in a precise and sustainable way that can help in enhancing the yield potential without depleting resources (Bernath and Tetrnyi 1981, Lisson 2007, Mahdavi-Damghani *et al.* 2010). Moreover, early yield prediction can help the pharmaceutical industry to plan post-harvest requirements (Laughlin *et al.* 1998, Zarco-Tejada, Ustin, *et al.* 2005, Harvest *et al.* 2009).

Some studies investigated multiple SVIs to predict yield (Vega *et al.* 2015, Zhou *et al.* 2017). These studies have explored SVIs and yield using simple linear or multiple linear regression models. There is a significant opportunity to test machine-learning

algorithms for yield estimation using UAS based remote sensing data. Statistical modelling based on machine learning algorithms can provide an alternative to traditional regression techniques and provides better prediction accuracy (Abdel-Rahman *et al.* 2013, Smith *et al.* 2013, Jeong *et al.* 2016). The Random Forest (RF) regression model, is a machine learning technique (Breiman 2001) used for feature selection to reduce the redundancy of variables (Smith *et al.* 2013, Adam *et al.* 2014, Wang *et al.* 2016). RF is a robust method and can handle a large number of input variables as well as an unbalanced dataset. The variable importance is very helpful measure in gaining insight about which SVIs are most useful for feature prediction when implemented on high dimensional data (Siroky and others 2009, Jones and Linder 2015). Several studies have tested RF for crop yield prediction using multiple variables (Abdel-Rahman *et al.* 2013, Jeong *et al.* 2016, Wang *et al.* 2016, Saeed *et al.* 2017). This study investigates the performance and potential of UAS multispectral SVIs using RF regression to estimate alkaloid yield. We investigate the accuracy obtained with high spatial and temporal resolution UAS imagery for measuring spatial and temporal variability of poppy alkaloids. Specifically, the objective of this research is to identify the optimal combination of SVIs that are associated to alkaloid yield.

7.2. Material and methods

7.2.1. Study area

This research was carried out in Sorell, Tasmania, Australia (42°45′ 58″S, 147° 35′ 38″E) on a commercial opium poppy crop (Figure 7.1). In Tasmania different varieties are cultivated to harvest different concentration of alkaloids. This particular study was conducted on a thebaine specific producing variety. Thus, this study focused on thebaine only. The experiment was designed based on a single season from June 2016 to January 2017. The poppy crop was sown in mid-July 2016 with the seedling emergence in the following 1-2 weeks. Flowering occurred in early December, with capsule formation starting in mid-December and poppy capsules were harvested on 16 January 2017. The crop was sown with a seed drill to maintain a seeding density of 80 seeds per square metre. To control the weeds, herbicides were applied prior to sowing and at early rosette stage.

7.2.2. Field data collection

The growth and development lifecycle of poppy is divided into the following stages; growth of seedlings, the formation of rosette-type leaves, stem elongation, hook, flowering and capsule formation (Shuljgin 1969, Bernath 1986, Wang *et al.* 1999, Miura

and Huete 2009, Mahdavi-Damghani *et al.* 2010). The critical period in opium development is from the hook stage until the capsule formation stage (Waine *et al.* 2014, Iqbal *et al.* 2017). Thus, UAS and field campaigns were conducted at hook stage (17th November), flowering (4th December), and at capsule formation stage (22nd December 2016).

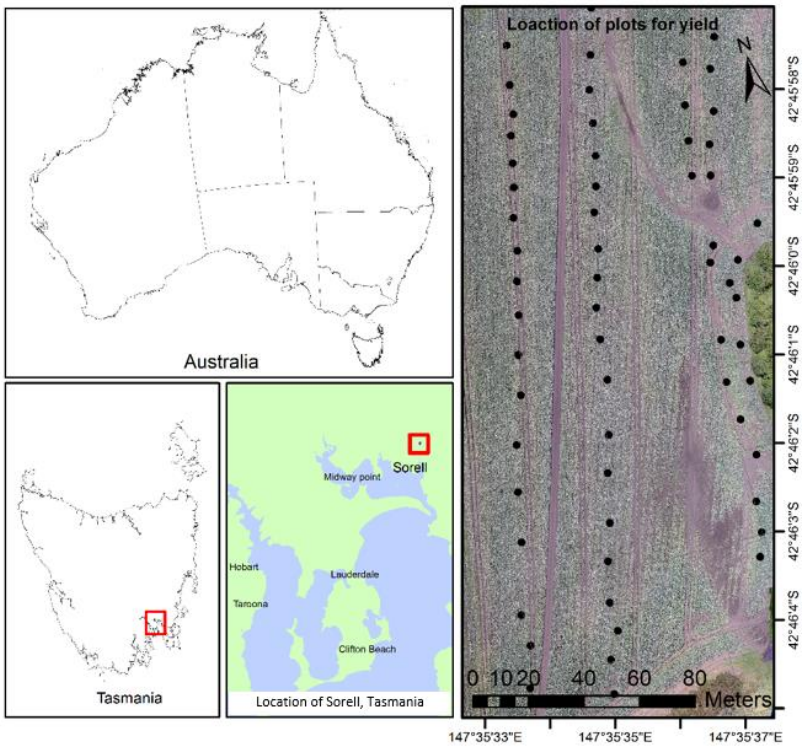

Figure 7.1. The general location of the study site and the overview of the image obtained from unmanned aircraft system (UAS) showing the location of field sampling plots.

Table 7.1. Field assessments and UAS campaigns at the study location

Survey date	Growth stage	Observation
Sorell		
17/11/2016	Hook	UAS, GPS
04/12/2016	Flowering	UAS
22/12/2016	Capsule formation	UAS
16/1/2017	Harvesting	Destructive sampling

Destructive sampling was conducted from 70 (0.5 x 0.5 m) sample plots, which included the collection of all capsules. The collected capsules were chemically analysed for the concentration of alkaloids by Tasmanian Alkaloid Pty. Ltd. In order to ensure that the

size and location of each plot was consistent, we used wooden stakes to mark each plot location and used a PVC quadrant (0.5 m x 0.5 m) to confine the plots. Moreover, global navigation satellite system (GNSS) coordinates of each sample plot and Ground Control Points (GCP) (0.5 m 0.5 m) were measured with survey-grade dual frequency real-time kinematic (RTK) GNNS (2 – 4 cm absolute coordinate accuracy).

7.2.3. UAS campaign Sorell site

Data was acquired using a 4-band multispectral MicaSense/Parrot Sequoia sensor, mounted on a 3DR Solo quadcopter (3D Robotics, Inc, city of supplier). The Sequoia sensor contains an RGB 16 megapixel sensor (4608 × 3456 pixel) with four single band sensors: the green band (530–570 nm), red band (640–680 nm), the red edge band (730–740 nm) which captures the rapid change from low red reflectance to near infrared reflectance, and near-infrared band (NIR, 770 nm to 810 nm). The spectral sensitivity of image sensors provides optimum sensitivity of 70% in the green band and gradual decrease to 55% at 650 nm, 35% at 730 nm and 30% around 800 nm in near-infrared. The sensor has a built-in navigation-grade GNSS and IMU for positioning and orientation. Moreover, it operates with an irradiance sensor, which allows self-calibration of spectral bands and provides the option to derive reflectance values. The sensitivity of the irradiance sensor is 98% in the red region and 82% to 84% in the near-infrared, red edge and green regions. The UAS campaigns were conducted under clear sky and low wind conditions between 12:00 pm and 2:00 pm local time. The Tower app was used to define the UAS flight lines. The UAS mission was planned with 75% overlap between adjacent flight strips, flight speed of 2.5 m/s, and flying height of 50 m, 25 m, and 25 m above ground level (AGL) for 17th November, 4th December, and 22nd December respectively. Flying height was reduced from 50 to 25 m to collect higher resolution imagery. MicaSense ATLAS was used to generate seamless 4-band orthomosaics for each date. The orthomosaics where further georeferenced with the GNSS coordinates for the GCPs by performing a 1st order polynomial geometric transformation in ArcGIS 10.3.

7.2.4. Computation of vegetation indices

Spectral indices that have been previously tested for crop yield estimation (Carlson and Ripley 1997, Zarco-Tejada, Ustin, *et al.* 2004, Zarco-Tejada, Gonzalez-Dugo, *et al.* 2012, Pradhan *et al.* 2014, Bendig *et al.* 2015, Zhou *et al.* 2017) were computed on the multispectral orthomosaic. The orthomosaic was clipped into 70 plots to collect the image spectra from each band (n = 4) to compute SVIs using Arc GIS 10.3. SVIs that

were possible to compute using the selected bands (550, 660, 735 and 790 nm) are presented in Table 7.2.

Table 7.2. Vegetation indices investigated in this study.

Acronym	Formula	Reference
VARI	$(\varrho\ 550 - \varrho\ 660) / (\varrho\ 550 + \varrho\ 660)$	(Gitelson *et al.* 2002)
MCARI	$1.2\ [2.5(\varrho\ 790 - \varrho\ 660) - 1.3(\varrho\ 790 - \varrho\ 550)]$	(Haboudane *et al.* 2004)
mTVI	$1.2\ [1.2(\varrho\ 790 - \varrho\ 550) - 2.5(\varrho\ 660 - \varrho\ 550)]$	(Haboudane *et al.* 2004)
NDVI	$(\varrho\ 790 - \varrho\ 660) / (\varrho\ 790 + \varrho\ 660)$	(Rouse Jr 1972)
GI	$\varrho\ 550\ /\ \varrho\ 660$	(Zarco-Tejada, Berjón, *et al.* 2005)
RGI	$\varrho\ 660\ /\ \varrho\ 550$	(Zarco-Tejada, Berjón, *et al.* 2005)
RDVI	$(\varrho\ 790 - \varrho\ 660) / (\varrho\ 790 + \varrho\ 660)^{0.5}$	(Roujean and Breon 1995)
SPVI	$0.4[3.7(\varrho\ 790 - \varrho\ 660) - 1.2\lvert \varrho\ 550 + \varrho\ 660\rvert]$	(Vincini *et al.* 2006)
OSAVI	$1.16(\varrho\ 790 - \varrho\ 660)/(\varrho\ 790 + \varrho\ 660 + 0.16)$	(Rondeaux *et al.* 1996)
GNDVI	$(\varrho\ 790 - \varrho\ 550) / (\varrho\ 790 + \varrho\ 550)$	(Gitelson *et al.* 1996)
MSAVI	$[2(\varrho\ 790 + 1 - [2\times \varrho\ 790+1)^2 - 8(\varrho\ 790 - \varrho\ 660)]^{0.5}]/2$	(Qi *et al.* 1994)
mSR	$(\varrho\ 790 / \varrho\ 660 - 1)/ (\varrho\ 790 / \varrho\ 660 + 1)^{0.5}$	(Chen and Cihlar 1996)
NDRE	$(\varrho\ 790 - \varrho\ 735) / (\varrho\ 790 + \varrho\ 735)$	(Clevers *et al.* 2002)
EVI	$2.5\ (\varrho\ 790 - \varrho\ 660) / (1 + \varrho\ 790 + 2.4 \times \varrho\ 660)$	(Jiang *et al.* 2008)

7.2.5. GVF estimation

Green vegetation fraction (GVF) is a ratio of the vertical projection of green leaves onto a horizontal surface (Carlson and Ripley 1997, Stark *et al.* 2000, Patel *et al.* 2007). To estimate GVF, supervised classification was performed based on field data collected using field campaign. The cropped and non-cropped areas were classified using training data which was collected from field. To calculate the ratio of vegetation cover, multiple plots were used (Figure 7.1) and the ratio of vegetation achieved using supervised classification was evaluated with field data. The accuracy achieved with supervised classification was also tested with the index-based technique for distinguishing soil patches that we presented in a previous study (Iqbal *et al.* 2017).

7.2.6. Data analysis for thebaine concentration estimation

For the remote prediction of poppy alkaloids, multi-temporal SVIs and GVF were used to train and test (validate) the RF regression models. Analysis was conducted by a combination of multiple multi-temporal SVIs and GVF to check the performance of all variables. Based on previous research (Breiman 2001, Abdel-Rahman *et al.* 2013) and investigation of conducted in this research, the number of trees (N_{tree}) in the RF regression was set to 500. Multiple number of variables (M_{try}) (1 to 49) were tested in the RF regression. The number of variables providing optimal prediction accuracy based on out-of-bag data were selected for further analysis. Variables providing improved accuracy were used to predict alkaloid concentration using multi-temporal

variables. Selected input variables with an optimal number of M_{try} and 500 N_{tree} were used to predict alkaloids. To check the consistency and robustness of the model, the dataset was randomly split into 10 equal size subsamples. During each iteration 70% of the data was used for training and the remaining 30% was used for validation. During the 10 iterations (K1 to K10), the dataset for validation and training was iterated in such a way that all the data points could be used for training and validation. However, a data point used in training was not used for validation simultaneously in a single iteration (Kohavi and John 1997, Breiman 2001, Cutler *et al.* 2007, Apuya *et al.* 2008). The performance of training and validation dataset during each iteration was calculated using well-known error statistics to analyse the difference between measured and predicted thebaine concentration, including root mean square error (RMSE) and relative root mean square error. The mean RMSE for all combinations was used as a summary indicator for model performance based on training and validation.

7.3. Results

7.3.1. Variable importance for alkaloid yield estimation

Analysis was conducted using all SVIs and GVF of three growth stages to estimate thebaine concentration. The optimisation of parameters, i.e. the number of variables or (M_{try}) selected were based on lowest RMSE. Analysis based on thebaine indicates that RF parameters (M_{try}) affect the prediction accuracy, as shown in Figure 7.2, where the optimal RMSE value was achieved with five M_{try}. Moreover, variable importance was estimated in terms of the increase of error rate, which represents the determination of the predictive performance of the model when each predictor is permuted. The mean decrease in accuracy illustrates the contribution of each variable to the RF regression model generated using multi-temporal SVIs and GVF (Figure 7.3).

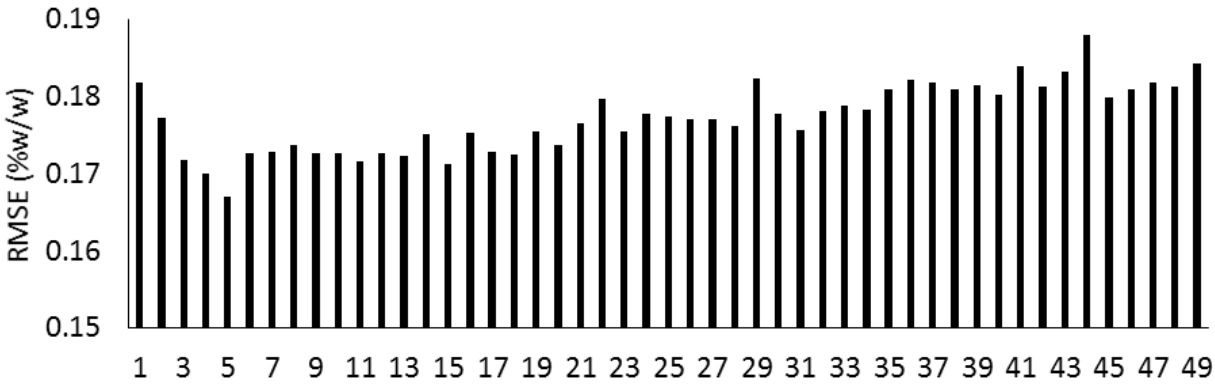

Figure 7.2. Optimal parameters (M_{try}) of random forest (RF) using RMSE.

Variables that have high mean decrease in accuracy value appear to be more important for thebaine prediction. According to the mean decrease in accuracy (% IncMSE), the most relevant variables in the RF model were MSAVI, mSR, OSAVI, NDVI and EVI (Figure 7.3 and 7.4). Results illustrate that the SVIs computed from capsule formation stage imagery contributed more significantly as compared to the variables computed from hook and flowering stage imagery. The ten most important variables are shown in Figure 7.4 by their importance in estimating thebaine concentration computed from capsule formation stage imagery. The importance scores indicate that SVIs formed using the NIR and red spectral bands dominate for predicting thebaine yield.

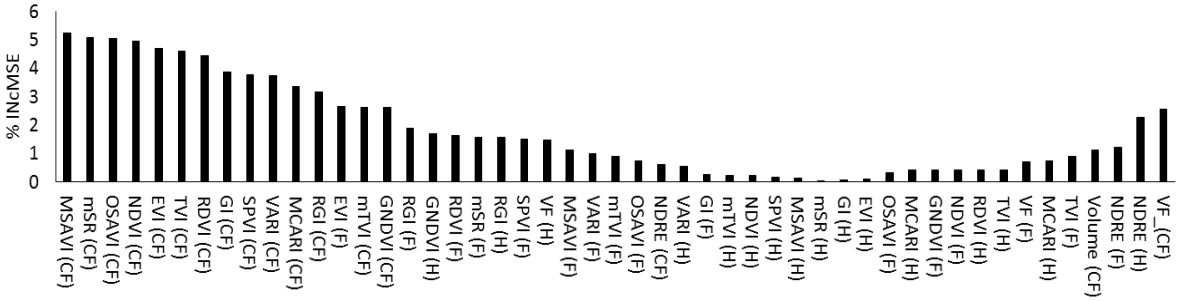

Figure 7.3. Importance of variables representing mean decrease accuracy values of optimal Random Forest regression model using SVIs and GVF of flowering, hook and capsule formation stage.

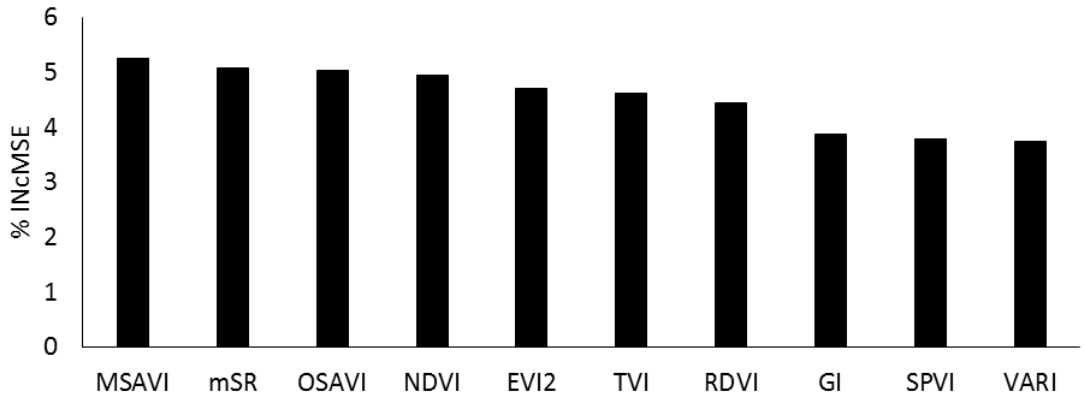

Figure 7.4. A subset of ten most importance of variables representing mean decrease accuracy values of optimal Random Forest regression model using SVIs and GVF of flowering, hook and capsule formation stage.

7.3.2. Determination of thebaine concentration using a combination of important variables.

The optimised RF model developed using MSAVI, mSR, OSAVI, NDVI and EVI were used to estimate thebaine concentration. Summary statistics based on training and

validation dataset are shown in Table 7.3 and Figure 7.5. The mean relative RMSE of 13.56 % (0.0907% w/w) with an R^2 of 0.82, (Figure 7.5a) was achieved from training data whereas, mean relative RMSE of 22.36 % (0.148 % w/w) with an R^2 of 0.63 was achieved with validation dataset (Figure 7.5b). Summary statistics based on training and validation dataset are shown in Table 7.3 and Figure 7.5.

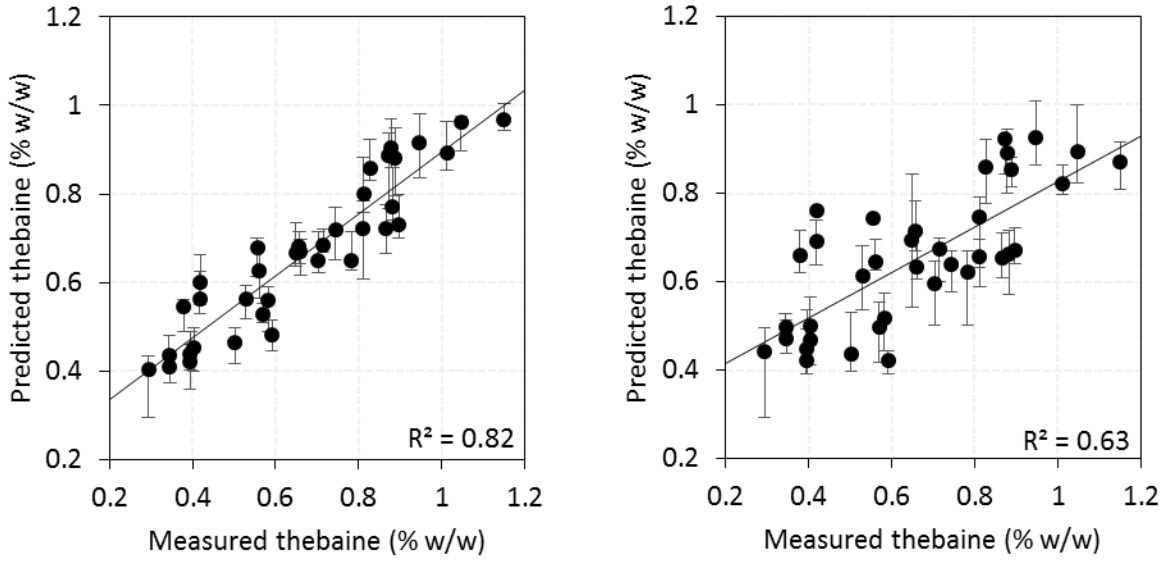

(a) **(b)**

Figure 7.5. Linear fit between measured and predicted thebaine: (a) training data; and (b) validation data.

Table 7.3. Average measured and predicted thebaine (%w/w).

	Training		**Validation**	
	Measured (%w/w)	Predicted (%w/w)	Measured (%w/w)	Predicted (%w/w)
Min	0.294	0.4045	0.294	0.421
Median	0.658	0.668	0.657	0.657
Mean	0.669	0.664	0.661	0.655
Max	1.15	0.967	1.15	0.923

Underestimation of thebaine was observed in plots with high measured concentrations, whereas overestimation was observed in plots with lower concentrations. The difference between measured and predicted thebaine of smaller capsules based on the training dataset showed an overestimation of 37.58% (0.11% w/w), and underestimation of 15.91 % (0.183 % w/w) in case of more concentration plots. In contrast, the validation dataset showed an overestimation of 43.19 % (0.127 % w/w) for plots with

lowerthebaine concentration and 19.73 % (0.227 % w/w) for higher thebaine concentration plots.

7.4. Discussion

The results from this study have shown that thebaine concentration in poppy capsules can be predicted using UAS imagery. The spectral information collected at the capsule formation stage was found to be most important for estimating thebaine concentration, compared to imagery collected at hook or flowering stage. Given alkaloid development starts at capsule formation stage, it is logical that information collected at that stage would relate more strongly. However, agronomic practices well before capsule formation stage and after flowering stage play an important role in the development of alkaloid concentration in the plants. SVIs computed from capsule formation stage showed higher importance as compared to hook and flowering stage SVIs. This is in accordance with the findings of previous research (Chung 1987, Mahdavi-Damghani *et al.* 2010), where they showed that alkaloid production per surface unit tended to increase by irrigation after flowering stage resulting in higher concentrations of alkaloids. Whereas, for the estimation of poppy capsule volume, 3-4 weeks around flowering stage are reported as suitable (Waine *et al.* 2014). Variable importance determined from RF showed that the SVIs with the combination of visible and NIR bands were ranked most highly and showed maximum influence to predict thebaine, as reported previously for poppy capsule volume and yield in other crops (Aparicio *et al.* 2000, Waine *et al.* 2014, Saeed *et al.* 2017).

The developed RF model using five key SVIs (MSAVI, mSR, OSAVI, NDVI and EVI) has illustrated that considerable information on thebaine concentration is contained in the red and NIR ranges computed from capsule formation stage data, which are associated with chlorophyll and protein contents (Curran *et al.* 1991, Liu *et al.* 2012, Abdel-Rahman *et al.* 2013, Wang *et al.* 2014, Onoyama *et al.* 2017). Especially, spectral indices that were selected by the RF model as important features for estimating thebaine concentration are related to nitrogen absorption features (Zhu *et al.* 2010, Cilia *et al.* 2014, Vega *et al.* 2015). It is interesting to note that the indices including red and NIR bands are found highly suitable for thebaine prediction, which are related to crop health and nitrogen status (Serrano *et al.* 2000, Zhu *et al.* 2010). Thus, these spectral indices can be associated with nutrient uptake after the flowering stage. Nutrient application between flowering and capsule formation are recommended to increase the alkaloid concentration (Jain 1990b, Losak and Richter 2004). Particularly nitrogen is vital for alkaloid production (Laughlin 1977), and formation of alkaloids is higher when N is applied at flowering

and capsule development stage (Losak and Palenicek 2005), whereas, N deficiency after flower initiation causes reduction in alkaloid yield (Temple-Smith *et al.* 1983). Thus, the relationship of SVIs computed from capsule formation stage to thebaine can be associated with nutrient application after flowering to capsule formation stage and hence, aids towards thebaine production. Moreover, continuous irrigation till capsule formation has been found to be significantly important for alkaloid production (Chung 1987, Mahdavi-Damghani *et al.* 2010). Water deficit around the capsule development stage reduces capsule mass and causes reduction in the concentration of codeine and thebaine indirectly (Mahdavi-Damghani *et al.* 2010). Irrigation required from flowering till capsule formation is critical due to the requirement of the biological processes in capsules (Laughlin and Chung 1990).

The model for estimation of thebaine used in this study is developed using multi-temporal stage data. However, results showed that combination of SVIs (MSAVI, mSR, OSAVI, NDVI and EVI) computed from capsule formation stage data can provide significant estimation of thebaine. Thus, this method could be further tested on other high-thebaine poppy varieties. In addition, several factors can influence the variable importance for estimating thebaine. These factors include mainly the genotype of crop, irrigation and nutrient condition around flowering and capsule formation stage, the use of growth regulators and extent of weed invasion. This implies that model calibration will be required based on field survey data for a new study site. This study predicted the alkaloids of summer crop only; however, in other parts of the world, poppy is sown in winter, thus, the difference of prediction conditions need to be reconciled by quantifying the effect of weather and genotype. In Tasmania, the world's largest licit producer of opium alkaloids, continuous research and development aims to use genetically improved crops for obtaining higher yields, thus, the applicability of RF models using selected SVIs would need to be investigated on new varieties. Overall, the combination of SVIs derived using red and NIR bands computed from capsule formation stage can provide significant information about prediction of alkaloid yield. This study can help farmers in optimising the irrigation and nutrient application to enhance the alkaloid yield in a sustainable way.

7.5. Conclusions

In this study, UAS-based multispectral imagery with random forest (RF) regression was used to predict the alkaloid concentration. As a result of the RF model optimisation, spectral indices computed from capsule formation stage imagery were found to predict thebaine with RMSE of 13.65 %. The RF model was trained and tested using optimal

number of variables (M_{try}) to predict thebaine. We conclude that multispectral imagery with red and NIR spectral bands acquired during capsule formation stage has the potential to predict thebaine concentration. The prediction results of the RF model showed a significant relationship with lab measured thebaine with an R^2 value of 0.63 for validation and an R^2 value of 0.82 for the training dataset. It can be concluded that the RF model with (MSAVI, mSR, OSAVI, NDVI and EVI) can estimate the thebaine concentration. However, further studies should be conducted to investigate the robustness of the proposed method. Detailed investigation in combination with information on chlorophyll, capsule moisture, nutrients and irrigation application can be explored to improve the accuracy. These investigations could provide useful information for utilisation of UAS remote sensing for precision agriculture.

7.6. Thesis context

Chapter 7 addressed the fourth objective of this thesis and described a successful methodology to predict thebaine using multi-temporal multispectral UAS data and a random forest (RF) machine learning approach.

Chapter 8

8. Conclusions

The aim of this research work was to investigate the potential of high spatial and temporal resolution UAS data for yield prediction of commercially grown Tasmanian poppies. The key goal was to identify methods for poppy capsule yield estimation by predicting poppy capsule volume and alkaloid yield potential at critical stages in the growing season. This information has the potential to help farmers and the alkaloid industry to monitor the crop proactively. This thesis followed a progressive pathway starting with a literature review, processing and correction of raw UAS data, through to advanced machine learning techniques of spectral and UAS data for crop yield modelling. As current yield estimation methods are based primarily on manual destructive sampling of samples which only cover a very small fraction of a poppy field, there was a need to assess the applicability and utility of UAS remotely sensed data to determine the spatial variability of growing conditions and yield within a poppy field. This thesis investigated the application of UAS remote sensing to estimate and predict poppy crop capsule yield. Each chapter of this thesis addresses to one or more of the thesis objectives, and has been published in peer-reviewed journals or submitted to scientific journals for publication. This final chapter aims to summarise the findings of this thesis. Firstly, it highlights the usability of developed methodologies and identifies the caveats and limitation of the research. Secondly, it provides the recommendations and future directions for the study. This thesis has demonstrated that data acquired from an unmanned aerial system (UAS), can be effectively used in a precision agriculture application for a high value crop. Based on the finding of this thesis, it is concluded that high spatial and temporal resolution data acquired from UAS can provide detailed spatially-explicit information for precision agriculture, in particular where time critical management is required.

8.1. Critical stages of poppy opium for the application of UAS remote sensing

Chapter 2 aimed to determine the critical stages of poppy crop that play a crucial role in biophysical and biochemical development of capsule yield. Review of literature shows that a number of environmental factors affect the growth and development of a poppy crop along its growth cycle. Therefore, identification of critical stages during crop development provided an important input for the timing of UAS-based remote sensing. The findings of Chapter 2 indicate that hook, flowering and capsule formation stages

are critical for capsule and alkaloid development. Thus, to estimate capsule volume and alkaloid yield, remote sensing data was acquired from these key stages.

8.2. Biophysical estimation using structural derivatives

Objective 1

To investigate the use of visible (RGB) imagery acquired using a single UAS flight for estimation of poppy crop height and capsule volume.

The goal of Chapter 3 was to determine whether high spatial resolution datasets acquired from a UAS-mounted visible sensor could be used to derive structural variables of poppy crop.

Chapter 3 presents a novel method to estimate plant height using a single-flight UAS dataset. Imagery acquired from the UAS was used to produce dense point clouds using structure from motion (SfM) and multi-view stereopsis (MVS) techniques. Dense point clouds were used to generate a digital surface model (DSM) and orthophoto mosaic. An RGB index was used to extract the bare ground patches and a bare ground mask was used to filter the points on the ground. A digital terrain model (DTM) was then interpolated from these points. Plant height values were estimated by subtracting the DSM and DTM to generate a Crop Height Model (CHM). UAS-derived plant height (PH) and field measured PH at the Cambridge, Tasmania study site were strongly correlated with an R^2 values ranging from 0.93 to 0.97. In addition, an R^2 of 0.74 with a relative error of 19.62% were found between UAS-derived PH and poppy capsule volume. It was demonstrated that the methodology used to estimate plant height is robust and repeatable as the techniques was successfully applied to a second study site at Cressy, Tasmania. Therefore, the proposed method can be considered an important step towards crop height estimation from a single UAS flight.

Overall, Chapter 3 provided a novel approach to estimating crop height using a single flight, in contrast to a more traditional approach requiring two flights to derive the height of the crop surface independently from the bare ground DTM. The new approach presented in Chapter 3 is highly suitable for Tasmania, where multiple flights are not always possible due to weather conditions. The results illustrate that plant height can be reliably estimated for poppy crops based on a single UAS flight and can be used to predict opium capsule volume at capsule formation stage.

Chapter 8

8.3. Biophysical estimation using combination of spectral and structural derivatives from capsule formation stage

Objective 2

To develop a machine learning workflow for estimating poppy capsule volume from UAS-based multispectral remote sensing data.

To compute spectral derivatives from multispectral data, digital numbers need to be converted to surface reflectance. The TetraCam Miniature Multiple Camera Array (Mini-MCA) multispectral camera was used for spectral reflectance measurements of poppy crop. This objective is covered in chapters 4 and 5. Chapter 4 aimed to address the correction of raw image data into surface reflectance and chapter 5 aimed to use spectral derivatives in combination with plant height (chapter 3) to estimate capsule volume.

Chapter 4 proposes an easy and cost-effective radiometric calibration process for UAS-based Mini-MCA multispectral camera. Prediction equations for DN values from six multispectral bands and surface reflectance showed a linear relationship with y-intercept value equal to zero. Y-intercept represents the minimal possible surface reflectance recorded by sensor and considered as a first point for calibration equation development. The spectral reflectance of white pseudo targets was used as a second point of the equation. The methodology developed in this chapter was used to calibrate the UAS acquired imagery for chapter 5.

The goal of chapter 5 was to determine whether the combination of structural and spectral derivatives of UAS data could provide improvement in capsule volume prediction results using a random forest (RF) machine learning approach. Analysis was undertaken using multiple sensor dataset, and field-based spectroscopy observations were convolved to simulate UAS Mini-MCA sensor data. Convolved data was used to develop random forest regression model. In addition, Mini-MCA and visual imagery were collected, and crop height data were computed from visible images (Chapter 3). Convolved data was used to compute spectral vegetation indices (SVIs). A combination of SVIs and plant height were used to develop a random forest regression model using k-fold approach to train and validate the model accuracy. The optimal number of trees (500) with lowest root mean square error (RMSE) value was used to rank the variable importance to predict poppy capsule volume.

Variable importance measures derived from the range of RF training models indicated that SVIs based on the visible and NIR portion of the spectrum (NDVI, SR, mTVI and RDVI) were the best for predicting capsule volume. Finally, the optimal number of variables (four) was used to train and test the RF model on UAS data. In Cambridge, Tasmania, Australia, RF models based on convolved to UAS multispectral data were used to predict capsule volume, which was strongly related to field measured capsule volume with an R^2 value of 0.70 for validation and an R^2 value of 0.86 for training dataset, whereas, UAS based RF model provided an R^2 value ranging from 0.77 to 0.82 from validation to training dataset respectively. Selected variables based on the first study site (Cambridge) were used to generate an RF model using UAS acquired data at the second site (Sorell) and significant relationship between measured and predicted capsule volume was observed, with an R^2 value of 0.72 and relative error of 26.25 %. The findings of this chapter indicate that poppy capsule volume can be estimated using a combination of SVIs and RF regression. Significantly improvement in prediction accuracy was observed with a relative error of 12.80 % as compared to capsule volume estimated using plant height only in chapter 3 with a relative error of 19.62 %.

8.4. Biophysical estimation using spectral derivatives from multi-temporal data

Objective 3

To assess the potential of multi-temporal UAS remote sensing with machine learning and linear regression techniques to predict poppy capsule volume.

Chapter 6 presents a multi-temporal analysis to estimate poppy capsule volume using random forest regression. This chapter aimed to identify the optimal number of variables and optimal crop growth stage to estimate poppy capsule volume. In this chapter, a small UAS with a 4-band Parrot Sequoia multispectral sensor was used to acquire very high resolution spatio-temporal images of a poppy crop. This study demonstrated the potential to estimate poppy capsule volume using multi-temporal spectral derivatives (spectral vegetation indices) and structural derivatives (green vegetation fractional cover) using random forest regression and multi linear regression techniques. It was concluded that the combination of green vegetation fractional cover acquired at the flowering stage with spectral indices acquired at the hook stage (RDVI, SPVI and mTVI) performed best with an R^2 of 0.88 and RMSE of 13.45 % to predict poppy capsule volume using random forest regression. Poppy capsule volume estimation using a combination of random forest regression with multi-temporal UAS variables is a novel approach, which has not been tested before. Moreover, the proposed

model was used to develop a spatial variability map of poppy yield for the study site. This chapter concluded that capsule volume can be predicted two months prior to harvesting. This information can help farmers and the pharmaceutical industry to enhance crop productivity by optimising nutrients and irrigation.

The findings of chapter 6 are in line with those of the previous prediction results presented in Chapter 5. The spectral regions identified as important for capsule volume estimation are similar to those found by the variable importance measures obtained by the random forest model in chapter 5. The identification of similar key spectral regions across capsule formation (Chapter 5), hook and flowering stage (Chapter 6) datasets is an important finding, as the two studies were undertaken at different temporal scales and locations, and represent two different agronomic practices. Thus, it can be concluded that the selected spectral derivatives can provide a robust methodology for mapping poppy capsule volume.

8.5. Bio-chemical estimation using structural and spectral derivatives from multi-temporal data

Objective 4

To develop a methodology for poppy opium alkaloid estimation before harvesting using multispectral imagery acquired from a UAS.

Chapter 7 presents a novel method to predict biochemical properties of poppy crop using UAS based multi-temporal spectral derivatives. In this chapter, UAS-based multispectral imagery with random forest (RF) regression was used to predict the alkaloid concentration. It was concluded that multispectral data collected from capsule formation stage can be used to predict thebaine concentration with a relative error of 13.56 % to 22.36 % in the training and validation dataset, respectively. Variable importance measures derived from the range of RF training models indicated that indices based on a combination of NIR and visible bands provided optimal results. This is in line with the results of chapter 5 and 6 and concluded that multispectral data acquired with red and NIR region from capsule formation stage have the potential to predict the thebaine concentration. The prediction results of proposed RF model showed significant relationship to lab measured thebaine. It was concluded that the RF model with (MSAVI, mSR, OSAVI, NDVI and EVI) can estimate the thebaine. However, further studies should be conducted to investigate the robustness of the proposed method.

8.6. Contributions to knowledge

The contributions to knowledge by this thesis fall into three major categories; poppy crop, UAS remote sensing and UAS remote sensing for crop yield estimation. The major contributions of this thesis are:

Poppy Crop

- This thesis systematically reviewed environmental factors that influence capsule volume and alkaloid yield.
- This thesis identified the critical growth stages for poppy crop yield estimation, and the importance of these stages for remotely sensed data collection.
- This thesis demonstrated that poppy capsule volume has a significant relationship with crop height, without considering the influence of growth regulators.

UAS remote sensing

- This study developed a novel and robust workflow to estimate plant height using a single UAS flight.
- This study demonstrated and tested a simplified radiometric calibration method to convert digital numbers from a multispectral Mini-MCA sensor to surface reflectance using a single pseudo target.

UAS Remote sensing for crop yield estimation

- This study demonstrated that a structural derivative (plant height) computed using overlapping visible UAS images can be used to estimate poppy capsule volume.
- This study demonstrated that multispectral sensor data acquired from a single stage (capsule formation) can be used to estimate poppy capsule volume.
- This study collected and analysed multi-temporal UAS remote sensing data for poppy capsule volume estimation and demonstrated that poppy capsule volume can be estimated two months prior to harvesting by collecting multispectral data from hook and flowering stage.
- This study demonstrated that multispectral data acquired from capsule formation stage can be used to estimate thebaine concentration in poppy capsules.

- This study demonstrated that low-cost UAS technology in combination with random forest regression can be used to monitor detailed spatial variability of poppy crop yield.
- This study demonstrated that random forest regression technique in combination with k-fold validation technique can provide much improved prediction modelling with multiple variables as compared to linear and multilinear modelling.

8.7. Limitations and future research

The findings presented in this research are in general promising and encourage further development of UAS remote sensing for precision management of poppy crops. Some of the limitations of this study will be identified in this section. This study was conducted on summer crops only; however, in other parts of the world poppy is sown in winter. Thus, the difference of prediction conditions needs to be reconciled by quantifying the effect of weather and genotype. In Tasmania, genetically improved crops are cultivated every year to get the maximum possible yield. Thus, the applicability of models using selected spectral variables would need to be investigated on new varieties. Moreover, the influence of growth regulators is not considered in this study, but should be considered in future research. One of the major limitations was the inaccessibility of soil data, as soil is one of the major factors for transport of nutrients and water to the plant. Therefore, the spatial variability of soil nutrients and moisture should be investigated to determine the influence of soil, irrigation and nutrients on capsule yield. Moreover, information on irrigation and nutrient condition was not available, and this information can further help to understand the poppy crop in more detail. In particular, irrigation and nutrient information around hook and capsule formation stages should be evaluated. Although the findings of this thesis have made significant contributions to the field of UAS remote sensing for precision agriculture, further could be done to improve the collection, processing and establishment of standardised automated procedures to convert sensor information into valuable information for farmers. Moreover, a huge amount of data is produced with each UAS campaign that could provide foundations to explore new avenues of knowledge. However, processing of such large datasets is computationally intensive and is beyond the ability of common computers. Therefore, the availability of powerful workstations or cloud-computing is one of the fundamental requirements for analysing these data and conversion into valuable information for agronomists and farmers. In addition, UAS driven information needs further investigation with on-ground sensors to improve

the confidence level and need to develop automated process to convert UAS acquired raw data into valuable maps for farmers use.

8.8. Recommendations

- Future research should further investigate and validate the models developed in this study in other areas of Tasmania, and across a range of poppy varieties and environmental conditions.
- The combination of green vegetation fractional cover and plant height should be further evaluated to predict poppy capsule volume. The use of these variables can facilitate prediction of poppy crop yield based on RGB imagery alone.
- The models developed in this study should be tested on other varieties of poppy using bigger sample size data, provided that a reliable field database is established. This allows optimal selection of UAS configurations and models for a range of poppy varieties and conditions of interest.
- Higher temporal resolution data from early hook stage till capsule formation stage can be investigated in combination with irrigation and nutrient application potentially further improving the prediction accuracy of capsule volume.
- The utility of hyperspectral data in predicting poppy capsule alkaloid yield could be evaluated. The narrow band poppy crop spectral features that are captured by hyperspectral sensors might accurately estimate poppy alkaloid and poppy capsule volume potential. Particularly high spectral resolution data acquired by hyperspectral sensors can be investigated by analysing the spectra's from capsule. Capsule-level spectral information may help to predict other alkaloids (e.g. morphine, codeine) and might help to improve the alkaloid prediction accuracy. In addition, spectral derivatives related to chlorophyll and protein contents can be evaluated to improve the alkaloid prediction.
- The utility of high spatial resolution thermal data in predicting moisture around poppy capsules could be evaluated to make more precise estimates of alkaloids.

8.9. Final Remarks

High spatial and temporal resolution data are essential for precise monitoring and management of poppy crop. Only UAS platforms can currently meet the remote sensing

requirement for precision agriculture. This thesis demonstrates that UAS with visible and multispectral sensors is a useful tool for poppy crop yield estimation and combination of UAS acquired data and machine learning random forest regression technique can be tested for other crop yield estimation. This thesis provides foundational techniques for the generation and analysis of high spatial and temporal resolution UAS data for poppy capsule yield estimation. Novel techniques are successfully demonstrated to estimate capsule volume using spectral and structural derivatives from UAS mounted sensors. The methods developed for poppy capsule yield estimation have broader applications and can potentially be used for site-specific crop management of a range of crops. The findings from this study can be applied to help farmers optimise agronomic practice to enhance alkaloid yield in a sustainable way.

References

Abdel-Rahman, E.M., Ahmed, F.B., and Ismail, R., 2013. Random forest regression and spectral band selection for estimating sugarcane leaf nitrogen concentration using EO-1 Hyperion hyperspectral data. *International Journal of Remote Sensing*, 34 (2), 712–728.

Abdullah, N.B., Hussin, M.S., Azhari, A.W., and Jaafar, M.N., 2011. Land suitability mapping for implementation of precision farming. *National Postgraduate Conference*. IEEE, 1–6.

Acock, M., Wang, Z., Acock, B., and Jones, R., 1996. Gum yield as affected by capsule age, firmness, gum collecting methods, and phenotypes in opium poppy. *HortScience*, 31 (7), 1156–1159.

Acock, M.C. and Pausch, R.C., 1997. Growth and development of opium poppy (*Papaver Somniferum L*) as a function of temperature. *Biotronics*, 26, 47–57.

Acock, M.C., Wang, Z., and Acock, B., 1996. Flowering and vegetative growth in opium poppy as affected by photoperiod and temperature treatments. *Biotronics*, 25, 11–21.

Adam, E., Mutanga, O., Odindi, J., and Abdel-Rahman, E.M., 2014. Land-use/cover classification in a heterogeneous coastal landscape using RapidEye imagery: evaluating the performance of random forest and support vector machines classifiers. *International Journal of Remote Sensing*, 35 (10), 3440–3458.

Adam, E.M., Mutanga, O., Rugege, D., and Ismail, R., 2012. Discriminating the papyrus vegetation (Cyperus papyrus L.) and its co-existent species using random forest and hyperspectral data resampled to HYMAP. *International Journal of Remote Sensing*, 33 (2), 552–569.

Ajayan, P.M. and Tour, J.M., 2007. Materials science: nanotube composites. *Nature*, 447 (7148), 1066–1068.

Alam, M., Samad, A., Khaliq, A., Ajayakumar, P. V, Dhawan, O.P., and Singh, H.N., 2011. Disease Incidence and Its Management on Opium Poppy: a Global Perspective. *In*: *International Symposium on Papaver 1036*. 123–139.

Albrechtova, J., Seidl, Z., Aitkenhead-Peterson, J., Lhotáková, Z., Rock, B.N., Alexander, J.E., Malenovský, Z., and McDowell, W.H., 2008. Spectral analysis of coniferous foliage and possible links to soil chemistry: Are spectral chlorophyll indices related to forest floor dissolved organic C and N, *Science of the Total Environment*, 404, 424–432.

Annett, H.E., 1920. Factors influencing alkaloidal content and yield of latex in the opium

poppy (Papaver somniferum). *Biochemical Journal*, 14 (5), 618.

Aparicio, N., Villegas, D., Casadesus, J., Araus, J.L., and Royo, C., 2000. Spectral vegetation indices as nondestructive tools for determining durum wheat yield. *Agronomy Journal*, 92 (1), 83–91.

Apuya, N.R., Park, J.-H., Zhang, L., Ahyow, M., Davidow, P., Van Fleet, J., Rarang, J.C., Hippley, M., Johnson, T.W., Yoo, H.-D., and Others, 2008. Enhancement of alkaloid production in opium and California poppy by transactivation using heterologous regulatory factors. *Plant Biotechnology Journal*, 6 (2), 160–175.

Awan, U.K., Ibrakhimov, M., Tischbein, B., Kamalov, P., Martius, C., and Lamers, J.P.A., 2011. Improving irrigation water operation in the lower reaches of the Amu Darya River - current status and suggestions. *Irrigation and Drainage*, 60 (5), 600–612.

Awan, U.K., Tischbein, B., Conrad, C., Martius, C., and Hafeez, M., 2011. Remote Sensing and Hydrological Measurements for Irrigation Performance Assessments in a Water User Association in the Lower Amu Darya River Basin. *Water Resources Management*, 25 (10), 2467–2485.

Bah, M., Hafiane, A., and Canals, R., 2018. Deep Learning with Unsupervised Data Labeling for Weed Detection in Line Crops in UAV Images. *Remote Sensing*, 10 (11), 1690.

Bakhsh, A. and Kanwar, R., 2006. GIS and Cluster Analysis of NO3-N Leaching Losses to Subsurface Drainage Water. *In*: *International Conference on Advances in Space Technologies*. 121–125.

Bakhsh, A., Kanwar, R.S., and Karlen, D.L., 2005. Effects of liquid swine manure applications on NO3–N leaching losses to subsurface drainage water from loamy soils in Iowa. *Agriculture, Ecosystems & Environment*, 109 (1–2), 118–128.

Baluja, J., Diago, M.P., Balda, P., Zorer, R., Meggio, F., Morales, F., and Tardaguila, J., 2012. Assessment of vineyard water status variability by thermal and multispectral imagery using an unmanned aerial vehicle (UAV). *Irrigation Science*, 30 (6), 511–522.

Barati, S., Rayegani, B., Saati, M., Sharifi, A., and Nasri, M., 2011. Comparison the accuracies of different spectral indices for estimation of vegetation cover fraction in sparse vegetated areas. *The Egyptian Journal of Remote Sensing and Space Science*, 14 (1), 49–56.

Baser, K.H.C. and Arslan, N., 2014. Opium Poppy (Papaver somniferum). *In*: *Medicinal and Aromatic Plants of the Middle-East*. Springer, 305–332.

Bastiaanssen, W.G.., Molden, D.J., and Makin, I.W., 2000. Remote sensing for irrigated

agriculture: examples from research and possible applications. *Agricultural Water Management*, 46 (2), 137–155.

Bastiaanssen, W.G.M. and Ali, S., 2003. A new crop yield forecasting model based on satellite measurements applied across the Indus Basin, Pakistan. *Agriculture, Ecosystems & environment*, 94 (3), 321–340.

Baugh, W.M. and Groeneveld, D.P., 2008. Empirical proof of the empirical line. *International Journal of Remote Sensing*, 29 (3), 665–672.

Bellvert, J., Zarco-Tejada, P.J., Girona, J., and Fereres, E., 2013. Mapping crop water stress index in a 'Pinot-noir' vineyard: comparing ground measurements with thermal remote sensing imagery from an unmanned aerial vehicle. *Precision Agriculture*, 15 (4), 361–376.

Bendig, J., Bolten, A., and Bareth, G., 2013. UAV-based Imaging for Multi-Temporal, very high Resolution Crop Surface Models to monitor Crop Growth Variability. *Photogrammetrie - Fernerkundung - Geoinformation*, 2013 (6), 551–562.

Bendig, J., Bolten, A., Bennertz, S., Broscheit, J., Eichfuss, S., and Bareth, G., 2014. Estimating Biomass of Barley Using Crop Surface Models (CSMs) Derived from UAV-Based RGB Imaging. *Remote Sensing*, 6 (11), 10395–10412.

Bendig, J., Yu, K., Aasen, H., Bolten, A., Bennertz, S., Broscheit, J., Gnyp, M.L., and Bareth, G., 2015. Combining UAV-based plant height from crop surface models, visible, and near infrared vegetation indices for biomass monitoring in barley. *International Journal of Applied Earth Observation and Geoinformation*, 39, 79–87.

Bernath, J., 1986. Complex physio-ecological evaluation of the alkaloid formation of the poppy (*Papaver Somniferum L*). *Herba Hung*, 25, 43–75.

Bernath, J., 1988. *Poppy: the genus Papaver*. Harwood Academic Publishers, Australia.

Bernath, J. and Tetrnyi, P., 1981. The effect of environmental factors on growth, development and alkaloid production of poppy. II. Interaction of light and temperature. *Biochem Phusiol Pflanzen*, 176 (7), 599–605.

Bernath, J. and Tetrnyi, P., 1986. Effect of environmental factos on growth, development and alkaloid productionof poppy III. NUtrition and light. *Acta Agronomica Hungarica*, 35 (1–2), 35–39.

Berni, J.. a. ., Zarco-Tejada, P.J., Suarez, L., and Fereres, E., 2009. Thermal and Narrowband Multispectral Remote Sensing for Vegetation Monitoring From an Unmanned Aerial Vehicle. *IEEE Transactions on Geoscience and Remote Sensing*, 47 (3), 722–738.

Berni, J.A.J., Zarco-Tejada, P.J., Sepulcre-Canto, G., Fereres Castiel, E., and Villalobos, F., 2009. Mapping canopy conductance and CWSI in olive orchards using high resolution thermal remote sensing imagery. *Remote Sensing of Environment*, 113 (11), 2380–2388.

Bos, M.G., Murray-Rust, D.H., Merrey, D.J., Johnson, H.G., and Snellen, W.B., 1994. Methodologies for assessing performance of irrigation and drainage management. *Irrigation and Drainage Systems*, 7 (4), 231–261.

Boschetti, L., Flasse, S.P., and Brivio, P.A., 2004. Analysis of the conflict between omission and commission in low spatial resolution dichotomic thematic products: The Pareto Boundary. *Remote Sensing of Environment*, 91 (3), 280–292.

Brandao, Z.N., Sofiatti, V., Bezerra, J.R.C., Ferreira, G.B., and Medeiros, J.C., 2015. Spectral reflectance for growth and yield assessment of irrigated cotton. *Australain Journal of Crop Science*, 9 (1), 75–84.

Breiman, L., 1996. Bagging predictors. *Machine Learning*, 24 (2), 123–140.

Breiman, L., 2001. Random forests. *Machine Learning*, 45 (1), 5–32.

Brisco, B., Brown, R.J., Hirose, T., McNairn, H., and Staenz, K., 1998. Precision agriculture and the role of remote sensing: a review. *Canadian Journal of Remote Sensing*, 24 (3), 315–327.

Broge, N.H. and Leblanc, E., 2001. Comparing prediction power and stability of broadband and hyperspectral vegetation indices for estimation of green leaf area index and canopy chlorophyll density. *Remote Sensing of Environment*, 76 (2), 156–172.

Brunet, Y., Nunez, M., and Lagouarde, J.-P., 1991. A simple method for estimating regional evapotranspiration from infrared surface temperature data. *ISPRS Journal of Photogrammetry and Remote Sensing*, 46 (6), 311–327.

Brunt, A.A., Crabtree, K., Dallwitz, M.J., Gibbs, A.J., Watson, L., and others, 1996. *Viruses of plants. Descriptions and lists from the VIDE database.* Cab International.

Calderón, R., Montes-Borrego, M., Landa, B.B., Navas-Cortés, J. a., and Zarco-Tejada, P.J., 2014. Detection of downy mildew of opium poppy using high-resolution multi-spectral and thermal imagery acquired with an unmanned aerial vehicle. *Precision Agriculture*, 15 (6), 639–661.

Candiago, S., Remondino, F., De Giglio, M., Dubbini, M., and Gattelli, M., 2015. Evaluating multispectral images and vegetation indices for precision farming applications from UAV images. *Remote Sensing*, 7 (4), 4026–4047.

Carbone, G.J., Narumalani, S., and King, M., 1996. Application of remote sensing and GIS technologies with physiological crop models. *Photogrammetric Engineering and Remote Sensing*, 62 (2), 171–179.

Carlson, T.N. and Ripley, D.A., 1997. On the relation between NDVI, fractional vegetation cover, and leaf area index. *Remote sensing of Environment*, 62 (3), 241–252.

Chartzoulakis, K. and Bertaki, M., 2015. Sustainable water management in agriculture under climate change. *Agriculture and Agricultural Science Procedia*, 4, 88–98.

Chavez Jr, P.S., 1989. Radiometric calibration of Landsat Thematic Mapper multispectral images. *Photogrammetric Engineering and Remote Sensing*, 55 (9), 1285–1294.

Chen, J.M. and Cihlar, J., 1996. Retrieving leaf area index of boreal conifer forests using Landsat TM images. *Remote sensing of Environment*, 55 (2), 153–162.

Cheng, Y.B., Zarco-Tejada, P.J., Riano, D., Rueda, C.A., and Ustin, S.L., 2006. Estimating vegetation water content with hyperspectral data for different canopy scenarios: Relationships between AVIRIS and MODIS indexes. *Remote Sensing of Environment*, 105 (4), 354–366.

Chiwocha, S.D.S., Abrams, S.R., Ambrose, S.J., Cutler, A.J., Loewen, M., Ross, A.R.S., and Kermode, A.R., 2003. A method for profiling classes of plant hormones and their metabolites using liquid chromatography-electrospray ionization tandem mass spectrometry: an analysis of hormone regulation of thermodormancy of lettuce (Lactuca sativa L.) seeds. *The Plant Journal*, 35 (3), 405–417.

Chuinsiri, S., Blasco, F., Bellan, M.-F., and Kergoat, L., 2010. A poppy survey using high resolution remote sensing data. *International Journal of Remote Sensing*, 18 (2), 393–407.

Chung, B., 1987. The effect of irrigation on the growth and yield components of poppies (*Papaver Somniferum L*). *Journal of Agricultural Science*, 108 (July 1986), 389–394.

Cilia, C., Panigada, C., Rossini, M., Meroni, M., Busetto, L., Amaducci, S., Boschetti, M., Picchi, V., and Colombo, R., 2014. Nitrogen Status Assessment for Variable Rate Fertilization in Maize through Hyperspectral Imagery. *Remote Sensing*, 6 (7), 6549–6565.

Clevers, J., De Jong, S.M., Epema, G.F., Van Der Meer, F.D., Bakker, W.H., Skidmore, A.K., and Scholte, K.H., 2002. Derivation of the red edge index using the MERIS standard band setting. *International Journal of Remote Sensing*, 23 (16), 3169–3184.

Cohen, Y., Alchanatis, V., Meron, M., Saranga, Y., and Tsipris, J., 2005. Estimation of leaf

water potential by thermal imagery and spatial analysis. *Journal of Experimental Botany*, 56 (417), 1843–1852.

Corcoles, J.I., Ortega, J.F., Hernández, D., and Moreno, M. a., 2013. Use of digital photography from unmanned aerial vehicles for estimation of leaf area index in onion (Allium cepa L.). *European Journal of Agronomy*, 45, 96–104.

Cotching, W.E., Sparrow, L. a., Hawkins, K., McCorkell, B.E., and Rowley, W., 2004. Linking Tasmanian potato and poppy yields to selected soil physical and chemical properties. *Australian Journal of Experimental Agriculture*, 44 (12), 1241.

Cotterill, P.J. and Pascoe, I.G., 1998. Downy mildew of Papaver somnifmum in Tasmania. *Australasian Plant Pathology*, 27 (4), 263–264.

Curran, P.J., Dungan, J.L., Macler, B.A., and Plummer, S.E., 1991. The effect of a red leaf pigment on the relationship between red edge and chlorophyll concentration. *Remote Sensing of Environment*, 35 (1), 69–76.

Cutler, D.R., Edwards, T.C., Beard, K.H., Cutler, A., Hess, K.T., Gibson, J., and Lawler, J.J., 2007. Random forests for classification in ecology. *Ecology*, 88 (11), 2783–2792.

Dandois, J.P. and Ellis, E.C., 2013. High spatial resolution three-dimensional mapping of vegetation spectral dynamics using computer vision. *Remote Sensing of Environment*, 136, 259–276.

Danielsen, S. and Munk, L., 2004. Evaluation of disease assessment methods in quinoa for their ability to predict yield loss caused by downy mildew. *Crop Protection*, 23 (3), 219–228.

Davies, P.J., 2010. The plant hormones: their nature, occurrence, and functions. *In*: *Plant Hormones*. Springer, 1–15.

De Castro, A.I., Torres-Sánchez, J., Peña, J.M., Jiménez-Brenes, F.M., Csillik, O., and López-Granados, F., 2018. An automatic random forest-obia algorithm for early weed mapping between and within crop rows using UAV imagery. *Remote Sensing*, 10 (2), 285.

Dean, G., 2011. Modifying poppy growth and alkaloid yield with plant growth regulators. University of Tamsania.

Delegido, J., Verrelst, J., Rivera, J.P., Ruiz-Verdú, A., and Moreno, J., 2015. Brown and green LAI mapping through spectral indices. *International Journal of Applied Earth Observation and Geoinformation*, 35, 350–358.

Dempewolf, J., Adusei, B., Becker-Reshef, I., Hansen, M., Potapov, P., Khan, A., and Barker, B., 2014. Wheat Yield Forecasting for Punjab Province from Vegetation

Index Time Series and Historic Crop Statistics. *Remote Sensing*, 6 (10), 9653–9675.

Dewick, P.M., 2002. *Medicinal natural products: a biosynthetic approach*. John Wiley & Sons.

Dieu, P. and Dunwell, J.M., 1988. Anther culture with different genotypes of opium poppy (*Papaver Somniferum L*): effect of cold treatment. *Plant Cell, Tissue and Organ Culture*, 12 (3), 263–271.

Doneus, M., Verhoeven, G., Fera, M., Briese, C., Kucera, M., and Neubauer, W., 2011. From deposit to point cloud--a study of low-cost computer vision approaches for the straightforward documentation of archaeological excavations. *Geoinformatics FCE CTU*, 6, 81–88.

Doran, J.W., 2002. Soil health and global sustainability: translating science into practice. *Agriculture Ecosystems & Environment*, 88 (2), 119–127.

Du, M. and Noguchi, N., 2017. Monitoring of Wheat Growth Status and Mapping of Wheat Yields within-Field Spatial Variations Using Color Images Acquired from UAV-camera System. *Remote Sensing*, 9 (3), 289.

Edelbauer, A. and Stangl, J., 1993. Nutrient removal of the waladviertler graumohn (*Papaver Somniferum L*) During Vegetative period. *Bodenkultur*, 44 (1), 15–27.

Ehlert, D., Horn, H.J., and Adamek, R., 2008. Measuring crop biomass density by laser triangulation. *Computers and Electronics in Agriculture*, 61 (2), 117–125.

Erten, E., Lopez-Sanchez, J.M., Yuzugullu, O., and Hajnsek, I., 2016. Retrieval of agricultural crop height from space: A comparison of SAR techniques. *Remote Sensing of Environment*, 187, 130–144.

van Evert, F.K., Gaitán-Cremaschi, D., Fountas, S., and Kempenaar, C., 2017. Can Precision Agriculture Increase the Profitability and Sustainability of the Production of Potatoes and Olives? *Sustainability*, 9 (10), 1863.

Ey, P.H.A.D.L., Adams, S.R., Pearson, S., Hadley, P., and Patefield, W.M., 1999. The Effects of Temperature and Light Integral on the Phases of Photoperiod Sensitivity inPetuniaxhybrida. *Annals of Botany*, 83, 263–269.

Facchini, P.J., Johnson, A.G., Poupart, J., and De Luca, V., 1996. Uncoupled defense gene expression and antimicrobial alkaloid accumulation in elicited opium poppy cell cultures. *Plant Physiology*, 111 (3), 687–697.

Fang, S., Tang, W., Peng, Y., Gong, Y., Dai, C., Chai, R., and Liu, K., 2016. Remote estimation of vegetation fraction and flower fraction in oilseed rape with unmanned aerial vehicle data. *Remote Sensing*, 8 (5), 416.

Far, S.T. and Rezaei-Moghaddam, K., 2018. Impacts of the precision agricultural technologies in Iran: An analysis experts' perception & their determinants. *Information Processing in Agriculture*, 5 (1), 173–184.

Fedotov, Y. and Osmani, Z.A.M., 2010. *Afghanistan Opium Survey 2010*. Kabul.

Fejer, J. and Salamon, I., 2011. Agro-Technology of the Poppy: Large-Scale Cultivation in Slovakia. *In*: *International Symposium on Papaver 1036*. 181–185.

Fist, A.J., 2000. *The Tasmanian poppy industry: A case study of the application of science and technology*. Tasmanian Alkaloids Pty Limited.

Frappell, B., 2010. Fifty years of poppies in Tasmania: The first ten years, 1960 to 1970. *In*: *Papers and Proceedings: Tasmanian Historical Research Association*. 73.

French, A.N., Hunsaker, D.J., and Thorp, K.R., 2015. Remote Sensing of Environment Remote sensing of evapotranspiration over cotton using the TSEB and METRIC energy balance models. *Remote Sensing of Environment*, 158, 281–294.

Gago, J., Douthe, C., Coopman, R.E., Gallego, P.P., Ribas-Carbo, M., Flexas, J., Escalona, J., and Medrano, H., 2015. UAVs challenge to assess water stress for sustainable agriculture. *Agricultural Water Management*, 153, 9–19.

Galewsky, S. and Nessler, C.L., 1986. Synthesis of morphinane alkaloids during opium poppy somatic embryogenesis. *Plant Science*, 45 (3), 215–222.

Gao, S., Niu, Z., Huang, N., and Hou, X., 2013. Estimating the Leaf Area Index, height and biomass of maize using HJ-1 and RADARSAT-2. *International Journal of Applied Earth Observation and Geoinformation*, 24, 1–8.

Gao, S., Niu, Z., Sun, G., Zhao, D., Jia, K., and Qin, Y., 2015. Height Extraction of Maize Using Airborne Full-Waveform LIDAR Data and a Deconvolution Algorithm. *IEEE Geoscience and Remote Sensing Letters*, 12 (9), 1978–1982.

Geipel, J., Link, J., and Claupein, W., 2014. Combined Spectral and Spatial Modeling of Corn Yield Based on Aerial Images and Crop Surface Models Acquired with an Unmanned Aircraft System. *Remote Sensing*, 6 (11), 10335–10355.

Gevaert, C.M., Suomalainen, J., Tang, J., and Kooistra, L., 2015. Generation of Spectral--Temporal Response Surfaces by Combining Multispectral Satellite and Hyperspectral UAV Imagery for Precision Agriculture Applications. *IEEE Journal of Selected Topics in Applied Earth Observations and Remote Sensing*, 8 (6), 3140–3146.

Gitelson, A.A., Gritz, Y., and Merzlyak, M.N., 2003. Relationships between leaf chlorophyll content and spectral reflectance and algorithms for non-destructive chlorophyll assessment in higher plant leaves. *Journal of Plant Physiology*, 148 (3),

271–282.

Gitelson, A.A., Kaufman, Y.J., and Merzlyak, M.N., 1996. Use of a green channel in remote sensing of global vegetation from EOS-MODIS. *Remote Sensing of Environment*, 58 (3), 289–298.

Gitelson, A.A., Kaufman, Y.J., Stark, R., and Rundquist, D., 2002. Novel algorithms for remote estimation of vegetation fraction. *Remote sensing of Environment*, 80 (1), 76–87.

Gitelson, A.A. and Merzlyak, M.N., 1997. Remote estimation of chlorophyll content in higher plant leaves. *International Journal of Remote Sensing*, 18 (12), 2691–2697.

Gomez-Candon, D., De Castro, A.I., and López-Granados, F., 2014. Assessing the accuracy of mosaics from unmanned aerial vehicle (UAV) imagery for precision agriculture purposes in wheat. *Precision Agriculture*, 15 (1), 44–56.

Green, S., Bevan, A., and Shapland, M., 2014. A comparative assessment of structure from motion methods for archaeological research. *Journal of Archaeological Science*, 46, 173–181.

Grenzdorffer, G.J., 2014. Crop height determination with UAS point clouds. *In*: *The International Archives of Photogrammetry, Remote Sensing and Spatial Information Sciences*. Copernicus GmbH, 135.

Gross, D. and Parthier, B., 1994. Novel natural substances acting in plant growth regulation. *Journal of Plant Growth Regulation*, 13, 93–114.

Guo, C., Zhang, L., Zhou, X., Zhu, Y., Cao, W., Qiu, X., Cheng, T., and Tian, Y., 2018. Integrating remote sensing information with crop model to monitor wheat growth and yield based on simulation zone partitioning. *Precision Agriculture*, 19 (1), 55–78.

Haboudane, D., Miller, J.R., Pattey, E., Zarco-Tejada, P.J., and Strachan, I.B., 2004. Hyperspectral vegetation indices and novel algorithms for predicting green LAI of crop canopies: Modeling and validation in the context of precision agriculture. *Remote Sensing of Environment*, 90 (3), 337–352.

Hagel, J.M., Macleod, B.P., and Facchini, P.J., 2007. Opium poppy. *In*: *Biotechnology in Agriculture and Forestry*. Springer, 169.

Ham, J.M., Kluitenberg, G.J., and Lamont, W.J., 1993. Optical properties of plastic mulches affect the field temperature regime. *Journal of the American Society for Horticultural Science*, 118 (2), 188–193.

Han-Ya, I., Ishii, K., and Noguchi, N., 2010. Satellite and aerial remote sensing for production estimates and crop assessment. *Environmental Control in Biology*, 48 (2),

51–58.

Harold, B., Annett, E., and College, A., 1920. Factor influancing alkaloid content and yield of latex in th eopium poppy. *Biochemical Journal*, 14 (5), 618–636.

Harrison, W.C. and Schmitt, C.G., 1972. *Diseases of the opium poppy*. Fort Detrick Frederick, Maryland.

Harvest, T., Brown, P.H., Fist, a., Gracie, a., Gregory, D., and Koutoulis, a., 2009. The latex capacity of opium poppy capsules is fixed early in capsule development and is not a major determinant in morphine yield. *Annals of Applied Biology*, 154 (2), 251–258.

Harwin, S. and Lucieer, A., 2012. Assessing the Accuracy of Georeferenced Point Clouds Produced via Multi-View Stereopsis from Unmanned Aerial Vehicle (UAV) Imagery. *Remote Sensing*, 4 (12), 1573–1599.

Harwin, S., Lucieer, A., and Osborn, J., 2015. The impact of the calibration method on the accuracy of point clouds derived using unmanned aerial vehicle multi-view stereopsis. *Remote Sensing*, 7 (9), 11933–11953.

Hasnain, Z., Abbas, G., Saeed, A., Shakeel, A., Muhammad, A., and Rahim, M.A., 2006. Combining ability for plant height and yield related traits in wheat (Triticum aestivum L.). *J. Agric. Res*, 44 (3), 167–173.

Hernández-Clemente, R., Navarro-Cerrillo, R.M., and Zarco-Tejada, P.J., 2012. Carotenoid content estimation in a heterogeneous conifer forest using narrow-band indices and PROSPECT+DART simulations. *Remote Sensing of Environment*, 127, 298–315.

Herrero-Huerta, M., Hernández-López, D., Rodriguez-Gonzalvez, P., González-Aguilera, D., and González-Piqueras, J., 2014. Vicarious radiometric calibration of a multispectral sensor from an aerial trike applied to precision agriculture. *Computers and Electronics in Agriculture*, 108, 28–38.

Herwitz, S.R., Johnson, L.F., Dunagan, S.E., Higgins, R.G., Sullivan, D. V, Zheng, J., Lobitz, B.M., Leung, J.G., Gallmeyer, B.A., Aoyagi, M., and others, 2004. Imaging from an unmanned aerial vehicle: agricultural surveillance and decision support. *Computers and Electronics in Agriculture*, 44 (1), 49–61.

Hofman, P.J. and Menary, R.C., 1984. Losses, by leaching, of alkaloids from the capsule of the poppy (*Papaver Somniferum L*) during maturation. *Crop and Pasture Science*, 35 (2), 253–261.

Hongoh, D., Kajiwara, K., and Honda, Y., 2001. Developing ground truth measurement

system using RC helicopter and BRDF model in forest area. *In*: *22nd Asian conference on remote sensing*. Singapore: National University of Singapore, 1–9.

Hoppert, B.D. and LaPlante, D.J., 1992. Enhanced metal filter/mirror coatings for use on engineering plastics.

Horrigan, L., Lawrence, R.S., and Walker, P., 2002. How sustainable agriculture can address the environmental and human health harms of industrial agriculture. *Environmental Health Perspectives*, 110 (5), 445.

Huang, J.Z., Shrestha, A., Tollenaar, M., Deen, W., Rajcan, I., Rahimian, H., and Swanton, C.J., 2001. Effect of temperature and photoperiod on the phenological development of wild mustard (Sinapis arvensis L.). *Field Crops Research*, 70 (1), 75–86.

Hunt, E.R., Doraiswamy, P.C., McMurtrey, J.E., Daughtry, C.S.T., Perry, E.M., and Akhmedov, B., 2013. A visible band index for remote sensing leaf chlorophyll content at the canopy scale. *International Journal of Applied Earth Observation and Geoinformation*, 21, 103–112.

Iqbal, F., 2010. *Remote Sensing and GIS Application for Site Specific Agriculture*. VDM Verlag.

Iqbal, F., 2011. Detection of salt affected soil in rice-wheat area using satellite image. *African Journal of Agriculture Research*, 6 (21), 4973–4982.

Iqbal, F., Lucieer, A., and Barry, K., 2018. Simplified radiometric calibration for UAS-mounted multispectral sensor. *European Journal of Remote Sensing*, 51 (1), 301–313.

Iqbal, F., Lucieer, A., Barry, K., and Wells, R., 2017. Poppy Crop Height and Capsule Volume Estimation from a Single UAS Flight. *Remote Sensing*, 9 (7), 647.

Iqbal, F. and Mehdi, M.R., 2008. Detection of suitable soils for Zero-Till Wheat Cultivation in Pakistan using GITs. *In*: *2008 International Workshop on Earth Observation and Remote Sensing Applications*. Beijing: IEEE, 1–6.

Ireson, J.E., 1993. Activity and pest status of surface-activie collembola in Tasmanian field crops and pastures. *Australian Journal of Entomology*, 32 (2), 155–167.

Jaakkola, A., Hyyppa, J., Kukko, A., Yu, X.W., Kaartinen, H., Lehtomaki, M., and Lin, Y., 2010. A low-cost multi-sensoral mobile mapping system and its feasibility for tree measurements. *ISPRS Journal of Photogrammetry and Remote Sensing*, 65 (6), 514–522.

Jackson, R.D. and Youngblood, J.W., 1983. Agriculture's eye in the sky: forever plane could give continuous crop data High Altitude Powered Platform, remote sensing,

research outlook. *Crops and Soils Magazine*, 1–5.

Jackson, S., 2009. Plant responses to photoperiod. *New Phytologist*, (2008), 517–531.

Jain, P.M., 1990a. Effect of phosphorus and potassium on yield of opium poppy. *Indian Journal of Agronomy*, 35 (3), 238–239.

Jain, P.M., 1990b. Effect of split application of nitrogen on opium poppy. *Indian Journal of Agronomy*, 35 (3), 240–242.

Jeong, J.H., Resop, J.P., Mueller, N.D., Fleisher, D.H., Yun, K., Butler, E.E., Timlin, D.J., Shim, K.-M., Gerber, J.S., Reddy, V.R., and others, 2016. Random forests for global and regional crop yield predictions. *PloS one*, 11 (6), e0156571.

Jia, K., Wu, B., Tian, Y., Li, Q., and Du, X., 2011. An effective biophysical indicator for opium yield estimation. *Computers and Electronics in Agriculture*, 75 (2), 272–277.

Jiang, Z., Huete, A.R., Didan, K., and Miura, T., 2008. Development of a two-band enhanced vegetation index without a blue band. *Remote Sensing of Environment*, 112 (10), 3833–3845.

Jiapaer, G., Chen, X., and Bao, A., 2011. A comparison of methods for estimating fractional vegetation cover in arid regions. *Agricultural and Forest Meteorology*, 151 (12), 1698–1710.

Jones, Z. and Linder, F., 2015. Exploratory data analysis using random forests. *In*: *Prepared for the 73rd annual MPSA conference*. Chicago.

Jordan, C.F., 1969. Derivation of leaf-area index from quality of light on the forest floor. *Ecology*, 50 (4), 663–666.

Joseph, W., Aerts, S., Vandenbossche, M., Thielens, A., and Martens, L., 2016. Drone based measurement system for radiofrequency exposure assessment. *Bioelectromagnetics*, 37 (3), 195–199.

Kamkar, B., Al-Alahmadi, M.J., Mahdavi-Damghani, A., and Villalobos, F.J., 2012. Quantification of the cardinal temperatures and thermal time requirement of opium poppy (*Papaver Somniferum L*) seeds to germinate using non-linear regression models. *Industrial Crops and Products*, 35 (1), 192–198.

Kang, H. and Primack, R.B., 1991. Temporal variation of flower and fruit size in relation to seed yield in celandine poppy (Chelidonium majus; Papaveraceae). *American Journal of Botany*, 711–722.

Karpouzli, E. and Malthus, T., 2003. The empirical line method for the atmospheric correction of IKONOS imagery. *International Journal of Remote Sensing*, 24 (5), 1143–

1150.

Kassem, M.A. and Jacquin, A., 2001. Somatic embryogenesis, rhizogenesis, and morphinan alkaloids production in two species of opium poppy. *Journal of Biomedicine and Biotechnology*, 2001, 70–78.

Kaur, R., Singh, B., Singh, M., and Thind, S.K., 2015. Hyperspectral indices, correlation and regression models for estimating growth parameters of wheat genotypes. *Journal of the Indian Society of Remote Sensing*, 43 (3), 551–558.

Kelcey, J. and Lucieer, A., 2012. Sensor correction of a 6-band multispectral imaging sensor for UAV remote sensing. *Remote Sensing*, 4 (5), 1462–1493.

Kempeneers, P., De Backer, S., Zarco-Tejada, P.J., Delalieux, S., Sepulcre-Canto, G., Iribas, F.M., Aardt, J., Coppin, P., Scheunders, P., and Spie, 2006. Stress detection in orchards with hyperspectral remote sensing data. *In*: *Conference on Remote Sensing for Agriculture, Ecosystems, and Hydrology VIII*. Stockholm, SWEDEN: Spie-Int Soc Optical Engineering, U242–U251.

Kempeneers, P., Zarco-Tejada, P.J., North, P.R.J., De Backer, S., Delalieux, S., Sepulcre-Canto, G., Morales, F., Van Aardt, J.A.N., Sagardoy, R., Coppin, P., and Scheunders, P., 2008. Model inversion for chlorophyll estimation in open canopies from hyperspectral imagery. *International Journal of Remote Sensing*, 29 (17–18), 5093–5111.

Khan, R., Khan, M.M.A., Singh, M., Nasir, S., Naeem, M., Siddiqui, M.H., and Mohammad, F., 2007. Gibberellic acid and triacontanol can ameliorate the opium yield and morphine production in opium poppy (*Papaver Somniferum L*). *Acta Agriculturae Scandinavica Section B-Soil and Plant Science*, 57 (4), 307–312.

Khan, Z.H., Khan, M.M.A., Aftab, T., Idrees, M., and Naeem, M., 2011. Influence of alginate oligosaccharides on growth, yield and alkaloid production of opium poppy (*Papaver Somniferum L*). *Frontiers of Agriculture in China*, 5 (1), 122–127.

Kogan, F., Kussul, N., Adamenko, T., Skakun, S., Kravchenko, O., Kryvobok, O., Shelestov, A., Kolotii, A., Kussul, O., and Lavrenyuk, A., 2013. Winter wheat yield forecasting in Ukraine based on Earth observation, meteorological data and biophysical models. *International Journal of Applied Earth Observation and Geoinformation*, 23, 192–203.

Kohavi, R. and John, G.H., 1997. Wrappers for feature subset selection. *Artificial intelligence*, 97 (1–2), 273–324.

Kothari, K.L. and Verma, A.C., 1972. Germination of conidia of poppy powdery mildew (Erysiphe polygoni DC). *Mycopathologia*, 47 (3), 253–260.

Kross, A., McNairn, H., Lapen, D., Sunohara, M., and Champagne, C., 2015. Assessment of RapidEye vegetation indices for estimation of leaf area index and biomass in corn and soybean crops. *International Journal of Applied Earth Observation and Geoinformation*, 34, 235–248.

Kumar, B., Singh, V.R., Ram, G., and Singh, H.P., 2011. Genetic Combining Ability Estimates for Inheritance of Economic Traits in Opium Poppy (*Papaver Somniferum L*). *In*: *International Symposium on Papaver 1036*. 43–50.

Kuo, C.-L., Sagare, A.P., Lo, S.-F., Lee, C.-Y., Chen, C.-C., and Tsay, H.-S., 2002. Abscisic acid promotes development of somatic embryos on converted somatic embryos of Corydalis yanhusuo (Fumariaceae). *Journal of Plant Physiology*, 159 (4), 423–427.

De la Rosa, J.M., Domingo, R., Gómez-Montiel, J., and Pérez-Pastor, a., 2015. Implementing deficit irrigation scheduling through plant water stress indicators in early nectarine trees. *Agricultural Water Management*, 152, 207–216.

Laliberte, A.S. and Rango, A., 2011. Image processing and classification procedures for analysis of sub-decimeter imagery acquired with an unmanned aircraft over arid rangelands. *GIScience & Remote Sensing*, 48 (1), 4–23.

Landa, B.B., Montes-Borrego, M., Muñoz-Ledesma, F.J., and Jiménez-Díaz, R.M., 2007. Phylogenetic analysis of downy mildew pathogens of opium poppy and PCR-based in planta and seed detection of *Peronospora arborescens*. *Phytopathology*, 97 (11), 1380–1390.

Laughlin, J.C., 1977. The effect of band placed nitrogen and phosphorus fertiliser on the yield of poppies (*Papaver Somniferum L*) grown on krasnozem soil. *In*: *I International Symposium on Spices and Medicinal Plants 73*. 165–172.

Laughlin, J.C., 1979. The boron nutrition of poppy (*Papaver Somniferum L*) on Kransoze and Alluvial soils of Tasmania. *In*: *II International Symposium on Spices and Medicinal Plants 96*. 227–234.

Laughlin, J.C., 1982. The effect of time of application and chemical formulation of nitrogen fertilisers on the morphine production of poppies (*Papaver Somniferum L*) in Tasmania. *In*: *III International Symposium on Spice and Medicinal Plants, XXI IHC 132*. 233–238.

Laughlin, J.C. and Chung, B., 1990. Nitrogen and Irrigation Effects on the Yield of Poppies (*Papaver Somniferum L*). *In*: *International Symposium on Medicinal and Aromatic Plants, XXIII IHC 306*. 466–473.

Laughlin, J.C., Chung, B., and Beattle, B.M., 1998. Poppy cultivation in Australia. *In*: *Poppy The Genus Papaver*. 249–277.

Laughlin, J.C. and Munro, D., 1982. The effect of fungal colonization on the morphine production of poppy (*Papaver Somniferum L*) capsules. *The Journal of Agricultural Science*, 98 (03), 679–687.

Lausch, A., Pause, M., Merbach, I., Zacharias, S., Doktor, D., Volk, M., and Seppelt, R., 2013. A new multiscale approach for monitoring vegetation using remote sensing-based indicators in laboratory, field, and landscape. *Environmental monitoring and Assessment*, 185 (2), 1215–1235.

Lecina, S., Neale, C.M.U., Merkley, G.P., and Dos Santos, C. a. C., 2011. Irrigation evaluation based on performance analysis and water accounting at the Bear River Irrigation Project (U.S.A.). *Agricultural Water Management*, 98 (9), 1349–1363.

Van Leeuwen, W.J.D., Orr, B.J., Marsh, S.E., and Herrmann, S.M., 2006. Multi-sensor NDVI data continuity: Uncertainties and implications for vegetation monitoring applications. *Remote Sensing of Environment*, 100 (1), 67–81.

Leh, M., Bajwa, S., and Chaubey, I., 2013. Impact of land use change on erosion risk: an integrated remote sensing, geographic information system and modeling methodology. *Land Degradation & Development*, 24 (5), 409–421.

Leroux, L., Jolivot, A., Bégué, A., Seen, D. Lo, and Zoungrana, B., 2014. How reliable is the MODIS land cover product for crop mapping Sub-Saharan agricultural landscapes? *Remote Sensing*, 6 (9), 8541–8564.

Li, W., Niu, Z., Chen, H., Li, D., Wu, M., and Zhao, W., 2016. Remote estimation of canopy height and aboveground biomass of maize using high-resolution stereo images from a low-cost unmanned aerial vehicle system. *Ecological Indicators*, 67, 637–648.

Liaw, A., Wiener, M., and others, 2002. Classification and regression by randomForest. *R news*, 2 (3), 18–22.

Lisson, S.N., 2007. Temperature and photoperiod effects on the growth and development of opium poppy (Papaver somniferum). *Australian Journal of Experimental Agriculture*, 47 (6), 742.

Lisson, S.N. and Cotching, W.E., 2011. Modelling the fate of water and nitrogen in the mixed vegetable farming systems of northern Tasmania, Australia. *Agricultural Systems*, 104 (8), 600–608.

Liu, J., Miller, J.R., Haboudane, D., Pattey, E., and Hochheim, K., 2008. Crop fraction estimation from casi hyperspectral data using linear spectral unmixing and vegetation indices. *Canadian Journal of Remote Sensing*, 34 (S1), S124--S138.

Liu, L., Wang, J., Bao, Y., Huang, W., Ma, Z., and Zhao, C., 2006. Predicting winter wheat condition, grain yield and protein content using multi-temporal EnviSat-ASAR and Landsat TM satellite images. *International Journal of Remote Sensing*, 27 (4), 737–753.

Liu, Z.A., Yang, J.P., and Yang, Z.C., 2012. Using a chlorophyll meter to estimate tea leaf chlorophyll and nitrogen contents. *Journal of soil science and plant nutrition*, 12 (2), 339–348.

Lopez-Granados, F., 2011. Weed detection for site-specific weed management: mapping and real-time approaches. *Weed Research*, 51 (1), 1–11.

Losak, T. and Palenicek, L., 2005. Using nitrogen and sulphur for the poppy (*Papaver Somniferum L*) nutrition. *In*: *Rosliny Oleiste-Oilseed Crops*. Yadda.

Losak, T. and Richter, R., 2004. Split nitrogen doses and their efficiency in poppy (*Papaver Somniferum L*) nutrition. *Growth*, 35 (11), 484–488.

Lu, Y., Song, S., Wang, R., Liu, Z., Meng, J., Sweetman, A.J., Jenkins, A., Ferrier, R.C., Li, H., Luo, W., and others, 2015. Impacts of soil and water pollution on food safety and health risks in China. *Environment International*, 77, 5–15.

Lucieer, A., de Jong, S., and Turner, D., 2014. Mapping landslide displacements using Structure from Motion (SfM) and image correlation of multi-temporal UAV photography. *Progress in Physical Geography*, 38 (1), 97–116.

Lucieer, A., Malenovský, Z., Veness, T., and Wallace, L., 2014. HyperUAS-Imaging Spectroscopy from a Multirotor Unmanned Aircraft System. *Journal of Field Robotics*, 31 (4), 571–590.

Mahdavi-Damghani, A., Kamkar, B., Al-Ahmadi, M.J., Testi, L., Muñoz-Ledesma, F.J., and Villalobos, F.J., 2010. Water stress effects on growth, development and yield of opium poppy (*Papaver Somniferum L*). *Agricultural Water Management*, 97 (10), 1582–1590.

Makynen, J., Holmlund, C., Saari, H., Ojala, K., and Antila, T., 2011. Unmanned aerial vehicle (UAV) operated megapixel spectral camera. *In*: *Electro-Optical Remote Sensing, Photonic Technologies, and Applications*. USA: International Society for Optics and Photonics, 8186.

Makynen, J., Saari, H., Holmlund, C., Mannila, R., and Antila, T., 2012. Multi- and hyperspectral UAV imaging system for forest and agriculture applications. *In*: *Next-Generation Spectroscopic Technologies*. Baltimore, MD: International Society for Optics and Photonics, 837409.

Malenovský, Z., Ufer, C., Lhotáková, Z., Clevers, J.G.P.W., Schaepman, M.E., Albrechtová, J., Cudlín, P., and Z Malenovský Z Lhotáková, J G P W Clevers, M E Schaepman, J Albrechtová & P Cudlín, C.U., 2006. A new hyperspectral index for chlorophyll estimation of a forest canopy: Area under curve normalised to maximal band depth between 650-725 nm. *EARSeL eProceedings*, 5, 161–172.

Mancini, F., Dubbini, M., Gattelli, M., Stecchi, F., Fabbri, S., and Gabbianelli, G., 2013. Using unmanned aerial vehicles (UAV) for high-resolution reconstruction of topography: the structure from motion approach on coastal environments. *Remote Sensing*, 5 (12), 6880–6898.

Mattar, C., Hernández, J., Santamar\'\ia-Artigas, A., Durán-Alarcón, C., Olivera-Guerra, L., Inzunza, M., Tapia, D., and Escobar-Lav\'\in, E., 2014. A first in-flight absolute calibration of the Chilean Earth Observation Satellite. *ISPRS Journal of Photogrammetry and Remote Sensing*, 92, 16–25.

Mika, E.S., 1955. Studies on the Growth and Development and Morphine Content of Opium Poppy Author. *Botanical Gazette*, 116 (4), 323–339.

Mishra, B.K., Rastogi, A., Siddiqui, A., Srivastava, M., Verma, N., Pandey, R., Sharma, N.C., and Shukla, S., 2013. Opium Poppy: Genetic Upgradation Through Intervention of Plant Breeding Techniques. *Plant Breeding from Laboratories to Fields, edited by SB Anderson, InTech*.

Mishra, B.K., Shukla, S., Rastogi, A., and Sharma, A., 2010. Heritability and genetic advance for effective selection in opium poppy (Papaver somniferum). *Indian Journal of Agricultural Scienceournal of Agricultural Science*, 80 (6), 470–476.

Miura, T. and Huete, A.R., 2009. Performance of three reflectance calibration methods for airborne hyperspectral spectrometer data. *Sensors (Basel, Switzerland)*, 9 (2), 794–813.

Montes-Borrego, M., Muñoz-Ledesma, F.J., Jiménez-Díaz, R.M., and Landa, B.B., 2008. *Peronospora arborescens* causes downy mildew disease in commercial opium poppy crops in France. *Plant Disease*, 92 (5), 834.

Moorthy, I., Miller, J.R., Noland, T.L., Nielsen, U., Zarco-Tejada, P.J., and Ieee, 2003. Chlorophyll content estimation of boreal conifers using hyperspectral remote sensing. *Igarss 2003: Ieee International Geoscience and Remote Sensing Symposium, Vols I - Vii, Proceedings: Learning from Earth's Shapes and Sizes*, 2568–2570.

Moran, M.S., Bryant, R., Thome, K., Ni, W., Nouvellon, Y., Gonzalez-Dugo, M.P., Qi, J., and Clarke, T.R., 2001. A refined empirical line approach for reflectance factor retrieval from Landsat-5 TM and Landsat-7 ETM+. *Remote Sensing of Environment*, 78 (1), 71–82.

Morel, J., Todoroff, P., Bégué, A., Bury, A., Martiné, J.-F., and Petit, M., 2014. Toward a Satellite-Based System of Sugarcane Yield Estimation and Forecasting in Smallholder Farming Conditions: A Case Study on Reunion Island. *Remote Sensing*, 6 (7), 6620–6635.

Moroni, M., Mei, A., Leonardi, A., Lupo, E., and Marca, F. La, 2015. PET and PVC separation with hyperspectral imagery. *Sensors*, 15 (1), 2205–2227.

Motohka, T., Nasahara, K.N., Oguma, H., and Tsuchida, S., 2010. Applicability of green-red vegetation index for remote sensing of vegetation phenology. *Remote Sensing*, 2 (10), 2369–2387.

Mulla, D.J., 2013. Twenty five years of remote sensing in precision agriculture: Key advances and remaining knowledge gaps. *Biosystems Engineering*, 114 (4), 358–371.

Murray-Krezan, J., Neumann, J.G., and Leathers, R.A., 2008. Small object hyperspectral detection from a low-flying UAV. *In*: USA, ed. *Signal and Data Processing of Small Targets 2008*. International Society for Optics and Photonics, 69691.

Murray, C., 2014. An overview of the tasmanian poppy indusrty [online]. *TPI Enterprises Ltd*. Available from: http://www.grdc.com.au/Research-and-Development/GRDC-Update-Papers/2014/07/An-overview-of-the-Tasmanian-poppy-industry.

Ncube, B., Mupangwa, W., and French, A., 2018. Precision agriculture and food security in Africa. *In*: *Systems Analysis Approach for Complex Global Challenges*. Springer, 159–178.

Nelson, L.B., 1972. Agricultural Chemicals in Relation to Environmental Quality: Chemical Fertilizers, Present and Future1. *Journal of Environmental Quality*, 1 (1), 2–5.

Nex, F. and Remondino, F., 2014. UAV for 3D mapping applications: a review. *Applied Geomatics*, 6 (1), 1–15.

Novotny, V., 1999. Diffuse pollution from agriculture-a worldwide outlook. *Water Science and Technology*, 39 (3), 1–13.

Omidi, M., Koohzadi, F., Solouki, M., Taghizad Farid, R., and Alizadeh, H., 2012. Comparison of morphinan alkaloids during different stages of growth in the medicinal plant opium poppy (*Papaver Somniferum L*). *Journal of Medicinal Plants*, 11 (44), 140–148.

Onoyama, H., Ryu, C., Suguri, M., and Iida, M., 2017. Estimation of rice protein content before harvest using ground-based hyperspectral imaging and region of interest

analysis. *Precision Agriculture*, 1–14.

Oovergaard, S.I., Isaksson, T., Kvaalc, K., Korsaeth, A., Oøvergaard, S.I., Isaksson, T., Kvaalc, K., and Korsaeth, A., 2010. Comparisons of two hand-held, multispectral field radiometers and a hyperspectral airborne imager in terms of predicting spring wheat grain yield and quality by means of powered partial least squares regression. *Journal of Near Infrared Spectroscopy*, 18 (4), 247–261.

Oudemans, P. V, Pozdnyakova, L., Hughes, M.G., and Rahman, F., 2002. GIS and Remote Sensing for Detecting Yield Loss in Cranberry Culture. *Journal of Nematology*, 34 (3), 207–212.

Pal, M. and Mather, P.M., 2005. Support vector machines for classification in remote sensing. *International Journal of Remote Sensing*, 26 (5), 1007–1011.

Papadavid, G., Hadjimitsis, D., Toulios, L., and Michaelides, S., 2011. Mapping potato crop height and leaf area index through vegetation indices using remote sensing in Cyprus. *Journal of Applied Remote Sensing*, 5 (1), 53526.

Park, S.-U. and Facchini, P.J., 2000. Agrobacterium rhizogenes-mediated transformation of opium poppy, *Papaver Somniferum L*, and California poppy, Eschscholzia californica Cham., root cultures. *Journal of experimental botany*, 51 (347), 1005–1016.

Patel, N.K., Saxena, R.K., and Shiwalkar, A., 2007. Study of fractional vegetation cover using high spectral resolution data. *Journal of the Indian Society of Remote Sensing*, 35 (1), 73–79.

Penka, M., 1968. Changes in water economy and morphine content in irrigated and non-irrigated plants of papaver somniferum. *Acta Univ. Agric. Fac. AGron*, 16, 579–590.

Pérez-Ortiz, M., Peña, J.M., Gutiérrez, P.A., Torres-Sánchez, J., Hervás-Martinez, C., and López-Granados, F., 2015. A semi-supervised system for weed mapping in sunflower crops using unmanned aerial vehicles and a crop row detection method. *Applied Soft Computing*, 37, 533–544.

Pethybridge, S.J., O Malley, T., Kile, R., and Wilsonc, C.R., 2005. Survey for viruses in oilseed poppy in Tasmania, Australia. *Australasian Plant Pathology*, 34 (4), 611–613.

Pinter Jr, P.J., Hatfield, J.L., Schepers, J.S., Barnes, E.M., Moran, M.S., Daughtry, C.S.T., and Upchurch, D.R., 2003. Remote sensing for crop management. *Photogrammetric Engineering & Remote Sensing*, 69 (6), 647–664.

Del Pozo, S., Rodríguez-Gonzálvez, P., Hernández-López, D., and Felipe-García, B., 2014. Vicarious Radiometric Calibration of a Multispectral Camera on Board an Unmanned Aerial System. *Remote Sensing*, 6 (3), 1918–1937.

Pradhan, S., Bandyopadhyay, K.K., and Sahoo, R.N., 2014. Predicting Wheat Grain and Biomass Yield Using Canopy Reflectance of Booting Stage. *Journal of the Indian Society of Remote Sensing*, 42 (4), 711–718.

Prasad, A.M., Iverson, L.R., and Liaw, A., 2006. Newer classification and regression tree techniques: bagging and random forests for ecological prediction. *Ecosystems*, 9 (2), 181–199.

Primicerio, J., Di Gennaro, S.F., Fiorillo, E., Genesio, L., Lugato, E., Matese, A., and Vaccari, F.P., 2012. A flexible unmanned aerial vehicle for precision agriculture. *Precision Agriculture*, 13 (4), 517–523.

Qi, J., Chehbouni, A., Huete, A.R., Kerr, Y.H., and Sorooshian, S., 1994. A modified soil adjusted vegetation index. *Remote Sensing of Environment*, 48 (2), 119–126.

Qi, Y., 2012. Random forest for bioinformatics. *In*: *Ensemble machine learning*. Springer, 307–323.

Quilter, M.C. and Anderson, V.J., 2000. Low altitude/large scale aerial photographs: A tool for range and resource managers. *Rangelands Archives*, 22 (2), 13–17.

R Core Team, 2015. R: A Language and Environment for Statistical Computing.

Rango, A., Laliberte, A., Herrick, J.E., Winters, C., Havstad, K., Steele, C., Browning, D., and others, 2009. Unmanned aerial vehicle-based remote sensing for rangeland assessment, monitoring, and management. *Journal of Applied Remote Sensing*, 3 (1), 33542.

Rasmussen, J., Ntakos, G., Nielsen, J., Svensgaard, J., Poulsen, R.N., and Christensen, S., 2016. Are vegetation indices derived from consumer-grade cameras mounted on UAVs sufficiently reliable for assessing experimental plots? *European Journal of Agronomy*, 74, 75–92.

Raven, P.H., Evert, R.F., and Eichhorn, S.E., 1999. Biology of the plant cell. *In*: *Biology of Plants*. W.H.Freeman and Compnay, 1–920.

Remondino, F., Del Pizzo, S., Kersten, T.P., and Troisi, S., 2012. Low-cost and open-source solutions for automated image orientation-A critical overview. *In*: *Euro-Mediterranean Conference*. 40–54.

Ries, S.K. and Wert, V.F., 1988. Rapid elicitation of second messengers by nanomolar doses of triacontanol and octacosanol. *Planta*, 173 (1), 79–87.

Rodriguez, M.G., Reynolds, M.P., Raun, W.R., Stone, M.L., and Klatt, A.R., 2009. Effect of morphological traits on spectral reflectance indices in spring wheat. *20th Annual Research Symposium, Research Week 2009*, (February 2015), 37–41.

Roger-Estrade, J., Anger, C., Bertrand, M., and Richard, G., 2010. Tillage and soil ecology: partners for sustainable agriculture. *Soil and Tillage Research*, 111 (1), 33–40.

Rondeaux, G., Steven, M., and Baret, F., 1996. Optimization of soil-adjusted vegetation indices. *Remote Sensing of Environment*, 55 (2), 95–107.

Roujean, J.-L. and Breon, F.-M., 1995. Estimating PAR absorbed by vegetation from bidirectional reflectance measurements. *Remote Sensing of Environment*, 51 (3), 375–384.

Rouse Jr, J.W., 1972. *Monitoring the vernal advancement and retrogradation (green wave effect) of natural vegetation*. College Station Teas USA.

Rowshon, M.K., Kwok, C.Y., and Lee, T.S., 2003. GIS-based scheduling and monitoring irrigation delivery for rice irrigation system. *Agricultural Water Management*, 62 (2), 117–126.

Rud, R., Cohen, Y., Alchanatis, V., Levi, a., Brikman, R., Shenderey, C., Heuer, B., Markovitch, T., Dar, Z., Rosen, C., Mulla, D., and Nigon, T., 2014. Crop water stress index derived from multi-year ground and aerial thermal images as an indicator of potato water status. *Precision Agriculture*, 15 (3), 273–289.

Rufino, G. and Moccia, A., 2005. Integrated VIS-NIR hyperspectral / thermal-IR electro-optical payload system for a mini-UAV. *Infotech@ Aerospace* 915–923.

Saari, H., Aallos, V. V, Akujärvi, A., Antila, T., Holmlund, C., Kantojärvi, U., Mäkynen, J., and Ollila, J., 2009. Novel miniaturized hyperspectral sensor for UAV and space applications. *In*: USA, ed. *Sensors, Systems, and Next-Generation Satellites XIII*. International Society for Optics and Photonics.

Saari, H., Pellikka, I., Pesonen, L., Tuominen, S., Heikkilä, J., Holmlund, C., Mäkynen, J., Ojala, K., and Antila, T., 2011. Unmanned aerial vehicle (UAV) operated spectral camera system for forest and agriculture applications. *In*: *Remote Sensing for Agriculture, Ecosystems, and Hydrology XIII*. USA: International Society for Optics and Photonics.

Saeed, U., Dempewolf, J., Becker-Reshef, I., Khan, A., Ahmad, A., and Wajid, S.A., 2017. Forecasting wheat yield from weather data and MODIS NDVI using Random Forests for Punjab province, Pakistan. *International Journal of Remote Sensing*, 38 (17), 4831–4854.

Sagare, A.P., Lee, Y.L., Lin, T.C., Chen, C.C., and Tsay, H.S., 2000. Cytokinin-induced somatic embryogenesis and plant regeneration in Corydalis yanhusuo (Fumariaceae) a medicinal plant. *Plant Science*, 160 (1), 139–147.

Salvatore, M., McCabe, M.F., Miller, P.E., Lucas, R., Pajuelo, V.M., and Tóth, B., 2018. On the Use of Unmanned Aerial Systems for Environmental Monitoring. *Remote Sensing*, 10 (4), 1–7.

Sandri, M.F. and Zuccolotto, P., 2006. Analysis of a bias effect in a tree-based variable importance measure. *In*: *Evaluation of an Empirical Adjustment Strategy*. Citeseer.

Schapire, R.E. and Singer, Y., 1999. Improved boosting algorithms using confidence-rated predictions. *Machine Learning*, 37 (3), 297–336.

Schiff, P., 2002. Opium and its alkaloids. *American Journal of Pharmaceutical Education*, 66, 186–194.

Schloter, M., Dilly, O., and Munch, J.C., 2003. Indicators for evaluating soil quality. *Agriculture, Ecosystems & Environment*, 98 (1–3), 255–262.

Schulz, H., Baranska, M., Quilitzsch, R., and Schütze, W., 2004. Determination of alkaloids in capsules, milk and ethanolic extracts of poppy (*Papaver Somniferum L*) by ATR-FT-IR and FT-Raman spectroscopy. *The Analyst*, 129, 917–920.

Scott, J.B., Hay, F.S., and Wilson, C.R., 2004. Phylogenetic analysis of the downy mildew pathogen of oilseed poppy in Tasmania, and its detection by PCR. *Mycological research*, 108 (02), 198–205.

Scott, J.B., Hay, F.S., Wilson, C.R., Cotterill, P.J., and Fist, A.J., 2003. Spatiotemporal analysis of epiphytotics of downy mildew of oilseed poppy in Tasmania, Australia. *Phytopathology*, 93 (6), 752–757.

Serrano, L., Filella, I., and Penuelas, J., 2000. Remote sensing of biomass and yield of winter wheat under different nitrogen supplies. *Crop Science*, 40 (3), 723–731.

Sharma, L.K., Bu, H., Franzen, D.W., and Denton, A., 2016. Use of corn height measured with an acoustic sensor improves yield estimation with ground based active optical sensors. *Computers and Electronics in Agriculture*, 124, 254–262.

Shibata, T., Miura, T., and Hatakeyama, Y., 1991. [Flower bud differentiation and development of opium poppy (*Papaver Somniferum L*) II. Effects of daylength and temperature]. *Eisei Shikenjo hokoku. Bulletin of National Institute of Hygienic Sciences*, (110), 53–59.

Shukla, S., Singh, S.P., Yadav, H.K., and Chatterjee, a., 2006. Alkaloid Spectrum of Different Germplasm Lines in Opium Poppy (*Papaver Somniferum L*). *Genetic Resources and Crop Evolution*, 53 (3), 533–540.

Shuljgin, G., 1969. *Cultivation of the opium poppy and the oil poppy in the Soviet Union Sections*.

Singh, S., Singh, A.K., and Kumar, B., 2011. Effect of Moisture Regimes and Field Practices on Germination and Establishment of Opium Poppy (*Papaver Somniferum L*). *In*: *International Symposium on Papaver 1036*. 169–173.

Siroky, D.S. and others, 2009. Navigating random forests and related advances in algorithmic modeling. *Statistics Surveys*, 3, 147–163.

Smith, G.M. and Milton, E.J., 1999. The use of the empirical line method to calibrate remotely sensed data to reflectance. *International Journal of Remote Sensing*, 20 (13), 2653–2662.

Smith, M.W., Carrivick, J.L., and Quincey, D.J., 2016. Structure from motion photogrammetry in physical geography. *Progress in Physical Geography*, 40 (2), 247–275.

Smith, P.F., Ganesh, S., and Liu, P., 2013. A comparison of random forest regression and multiple linear regression for prediction in neuroscience. *Journal of Neuroscience Methods*, 220 (1), 85–91.

Solanki, N.S., Sharma, O.L., and Sahu, M.P., 1999. Phosphorus management in opium-poppy (Papaver somniferum)--Based cropping system. *Indian Journal of Agronomy*, 44 (3), 499–503.

Srivastava, N.K. and Sharma, S., 1990. Effect of triacontanol on photosynthesis, alkaloid content and growth in opium poppy (*Papaver Somniferum L*). *Plant Growth Regulation*, 9, 65–71.

Staben, G.W., Pfitzner, K., Bartolo, R., and Lucieer, A., 2012. Empirical line calibration of WorldView-2 satellite imagery to reflectance data: using quadratic prediction equations. *Remote Sensing Letters*, 3 (6), 521–530.

Stadler, A., Rudolph, S., Kupisch, M., Langensiepen, M., van der Kruk, J., and Ewert, F., 2015. Quantifying the effects of soil variability on crop growth using apparent soil electrical conductivity measurements. *European Journal of Agronomy*, 64, 8–20.

Stafford, J. V, 2000. Implementing precision agriculture in the 21st century. *Journal of Agricultural Engineering Research*, 76 (3), 267–275.

Stagakis, S., González-Dugo, V., Cid, P., Guillén-Climent, M.L., and Zarco-Tejada, P.J., 2012. Monitoring water stress and fruit quality in an orange orchard under regulated deficit irrigation using narrow-band structural and physiological remote sensing indices. *ISPRS Journal of Photogrammetry and Remote Sensing*, 71, 47–61.

Stagakis, S., Gonzalez-Dugo, V., Cid, P., Guillen-Climent, M.L., Zarco-Tejada, P.J.J., González-Dugo, V., Cid, P., Guillén-Climent, M.L., and Zarco-Tejada, P.J.J., 2012.

Monitoring water stress and fruit quality in an orange orchard under regulated deficit irrigation using narrow-band structural and physiological remote sensing indices. *ISPRS Journal of Photogrammetry and Remote Sensing*, 71, 47–61.

Stark, R., Gitelson, A.A., Grits, U., Rundquist, D., Kaufman, Y., and others, 2000. New technique for remote estimation of vegetation fraction: principles, algorithms and validation. *Aspects of Applied Biology*, 60, 241–246.

Steduto, P., Hsiao, T.C., Raes, D., and Fereres, E., 2009. AquaCrop-The FAO crop model to simulate yield response to water: I. Concepts and underlying principles. *Agronomy Journal*, 101 (3), 426–437.

Stellman, C.M., Olchowski, F.M., and Michalowicz, J. V, 2001. WAR HORSE wide area reconnaissance - Hyperspectral overhead real-time surveillance experiment. International *Society for Optics and Photonics* 339–346.

Stevens, A. and Ramirez-Lopez, L., 2014. An introduction to the prospectr package. *R Package Vignette, Report No.: R Package Version 0.1*, 3.

Stow, D., Hope, A., Nguyen, A.T., Phinn, S., and Benkelman, C.A., 1996. Monitoring detailed land surface changes using an airborne multispectral digital camera system. *IEEE Transactions on Geoscience and Remote Sensing*, 34 (5), 1191–1203.

Swain, K.C., Thomson, S.J., Jayasuriya, H.P.W., and others, 2010. Adoption of an unmanned helicopter for low-altitude remote sensing to estimate yield and total biomass of a rice crop. *Transactions of the ASAE (American Society of Agricultural Engineers)*, 53 (1), 21.

Tan, G. and Shibasaki, R., 2003. Global estimation of crop productivity and the impacts of global warming by GIS and EPIC integration. *Ecological Modelling*, 168 (3), 357–370.

Tattaris, M., Reynolds, M.P., and Chapman, S.C., 2016. A direct comparison of remote sensing approaches for high-throughput phenotyping in plant breeding. *Frontiers in Plant Science*, 7, 1131.

Teillet, P.M., Fedosejevs, G., Thome, K.J., and Barker, J.L., 2007. Impacts of spectral band difference effects on radiometric cross-calibration between satellite sensors in the solar-reflective spectral domain. *Remote Sensing of Environment*, 110 (3), 393–409.

Temple-Smith, M.G., Wright, D.N., Laughlin, J.C., and Hoare, B.J., 1983. Field response of poppies (*Papaver Somniferum L*) to lime application on acid krasnozems in Tasmania. *The Journal of Agricultural Science*, 100 (02), 485–492.

Thangavel, T., Wilson, C.R., Jones, S., Scott, J.B., and Voglmayr, H., 2017. First Report of

Systemic Downy Mildew of Opium Poppy Caused by Peronospora somniferi in Australia. *Plant Disease*, 101 (2), 392–392.

Thenkabail, P.S., Smith, R.B., and De Pauw, E., 2000. Hyperspectral vegetation indices and their relationships with agricultural crop characteristics. *Remote Sensing of Environment*, 71 (2), 158–182.

Thornton, P., 2002. *Mapping poverty and livestock in the developing world*. 1st ed. Nairobi, Kenya: ILRI.

Tilly, N., Hoffmeister, D., Cao, Q., Huang, S., Lenz-Wiedemann, V., Miao, Y., and Bareth, G., 2014. Multitemporal crop surface models: accurate plant height measurement and biomass estimation with terrestrial laser scanning in paddy rice. *Journal of Applied Remote Sensing*, 8 (1), 83671.

Tirado, R., 2007. Nitrates in drinking water in the Philippines and Thailand. *Greenpeace Research Laboratories Technical Note*, 11, 2007.

Tomlins, G.F. and Lee, Y.J., 1983. Remotely Piloted Aircraft An Inexpensive Option for Large-Scale Aerial Photography in Forestry Applications. *Canadian Journal of Remote Sensing*, 9 (2), 76–85.

Torres-Sánchez, J., López-Granados, F., and Peña, J.M., 2015. An automatic object-based method for optimal thresholding in UAV images: Application for vegetation detection in herbaceous crops. *Computers and Electronics in Agriculture*, 114, 43–52.

Tripathi, L. and Tripathi, J.N., 2005. Role of biotechnology in medicinal plants. *Tropical Journal of Pharmaceutical Research*, 2 (December), 243–253.

Trishchenko, A.P., Cihlar, J., and Li, Z., 2002. Effects of spectral response function on surface reflectance and NDVI measured with moderate resolution satellite sensors. *Remote Sensing of Environment*, 81 (1), 1–18.

Tucker, C.J., Holben, B.N., Elgin Jr, J.H., McMurtrey III, J.E., and others, 1980. Relationship of spectral data to grain yield variation. *Photogrammetric Engineering and Remote Sensing*, 46 (5), 657–666.

Turechek, W.W. and Mahaffee, W.F., 2004. Spatial pattern analysis of hop powdery mildew in the Pacific Northwest: Implications for sampling. *Phytopathology*, 94 (10), 1116–1128.

Turner, D., Lucieer, A., and Wallace, L., 2014. Direct georeferencing of ultrahigh-resolution UAV imagery. *IEEE Transactions on Geoscience and Remote Sensing*, 52 (5), 2738–2745.

Turner, D., Lucieer, A., and Watson, C., 2012. An automated technique for generating

georectified mosaics from ultra-high resolution unmanned aerial vehicle (UAV) imagery, based on structure from motion (SfM) point clouds. *Remote Sensing*, 4 (5), 1392–1410.

Uto, K., Seki, H., Saito, G., and Kosugi, Y., 2013. Characterization of rice paddies by a UAV-mounted miniature hyperspectral sensor system. *IEEE Journal of Selected Topics in Applied Earth Observations and Remote Sensing*, 6 (2), 851–860.

Vega, F.A., Ramirez, F.C., Saiz, M.P., and Rosua, F.O., 2015. Multi-temporal imaging using an unmanned aerial vehicle for monitoring a sunflower crop. *Biosystems Engineering*, 132 (0), 19–27.

Veres, T., 2011. Variation in Alkaloid Production in Poppy Ecotypes: Responses to Different Environments, *Biochemical Systematics and Ecology,* 16 (2), 171–178.

Verhoeven, G., Doneus, M., Briese, C., and Vermeulen, F., 2012. Mapping by matching: a computer vision-based approach to fast and accurate georeferencing of archaeological aerial photographs. *Journal of Archaeological Science*, 39 (7), 2060–2070.

Verhoeven, G. and Vermeulen, F., 2016. Engaging with the Canopy-Multi-Dimensional Vegetation Mark Visualisation Using Archived Aerial Images. *Remote Sensing*, 8 (9), 752.

Verma, N., Shukla, S., Prasad, B., Parmar, D., Parmar, N.C., Mishra, B.K., and Rastogi, A., 2011. Effect of Genotype, Environment and Their Interaction on Seed and Opium Yield in Opium Poppy (*Papaver Somniferum L*) and Comparison of Different Stability Models for GEI. *In*: *International Symposium on Papaver 1036*. 163–168.

Vicente-Serrano, S.M., Pérez-Cabello, F., and Lasanta, T., 2008. Assessment of radiometric correction techniques in analyzing vegetation variability and change using time series of Landsat images. *Remote Sensing of Environment*, 112 (10), 3916–3934.

Vincini, M., Frazzi, E., and D Alessio, P., 2008. A broad-band leaf chlorophyll vegetation index at the canopy scale. *Precision Agriculture*, 9 (5), 303–319.

Vincini, M., Frazzi, E., and DAlessio, P., 2006. Angular dependence of maize and sugar beet VIs from directional CHRIS/Proba data. *In*: *Proc. 4th ESA CHRIS PROBA Workshop*. 19–21.

Waine, T.W., Simms, D.M., Taylor, J.C., and Juniper, G.R., 2014. Towards improving the accuracy of opium yield estimates with remote sensing. *International Journal of Remote Sensing*, 35 (16), 6292–6309.

Wang, Zhongchun and Acock, Mary C and Acock, B., 1997. Phases of development to flowering in opium poppy (*Papaver Somniferum L*) under various temperatures. *Annals of Botany*, 80 (4), 547–552.

Wang, C. and Myint, S.W., 2015. A simplified empirical line method of radiometric calibration for small unmanned aircraft systems-based remote sensing. *IEEE Journal of Selected Topics in Applied Earth Observations and Remote Sensing*, 8 (5), 1876–1885.

Wang, J., 2013. *Unsupervised detection of opium poppy fields in Afghanistan from EO-1 Hyperion data*. Fredericton , N.B., Canada.

Wang, L., Tian, Y., Yao, X., Zhu, Y., and Cao, W., 2014. Predicting grain yield and protein content in wheat by fusing multi-sensor and multi-temporal remote-sensing images. *Field Crops Research*, 164, 178–188.

Wang, L., Zhou, X., Zhu, X., Dong, Z., and Guo, W., 2016. Estimation of biomass in wheat using random forest regression algorithm and remote sensing data. *The Crop Journal*, 4 (3), 212–219.

Wang, Z., Acock, M.C., Liu, Q., and Acock, B., 1999. Growth, opium gum yield, and photoperiod response of five opium poppy accessions. *HortScience*, 34 (6), 1060–1063.

Wang, Z., Aoock, M., Acock, B., Acock, M., and Acock, B., 1997. Photoperiod sensitivity during flower development of opium poppy (*Papaver Somniferum L*). *Annals of Botany*, 79 (2), 129–132.

Warren, C.P., Pfister, W., Even, D., Velasco, A., Yee, S., Breitwieser, D., and Naungayan, J., 2011. Miniaturization of a SWIR Hyperspectral imager. *In*: *Airborne Intelligence, Surveillance, Reconnaissance (ISR) Systems and Applications VIII*. USA: International Society for Optics and Photonics.

Warren, G. and Metternicht, G., 2005. Agricultural Applications of High-Resolution Digital Multispectral Imagery. *Photogrammetric Engineering & Remote Sensing*, 71 (5), 595–602.

Wester-Ebbinghaus, W., 1980. Aerial photography by radio controlled model helicopter. *The Photogrammetric Record*, 10 (55), 85–92.

Whiting, M.L., Ustin, S.L., Zarco-Tejada, P., Palacios-Orueta, A., Vanderbilt, V.C., and Spie, 2006. Hyperspectral mapping of crop and soils for precision agriculture. *In*: *Conference on Remote Sensing and Modeling of Ecosystems for Sustainability III*. San Diego, CA: Spie-Int Soc Optical Engineering.

Williams, G., 2008. Data mining desktop survival guide. *dim (survey)*, 1 (32561), 15.

Woebbecke, D.M., Meyer, G.E., Von Bargen, K., and Mortensen, D.A., 1995. Color indices for weed identification under various soil, residue, and lighting conditions. *Transactions of the ASAE*, 38 (1), 259–269.

Wu, M., Yang, C., Song, X., Hoffmann, W.C., Huang, W., Niu, Z., Wang, C., and Li, W., 2017. Evaluation of Orthomosics and Digital Surface Models Derived from Aerial Imagery for Crop Type Mapping. *Remote Sensing*, 9 (3), 239.

Xing, S., Pan, Q., Tian, Y., Wang, Q., Liu, P., Zhao, J., Wang, G., Sun, X., and Tang, K., 2011. Effect of plant growth regulator combinations on the biosynthesis of terpenoid indole alkaloids in Catharanthus roseus. *Journal of Medicinal Plants Research*, 5 (9), 1692–1700.

XUE, L., CAO, W., LUO, W., and others, 2005. Rice Yield Forecasting Model with Canopy Reflectance Spectra [J]. *Journal of Remote Sensing*, 1, 14–19.

Yadav, Hemant K and Shukla, S and Singh, S., 2006. Genetic Variability and Interrelationship Among Opium and its Alkaloids in Opium Poppy (*Papaver Somniferum L*). *Euphytica*, 150 (1–2), 207–214.

Yadav, H.K., Shukla, S., and Singh, S.P., 2007. Assessment of genotype x environment interactions for yield and morphine content in opium poppy (*Papaver Somniferum L*). *Acta Agronomica Hungarica*, 55 (3), 331–338.

Yadav, H.K., Shukla, S., Singh, S.P., and Yadav, Hemant K and Shukla, S and Singh, S., 2006. Genetic Variability and Interrelationship Among Opium and its Alkaloids in Opium Poppy (*Papaver Somniferum L*). *Euphytica*, 150 (1–2), 207–214.

Yadav, R.L., Mohan, R., Singh, R., and Verma, R.K., 1984. The effect of application of nitrogen fertilizer on the growth of opium poppy in north central India. *The Journal of Agricultural Science*, 102 (02), 361–366.

Yang, G., Liu, J., Zhao, C., Li, Z., Huang, Y., Yu, H., Xu, B., Yang, X., Zhu, D., Zhang, X., and others, 2017. Unmanned aerial vehicle remote sensing for field-based crop phenotyping: current status and perspectives. *Frontiers in plant science*, 8 (111), 1–26.

Yin, X., McClure, M.A., Jaja, N., Tyler, D.D., and Hayes, R.M., 2011. In-season prediction of corn yield using plant height under major production systems. *Agronomy Journal*, 103 (3), 923–929.

Zarco-Tejada, P.J., Berjón, A., López-Lozano, R., Miller, J.R., Martin, P., Cachorro, V., González, M.R., and De Frutos, A., 2005. Assessing vineyard condition with hyperspectral indices: Leaf and canopy reflectance simulation in a row-structured discontinuous canopy. *Remote Sensing of Environment*, 99 (3), 271–287.

Zarco-Tejada, P.J., Diaz-Varela, R., Angileri, V., and Loudjani, P., 2014. Tree height quantification using very high resolution imagery acquired from an unmanned aerial vehicle (UAV) and automatic 3D photo-reconstruction methods. *European Journal of Agronomy*, 55, 89–99.

Zarco-Tejada, P.J., Gonzalez-Dugo, V., and Berni, J.A.J., 2012. Fluorescence, temperature and narrow-band indices acquired from a UAV platform for water stress detection using a micro-hyperspectral imager and a thermal camera. *Remote Sensing of Environment*, 117, 322–337.

Zarco-Tejada, P.J., Miller, J.R., Haboudane, D., Tremblay, N., Apostol, S., and Ieee, 2003. Detection of chlorophyll fluorescence in vegetation from airborne hyperspectral CASI imagery in the red edge spectral region. *Igarss 2003: Ieee International Geoscience and Remote Sensing Symposium, Vols I - Vii, Proceedings: Learning from Earth's Shapes and Sizes*, 598–600.

Zarco-Tejada, P.J., Miller, J.R., Morales, A., Berjon, A., and Aguera, J., 2004. Hyperspectral indices and model simulation for chlorophyll estimation in open-canopy tree crops. *Remote Sensing of Environment*, 90 (4), 463–476.

Zarco-Tejada, P.J., Morales, A., Testi, L., and Villalobos, F.J., 2013. Spatio-temporal patterns of chlorophyll fluorescence and physiological and structural indices acquired from hyperspectral imagery as compared with carbon fluxes measured with eddy covariance. *Remote Sensing of Environment*, 133, 102–115.

Zarco-Tejada, P.J., Ustin, S.L., and Whiting, M., 2004. Temporal and spatial relationships between cotton yield and high-spatial hyperspectral remote sensing imagery. *In*: D.J. Mulla, ed. *Proceedings of the 7th International Conference on Precision Agriculture and Other Precision Resources Management, Hyatt Regency, Minneapolis, MN, USA, 25-28 July, 2004*. St. Paul,: Precision Agriculture Center, University of Minnesota, Department of Soil, Water and Climate, 1204–1217.

Zarco-Tejada, P.J., Ustin, S.L., and Whiting, M.L., 2005. Temporal and spatial relationships between within-field yield variability in cotton and high-spatial hyperspectral remote sensing imagery. *Agronomy Journal*, 97 (3), 641–653.

Zarco-Tejada, P.J.J., González-Dugo, V., Berni, J. a. J.A.J., and Gonzalez-Dugo, V., 2012. Fluorescence, temperature and narrow-band indices acquired from a UAV platform for water stress detection using a micro-hyperspectral imager and a thermal camera. *Remote Sensing of Environment*, 117, 322–337.

Zarco-Tejada, P.J.J., Guillen-Climent, M.L., Hernandez-Clemente, R., Catalina, a., Gonzalez, M.R., Martin, P., Guillén-Climent, M.L., Hernández-Clemente, R., Catalina, a., González, M.R., Martín, P., Guillen-Climent, M.L., Hernandez-Clemente, R., Catalina, a., Gonzalez, M.R., and Martin, P., 2013. Estimating leaf

carotenoid content in vineyards using high resolution hyperspectral imagery acquired from an unmanned aerial vehicle (UAV). *Agricultural and Forest Meteorology*, 171, 281–294.

Zenk, M.H. and Juenger, M., 2007. Evolution and current status of the phytochemistry of nitrogenous compounds. *Phytochemistry*, 68 (22), 2757–2772.

Zhang, C.H. and Kovacs, J.M., 2012. The application of small unmanned aerial systems for precision agriculture: A review. *Precision Agriculture*, 13 (6), 693–712.

Zhang, N., Wang, M., and Wang, N., 2002. Precision agriculture a worldwide overview. *Computers and Electronics in Agriculture*, 36 (2), 113–132.

Zheng, G. and Moskal, L.M., 2009. Retrieving Leaf Area Index (LAI) Using Remote Sensing: Theories, Methods and Sensors. *Sensors (Basel, Switzerland)*, 9 (4), 2719–45.

Zhou, X., Zheng, H.B., Xu, X.Q., He, J.Y., Ge, X.K., Yao, X., Cheng, T., Zhu, Y., Cao, W.X., and Tian, Y.C., 2017. Predicting grain yield in rice using multi-temporal vegetation indices from UAV-based multispectral and digital imagery. *ISPRS Journal of Photogrammetry and Remote Sensing*, 130, 246–255.

Zhu, J., Wang, K., Deng, J., and Harmon, T., 2010. Quantifying Nitrogen status of rice using low altitude UAV-mounted system and object-oriented segmentation methodology. *In*: *ASME 2009 International Design Engineering Technical Conferences and Computers and Information in Engineering Conference*. USA: American Society of Mechanical Engineers, 603–609.

Zhu, Y.T., Lowe, T.C., and Langdon, T.G., 2004. Performance and applications of nanostructured materials produced by severe plastic deformation. *Scripta Materialia*, 51 (8), 825–830.

Ziegler, J. and Facchini, P.J., 2008. Alkaloid biosynthesis: metabolism and trafficking. *Annu. Rev. Plant Biol.*, 59, 735–769.